Studies on Development of Environmentally Benign Lactone based Polymers and their Composites for Biomedical Applications

Thesis submitted in the partial fulfilment of the requirements for the degree of

DOCTOR OF PHILOSOPHY

by

Neha Manojkumar Mulchandani

(Roll No. 166107006)

Department of Chemical Engineering
Indian Institute of Technology Guwahati
Guwahati-781039, Assam, India

June, 2021

INDIAN INSTITUTE OF TECHNOLOGY GUWAHATI

Guwahati-781039, Assam, India

Department of Chemical Engineering

STATEMENT

This is to certify that the research work in the thesis entitled "**Studies on Development of Environmentally Benign Lactone based Polymers and their Composites for Biomedical Applications**", is carried out by me at CoE-SusPol laboratory, Department of Chemical Engineering, Indian Institute of Technology Guwahati, under the supervision of **Prof. Vimal Katiyar**. The results documented in this thesis achieved by me are reproducible and have not been submitted to any other University or Institute for the award of any degree or diploma.

Neha Manojkumar Mulchandani

Roll No. 166107006
Department of Chemical Engineering
Indian Institute of Technology Guwahati
Guwahati-781039, Assam, India.

Guwahati, June 2021.

Prof. Vimal Katiyar

Professor
Department of Chemical Engineering
Indian Institute of Technology Guwahati
Guwahati-781039, Assam, India
Tel: +91-361-258-2278;
Email: vkatiyar@iitg.ac.in

CERTIFICATE

This is to certify that the thesis entitled "**Studies Development of Environmentally Benign Lactone based Polymers and their Composites for Biomedical Applications**", submitted by **Ms. Neha Manojkumar Mulchandani** for the award of Ph.D. degree has been carried out by her at CoE-SusPol, Department of Chemical Engineering, Indian Institute of Technology Guwahati under my supervision. The work documented in this thesis has not been submitted to any other University or Institute for the award of any degree or diploma.

Guwahati

June, 2021

Prof. Vimal Katiyar

Thesis Supervisor

This thesis is dedicated to my parents for their love, support and belief in me.

Acknowledgement

I sincerely express my earnest sense of gratitude to my learned mentor and PhD supervisor Prof. Vimal Katiyar for his valuable supervision and guidance throughout my whole research endeavour. He is an embodiment of knowledge, tolerance and perseverance. His true scientific spirit, independence and self-reliance has helped me immensely to develop the quality of my research work. I am extremely fortunate to be involved in a challenging research work assigned by him. It has enriched my life. This work enhanced my thinking abilities and understanding capability. I experienced a feeling of self-satisfaction after completion of my work. Without his continual guidance, this would not have been materialized. I shall remain grateful to him forever.

I would also like to thank my doctoral committee members Professor Vijayanand S. Moholkar, Prof. Sachin Kumar, Prof. Achalkumar A. Sudhakar for their valuable suggestions, comments, encouragement and valuable criticism during all assessments of my Ph.D. programme. I would like to place on record the use of facilities and sophisticated instruments available at Centre of Excellence for Sustainable Polymers (CoE-SusPol) and Central Instruments Facility (CIF), IIT Guwahati for carrying out instrumental analysis part of my research work. I would also like to thank the head and all the authorities of the Department of Chemical Engineering for providing me all research and analytical facilities required for my work. I am extremely thankful to the technical staff (teaching and non-teaching) of the chemical engineering department, particularly Deep Jyoti Sinha, Sailen Das, Bhagya Boro, Harsaraj Biswanath, Jayanta Kumar Mout and Ariful Haque for providing me all help and assistance for the completion of my work.

I am highly indebted to Prof. Yoshiharu Kimura, Prof. Shinichi Sakurai, Prof. Sono Sasaki, Dr. Kazunari Masutani, at Department of Biobased material science, Kyoto Institute of

Technology (KIT), Kyoto, Japan for their constant guidance and support during the entire duration of my stay in Japan. I am also thankful to Prof. Aoki, Prof. Sakai, Dr. Rasha, Dr. Shinichi Yagi, Mr. Ouchi for their help during my stay in KIT, Japan.

I owe my sincere gratitude to my fellow lab members Dr. Arvind Gupta, Dr. Surendra Singh Gaur, Dr. Prodyut Dhar, Dr. Rahul Patwa, Dr. Akhilesh Pal, Dr. Gourhari Chakraborty, Dr. Shasanka, Dr. Monika, Dr. Narendren S., Dr. Siddhartha Mohan Bhasney, Dr. Kiran Kumar Gali, Dr. Naba Kumar Kalita, Mr. Pankaj Boruah, Ms. Munmi Das, Ms. Chethana Mudenur, Ms. Doli Hazarika, Ms. Deepshikha Das, Ms. Bhanupriya Das for helping me in every way they could and for making the past couple of years more delightful in the laboratory. I wish to place on record, my thankfulness to Ms. Kona Mondal and Ms. Tabli Ghosh for their presence in my life.

Finally, I would like to convey my sincere gratitude to my parents for their sustained help and encouragement in my all academic ventures. I feel deeply indebted to them for whatever I have achieved so far.

Neha Manojkumar Mulchandani

Abstract

The current research work deals with various strategies to chemically connect the monomers (lactide and ε-caprolactone) at the molecular level and reduce the macrophase separation between them which is often witnessed when blending their respective polymers (PLA and PCL). This has been done by the random and block copolymerization techniques, where the block copolymerization (step ring opening polymerization) leads to the improved mechanical properties (strength, elongation, toughness and modulus) with the increasing block length of PLA. The diblock copolymers (PCL-PLA) and their stereocomplex blends are thermally processed by injection molding to form cortical and cancellous bone screws which are further tested for their thermomechanical stability at the sterilization temperature of biomedical devices. The linear triblock copolymers (PLA-PCL-PLA) result in the significant improvement in the mechanical properties as compared to the diblock copolymers. The triblock copolymer is thermally processed by twin-screw extruder to fabricate the filament followed by 3D printing to form a scaffold. The biocompatibility of the block copolymers is ascertained by performing MTT assay using human/rat bone osteosarcoma cells. Preferential formation of stereocomplexation is achieved upon synthesizing stereoblock terpolymers of PLA and PCL. Further, random copolymerization of L-lactide and ε-caprolactone (single step) leads to the development of copolymers which are chemically mixed (giving rise to a single T_g) and varying the content of caproyl and lactyl segments provide the range of materials with variable mechanical properties. Random copolymerization turns out to be an effective strategy for developing thermoresponsive copolymers and/or elastomeric materials. The random copolymer of L-lactide and ε-caprolactone is reinforced with bioglass (upto 50%) by solution casting method. The composites are characterized to determine their mechanical and thermal

properties and are found to behave as near elastomeric materials (with the strain recovery of 500%).

Furthermore, carbon dioxide (CO_2) is used along with 1,3-butadiene gas to develop a precursor (δ-lactone) via high pressure reaction. The use of highly reactive acid such as trifluoromethanesulfonic acid has been made to achieve the cationic polymerization of the metastable monomer. The use of metal catalyst such as Grubb's II generation catalyst in achieving the metathesis polymerization of metastable lactone has been attempted. The metal catalyst has been removed by the metal scavenger and the polymeric product has been isolated and its structure determined by nuclear magnetic resonance (NMR) spectroscopy.

Contents

List of Figures

List of Schemes

List of Tables

List of Abbreviations

3D	Three dimensional
c.a.	Approximately
PLA	Polylactic acid
PP	Polypropylene
PE	Polyethylene
PET	Polyethylene terephthalate
PLLA	Poly(L-lactic acid)
PDLA	Poly(D-lactic acid)
HAP	Hydroxyapatite
ROP	Ring opening polymerization
SC	Stereocomplex
scPLA	Stereocomplex PLA
T_m	Melting temperature
NMR	Nuclear magnetic resonance
DSC	Differential scanning calorimetry
XRD	X-ray diffraction
HFIP	Hexafluoroisopropanol
PEG	Polyethylene glycol
FESEM	Field emission scanning electron microscopy
POM	Polarizing optical microscopy
TEM	Transmission electron microscopy
FTIR	Fourier transform infrared
KBr	Potassium bromide
$CDCl_3$	Deuterated chloroform
TGA	Thermogravimetric analysis
MS	Mass spectroscopy
UTM	Universal testing machine
ASTM	American society for testing and materials
DMA	Dynamic mechanical analyzer
OTR	Oxygen transmission rate
WVTR	Water vapor transmission rate

GPC	Gel permeation chromatography
Mw	Molecular weight
N_2	Nitrogen
^{1}H-NMR	Proton-NMR
PDI	Polydispersity index
Da	Dalton
ppm	Part per million
RH	Relative humidity
T_g	Glass transition temperature
HDT	Heat deflection temperature
LA	Lactide
WAXD	Wide angle X-ray diffraction
rpm	Revolution per minute
EDX	Energy dispersive X-ray spectroscopy
hc	Homocrystals
HMW	High molecular weight
rac-LA	Racemic lactide
Sn	Tin
Oct	Octoate
Di-sb-PLA	Di stereoblock PLA
Tri-sb-PLA	Tri stereoblock PLA
Penta-sb-PLA	Pentablock PLA
CMC	Cellulose microcrystal
HAP	Hydroxyapatite
CO_2	Carbon dioxide
PCL	Poly(ε-caprolactone)
Sb-PLA	Stereoblock PLA
EVV	3-ethylidene-6-vinyltetrahydro-2H-pyran-2-one
EVV	α-ethylidene-δ-vinylvalerolactone
OH	Hydroxyl
COOH	Carboxylic acid
^{13}C-NMR	Carbon NMR
Et-soluble	Soluble in diethyl ether

Chapter: 1

Introduction

1.1 Introduction

The discovery of petroleum was a stepping stone for the development of modern human civilization leading to the industrial revolution. In the current world scenario, petroleum fulfils a larger part of the energy demand of industries and day to day human life. Due to the vast variety of its applications such as electricity, propelling vehicles, plastics production, solvent for extractions, etc., petroleum is a crucial entity which governs the global economy and affects every human being. Increased rate of petroleum exploitation with time has led to the significant concerns such as global warming, harmful greenhouse gases generation i.e. carbon dioxide (CO_2), environmental pollution and ultimately affected life and health of several species on the planet. Conventional plastics and CO_2 are the products derived from petroleum which are now considered as prime polluter of marine, water, food etc. and global warming, respectively.

Polymers are an indispensable part of human life and are usually derived from the petroleum feedstock which is available in limited amount on the planet. At the current rate of consumption of petroleum feedstock, these resources are predicted to be exhausted by the next century[1-4]. Additionally, burning of fossil fuel leads to the accumulation of carbon dioxide (CO_2) in the atmosphere at a rate which is significantly higher than its usage by green plants during photosynthesis[5]. Thus, finding the alternatives for the petroleum based resources is the prime concern of the present age[6,7]. Considering the fact, several scientists and researchers are constantly putting efforts towards developing polymers from the environmentally benign routes. The term "environmentally benign" refers to the eco-friendly/greener routes which may

be employed for developing desired materials. The biopolymers such as polylactic acid (PLA), poly(hydroxyalkanoates) (PHA), polyglycolic acid (PGA) are derived from the renewable resources which degrade into the non-toxic by-products after their service life. The polymers thus obtained from greener routes are termed as bioplastics, which have lately achieved significant scientific and commercial recognition.

The production capacities of the biodegradable and non-biodegradable plastics from the year 2017 to 2024 are shown in **Figure 1.1.** The *non-biodegradable polymers* include polyamides (PA), polyethylene (PE), polytrimethylene terephthalate (PTT), polyethylene terephthalate (PET), polypropylene (PP), whereas the *biodegradable plastics* include polylactic acid (PLA), starch blends, polybutylene adipate terephthalate (PBAT), polybutylene succinate (PBS), polyhydroxyalkanoates (PHA) and others. The global production capacities of bioplastics in the year 2020 was 2.15 million metric tonnes, of which PLA accounted for 18.7% of the production capacities, and PET accounted for 7.8%. On the other hand, biobased/non-biodegradable bioplastics accounted for 42% of the production capacities. This is further expected to rise to 2.43 million metric tonnes by 2024, of which PLA is expected to account for 19.5% of its share. This clearly discerns the global need and acceptance for the bioplastics as compared to the conventional polymers with respect to the current environmental scenario[8].

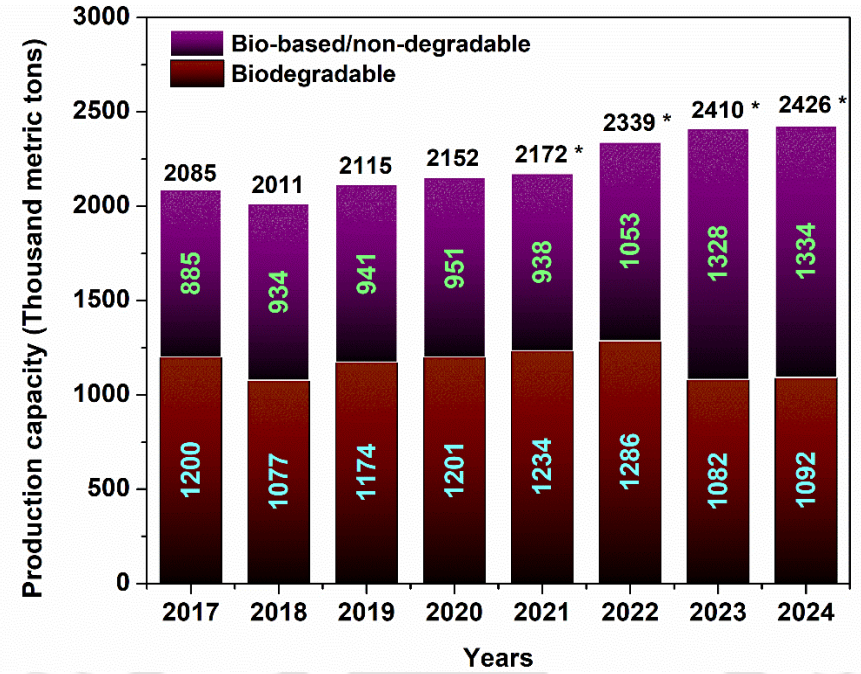

(Source: Statistica, Production capacities of bioplastics worldwide by material type)

Figure 1.1: Global production capacities of bioplastics.

Apart from the well-known bioplastics, there has been a constant exploration for developing novel materials or their precursors from the greener routes. The greenhouse gas CO_2 being available in abundant amount has been utilized for the synthesis of thermoplastics including polycarbonates, which have also gained commercial acceptance. However, several possibilities of utilizing CO_2 as a precursor in the organic synthesis are currently under investigation.

1.2 Motivation

One of the major constituents of the environment is "carbon" which is considered to be the building block of life on the earth and the primary component of macromolecules. Carbon circulates constantly in the environment over the living and non-living species, thus forming a carbon cycle. One such form of the carbon in the environment is CO_2 which is available in an abundant amount in the atmosphere. The interesting properties of CO_2 at supercritical conditions i.e. the viscosity and surface tension of CO_2 being comparable to that of gases while its solubility parameter, density and dielectric constant being comparable to that of liquids have witnessed its exploration in replacing the organic solvents[9-11].

CO_2 which is considered as one of the major causes of the global warming, is also a key element for the photosynthesis in plants. It is a crucial entity for the major complex reactions occurring daily in the plants as well as human life, and a closer examination at the function of CO_2 manifests the principles of basic chemistry. However, it is difficult to fix CO_2 in the chemistry of polymerization due to its low reactivity and usually require extreme conditions of temperature and pressure for its reaction. Catalysis is perhaps, one of the best solutions to overcome the thermodynamic stability of the most abundant C1 resource[12-14].

The potential of CO_2 in the organic synthesis has been realized ever since the discovery of cyclic lactone "3-ethylidene-6-vinyltetrahydro-2H-pyranone" from the reaction of CO_2 with 1,3-butadiene by Inoue and coworkers[15]. This process directly fixes CO_2 in the chemistry of organic synthesis employing a palladium catalyst complex. Since them attempts have been made to increase the yield and selectivity of this novel precursor[16-19] and its subsequent polymerization[20, 21].

Furthermore, the process of conversion of lactide (cyclic lactone) to PLA was developed by Wallace Hume Carothers[22]. However, PLA was first discovered by Theophile-Jules Pelouze as a condensation product of 2-hydroxypropanoic acid (lactic acid). Lactic acid is industrially obtained by the fermentation of carbohydrates such as glucose, sucrose or galactose[23]. The major form of carbohydrates include corn and corn starch which are a result of plant photosynthesis. Thus, CO_2 indirectly acts as a precursor for the synthesis of lactide, which is then used for the production of polylactic acid (PLA), a well-known biobased polymer[24].

These environmentally benign cyclic esters (lactones) thus set out to be the potential monomers for a different class of materials, thereby expanding the horizons of material chemistry [25]. In this regard, the current research majorly employs the use of these cyclic lactones to develop environmentally benign polymers. Yet, another class of lactone i.e. ε-caprolactone[26, 27] has also

been used in the present research, which is currently derived from the petroleum based feedstock. Attempts are being made to synthesize biobased ε-caprolactone, however, it is at a very naïve stage[28].

1.2.1 Lactide and ε-caprolactone based copolymers/composites

In the current research, the use of lactide and ε-caprolactone monomers has been made to develop a series of random, diblock, triblock and pentablock copolymers, and their composites by using bioceramic filler such as bioglass.

The copolymers have been synthesized by using the tandem ring opening polymerization (ROP) strategy in presence of suitable catalyst and initiator. It is noteworthy to observe the effect of molecular architecture on the properties of the copolymers and this research provides a methodology for the synthesis of customized materials with tailored properties. Additionally, the concept of "stereocomplexation" in PLA has been remarked in the block copolymer system which has the potential of achieving improved thermal stability. The random and block copolymers are made for the biomedical applications and their biocompatibility has been demonstrated by performing the *in vitro* studies. Furthermore, the processability of these copolymers has been demonstrated to develop representative biomedical implants.

1.2.2 New class of materials from "3-ethylidene-6-vinyltetrahydro-2H-pyranone"

A new class of materials have been made from "3-ethylidene-6-vinyltetrahydro-2H-pyranone" or "α-ethylidene, δ-vinyl valerolactone" precursor which has a high substitution on its ring. The precursor is synthesized from the reaction of CO_2 and 1,3-butadiene, which is subjected to metathesis and cationic polymerization processes in presence of suitable catalysts to develop novel materials.

1.3 Organization of thesis

Chapter 2: *Literature review*

The progress in the field of polymer chemistry has been highlighted from the perspective of environmentally benign polymers including polylactic acid (PLA) and poly(ε-caprolactone) (PCL). The importance of bioglass in biomedical implants has been remarked. The advancements in the field of CO_2 derived lactone based polymers have been presented.

Chapter 3: *Diblock Copolymers based on Poly(lactic acid) and Poly(ε-caprolactone), and their Stereocomplex Blends*

The formation of diblock (PCL-PLLA & PCL-PDLA) copolymers and their enantiomeric blends have been demonstrated in this chapter which the effect of block length on the thermal, mechanical and crystal behaviours. The copolymers have been processed to fabricate orthopaedic implants and their thermomechanical stability and biocompatibility has been determined.

Chapter 4: *Triblock Copolymers based on Poly(lactic acid) and Poly(ε-caprolactone), and their Stereocomplex Blends*

This chapter focuses on the synthesis and characterization of triblock copolymers (PLLA-PCL-PLLA & PDLA-PCL-PDLA) and their enantiomeric blends by tandem ROP. The effect of block length as well the content of PLA and PCL on the mechanical properties of triblock copolymers have been investigated. A structure model has been given from the SAXS analysis. The process of triblock copolymer synthesis has been scaled up to 500 g batch which is processed by twin-screw extrusion to make filaments and its subsequent 3D printing to develop mesh-type scaffold. The biocompatibility of the materials have been determined.

Chapter 5: *Stereoblock Terpolymers based on Poly(lactic acid) and Poly(ε-caprolactone) with Preferential Stereocomplexation*

The stereoblock terpolymers have been made by tandem ROP where PCL is used as a middle segment to obtain preferential stereocomplexation. The effect of blending the enantiomeric penta-stereoblock copolymers have been presented in terms of its thermal and mechanical properties. The morphological structure of the stereoblock copolymer is further remarked.

Chapter 6: *Random Copolymers based on L-lactide and ε-caprolactone, and its Composites*

This chapter focuses on the synthesis of random copolymers of L-lactide and ε-caprolactone with the varying molar ratio of the two monomers resulting in molecularly mixed copolymers with tailored thermal and mechanical properties. The shape memory and elastomeric properties of the random copolymers have been underlined. Further, bioglass has been incorporated to the random copolymer matrix and the properties of the composites are investigated. The near-elastomeric character of the composites of the random copolymers have been remarked.

Chapter 7: *Metathesis Polymerization of a CO_2 Derived Lactone*

The CO_2 derived monomer "α-ethylidene, δ-vinyl valerolactone" due to its high ring substitution was subjected to olefin metathesis in presence of a metathesis catalyst (Hoveyda-Grubb's II generation) to obtain novel materials. The structure of the obtained material is ascertained from ^{13}C-NMR and ^{1}H-NMR spectroscopy.

Chapter 8: *Cationic Polymerization of a CO_2 Derived Lactone*

This chapter presents the synthesis of "α-ethylidene, δ-vinylvalerolactone" from the reaction of CO_2 and 1,3-butadiene, which is further subjected to cationic polymerization in presence of a highly reactive acid catalyst. The structural analysis of the obtained material is further presented.

Chapter 9: *Conclusions and Future scope*

The summary of the present research work and its future scope has been presented in this chapter.

The schematic representation of the current research work is shown in **Figure 1.2**.

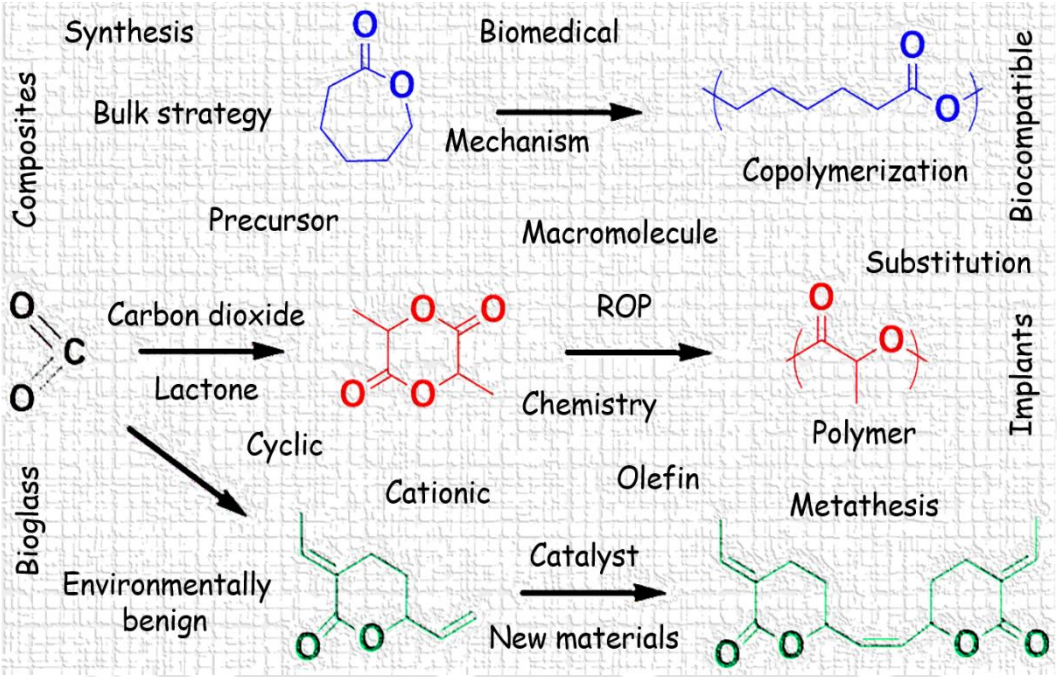

Figure 1.2: Schematic representation of the thesis work.

Chapter: 2

Literature Review

Graphical Abstract

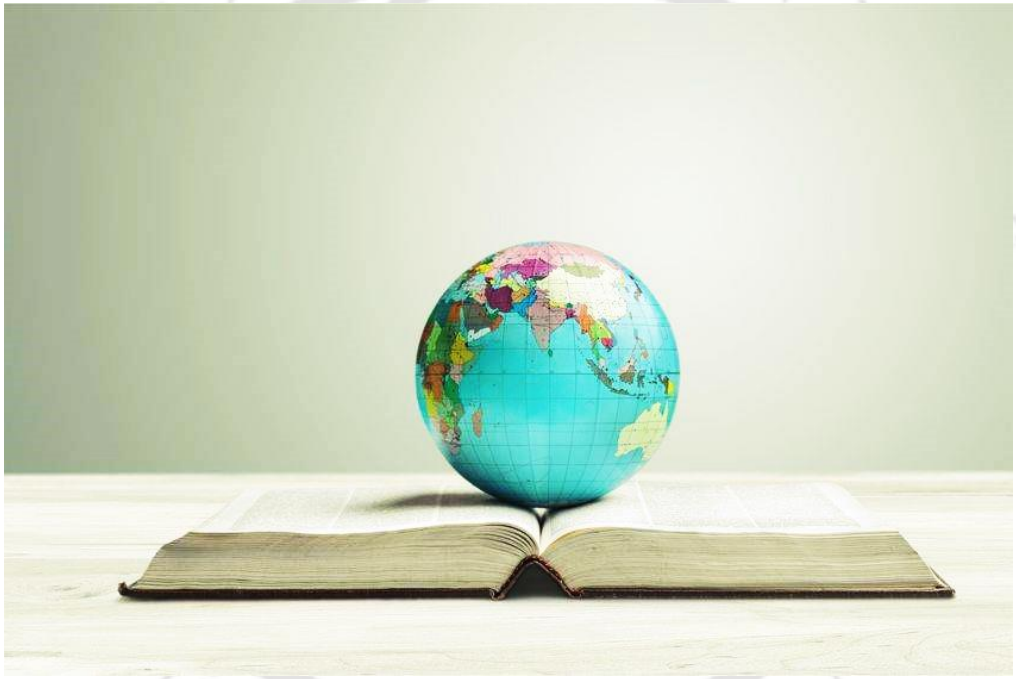

Outcome:

- *Advances in Sustainable Polymers: Synthesis, Fabrication and Characterization. Springer Nature, 2020.*
- *Bioactive Glasses: Prospects in Bone Tissue Engineering. Advances in Sustainable Polymers. Springer, Singapore, 2019. 67-83.*
- *Resorbable polymers in bone repair and regeneration. Materials for Biomedical Engineering. Elsevier, 2019. 87-125.*
- *Polylactic Acid Based Hydrogels and Its Renewable Characters: Tissue Engineering Applications." Springer International Publishing: Cham, Switzerland, 2018. 1-24.*

2.1 General Introduction

Much of the global industrial advancements are a result of the processes that are inspired from nature. Although the inception of research in the organic synthesis lasts back to centuries, there has been a perpetual exploration and application of greener/environmentally benign routes to develop a new class of materials. While nature has unfolded a number of its components/sources to the scientific society, it still retains infinite unexplored/underexplored things. One such natural source is carbon dioxide which is present in abundance in the environment and has an immense potential to be utilized for the chemical processes accounting to its renewability, non-toxicity and economic efficiency. Lately, carbon dioxide has attracted a significant attention of the human society. It can either be directly fixed into the chemistry of organic synthesis, or indirectly act as a precursor for the synthesis of biobased polymers such as PLA. The purpose of this research is to utilize environmentally benign lactones for the development of polymers/composites for biomedical applications. In line to this, the current chapter presents an extensive literature review on lactone based polymers and their composites in order to explore them for potential biomedical applications.

2.2 Polylactic acid (PLA)

PLA is an aliphatic polyester which belongs to the family of α-hydroxy acids. Being derived from renewable sources such as corn starch, sugarcane, cassava roots, potatoes, etc., PLA has been widely accepted as an alternative to petroleum based polymers such as polyethylene, polypropylene, polyethylene terephthalate, etc. PLA can be synthesized from lactic acid by polycondensation. Lactide is another precursor, derived from lactic acid which leads to the formation of PLA by ring opening polymerization. Reinhold Gruter first patented the process for the synthesis of lactide in 1913. PLA is thus produced by combined fermentation and

polymerization processes. The synthesized PLA can further be processed using different approaches for intended applications. Swedish Chemist Carl Wilhelm Scheele isolated lactic acid (basic constituent of PLA) from sour milk in the eighteenth century[29]. The chiral nature of lactic acid leads to the formation of two enantiomerically pure homopolymers of PLA i.e. poly(L-lactic acid) (PLLA) and poly(D-lactic acid) (PDLA) acid[30]. The two enantiomers are found to have different rates of degradation. PLLA is known for its prolonged biodegradation and superior biocompatibility as compared to that of PDLA. Further, the strength and modulus of PDLA are relatively low as compared to PLLA. These polymers are found to have a crystalline nature[31]. Racemic mixture of D-lactic acid and L-lactic acid, on polymerization forms poly(DL-lactic acid) (PDLLA) which is amorphous in nature. Various techniques such as ring opening polymerization, solid-state polymerization, condensation polymerization and azeotropic dehydrative condensation have been adopted to produce enantiopure PLA. The properties of PLA vary with the molecular weight and therefore it is essential to consider the molecular weight for intended applications. PLA can be synthesized via polycondensation or ring opening polymerization. However, ring opening polymerization takes relatively less time for the production of PLA. Wallace. H Carothers reported the ring opening polymerization of lactide in 1932. PLA was considered to be an undesirable material due to its instability in the humid conditions. However, PLA started gaining importance in biomedical field in 1966 due to its biodegradable, bioresorbable, biocompatible and non-toxic nature. The synthesis of PLA usually involves the use of tin octoate ($Sn(Oct)_2$) as a catalyst which is less toxic to human body and has been approved by Food and Drug Administration (FDA) for pharmaceutical and biomedical applications[32]. The recent approaches involve the use of lipase for the synthesis of PLA which will eliminate the use of metal based catalysts. Such greener approaches are still at the stage of development. The

degradation products of PLA are usually water and carbon dioxide which are non-toxic and non-carcinogenic to the body. PLA has therefore gained significant attention due to its excellent biodegradability and biocompatibility. It has been studied for its application in the biomedical field such as drug delivery, orthopedic fixation devices, surgical sutures, dental implants and scaffolds for engineering damaged tissues. The structure of PLA is shown in **Figure 2.1**.

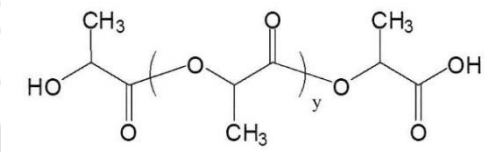

Figure 2.1 Structure of polylactic acid.

2.2.1 Advantages and Limitations of PLA

PLA is a versatile polymer which is known to have high mechanical strength and modulus and has been explored in various applications including food packaging, agriculture, electronics, textile, paper coating, etc. due to its unique properties. The conventional petroleum based polymers take several hundred years to degrade completely whereas PLA, after its service life can go back to nature in the form of water and carbon dioxide and degrade completely over several months to few years. However, it has low impact toughness and small window for processing which may be improved by blending, stereocomplexation or co-polymerization. A small amount of PDLA is generally added to PLLA in order to improve the processability, however it decreases the crystallinity of the polymer. Blending of PLA with suitable polymers enables to achieve increased crystallinity, improved toughness and elongation at break along with tailored hydrolytic degradation [33]. PLA, although having significant potential for replacing conventional plastics, the cost of manufacturing PLA is higher as compared to that of petroleum based polymers due to the complicated steps of synthesis. Additionally, the low heat deflection temperature, relatively low

glass transition temperature, low melting temperature, relatively poor barrier properties and slow crystallization have limited its use in many applications. Various scientific groups have attempted to enhance these properties of PLA by utilizing methods such as formation of biocomposites[34, 35], copolymerization, blending of polymers, formation of stereocomplex[36, 37], etc. Addition of biofillers such as chitosan, clay, cellulose, hydroxyapatite, bioglass, etc. into the PLA matrix leads to the formation of biocomposite with improved properties. Further, the incorporation of bioactive fillers such as bioglass will allow for the regeneration of bone tissue which has gained significant attention in the recent past [38]. Thermal, mechanical as well as thermomechanical properties of PLA can be enhanced by blending with suitable polymers. Stereocomplexation involves mixing of enantiomers in 1:1 ratio which is found to increase the melting temperature by 50°C as compared to that of pure enantiomeric PLA. Thermal, mechanical and gas barrier properties can significantly be improved by stereocomplexation which is a crystal formed by the interaction between enantiomers of PLA. Further, PLA is known to be hydrophobic in nature along with slower rate of degradation which is undesirable for many biomedical applications. However, co-polymerization with hydrophilic monomers or the incorporation of polyethylene glycol (PEG) chains in the backbone of PLA can lead to the formation of water soluble PLA based polymers which can be explored for the formation of hydrogels for engineering diseased or damaged tissues [39]. Stereocomplexation of copolymers can further enhance the mechanical, physical and chemical properties of the hydrogels which can be tailored for desired specific applications. The properties and degradation rates of polyesters have been displayed in **Table 2.1.** The rate of degradation of the polymer can be tailored by using different combination of polymers for desired tissue regeneration.

Table 2.1 Thermal and mechanical properties of polyesters.

Sr. No.	Polymer	T_m (°C)	T_g (°C)	Tensile strength (MPa)	Modulus (MPa)	Time of degradation (months)	References
1.	PLLA	~175	~62	~41	~1196	24-60	40-42
2.	PDLA	~177	~61	~46	--	24-60	40, 43-45
3.	scPLA	~206-230	65-72	~880	~8600	--	36, 40, 41
4.	PGA	225-230	35-40	~384	~12.8	6-12	40, 46-48
5.	PLGA	--	45-55	~4.3	1000-2000	1-6	40, 49
6.	PCL	60	-60	10-16	400	>24	40, 50

PLLA: Poly(L-lactic acid), PDLA: Poly(D-lactic acid), scPLA: stereocomplex PLA, PGA: polyglycolic acid, PLGA: poly(lactic-co-glycolic acid), PCLA: poly(caprolactone-co-lactic acid)

2.3 Stereocomplexation in PLA

An intermolecular complex formed by the macromolecules having identical chemical composition but different configuration of the repeating units is known as stereocomplex (sc)[51]. The co-crystallization of the stereoisomers PLLA and PDLA results in the formation of a well-known crystal structure "stereocomplex PLA (sc-PLA)". The sc-PLA gained widespread recognition and acceptance ever since its discovery by Ikada et al. in 1987[52], patented by Murdoch and Loomis[53]. Stereocomplexation in PLA is attributed to the non-covalent interaction of the enantiomeric macromolecular chains. The sc-PLA crystals melt at a temperature (T_m) 50 °C higher than the homochiral (hc) PLLA or PDLA crystals[54]. Apart from the improved heat resistance, stereocomplexation in PLA provides better mechanical performance and resistance to hydrolysis[55, 56] as compared to PLLA or PDLA allowing its exploration in pharmaceutical and biomedical applications. The homopolymers PLLA or PDLA have been utilized for several applications such as agricultural mulch-films, disposable trays, etc. which have a short life. On the other hand, sc-PLA can be specifically adopted for high performance applications such as structural and engineering plastics[57].

The stereoselective interaction of the optically active enantiomers PLLA and PDLA result in the formation of optically inactive sc-PLA, when mixed in an equimolar ratio[58, 59]. The formation of sc crystals was initially remarked from the solution mixing and later from the melt, where the sc crystals melted at a temperature (T_m) ~50ºC higher than that of hc PLLA or PDLA[52]. The enantiomers PLLA and PDLA are packed side by side in a sc crystal lattice. PLA being semi-crystalline in nature, leads to the development of unique morphologies in block copolymers due to the competition between crystallization and microphase separation which expands their application in materials science[60]. The

spherulites of sc-PLA does not have a ring-band structure at any crystallization temperature unlike those of PLLA or PDLA homopolymers. The stereocomplexation is largely driven by the molecular weight of PLLA and PDLA. An equimolar blending of PLLA and PDLA (1:1) with high molecular weight (>100 kg/mol) often lead to the formation of hc crystals along with sc crystals. Improved miscibility between the PLLA and PDLA chains can enhance the formation of sc in the PLLA/PDLA blend. The mesophase (an ordering of molecules which is intermediate between crystalline and amorphous state) in sc-PLA can be observed by annealing the equimolar blends of PLLA/PDLA just above their T_g due the prevailing weak intermolecular interactions between PLLA and PDLA chains[61]. The stereocomplex mesophase is more prevalent at the lower temperature due to the reduced molecular mobility. An increased molecular mobility is observed at higher temperature leading to the increased formation of hc crystals. Further, blending non-equimolar mixture of PDLA and PLLA result in various fractions of hc and sc crystallites. However, as reported by Woo. et al., the non-equimolar blends of PDLA and low-molecular weight PLLA where the content of PLLA is between 30 and 50 wt%, there is an existence of only sc-PLA crystals. In such a case, a large amount of homopolymer PLA chains may be trapped and dispersed in the spherulites of sc-PLA crystals thereby resulting in the fluffy lamellae stacking of sc crystals[62].

Lately, attention has been paid on improving the melt crystallizability of sc-PLA for the efficient formation of sc crystals in order to expand its applications, particularly in industry where melt processing of polymers is often employed. The viscosity average molecular weight ($\overline{M_v}$) for the stereocomplexation from the melt is 6×10^3 g/mol, whereas that from the solution casting is 4×10^4 g/mol. However, sc crystals upon melt crystallization lead to the formation of hc along with sc crystals. Therefore, efforts have

been laid on to achieve exclusive formation of sc-crystals from the melt[63, 64]. The use of polyethylene glycol (PEG) as a plasticizer has been reported to enhance the formation of sc crystallites in the high molecular weight (HMW) blends of PLLA and PDLA. Several studies have also made use of sc-PLA in the drug delivery application in lieu of its improved barrier properties which prevents the burst release/prolongs the release of drug[65]. The formation of sc crystals may therefore lead to the development PLA based materials with enhanced performance. The molecular weight, optical purity of enantiomeric PLA, and tacticity are the governing parameters for the sc crystallization, where the lower optical purity or higher molecular weight affects the sc crystallization[66, 67]. The formation of hc crystals is often more kinetically favourable than that of sc crystals during the crystallization of high molecular weight PLLA/PDLA blend. However, enhancing the interchain interactions between PLLA and PDLA by covalent or non-covalent means can improve the formation of sc crystallites[68]. Also, sc crystallizes much faster from the melt as compared to the α-form. Due to its distinctive behaviour, sc-PLA is attracting several industrial applications. Several researchers have therefore been constantly involved in understanding the crystal structure of sc-PLA, which may be the governing parameter for its explicit behaviour. A preferential formation of sc may be obtained by blending PLLA/PDLA (in solution) in equimolar (1:1) ratio which has the melting temperature ~230 °C. However, varying the ratios of PLLA/PDLA in the blend give rise to the formation of hc-PLA (T_m ~ 180 °C) along with sc-PLA. In order to improve the sc formation in non-equimolar blends of PLLA/PDLA, several methodologies have been adopted and some of them have been highlighted in the subsequent sections.

2.3.1 Crystal structure of sc-PLA

Sc-PLA often crystallizes in a triclinic or trigonal unit cell with both 3_1 (or 3_1 and 3_2) PLLA and PDLA chains packed side by side[69] unlike the orthorhombic or pseudo-orthorhomic crystal forms of hc-PLA[70]. The crystal structure consisting of a triclinic unit cell (P1 symmetry with parallel chain orientation) was proposed in 1991 by Okihara et al., who reported 3_1 helical structure of PLLA and PDLA chains having a lamellar thickness of 0.87 nm, where the three enantiomeric chains penetrate one unit cell[71]. The unit cell parameters of a triclinic cell are given as a = b = 9.16 Å, c = 8.7 Å; α = β = 109.2°, γ = 109.8°. The structure was revised to that of a trigonal unit cell (R3c or R-3C group) by Cartier et al. in 1997, where the PLLA and PDLA chains have 3_2 and 3_1 conformations respectively[72]. According to the modified trigonal structure, the triclinic cell was assumed to be a subcell of the larger trigonal cell where six helices penetrate one unit cell. The trigonal unit cell parameters may be given as a = b = 14.98 Å, c = 8.7 Å; α = β = 90°, γ = 120°. The crystal was grown from the non-equimolar blends of PLLA and PDLA which indicated the cocrystallization of PLLA and PDLA chains could occur from their asymmetric ratio. However, the model was proposed by taking into consideration only 1:1 ratio of PLLA and PDLA chains. Further, the stereocomplex structures with parallel and antiparallel orientation of the molecular chains were proposed by the molecular simulations conducted by Brizzolara et al. who also revealed that the parallel structure (P1) was more stable than the anti-parallel structure (P/1). The structures were considered to be triclinic having the cell parameters a = 0.912, b = 0.913, c = 0.930 nm, α = β = 110°, γ = 109° for the parallel structure (P1); and a = 0.930, b = 0.940, c = 0.930 nm, α = 111°, β = 112°, γ = 108° for the antiparallel structure (P/1). The growth mechanism of the triangular lamellar crystals in the sc formation was well supported by

the simulations[73]. Further, the highly oriented stereocomplex samples were prepared in study reported by Sawai et al. who adopted the solvent casting technique to prepare the films followed by their co-extrusion (draw ratio = 14). The oriented samples showed 20 wide angle X-ray reflections that were reasonably indexed with a trigonal unit cell as proposed by Cartier et al. with a slight variation of the parameters, which are given as : a = b = 1.50, c = 0.823 nm, $\alpha = \beta = 90$ and $\gamma = 120^{o}$ with R3c space group[74].

These structure models were mainly proposed for the PLLA/PDLA blend having a ratio of 50/50. However, stereocomplexation is also evident in the PLLA/PDLA blend having the ratios of 30/70 - 70/30, for which a new structure model (space group P3) was proposed by Tashiro et al. (2017) on the basis of X-ray Diffraction analysis. According to the model, the co-existence of PLLA and PDLA chains between the sc crystal lattice is profound for the PLLA/PDLA blend ratios in the range of 30/70 – 50/50 – 70/30. Beyond this, the coexistence of PLLA and PDLA chains is not realizable due to their instability. A statistically disordered packing of PLLA and PDLA chains can be perceived from the P3 space group, unlike the symmetrical R3c model[75, 76]. The unit cell parameters reported by several researchers have been tabulated in **Table 2.2.**

Table 2.2: Unit cell parameters reported for the sc crystals.

	Okihara et al.	Brizzolara et al.	Cartier et al.	Sawai et al.	Tashiro et al.
Crystal system	Triclinic	Triclinic	Trigonal	Trigonal	Trigonal
Chain conformation	3_1	3_1	3_1 and 3_2	3_1 and 3_2	3_1
Unit cell parameters					
a (nm)	0.916	0.912	1.498	1.50	1.494
b (nm)	0.916	0.913	1.498	1.50	1.494
c (nm)	0.870	0.930	0.870	0.823	0.862
α (degree)	109.2	110	90	90	90
β (degree)	109.2	110	90	90	90
γ (degree)	109.8	109	120	120	120
ρ_{calc} (g/cm^3)	1.27	1.21	1.27	1.342	-

2.3.2 Stereoblock PLA formation

The stereoblock formation allows for the intermolecular as well as intramolecular mixing of the neighbouring L- and D- stereosequences, thereby leading to the preferential formation of sc crystallites. This is particularly important when synthesizing sc polymers with HMW. Block copolymerization has received enormous recognition in achieving the desired properties of the resulting materials. The composition of PLLA/PDLA along with the number of blocks and chain length can be varied in order to obtain a variety of diblock, multiblock copolymers with tailored properties. The molecular mixing of the enantiomeric PLLA and PDLA chains in the sb copolymers lead to the improved crystallinity[77-79].

2.3.2.1 Single step process

The formation of sc-PLA usually occurs by blending of PLLA/PDLA chains, which requires the individual ROP of L- and D-lactide prior to blending the respective enantiomeric PLA chains. The sc-PLA thus formed exhibits improved thermal and mechanical properties, however the process requires the formation of enantiopure polymers from the respective enantiopure monomers which restricts its practical applications. In this regard, the single step preparation of sc-PLA has been explored from the readily available racemic lactide (rac-LA) which is inexpensive (**Figure 2.2**). The ROP of rac-LA (1:1 mixture of D- and L- lactide) usually yields the amorphous polymers (atactic or heterotactic) having much lower melting and glass transition temperatures as compared to the isotactic PLA. The random arrangement of L- and D- lactide units in the backbone chain is usually observed upon polymerizing rac-LA with a limited scope of application. In order to extend the utilization of rac-LA precursor, significant efforts have been made in achieving the stereoselective polymerization of rac-LA by tailoring the stereochemistry of the resulting PLA[80-82].

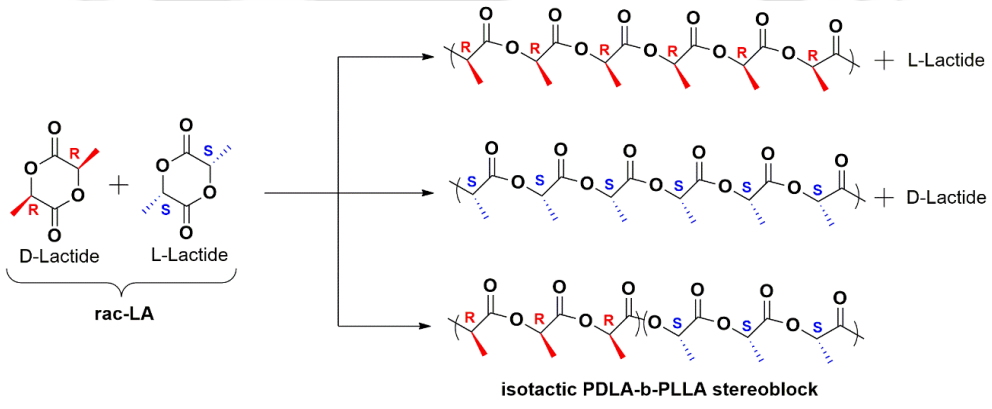

Figure 2.2: Stereoblock PLA formation from rac-LA in a single step.

2.3.2.2 Stepwise ROP

The well-known sequential polymerization has largely been employed to develop stereoblock PLA with high molecular weight and crystallinity[83]. The formation of diblock copolymers of PLLA and PDLA was first reported by Yui et al. by adopting the sequential ring opening polymerization strategy using aluminium tris(2-propanolate) as a catalyst. The easy interaction of the enantiomeric block sequences resulted in the formation of di-stereoblock copolymers consisting of sc crystals with little hc crystallization. The molecular weight of the diblock copolymers was reported to be ~20 kDa, however it is often essential to obtain the polymers with HMW in order to render them processable for possible applications. The two-step ROP of L- and D-lactides have been conducted to form PLLA-PDLA (di-sb copolymers) where stannous octoate ($Sn(Oct)_2$) was employed as a catalyst (**Figure 2.3**). The prepolymer (PLLA or PDLA) was prepared in the first step having a molecular weight of <50 kDa which was purified to remove the residual lactide prior to synthesizing di-sb PLA (having non-equivalent ratio of PLLA/PDLA) in the second stage of ROP. The di-sb PLA had the Mw > 150kDa and the solution cast films showed the formation of exclusive sc crystals. The heat deflection temperature of di-sb PLA was however limited, and the sc crystallinity was found to enhance upon blending the enantiomeric di sb-PLAs[84]. Further, the stereo triblock PLAs (ABA) having non-equivalent block compositions were prepared by two-step ROP in presence of 1,12-dodecanediol as an initiator. The bis-hydroxyl terminated PDLA was prepared in the first stage of ROP which was purified to remove the residual D-lactide. In the second stage of ROP, L-lactide was used as a monomer to develop PLLA-PDLA-PLLA with different compositions of PLLA and PDLA blocks (**Figure 2.4**). The molecular weights

of tri-sb PLAs was higher than 100 kDa, which gave the exclusive formation of sc crystals without hc crystallization[85].

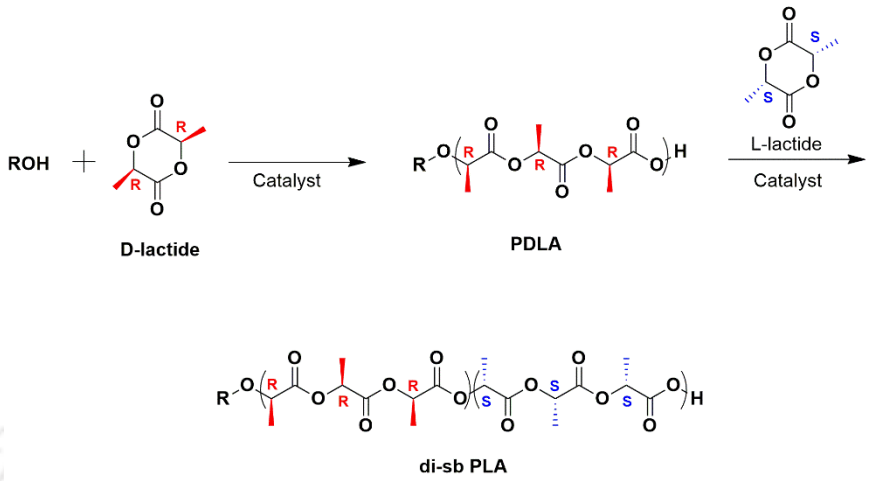

Figure 2.3: Two-step ROP for the synthesis of di-sb PLA.

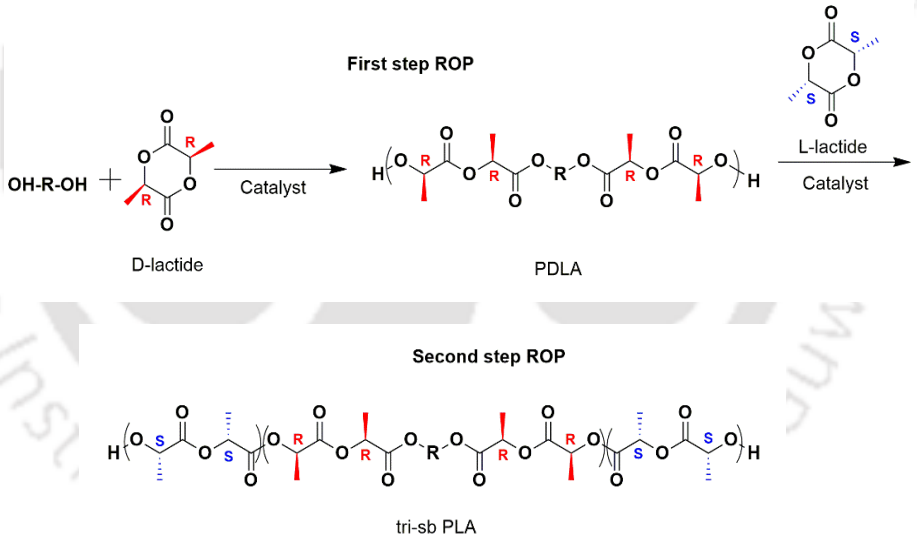

Figure 2.4: Two-step ROP for the synthesis of tri-sb PLA.

2.4 Stereocomplexation in PLA based Copolymers

The copolymerization of sc-PLA has been studied with the well-known biobased/biodegradable polymers such as PCL, PEG, etc. due to the complementary properties of the counterparts which may lead to the achievement of materials with

customized properties. The mechanical and thermal properties of the representative biobased/biodegradable polymers have been highlighted in **Table 2.3**.

2.4.1 sc-PLA-PCL Copolymers

The sc blends of PLA have lately witnessed importance in biomedical implants as well. In a study reported by us[86], the synthesis of diblock copolymers of PCL-PLLA and PCL-PDLA has been done by two-step ROP followed by blending them in 1:1 ratio to achieve sc blends of diblock copolymers. Using this strategy, it was possible to achieve the enhanced mechanical properties (28 MPa strength and ~80% elongation at break) which was also processed by the conventional injection molding machine to develop cancellous bone screws (orthopedic implants). The study reported the thermomechanical stability of the cancellous bone screw at 121 °C in comparison to the commercial PLA (NatureWorks). The synthesized formulation of sc blend was found to be stable at the sterilization temperature of biomedical devices, unlike that of commercial PLA.

Table 2.3: Mechanical and Thermal Properties of the Representative Bio-based /Bio-Degradable Polymers.

	PLLA	sc-PLA	PGA	PHB	PCL
T_m (°C)	170 - 190	220 - 240	225 - 230	188 - 197	55 - 65
T_g (°C)	50 - 65	65 - 72	40	5	-60
ΔH_m (J/g)	93 -203	142 - 155	180 - 207	146	136
Density (g/cm^3)	1.25 - 1.3	1.21 - 1.342	1.50 - 1.69	1.18 - 1.26	1.1 - 1.15
Tensile strength (MPa)	120 - 2260	880	80 - 980	180 - 200	8 - 16
Young's modulus (GPa)	6.9 - 9.8	8.6	3.9 - 1.4	4.9 - 5.9	0.1 - 0.4
Elongation at break (%)	12 - 16	30	30 - 40	50 - 70	100 - 2000

2.4.2 scPLA-PEG Copolymers

Polyethylene glycol (PEG) being hydrophilic in nature, leads to the development of amphiphilic materials when used in combination with hydrophobic polymers[87, 88]. The amphiphilic copolymers based on PLA[89] have received attention in several applications including pharmaceutical, drug delivery[90, 91], hydrogels for tissue engineering, etc.[92]. The aqueous self-assembly of amphiphilic PEG/scPLLA copolymers has been reported by Noack et al., where the block copolymers PEG/PLLA and PEG/PDLA were synthesized by ring opening polymerization using PEG-OH as a macroinitiator. The decreasing content of hydrophobic unit (lactide) led to the increased formation of worm-like aggregates at ambient conditions. The preferential formation of spherical micelles was observed for the most hydrophilic block copolymer (ascertained from dynamic light scattering), which were said to become colloidally unstable upon increasing the crystalline PLA and leading to the formation of worm-like aggregates[93]. The biofunctional injectable hydrogels based on PEG-scPLA have been reported by Wang et al. for cartilage tissue engineering[94]. The ROP of D- and L-lactides was performed using 4-arm PEG as a macroinitiator to develop 4-arm PEG-PDLA and PEG-PLLA copolymers respectively. This was followed by synthesizing their cholesterol modified derivatives namely 4-arm PEG-PDLA-Chol and 4-arm PEG-PLLA-Chol by condensation reaction. The sc blends of the respective enantiomers resulted in the stereocomplexes scPLA (4-arm-PEG-PLA) and scPLA-Chol (4-arm PEG-PLA-Chol) which were employed as 3D scaffolds for the cartilage tissue engineering. The cholesterol modified sc-PLA had the higher critical gelation temperature, improved mechanical properties, better adhesion of chondrocytes and slower degradation which served as appropriate materials for

cartilage regeneration. The thermal and mechanical properties for the sc-PLA based copolymers and composites have been reported in **Table 2.4**.

Table 2.4: Thermal and mechanical properties reported for the sc-PLA based copolymers and composites.

	Mulchandani et al.	Noack et al.	Sun et al.	Gupta et al.	Gupta et al.	Gupta et al.
Copolymer/ Composite	sc-PLA/PCL	sc-PLA/ PEG	sc-PLA/GO	sc-PLA/ chitosan	sc-PLA/CMC	sc-PLA/ n-HAP
$T_{m,hc}$ (°C)	171 - 177	-	150	-	152 – 180	152 - 178
$T_{m,sc}$ (°C)	210 - 235	140 - 200	210	192 - 208	211	210
$\Delta H_{m,hc}$ (J/g)	10 - 23	-	-	-	-	0 -28
$\Delta H_{m,sc}$ (J/g)	30 - 42	-	-	20 - 40	-	17 - 55
Crystallinity, sc (%)	-	-	40 - 70	~70	55	12 - 39
Tensile strength (MPa)	14 - 30	-	-	29 - 63	29 - 57	33 - 40
Elongation at break (%)	7 – 80	-	-	-	1.9 - 36	6.3 - 131
Young's modulus (GPa)	0.3 – 0.7	-	-	1.9 – 2.8	-	-

2.5 Stereocomplex PLA based Composites

The application of stereocomplexation in composites has often been made to impart heat stability to the resulting composites. In principle, when the desired properties cannot be achieved by a single component, incorporation of several fillers may lead to the tailored/desired properties. Stereocomplex PLA, which is known for its better thermal resistance has been incorporated/modified with the fillers such as hydroxyapatite, chitosan,

cellulose, graphene, etc. to obtain the materials with customized properties. In line to this, Sun et al. have grafted graphene oxide (GO) to PDLA by ring opening polymerization of D-lactide, where the OH groups on the GO acted as initiator[95]. The grafted PDLA was then blended with PLLA in solution to develop the solution cast films of sc nanocomposites. The activation energy of crystallization was lowered along with an increased fraction of sc crystallites and improved crystallinity for the nanocomposites, as compared to the PLLA/PDLA blends without filler (GO). This effect may be reasonably attributed to the heterogeneous nucleation of GO. The cold crystallization however lead to the lower crystallinity possibly due to the reduced chain mobility and hindered crystal growth accounting to the exfoliated GO sheets.

Furthermore, Gupta et al. have demonstrated the use of nano-amphiphilic chitosan in developing high heat stable sc-PLA[96]. The grafting of chitosan to the oligomeric PLA was done via in situ polycondensation of L-lactic acid to synthesize nano-amphiphilic chitosan. The modified chitosan (0.5 – 1.5%) along with PLLA/PDLA (50/50) was melt blended using extrusion followed by injection molding to form the dumbbells of sc nanocomposite. The heat treatment (annealing above 160 ºC) lead to the exclusive formation of sc crsytals with a degree of crystallinity ~40%. Also, cooling the nanocomposite from the melt at 2º/min, increased the crystallinity to ~70% with an exclusive formation of sc crystals. The heat distortion temperature was elevated from 70 ºC (sc-PLA) to 145 ºC for the sc nanocomposite containing 1.5% filler. In another study, the use of nano-amphiphilic chitosan (1 – 3%) into the blends of PLLA/PDLA (1:1) has been demonstrated[97]. The filler was mixed with the equal amounts of PLLA and PDLA and mixed by stirring followed by making films by solution casting. The solvent was allowed to evaporate at room temperature for 24h followed by drying the films under vacuum at 50 ºC for 24h and

annealing them at 120 ºC for 2h. The sc crystallites were formed in the nanocomposites having the crystallinity of ~56%, where the stereocomplexation was higher upon melt cooling as compared to annealing the nanocomposites. The oxygen barrier capacity of the films were evaluated and the nanocomposite films showed ~56% reduction in the oxygen barrier as compared to the blend of PLLA/PDLA film (sc-PLA). Addition of the nanofiller also led to the increased hydrophobicity of the nanocomposite which is attributed to the increased surface roughness as well as crystallinity. The viability of the fibroblast cells (BHK-21) on the surface of the nanocomposites have been determined manifesting the biocompatible behaviour of the developed materials.

The biocomposites of sc-PLA were prepared by employing cellulose microcrystals (CMC) as a filler (1 – 10%). The ROP technique was used to develop PDLA grafted CMC which was mixed with PLLA in 50/50 ratio and melt extruded followed by injection molding to prepare the biocomposite specimens. The improved dispersion of CMC led to the formation of sc crystallites and suppressing the hc formation. The sc-PLA biocomposites resulted in significant improvement of the tensile strength (~96%) as compared to sc-PLA along with high value of storage modulus (~3500 Pa). The enhanced sc formation and incorporation of CMC reduced the permeability of oxygen as well as water vapor suggesting its use in engineering and packaging applications [30].

The use of nano-hydroxyapatite (n-HAP) has witnessed an enormous attention in the biomedical field as it remains to be the reinforcement form of the natural bone. In order to exploit the use of sc-PLA and n-HAP for biomedical applications, the biocomposites were prepared by Gupta et al., where n-HAP was grafted to PDLA via in situ ROP where the OH groups on n-HAP acted as initiating species. The grafting was confirmed by ^{13}C-NMR and thermogravimetric analysis [37]. The grafted PDLA was blended with PLLA to develop

sc biocomposites which gave the exclusive formation of sc crystallites due to improved dispersion of n-HAP and extended molecular surface area provided by the PDLA chains. The nanocomposites with improved mechanical properties were obtained (~40 MPa strength, ~132% elongation at break and ~47% storage modulus). An improved degree of crystallinity was achieved which resulted in the hindered diffusion of water vapour thereby improving the resistance to moisture. The viability of BHK-21 cells on the nanocomposite materials revealed their applicability as a biomaterial.

It may be perceived that the sc-PLA based copolymers and composites are addressing the concerns of the polymer processing and their applicability for packaging and biomedical domains. The illustration of the application of sc-PLA based copolymers and composites is shown in **Figure 2.5**.

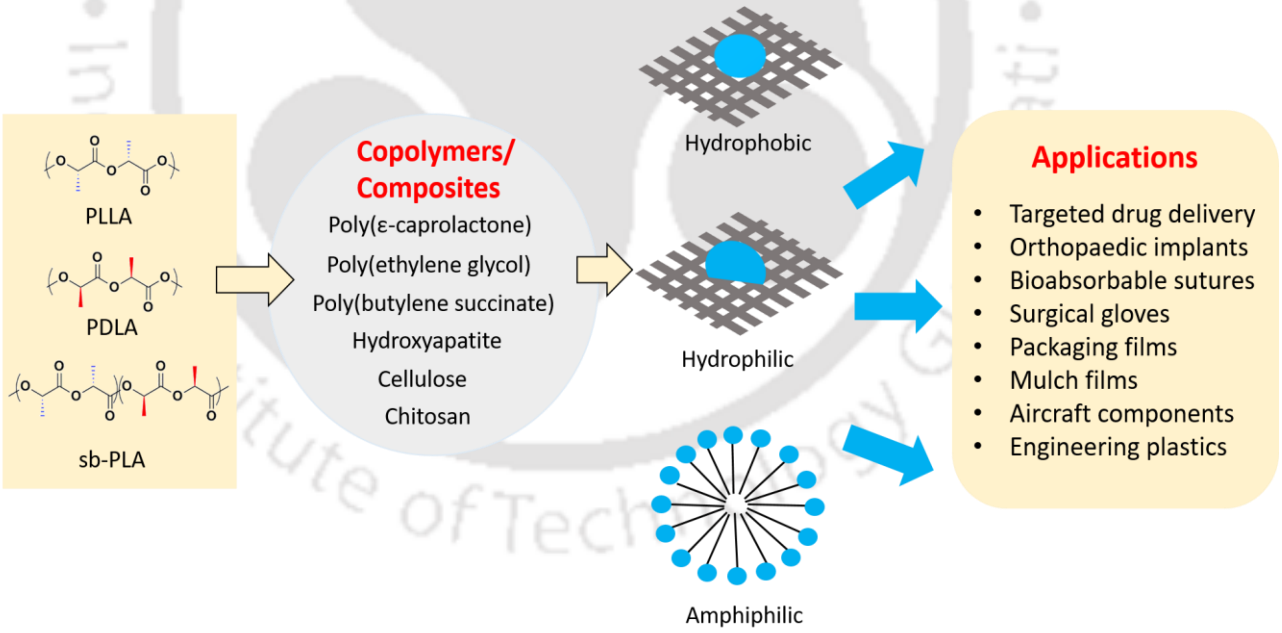

Figure 2.5: Applications of the sc-PLA based copolymers and composites.

2.6 Biomaterials

The conventional methods of repairing the damaged tissues include autografts, allografts, and xenografts which suffer from several drawbacks such as scarcity of donors, disease transmission, low clinical success, etc. Tissue engineering has emerged as one of the promising alternatives for the repair/regeneration of damaged tissues. In order to cure the diseased tissues, various methods have been developed incorporating the use of polymers, ceramics, metals, etc. and the materials thereof are regarded as biomaterials.

Resorbable sutures were made for the first time by American Cyanamide Co. from polyglycolide in 1962 which was commercialized under the trade name "Dexon". A few years later, co-polymer of PLLA (8%) and PGA (92%) [poly(L-lactide-co-glycolide)] was developed as a biodegradable suture with the trade name "Vicryl." Aliphatic polymers were then explored for their potential in various biomedical applications including bone repair and regeneration. These are considered to be versatile polymers with good mechanical properties and biocompatibility when prepared by ring opening polymerization of lactides and lactones. The properties required for the intended application may be significantly different. It is possible to control the physical properties and biodegradability of aliphatic polyesters which are made by ring opening polymerization of lactides and lactones. This can possibly be done by changing the structure and composition of the repeat units, presence of polar groups, crystallinity, molecular mass, orientation and flexibility of the chain. It is essential for a biomaterial to have biochemical as well as biomechanical compatibility. For an implant to replace the bone, it must have physical and mechanical properties that would match with the host

tissue. Stress shielding of the bone is due to the high Young's modulus of the implant which carries all the load and leads to the failure of the implant.

The first generation biomaterials were intended to be bio-inert in order to minimize the formation of scar tissue. Bioactive glasses emerged as the second generation materials providing interfacial bonding between the implant and the host tissue. The third generation of biomaterials involved tissue regeneration and repair combining the resorbable and bioactive characteristics such as the bioactive glasses with gene activation properties[98]. The revolution in biomaterials from tissue replacement to tissue regeneration is shown in **Figure 2.6**. Bioactive glasses gained enormous attention in the field of tissue engineering due to its extraordinary characteristics such as bioactivity, biocompatibility, osteoconductivity, and biodegradability. The remarkable discovery of bioactive glass by Prof. Larry Hench was made in 1969 (University of Florida, USA). The glass composition of 45% SiO_2, 24.5% CaO, 24.5% Na_2O and 6% P_2O_5 was found to be close to a ternary eutectic which was melted, cast and tested as an implant in rats and the implants were found to be bonded with the bone. The *in vitro* and *in vivo* tests resulted in the formation of hydroxyapatite (HA) layer which was bonded to the collagen. A strong bonding between the collagen and HA was observed and thus was the most fascinating material discovered which was recognized as 45S5 Bioglass® [99]. Since its discovery, it has been widely used by the researchers for testing its widespread applications.

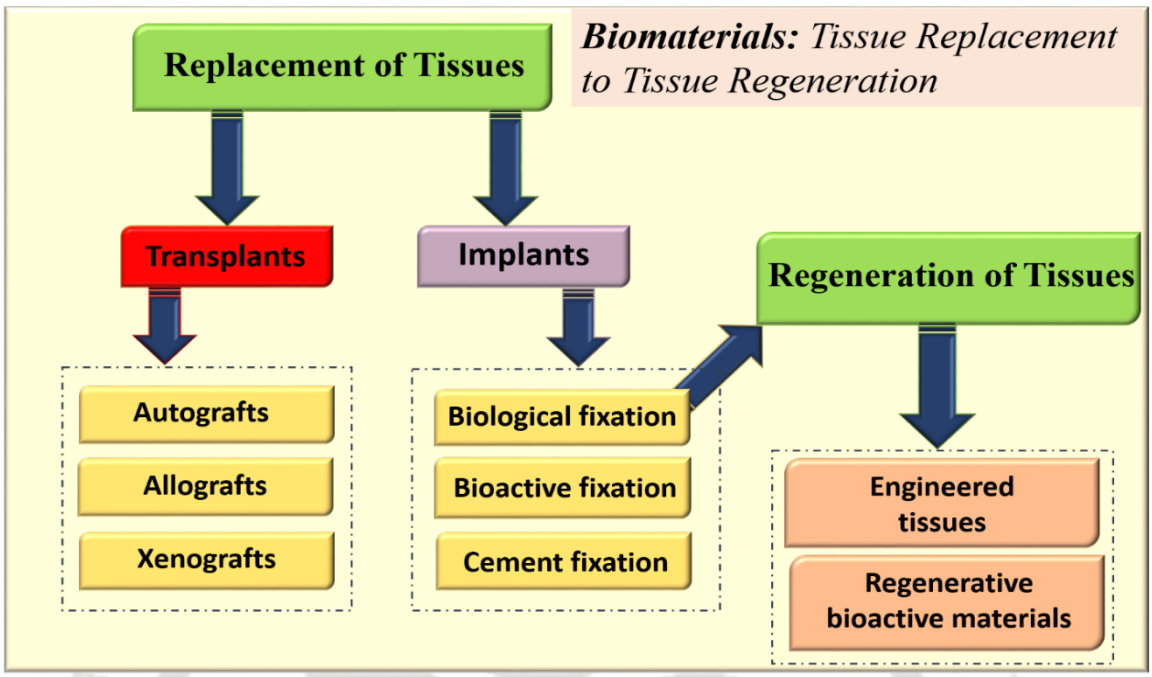

Figure 2.6: Revolution in biomaterials: Tissue replacement to tissue regeneration.

2.7 Bioactive glass

One of the most important criterion for the biomaterials to serve as an ideal scaffold material is to mimic the extracellular matrix (ECM) onto which the cells would adhere, multiply, and function. The ability of a biomaterial to form a bond with the living tissues is termed as "bioactivity." The major compositional characteristics of bioactive glasses that distinguish it from the traditional soda-lime glasses are: a) SiO_2 content less than 60 mole percent, b) high CaO and Na_2O content, and c) higher ratio of $CaO:P_2O_5$[100]. Bioactive glasses suffer from several disadvantages such as their brittle and stiff nature which restricts them to be molded into complex shapes and often leads to the fracture under mechanical loads. Additionally, trauma and infections also lead to the critical size bone defects and their treatment using conventional methods is often encountered by immune rejection, high cost, limited availability, scar tissue formation, painful secondary

surgeries, little or no integration with the host tissue, etc. Bioactive glass, on the other hand, being bioactive in nature is considered to be the most suitable alternative to allografts with a great potential in orthopedic applications. Bioactive glass undergoes dissolution inducing an apatite layer which is similar to that of natural bone thereby stimulating osteogenesis and angiogenesis which in turn allow the interfacial bonding between the bone and the implant leading to osteointegration. However, it is essential for the implant to mimic the structure of the bone in order to promote the regeneration of the bone. Bioactive glass has the ability to bind to both bone as well as soft tissues, however, it has been mainly studied in orthopedic applications as it promotes the formation of bone like apatite layer. Bioactive glass has been reported for the adhesion and proliferation of osteoblast cells like MC3T3-E1 and MLO-A5. Furthermore, the bioglass undergoes dissolution creating ions such as Si, P, Ca, Cu which are involved in enhancing the proliferation of osteoblast cells and in turn formation of bone[101]. The bioactive behavior of HA may be increased on adding Si during its synthesis. In case of bioactive glass, the silanol groups work as catalysts leading to the nucleation of apatite phase in order to form apatite layers on the surface. The mechanism of bone formation in shown in **Figure 2.7**.

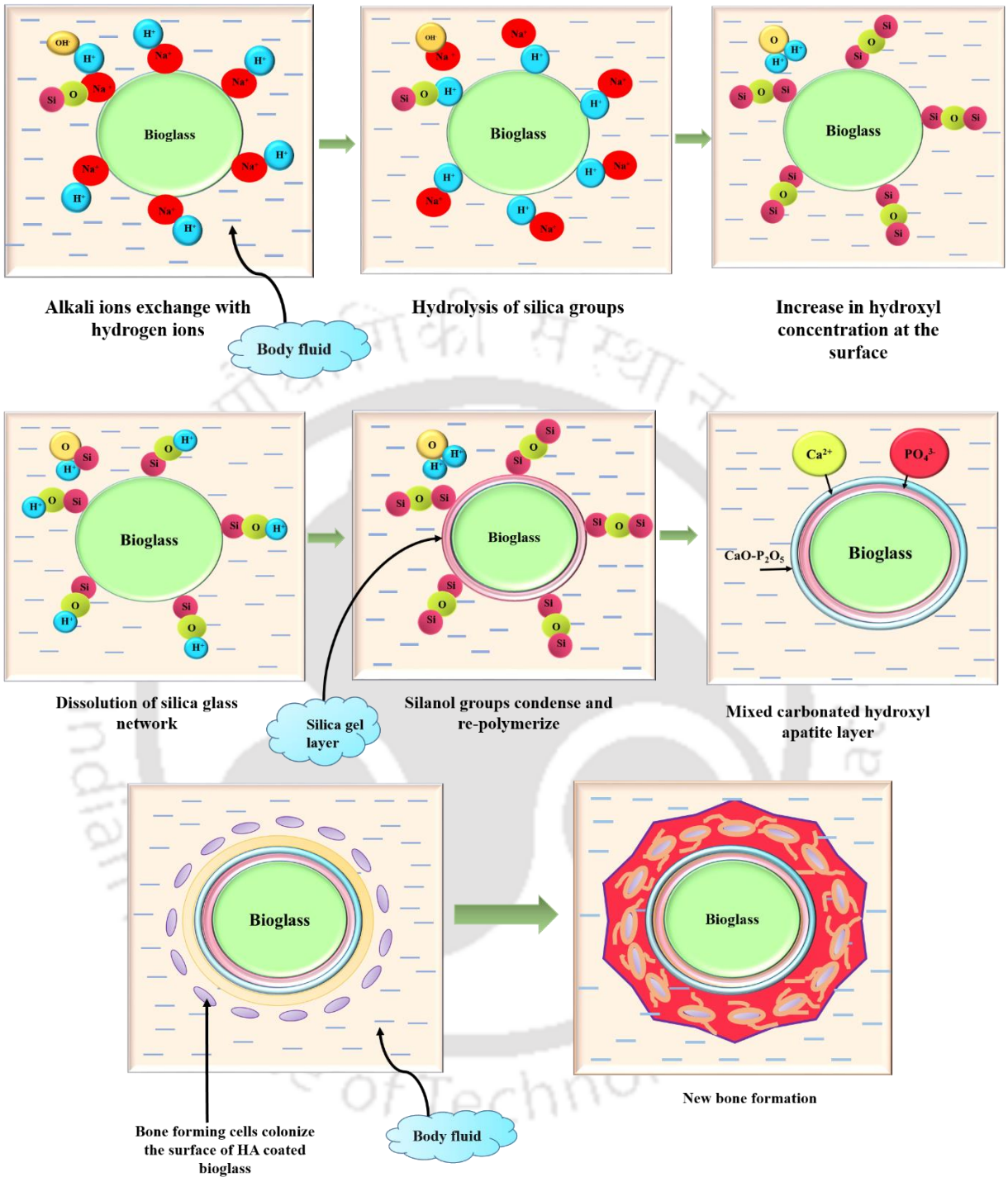

Figure 2.7: Mechanism of integration of bioglass with the bone.

2.7.1 Types of Bioactive Glasses

Various types of bioactive glasses can be fabricated for different applications which have varied composition. The parameters affecting the rate of dissolution of bioactive glasses and their ability to form apatite layer are:

1. Composition of bioactive glasses
2. Morphology
3. Technique used to fabricate the glass

It may be imperative to choose the bioactive glasses based on the ability of apatite formation which is highly dependent on the above stated parameters. The commercially available bioactive glasses with their composition are shown in **Table 2.5**. The patients (over 1 million) have been implanted with NovaBone^{TM} which is known for its use as an osseous defect filler and the capability of inducing new bone formation.

Table 2.5: Commercially available bioactive glasses with their composition.

Bioactive glasses (commercial)	**Composition**								**Origin**
	SiO_2	**Na_2O**	**CaO**	**P_2O_5**	**SrO**	**MgO**	**CaF_2**	**K_2O**	
NovaBone	46.1	24.4	26.9	2.6	-	-	-	-	Novabone LLC, Jacksonville, Florida
BonAlive	53.8	22.7	21.9	1.7	-	-	-	-	Turku, Finland
Cerabone	34.0	-	44.7	16.2	-	4.6	0.5	-	Straumann group, Switzerland
45S5	46.1	24.4	26.9	2.6	-	-	-	-	Mo-Sci, Rolla, Missouri
13-93	54.6	6.0	22.1	1.7	-	-	-	-	Mo-Sci, Rolla, Missouri
StonBone	44.5	27.2	21.5	4.4	2.4	7.7	-	7.9	RepRegen Ltd, London, UK

It is essential for the implants to form an interfacial bond with the living tissue in order to function as an ideal material for bone repair/growth. Hench and Ethridge expressed the criterion for biomaterials for bone fixing which described the materials to be equivalent to the host tissue being able to form a stable interfacial bond between the host tissue and itself and its ability to respond to the external stimuli (physical) in the same manner as that of the host tissue. Additionally, the mechanical and physical properties of biomaterials are of prime importance apart from its bioactivity. For bone repair and regeneration, the major problem often accounted is that of stress shielding which is mainly due to the higher Young's modulus of the implant carrying all its load (or) leading to the improper distribution of load. Thus, it is important to design materials that would bind with the natural tissues and withstand the mechanical loads when implanted into the body.

2.7.2 Biomedical applications

Bioactive Glass Hybrids

While fabricating materials for bone tissue engineering applications, it is important to design the scaffolds that are biodegradable and their rate of degradation is similar to the rate of new bone where the newly formed bone would eventually replace the scaffold. The mechanical integrity of the scaffold must be sufficient to support the bone regeneration process. However, it is difficult to combine all these properties in a single material and therefore the composites are often considered to be advantageous while fabricating scaffolds. The conventional composite materials consist of phases that are distinct at macroscale, thus are not suitable as scaffold materials that require the homogenous phases at molecular level along with uniform mechanical, physical,

chemical, and biological properties. In line to this, Mondal et al.[102] demonstrated the possibility of using hybrid biomaterials consisting of organic and inorganic components for bone tissue engineering applications due to the molecular level interactions among them leading to the formation of single-phase materials. They prepared class II hybrid biomaterials consisting of tertiary bioactive glasses as inorganic phase covalently crosslinked to organic polymers. Firstly, they synthesized the copolymers of vinylpyrrolidone and triethoxysilane in varying molar ratios so as to vary the amount of silane groups in the copolymer. Thereafter, tertiary bioglass was mixed with the copolymer in order to allow for hydrolysis and polycondensation leading to the formation of Si-O-Si and Si-O-P networks between the two phases. They found that the covalent bonding between copolymer and bioglass was increased with the increasing number of functional groups whereas the degradation was decreased along with the decrease in the dissolution products of bioglass. Incorporation in SBF led to the formation of apatite layer of the surface of materials which was found to be dependent on the weight ratios of organic and inorganic materials. Further, they reported that the increased content of bioglass led to the improved deposition of apatite layer along with the improved biocompatibility of the fabricated hybrid materials. Furthermore, Allo et al.[103] chose the combination of biodegradable polymers i.e. poly(ε-caprolactone) (PCL) and bioactive glasses in order to make hybrid biomaterials with the aim of tailoring the physical, mechanical, biological and degradation behavior of the resulting materials. The combination of inorganic and organic materials in different ratios were synthesized using the sol-gel process. In a typical sol-gel process, the hydroxyl groups are formed by the hydrolysis of metal alkoxides which is followed by the formation of a three-dimensional network due to the polycondensation reaction. The stiffness and the brittleness of

bioactive glasses restrict their formation into the complex shapes and promote their fracture under loads. On the other hand, the flexibility of PCL along with its biodegradable and biocompatible nature allows its easy processing into complex three-dimensional structures. The properties of the two materials being complementary to each other were speculated to be favorable in developing materials with desired toughness, biocompatibility, bioactivity, and predictable degradation and thus were explored for their potential as three-dimensional scaffolds for bone regeneration which were fabricated by electrospinning. The polymer chains (dissolved in “methyl ethyl ketone" which is water miscible and has the ability to dissolve inorganic materials) were introduced into the sol during the formation of inorganic network in order to allow for the chemical interactions between the polymer chains and bioactive glass in order to form homogenous hybrid materials. The intermolecular interaction between the organic polymer chains and the inorganic bioactive glass was determined by FTIR which confirmed the molecular interaction of the two phases by H bonding between the silanol hydroxyl groups of glass and the carbonyl group of PCL. The developed hybrids were found to have immense potential in bone tissue engineering applications.

Large Bone Defects

Although tissue engineering has made its impact in treating the several bone related diseases and disorders, the treatment of large bone disorders is still a challenge for the clinicians. The major causes of such disorders could be trauma, infections, accidents, tumors, etc. and the major issues often witnessed in their treatment are accelerating the bone formation as well the bone healing. Furthermore, it is important to track the degradation products from the scaffolds that would possibly accumulate in the tissues and

organs in order to identify the degradation mechanism of the biomaterials. In this context, Wu et al.[104] developed biofunctional materials for biolabeling by incorporating Europium (Eu) into the bioactive glass scaffolds (*in situ*) using polyurethane sponge co-templates. Eu is also known for its ability to bind with HA [105] along with pro-angiogenic properties[106, 107]. The scaffolds thus fabricated were found to have luminescence property that allowed the labelling of bone marrow stromal cells (BMSCs) *in vitro* as the degradation of scaffolds occurred by releasing the ionic products which influenced the luminescence change of the scaffolds. Further, *in vivo* studies were conducted by using the ovariectomized rat models (OVX) for the reconstruction of the femoral defects and inducing bone defects (3.5 mm dia) in the distal region of femur. The bone defects were filled randomly with MBG along with Eu-inocrporated MBG (2 and 5 mol %) and the rats were sacrificed after 4 and 8 weeks and observed under Micro-CT and evaluated for histological analysis. The bone formation was seen to be higher along with higher amount of bone formation area for the bioactive glasses with Eu content as compared to MBG alone. Thus, the scaffolds with Eu showed the improved bone formation by promoting the osteogenic differentiation of BMSCs suggesting their potential for biolabeling and regeneration of bone.

Osteosarcoma Treatment

Osteosarcoma is a type of bone cancer that leads to the formation of immature bone and has affected a large number of people. The treatment methods such as radiation or chemotherapy are ineffective in curing the disease and it is often difficult for the patients to survive. With the aim of developing safe and effective biomaterials for the clinical cure of osteosarcoma, Rana et al. [108] developed gallium doped bioactive glasses. Gallium,

which is known for its effective use against cancer[109, 110] was doped during the melt-quench process in different ratios followed by producing glass rods which were cut into discs. The synthesized materials were characterized to identify their structure, morphology, biocompatibility, and formation of apatite layer. The human osteosarcoma cells (Saos-2) were used to determine the viability of the cells in the glasses in presence and absence of gallium. It was observed that the viability of the tumor (osteosarcoma) cells was reduced to ~50% in presence of gallium containing bioactive glasses which was further dependent on the dosage. Additionally, no adverse effects were observed on the cell growth in case of normal human osteoblast cells. The HA formation was observed for all the glasses (those containing gallium and control). Furthermore, the glasses doped with gallium preferentially led to the localized delivery of gallium ions at the targeted site and thus has a substantial potential in the treatment of the bone cancer.

2.8 Carbon Dioxide: Potential Precursor in Organic Synthesis

Carbon dioxide is a greenhouse gas which is available in abundant amount in the atmosphere. The average lifetime of CO_2 molecule may be considered to be of the order of 10 years before it is dissolved into the oceans[111]. CO_2 is not only available in the large amount in the atmosphere but is also regenerative in nature as it gets integrated with the natural cycle. The constant rise in the CO_2 levels have led the researchers to focus towards the mitigation[112] or finding alternate uses of this greenhouse gas in order to reduce the global environmental impact[113-116]. In order to reduce the greenhouse gas from further accumulating in environment, the strategy of capturing of CO_2 has been adopted by several researchers. However, converting CO_2 into useful end products is preferred over storing it because of its non-toxic, renewable and inexpensive nature[117-121]. One such

possibility is exploring its potential in developing monomers/precursors which would be utilized for the synthesis of polymers[122, 123]. Conventional polymers are usually derived from petroleum based feedstock which is available in limited amount on the planet. At the current rate of consumption of petroleum based feedstock, these resources are predicted to be exhausted by the next century[1-4]. Additionally, burning of fossil fuel leads to the accumulation of CO_2 in the atmosphere at a rate which is significantly higher than its usage by green plants during photosynthesis[5]. Thus, finding the alternatives for the petroleum based resources is the prime concern of the present age[6, 7]. Considering this situation, using CO_2 as a precursor in the synthesis of polymers would not only reduce the human dependence on the fossil fuels but would also reduce the accumulations of the potential greenhouse gas in the atmosphere along with developing polymers from a greener route. This strategy may aid in combating with the ongoing environmental issues. The interesting properties of CO_2 at supercritical conditions i.e. the viscosity and surface tension of CO_2 being comparable to that of gases while its solubility parameter, density and dielectric constant being comparable to that of liquids have witnessed its exploration in replacing the organic solvents[9-11]. However, it is difficult to fix CO_2 in the chemistry of polymerization due to its low reactivity and usually require extreme conditions of temperature and pressure for its reaction. Catalysis is perhaps, one of the best solutions to overcome the thermodynamic stability of the most abundant C1 resource[12-14]. The possible exploitation of CO_2 for the effective synthesis of polycarbonate, polylactone, poly(limonene oxide), etc. have been discussed in the subsequent sections followed by the existing technologies for the commercial production of polymers from CO_2.

2.8.1 Synthesis of polycarbonate

One of the most fascinating discovery is the synthesis of aliphatic polycarbonate by the ring opening copolymerization of CO_2 with epoxides. Epoxides are the cyclic ethers containing a three-atom ring and their high reactivity is accounted for their strained ring structure which is due to the equilateral triangle formed by the ring. It is known that catalyst plays a crucial role in fixing CO_2 in the backbone of polymers. Additionally, the catalyst lays an essential effect on the yield, properties and applications of the polymers that are produced. In view of this, Trott et al. have reported the important findings in the field of catalysis for the ring opening polymerization of CO_2 and epoxide[124]. The copolymerization of CO_2 with epoxide was successfully carried out by Inoue and co-workers in 1969 using organometallic catalysts[125]. They reported the synthesis of high molecular weight polycarbonates by alternating copolymerization of CO_2 with propylene oxide. Polycarbonates have been conventionally manufactured industrially by using bisphenol A (BPA) and phosgene precursors which are known for their harmful (during fetal development)[126] and toxic natures[127], respectively. In the work reported by Inoue et al., various organometallic catalysts were tested for the copolymerization of CO_2 and propylene oxide to yield polypropylene oxide. Among various catalyst systems, diethylzinc/water (1:1) system was found to be the most effective which yielded the methanol insoluble copolymer at 20-50 atm CO_2 pressure and 80 ºC. Owing to its high efficiency, the same catalyst system was chosen for the copolymerization of CO_2 with other epoxides such as ethylene oxide, isobutylene oxide, styrene oxide and epichlorohydrin which were found to be soluble in methylene chloride. Their study led to the development of polypropylene carbonate with high molecular weight ($\overline{Mn}\ (osm.) = 115{,}000$. Although several epoxides have been explored for the reaction with CO_2, not

much focus has been laid on the bioderived epoxides. D-limonene is the cyclic monoterpene which is usually extracted from the orange peel. Limonene oxide is available in abundant amount which is structurally similar to cyclohexene oxide and has low cost. The alternating copolymerization of limonene oxide and CO_2 was reported by Byrne et al. under mild conditions to yield polycarbonates[128]. The copolymerization was carried out using β-diiminate zinc acetate as catalyst. They observed that the catalyst led to the formation of *regioregular* polycarbonate with high selectivity of trans isomer at 25 °C and 100 psi pressure of CO_2. The resulting copolymer was found to have a narrow molecular weight distribution with >99% carbon linkage. Furthermore, Kindermann et al. reported the reaction of limonene oxide with CO_2 in presence of Al(III) complex catalyst to develop poly(limonene) dicarbonate[129]. They mixed limonene oxide (cis/trans mixture), bis-triphenylphosphine iminium chloride (PPNCl) and catalyst were mixed and placed inside the stainless steel reactor followed by purging with CO_2 thrice. The reactor pressure was increased to 15 bar with temperature 45 °C and the reaction was carried out for 48h. The resulting material was poly (limonene carbonate) which was dissolved in dichloromethane and oxidized at 0 °C using 3-chlorperbenzoic acid for 12h to form poly(limonene-8,9-oxide carbonate) (**Figure 2.8**). The developed polycarbonates find applications as precursors for the coating materials and formation of polymer blends with tailored properties.

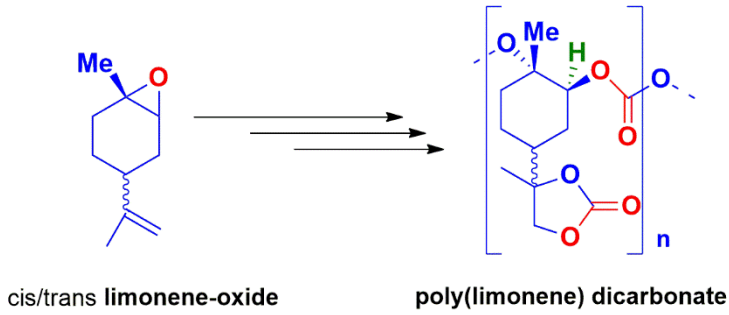

Figure 2.8: Limonene oxide to poly(limonene) dicarbonate.

2.8.2 Synthesis of polyalkanoates

Copolymerization of CO_2 with alkynes involves the carbon-carbon triple bonds as the building blocks for the reaction. This is a unique technique developed to yield poly(alkanoate)s with high weight average molecular weight (Mw ~31,400). The reaction of CO_2 with alkyl dihalides and diynes in presence of Ag_2WO_4 catalyst, Cs_2CO_3 additive along with N,N-dimethylacetamide (**Figure 2.9**) was reported by Song et al. which resulted in poly(alkanoate)s with high yields (~95%) possessing superior thermal and chemical stability [130]. The reactions were conducted at very mild conditions (80 ºC, 12h). Such efficient and robust reaction resulting in high yield of the final product may be considered as industrially viable process. Furthermore, the reaction of CO_2 with alkyl dihalide and triphenylamine (TPA) containing diyne led to the formation of telechelic polymer via step growth polymerization. The synthesized telechelic polymer can be used for the synthesis of high molecular weight functional polymers by continuously adding alkyl dihalide in presence of catalyst and CO_2. The direct conversion of CO_2 into useful end products such as poly(alkanoate)s reports the potential of the greenhouse gas in useful chemical reactions under mild conditions. The synthesized poly(alkanoate)s may be considered as polyesters due to their structure and may be hydrolyzed under alkaline

environment at ambient conditions in few minutes which makes them as promising materials for biomedical as well as engineering applications. In this regard, utilization of CO_2 for the development of end product that is biodegradable lays a significant impact and may be a solution to the current environmental issues.

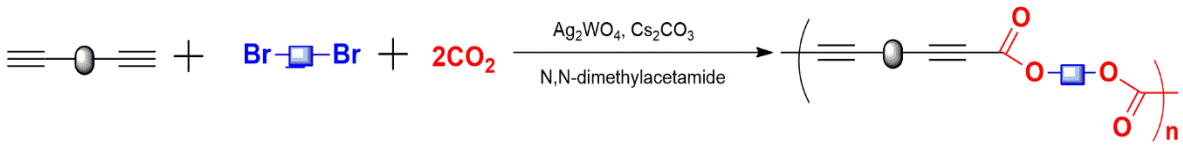

Figure 2.9: Reaction of diene, alkyl halide and CO_2 to form polyalkanoate.

2.8.3 Synthesis of lactone

The copolymerization of CO_2 with olefins has been a subject of broad interest, however, it is restricted by the propagation step which is endothermic; and on several occasions homopolymerization of olefin takes place due to the reaction failure. In this regard, Nakano et al. have adopted a unique strategy to overcome the barriers associated in the reaction by using a lactone intermediate. The copolymerization of CO_2 with 1,3-butadiene led to the formation of 3-ethylidene-6-vinyltetrahydro-2H-pyran-2-one (lactone) which was followed by the homopolymerization of lactone [131] as shown in **Figure 2.10**. The synthesized copolymers consisted of 33 mol% CO_2 which was consistent with the theoretical values. Furthermore, they extended their research to develop one-pot copolymerization process of CO_2 and butadiene along with one-pot terpolymerization process which was considered to be a sustainable and scalable process. They had used a mixture of dienes such as butadiene, isoprene and 1,3-pentadiene by varying their molar ratios and reacted with CO_2 in presence of palladium acetylactenoate, triisopropylphosphine and ethylene carbonate at 80 ºC. The reaction time was varied from

3 to 20 hours for the mixture of dienes. Furthermore, the synthesized lactones were subjected to polymerization in presence of 1-1′-azobis(cyclohexane-1-carbonitrile) and zinc chloride which resulted in the formation of terpolymers i.e. (CO_2/butadiene/isorprene and CO_2/butadiene/1,3-pentadiene) with molecular weights (Mn) 5,500 and 16,000 and yields of 46% and 35% respectively. Additionally, the glass transition temperature of these polymers was found to be 63 ºC and 33 ºC respectively. The authors concluded their process had the potential to be utilized on a large scale in order to synthesize the synthetic polymers via a green and sustainable route.

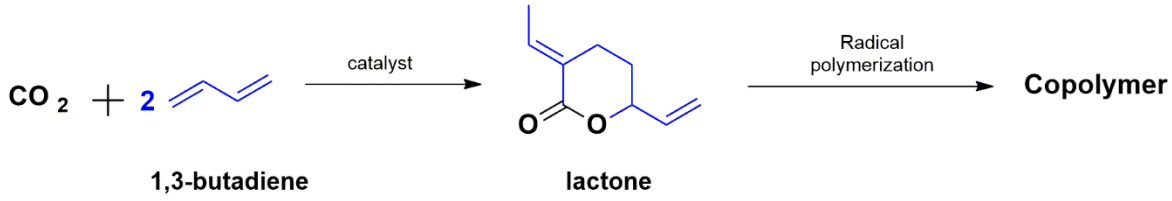

Figure 2.10: Lactone from CO_2 and 1,3-butadiene and its subsequent polymerization.

2.8.4 Existing technologies for making polymers from CO_2

Novomer Inc. (USA) founded by Geoffrey Coates (Cornell University graduate) has initiated the production of polyols (copolymers resulting from epoxides and CO_2) which have the applications in light-weight polyurethane foams. The Novomer technology may also be adopted by Ford Motor Co. to use polyols in the cushions of the automobile seats. This will indeed lay a great impact on the society[132]. Also, the industrial production of poly(propylene carbonate) has been witnessed in China which aims at producing poly(propylene carbonate) (average mol wt. of tens of thousands) by using diethylzinc-glycerol system ($Nd(CCl_3COO)_3$)[133]. Norner™, a Norway based company has also actively been involved in the development of CO_2 based polycarbonates. It has been able to design a continuous process for the production of polycarbonates and is aiming towards

developing pilot scale process and commercialization of the product [134]. Researchers from Rutgers University have established a start-up "RENEWCO_2" which is the outcome of the project carried out under Prof. Charles Dismukes. They have developed an electrochemical method to convert CO_2 and water into polymers using the nickel and phosphorous based catalysts [135]. A German based company "Covestro" headed by Markus Steilemann has developed the CO_2 based polyols which are used to make the synthetic sports flooring. They have made a novel CO_2-based binder for sports flooring which has been installed at the Crefelder Hockey and Tennis Club which is one of the leading hockey facilities in Germany. These CO_2 based materials are replacing ~20% of fossil fuels that are required for the production of polymers.

2.9 Research Gap

It is observed from the literature that the biodegradable aliphatic polyesters such as PLA, PGA, etc. have witnessed enormous attention in the developing biomedical implants. However, the homopolymers or copolymers of these often lead to the development of a brittle material with a higher tensile modulus leading to the implant failure. The biological tissues such as bones, tendons, cartilage, skin, etc. are flexible or elastic and thus require toughened materials in order to replace them into the body. In this regard, several attempts have been made by incorporating soft materials such as PCL in order to evoke toughness into the brittle polymers. However, the content of soft and hard segments play an essential role in determining the properties of the developed copolymers and it is therefore essential to develop an understanding regarding the same. The literature reports the copolymerization strategies to develop random and multiblock copolymers of PLA and PCL, however little attention has been paid on the content of PLA and PCL in the

copolymer system. Furthermore, it lacks the essence of stereocomplexation in the block copolymers or developing their composites by choosing the appropriate reinforcing materials/fillers. Additionally, scaling up the polymerization process and processing of the biodegradable copolymers by conventional techniques, is the need of the hour. Therefore, attempts have been made in this work to overcome the existing research gap and develop the biodegradable copolymers/composites which can be scaled-up and processed by the existing techniques. Furthermore, insights have been made on the structure-property relationship of block copolymers by relating to their nanostructure.

Since the current work reports the development of environmentally benign lactone based polymers, an attempt has also been made to develop new polymers from the environmentally benign routes. The literature reports the use of greenhouse gas carbon dioxide in developing a six-membered cyclic monomer (δ-lactone) which has been used by the researchers for free-radical polymerization. Herein, we report the novel strategies of polymerizing the carbon dioxide derived monomer using metathesis and cationic polymerization strategies, and challenges associated with it.

2.10 Objectives

In order to overcome the above mentioned research gaps, the objectives of the current thesis are as follows:

1. Synthesis of linear diblock copolymers based on PLA and PCL and their stereocomplex blends by changing the block length of PLA segment.
    a. Determining the processability of the diblock copolymers to develop implants
    b. Determining the thermomechanical stability of the implants

2. Varying the molecular architecture to synthesize linear triblock copolymers based on PLA and PCL to develop toughened materials.
    a. Scaling-up the synthesis process to a batch of 500 g and processing it to develop 3D printed scaffold.
    b. Proposing a structure model for gaining insights into the mechanical properties.
3. Developing stereo-pentablock copolymers of PLA and PCL and providing insights into the preferential stereocomplexation.
4. Random copolymerization of lactide and caprolactone by varying the content of lactyl and caproyl segments
    a. Synthesis of random copolymers by single step ring opening polymerization
    b. Scaling up the synthesis process to the batch of 100 g
5. Further, developing composites of random copolymers by incorporating bioactive glass as a filler and evaluation of its properties.
6. Strategies to polymerize the metastable carbon dioxide derived monomer (δ-lactone) by novel strategies to explore a new class of materials.
    a. Metathesis polymerization strategy
    b. Cationic pathway

Chapter: 3

Diblock Copolymers based on PLA and PCL, and their Stereocomplex Blends

Graphical Abstract

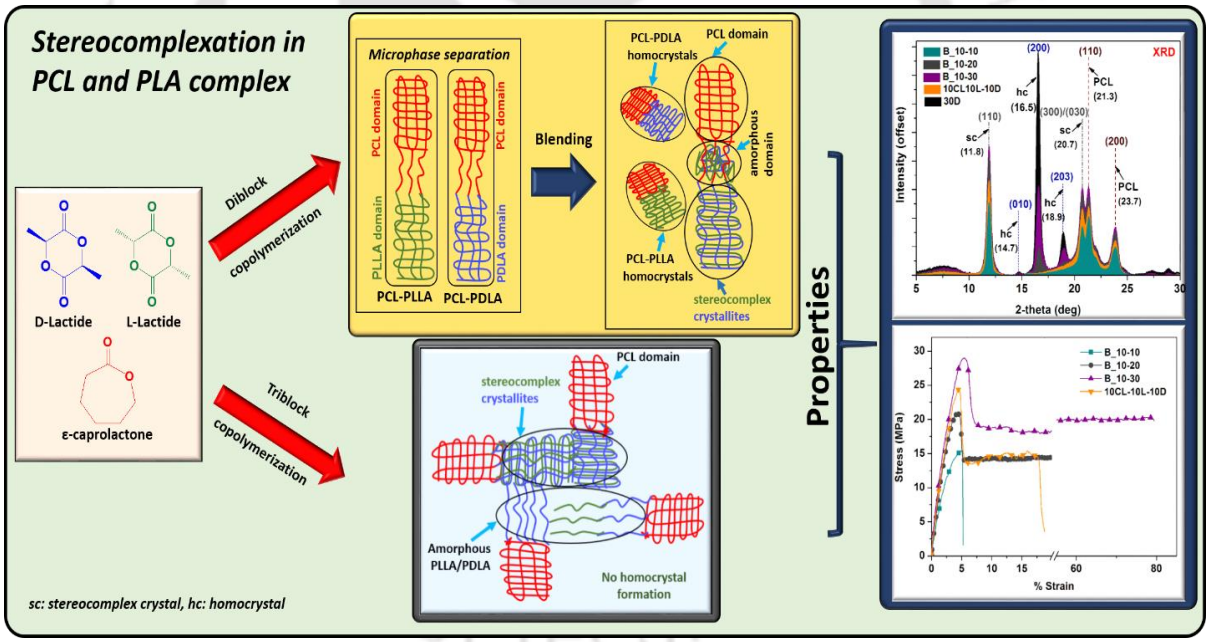

Outcome:

- *Effect of Block Length and Stereocomplexation on the Thermally Processable Poly (ε-caprolactone) and Poly (Lactic acid) Block Copolymers for Biomedical Applications. ACS Applied Polymer Materials 1.12 (2019): 3354-3365.*

Abstract

The current chapter concentrates on the synthesis of linear block copolymers with their backbone consisting of hard and soft segments i.e. poly(L-lactic acid) (PLLA)/ poly(D-lactic acid) (PDLA) and poly(ε-caprolactone) (PCL) with the detailed investigation of the effect of block length on the thermal, mechanical and crystallization behavior followed by their processing and biocompatibility evaluation. Here, the sequential ring opening polymerization has been employed wherein PCL is used as a macro-initiator for the synthesis of diblock (PCL-PDLA and PCL-PLLA) and stereo-triblock copolymer (PCL-PLLA-PDLA) of targeted molecular weight, which is confirmed by ^{1}H-NMR spectroscopy. The block length of PCL, in case of diblock copolymer, is fixed whereas that of PLLA/PDLA is varied and the enantiomeric blends thereof are made to achieve the merits of stereocomplexation. The length of the individual blocks is same in case of stereo-triblock copolymer. The presence of two crystalline domains is manifested from differential scanning calorimetry and thermogravimetric analysis. An interesting "strain induced plastic to rubber transition" phenomena is observed upon increasing the block length of PDLA/PLLA in the block copolymer system which accounts for the improved overall mechanical properties. Additionally, the synthesized materials are found to support the adhesion of MG-63 cells as determined from in vitro studies indicating their potential in bone repair and regeneration. Further, the block copolymers possessing superior mechanical properties are thermally processed by injection molding to fabricate representative orthopedic fixation devices such as cancellous and cortical bone screws. Eventually, the thermo-mechanical stability of the cancellous bone screw made from the synthesized block copolymer is presented as compared to that made from the commercial PLA at the sterilization temperature of the biomedical devices.

3.1 Introduction

Block copolymerization of aliphatic polyesters has widely been studied in order to obtain the materials with tailored properties[136,137]. Poly(lactic acid) (PLA) and poly(ε-caprolactone) (PCL) are the biodegradable aliphatic polyesters with complementary properties and found to have substantial potential in biomedical applications[138]. PLA is a biobased and bioabsorbable material and has a potential to replace the conventional petroleum derived polymers owing to its superior mechanical strength, transparency and processability[139]. However, the inherent brittle nature[140] (T_g ~ 60 °C) and inferior thermal resistance[79] of PLA often limit its use in several engineering and biomedical applications. PCL on the other hand is flexible in nature thereby possessing inherent toughness[141]. Further, it has ever been used in the Food and Drug Administration (FDA) approved biomedical devices[142,143]. However, the melting temperature of PCL is very low (~ 60º C) along with very low glass transition temperature (~ -60º C) which has limited its use in various engineering applications. Furthermore, stereocomplexation, which is a special crystal form between the enantiomeric PLA chains, is known to improve the thermal resistance of PLA materials. Due to the increased chain packing leading to the improved crystalline density, the melting temperature (T_m) of the stereocomplex crystallites is enhanced to ~230 ºC which is ~50 ºC uplifted as compared to that of pure enantiomeric PLA.[30] The preferential stereocomplexation is observed in case of stereoblock PLA copolymers (sb-PLA) where the enantiomeric polymer chains interact at the molecular level to enhance the formation of stereocomplex crystallites.[85]

In order to develop materials with customized properties, PCL and PLA are often used in combination. Various approaches have been made to combine PCL and PLA including

blending[144], copolymerization[145], formation of biocomposite[146], etc. However, due to the immiscibility of PCL and PLA, blending the two polymers often leads to the phase separation and inhomogeneity.[147] Consequently, in the polymer blending of PCL and PLA, several compatibilizers have been used to improve the compatibility of these polymers.[148] In line to this, Shuai et al. synthesized diblock copolymers of PCL and PLLA (PLLA) where they formed host-guest complex with α-cyclodextrin (CD) molecules in water. By elevating the temperature of the aqueous dispersion, the PCL-PLLA chains were decoupled from CD and then precipitated in water. This method led to the formation of single phase of PCL-PLLA without microphase separation because of quick formation of precipitates similar to the freeze-drying method.[149] However, this method may not be an industrially viable process because of many complicated steps. The copolymers of PCL and PLA are semi-crystalline in nature, and therefore crystallinity plays a key role to ascertain their structure and properties. Further, the composition of copolymers, block length, and overall molecular weight are also important parameters in tailoring their properties.

Block copolymerization may significantly enhance the properties of the resulting material by taking into account the advantages of both the individual monomer segments along with retarding macro-phase separation. In this regard, the block copolymerization of PCL and PLA would lead to the development of materials with enhanced thermal stability and high toughness. Until now several methods have been adopted by various researchers for synthesizing block copolymers based on PCL and PLA. Liu et al. synthesized novel aluminum complex based catalysts and tested them for ring opening polymerization (ROP) of L-lactide and ε-caprolactone using 2-propanol as an initiator where the reaction time taken for the maximum conversion of L-lactide was 4 h.[150] In contrary to this, the

FDA (Food and Drug Administration) approved tin octoate catalyst[151,152] takes much shorter time for the maximum conversion of lactide and ε-caprolactone monomers during their ROP along with having an ability to yield polymers with high molecular weight. Wei et al. have reported the synthesis of PCL-PLLA block copolymers by melt or solution sequential copolymerization technique using dibutyl magnesium as initiator. The reaction time for the synthesis was 24 h along with relatively lower molecular weights of the individual blocks (~5 kDa) as determined from ^{1}H-NMR.[153] The earlier reports based on PCL and PLA block/random copolymers and their blends mainly focus on the synthesis, thermal and mechanical properties along with their biodegradability. These studies have reported relatively long reaction time required for the synthesis of block copolymers[154,155] or the formation of block copolymers with lower molecular weight in some cases and requirement of suitable solvent for the polymerization. Furthermore, the thermal processability of the biodegradable block copolymers using conventional processing technique is often restricted by their molecular weight, or requires the incorporation of flow rate enhancing components[156] or thermal stabilizers[157]. The block copolymers possessing stereocomplexation may lead to the development of materials with improved thermal and thermomechanical properties, which may be achieved either by blending the enantiomeric block copolymers or developing stereo-block copolymers.

Considering the advantages and limitations of PCL and PLA along with the merits of stereocomplexation, the current work reports the synthesis of linear block copolymers which are directly thermally processable. The enantiomeric block copolymers have been synthesized in such a way that the chain length of PCL is fixed and that of PLLA/PDLA is varied and the blends thereof are made to obtain stereocomplexation. The influence of block length on the thermal, mechanical and crystallization properties of the block

copolymers and their blends have been addressed. Additionally, a stereo-triblock copolymer is synthesized to compare with the properties of enantiomeric blends. Among various synthesized materials, the block copolymer possessing superior mechanical and thermomechanical properties is chosen for direct thermal processing using an injection molding machine so as to fabricate representative three-dimensional articles such as cancellous and cortical bone screws which may be regarded as resorabable orthopedic fixation devices. The thermo-mechanical stability of the cancellous screw made from the enantiomeric diblock copolymer is compared with that of commercial PLA at 121 °C, which is usually the sterilization temperature of the biomedical devices[158]. Eventually, the *in vitro* biocompatibility studies have been conducted using MG-63 cells to ascertain the adhesion of cells on the surface of the synthesized materials.

3.2 Experimental section

3.2.1 Materials

D- and L- Lactides (99% optical purities) were obtained from Musashino Chemical Laboratories Ltd., Tokyo, Japan. ε-Caprolactone was procured from Nacalai Tesque, Kyoto, Japan, and stored under N_2 atmosphere after distillation. 1-Octadecanol (1-Oct) was supplied by Wako Pure Chemical Industries Ltd., Tokyo, Japan. Tin octoate ($Sn(Oct)_2$, 95%) was acquired from Sigma Aldrich, St. Louis, USA, via Nacalai Tesque and used after distillation under high vacuum. The distilled $Sn(Oct)_2$ was dissolved in dried toluene (0.1 g/ml and 0.2 g/ml) prior to its use. Dichloromethane and methanol were supplied by Nacalai Tesque and used without further purification. 1,1,1,3,3,3-Hexafluoro-2-propanol (HFIP) was obtained from Central Glass Co. Ltd., Yamaguchi, Japan.

3.2.2 Synthesis of PCL

As shown in **Scheme 3.1 (a),** a mono-hydroxyl terminated PCL was obtained by the first-step ROP of ε-caprolactone using 1-Oct as an initiator and $Sn(Oct)_2$ as a catalyst. 1-Oct (4.95×10^{-4} mol) was added to the polymerization tube equipped with a three-way connector and a magnetic stirrer and kept under vacuum (10 Pa) for 3 h with intermediate N_2 gas purging. Then, a pre-distilled monomer (ε-caprolactone, 4.38×10^{-2} mol) and a tin octoate solution (1.75×10^{-5} mol) were added into the system under N_2 environment. The tube was sealed under N_2 atmosphere and immersed in an oil-bath at 180° C for 25 min to conduct polymerization. After the polymerization, a portion of product was taken out in order to determine the monomer conversion by ^{1}H-NMR. When the conversion was higher than 99%, the product PCL was directly subjected to the next step without reprecipitation.

PCL: ^{1}H NMR (600 MHz, $CDCl_3$): δ = 4.06 ($CH_3(CH_2)_{15}CH_2C\underline{H}_2O$-, 2H), 3.65 ($CH_2CH_2C\underline{H}_2OH$, 2H), 2.3 ($OC\underline{H}_2CH_2$-, 2H), 1.64 ($CH_3(CH_2)_{15}C\underline{H}_2CH_2O(=OCH_2C\underline{H}_2CH_2C\underline{H}_2CH_2O)$, 2H), 1.38 ($OCH_2CH_2C\underline{H}_2CH_2CH_2O$, 2H), 1.25 ($CH_3(C\underline{H}_2)_{15}CH_2CH_2O$, 2H), 0.88 ($C\underline{H}_3(CH_2)_{15}CH_2CH_2O$, 3H) ppm.

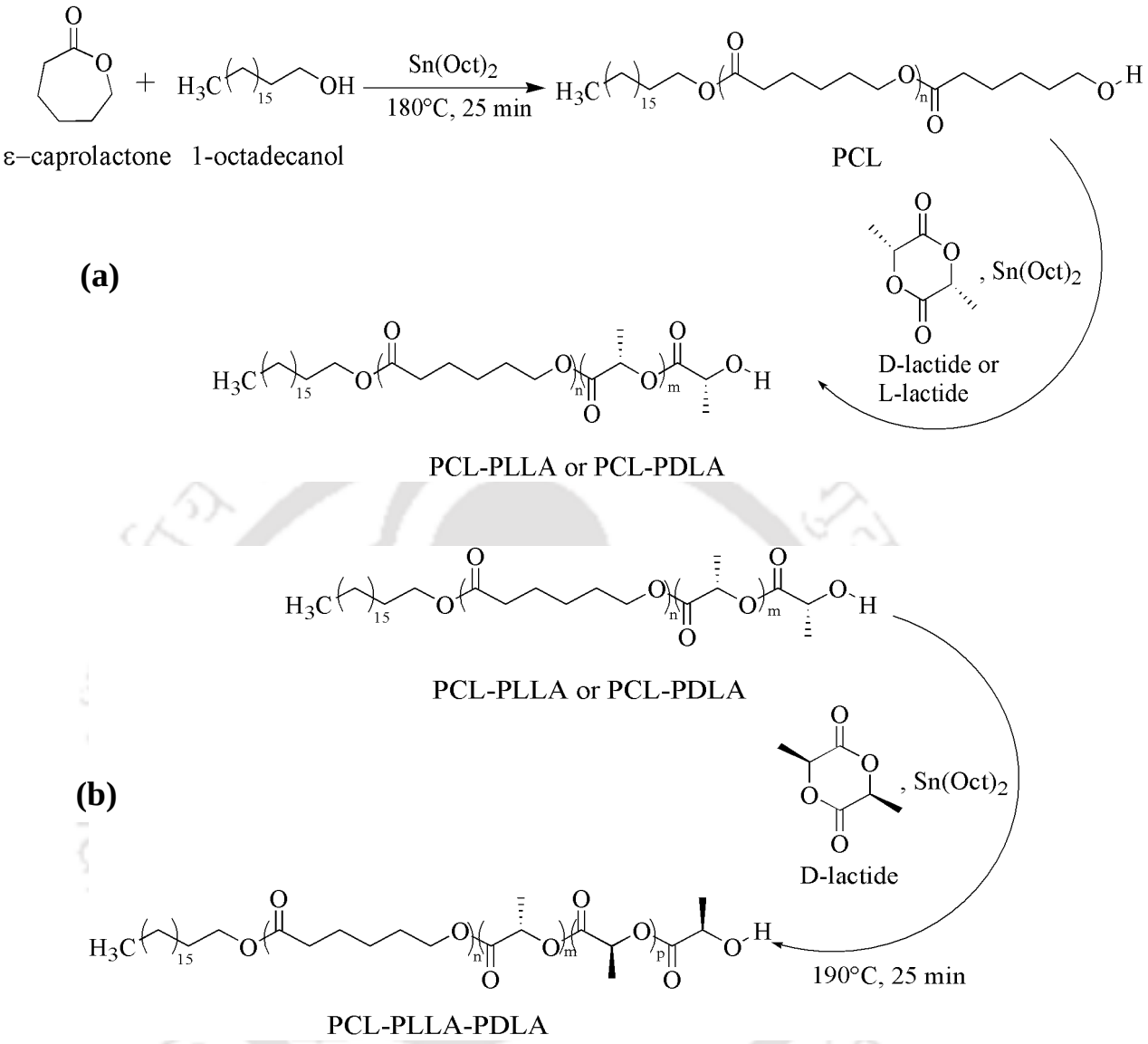

Scheme 3.1: Synthesis of (a) diblock and (b) stereo-triblock copolymers.

3.2.3 Synthesis of AB/AC diblock copolymers

In the second step, the mono-hydroxyl PCL obtained above was used as the macro-initiator for the synthesis of diblock copolymers, PCL-PLLA (AB) and PCL-PDLA (AC), which were prepared by the following ROP of L- and D-lactides respectively. Typically, the polymerization tube containing PCL (4.8×10^{-4} mol) was evacuated at 10 Pa for 1 h at ambient temperature followed by purging with nitrogen. A pre-determined amount of

D-lactide (0.1 mol, in case of 10CL-30D) was added, and the tube evacuated at 10 Pa for 1 h at ambient temperature with N_2 purging periodically. Later, the temperature was raised to 40 °C, and the system was kept at 10 Pa in pressure for 12 h so as to remove the bound moisture. It was observed that a portion of lactide was sublimated on the upper part of the reactor. For minimizing this sublimation the tube was purged with N_2 gas several times. Finally, the vacuum was removed, and the mixture of prepolymer and monomer in the tube was heated at 180 °C under stirring. The PCL polymer started to melt and solubilize into the melt of D-lactide. After complete mixing, a certain amount of the catalyst solution (4.2×10^{-5} mol) was added into the mixture under N_2 environment. The tube was sealed under N_2 atmosphere, and the reaction was carried out at 180 °C for 25 min. A sample was taken out to check the monomer conversion by ^{1}H-NMR after the reaction. Finally, the obtained product was brought down to room temperature followed by dissolving in dichloromethane and reprecipitation in excess methanol. The obtained polymer precipitates were then filtered and dried in a vacuum oven at 80 °C for 12 h. The dried product was used for the determination of number average molecular weight (Mn) by ^{1}H-NMR. The AB/AC diblock copolymers are represented by XCL-YL/XCL-YD where X and Y denote the number-average molecular weights (Mn) in kDa of the component PCL (CL), PLLA (L), and PDLA (D) blocks.

PDLA: ^{1}H NMR (600 MHz, $CDCl_3$): δ = 5.17 ($OCC\underline{H}_2CH_3O$, 3H), 4.36 ($OCC\underline{H}_2CH_3OH$, 2H), 4.12 ($CH_3(CH_2)_{15}CH_2C\underline{H}_2O$, 2H), 1.57 ($OCCH_2C\underline{H}_3O$), 3H), 1.25 ($CH_3(C\underline{H}_2)_{15}CH_2CH_2$-O-, 2H), 0.88 ($C\underline{H}_3(CH_2)_{15}CH$-, 3H) ppm.

Diblock copolymer: ^{1}H NMR (600 MHz, $CDCl_3$): δ = 5.17 ($OCC\underline{H}_2CH_3O$, 3H), 4.36 ($OCC\underline{H}_2CH_3OH$, 2H), 4.06 ($CH_3(CH_2)_{15}CH_2C\underline{H}_2O$-, 2H), 2.3 ($OC\underline{H}_2CH_2$-, 2H),

1.64 ($CH_3(CH_2)_{15}C\underline{H}_2CH_2O(=OCH_2C\underline{H}_2CH_2C\underline{H}_2CH_2O)$, 2H), 1.38 ($OCH_2CH_2C\underline{H}_2CH_2CH_2O$, 2H), 1.25 ($CH_3(C\underline{H}_2)_{15}CH_2CH_2O$, 2H), 0.88 ($C\underline{H}_3(CH_2)_{15}CH_2CH_2O$, 3H) ppm.

3.2.4 Synthesis of ABC stereo-triblock copolymer:

In the third step, the AB diblock copolymer (10CL-10L) obtained above was used as the macro-initiator for the synthesis of stereo-triblock (tri-sb) copolymer PCL-PLLA-PDLA (**Scheme 3.1(b)**). Typically, 10CL-10L (1×10^{-4} mol) was added to the polymerization tube equipped with a three-way connector and a magnetic stirrer. It was evacuated to 10 Pa at 120 ºC for 3 h with N_2 purging several times. Then, a predetermined amount of D-lactide (7.7×10^{-3} mol) was added under N_2 atmosphere and evacuated again at 10 Pa at 80 ºC overnight. The sublimation of lactide was observed on the upper part of the polymerization tube, and it was dropped off to the bottom by heating the upper part of the tube. This was followed by adding a certain amount of the catalyst solution (3.08×10^{-6} mol) to the polymerization tube. After the tube had been evacuated for removing the solvent, it was purged with N_2 gas followed by immersing in an oil bath at 190º C. The diblock copolymer (10CL-10L) first melted and was stirred for 1-2 min so as to allow for its mixing with the catalyst. In the next step, the lactide began to melt and mixed with the melt of 10CL-10L. The polymerization reaction was continued for 25 min at 190 ºC. Finally, the polymerization system was brought down to ambient temperature, and a portion of the product was taken out and subjected to ^{1}H-NMR spectroscopy to determine the conversion. The final product was dissolved (dichloromethane + 10% HFIP) and reprecipitated in excess methanol followed by filtering the precipitates and drying in a vacuum oven at 80 ºC for 12 h. The ABC tri-sb copolymers are represented by XCL-YL-

ZD where X, Y, and Z denote the Mn values in kDa of its following block sequences shown by the abbreviated symbols.

Tri-sb copolymer: ^{1}H NMR (600 MHz, $CDCl_3$): δ = 5.17 ($OCC\underline{H}_2CH_3O$, 3H), 4.36 ($OCC\underline{H}_2CH_3OH$, 2H), 4.06 ($CH_3(CH_2)_{15}CH_2C\underline{H}_2O$-, 2H), 2.3 ($OC\underline{H}_2CH_2$-, 2H), 1.64 ($CH_3(CH_2)_{15}C\underline{H}_2CH_2O(=OCH_2C\underline{H}_2CH_2C\underline{H}_2CH_2O)$, 2H), 1.38 ($OCH_2CH_2C\underline{H}_2CH_2CH_2O$, 2H), 1.25 ($CH_3(C\underline{H}_2)_{15}CH_2CH_2O$, 2H), 0.88 ($C\underline{H}_3(CH_2)_{15}CH_2CH_2O$, 3H) ppm.

3.2.5 Blending of diblock copolymers

The synthesized diblock copolymers were blended with their corresponding enantiomers. Typically, 2 g each of 10CL-10L and 10CL-10D were weighed and mixed in 50 ml of (dichloromethane + 10% HFIP). The mixture was allowed to stir at ambient temperature until a clear solution was obtained. This clear solution was poured into excess methanol followed by filtering the precipitates and drying in a vacuum oven at 80 ºC for 12 h. The dried polymer is represented as B_10-10. In the same way, 10CL-20L and 10CL-20D; 10CL-30L and 10CL-30D were blended to form enantiomeric blends which are represented as B_10-20 and B_10-30 respectively.

3.2.6 Preparation of polymer films

A polymer sample (1.5 g) was laid between two teflon sheets with a metal spacer having a window size of 70 mm × 70 mm × 0.230 mm followed by compression molding on a Mini Test Press (MP-2FH, Toyoseiki Co. Ltd., Japan). The polymer was hot pressed at 2 MPa in pressure for 3 min thereby quenching in ice water to obtain a polymer film. The hot-pressing temperature of PDLA was 190 ºC while that of PCL was 90 ºC. The hot-pressing temperature of a diblock copolymer was 210 ºC and that of a triblock copolymer

and a blend of the enantiomeric block copolymers was 240 ºC. The hot pressed (melt quenched) films were used for the thermal, mechanical and crystallization studies.

3.2.7 Characterization

^{1}H NMR and ^{13}C NMR (600 MHz) spectra were measured on an AV600 spectrometer (Bruker, Germany). The synthesized samples (50-70 mg) were dissolved in 0.7 ml of deuterated chloroform ($CDCl_3$) containing 0.03 vol-% tetramethylsilane (TMS) as an internal reference.

Mn of the synthesized samples is ascertained from ^{1}H-NMR by using the following equations:

$$DP\ (PCL) = \frac{e}{j} + 1 \quad \text{(i)}$$

$$DP\ (PDLA) = \frac{l}{m} + 1 \quad \text{(ii)}$$

$$Mn\ (PCL) = 114\big(DP(PCL)\big) + M_{1-oct} = 114\left(\frac{e}{j} + 1\right) + 270.49 \quad \text{(iii)}$$

$$Mn\ (PLA) = 72\big(DP(PLA)\big) + M_{1-oct} = 72\left(\frac{l}{m} + 1\right) + 270.49 \quad \text{(iv)}$$

$$Mn\ (diblock) = Mn(PCL) + Mn(PLA) + M_{1-oct} = 114\left(\frac{e}{m} + 1\right) + 72\left(\frac{l}{m} + 1\right) + 270.49 \quad \text{(v)}$$

$$Mn\ (tri-sb) = Mn(PCL) + Mn(PLA) + M_{1-oct} = 114\left(\frac{e}{m} + 1\right) + 72\left(\frac{l}{m} + 1\right) + 270.49 \quad \text{(vi)}$$

where, DP = Degree of polymerization,

$M_{1\text{-oct}}$ = molecular weight of 1-Oct (initiator)

For determining the Mn of PDLA and PLLA, the same formula is used.

The number- (Mn) and weight-average molecular weights (Mw) of the synthesized samples were analysed by gel permeation chromatography (Shimadzu, Japan). The system comprised of LC-20AD pump, SIL-20A HT auto sampler and RID-10A refractive index detector. The measurement was conducted at 40 ºC using HPLC grade chloroform as an eluent (flow rate: 1 ml/min). Polystyrene monodispersed standards ranging from 370 Da to 500 kDa were used for the calibration. The materials were dissolved in chloroform (20 mg/ml) and filtered with PTFE syringe filters (0.45 µm) before analysis.

Differential scanning calorimetery (DSC) measurements were conducted using DSC 214 Polyma (NETZSCH, Germany) under nitrogen atmosphere. The films (~7 mg) were heated from 0 ℃ to 250 ℃ at the rate of 10 ℃/min.

Thermal degradation of the films was analyzed using a thermogravimetric analyser (TGA 4000, Perkin Elmer, US) under inert (N_2) atmosphere. The samples (5-8 mg) were heated from 30 ºC to 700 ºC at the rate of 10 ºC/min. The weight loss (%) and its derivative were measured with the increasing temperature.

The polymer films (5 mm width and 20 mm gauge length) were used to determine the mechanical properties under tensile mode using a universal testing machine (KIC 2-050-C, Kalpak Instruments and Controls, India) provided with a 500 N load cell and the cross head speed was set to 5 mm/min. The measurements were conducted at ambient temperature. Five specimens of each sample were tested to analyse the tensile strength, modulus, elongation (at break) and toughness, and the results were reported as an average of five specimens along with standard deviation. Tensile toughness was determined from the area under the stress-strain curve. Young's modulus was determined by the slope of the straight line at 2% strain.

Dynamic mechanical analysis (DMA) was conducted on a DMA equipment (242 E, NETZSCH GmbH, Germany). The film samples were subjected to analysis under 1 Hz frequency and 10 μm displacement amplitude at the rate of 2 ºC/min. The temperature range for PDLA and diblock copolymers was kept as 25-160 ºC and that for enantiomeric blends and stereo-triblock copolymer was 25-180 ºC. The temperature range for PCL was 25-50 ºC.

X-ray diffraction studies were performed on a Powder X-ray Diffractometer (Rigaku, SmartLab) which comprised of a 9kW rotating anode coupled with HyPix-3000 semiconductor operating at 45 kV and 112 mA (CuKα radiation, $\lambda = 0.154$ nm). The analysis of hot pressed films in the melt quenched state as well as after annealing at 120 °C for 1 h, was carried out at the rate of 4º/min in the scanning (2θ) range of 3º - 40º at room temperature. The data were acquired by Rigaku SmartLab Studio II software.

3.2.8 Thermal processing of synthesized block copolymers

The selected diblock copolymers and enantiomeric blends were cut into thin films and processed using an injection molding machine (HAAKE Minijet Pro, Thermo Fisher Scientific) to make three-dimensional articles. The diblock copolymer was processed at 200 ºC whereas the enantiomeric blend was processed at 225 ºC at 750 bar pressure for 5 s to make cortical and cancellous screws respectively. The temperature of the mold was set to 90 ºC. The commercial PLA 2003D (NatureWorks®) was also processed in the same way to fabricate the cancellous bone screws.

3.2.9 Thermo-mechanical stability of cancellous bone screws

The cancellous bone screws made using the enantiomeric blend possessing stereocomplexation and that made using commercial PLA 2003D (Nature Works®) were

held (at one end) between the two blocks and kept in an oven at 121 °C for 1 hour to determine their thermo-mechanical stability.

3.2.10 *In vitro* studies

Cell culture and seeding:

MG-63 (human bone osteosarcoma cells)[159] were cultivated in T25 flasks using Dulbecco's modified eagle's medium (DMEM) supplemented with 20% fetal bovine serum (FBS) and 2% penicillin streptomycin. The cells were detached from the flasks prior to seeding by using trypsin. The polymer samples were sterilized with ethanol followed by washing with phosphate buffer saline (PBS) and were placed in 96 well-plates. The samples were then subjected to UV radiation. Trypan blue (Sisco Research Laboratories) stain was used to count the cells prior to seeding by an automated cell counter (Countess® II FL, Thermo Fisher Scientific) and 1×10^3 cells/well were seeded in 96 well plates containing samples along with control (polystyrene) in triplicates. The plates were kept under incubation with 5% CO_2 and 37º C temperature.

MTT assay

In order to determine the mitochondrial activity of MG-63 cells onto the polymers/copolymers, MTT (3-(4,5-dimethylthiazol-2-yl)-2,5-diphenyltetrazolium bromide) assay was conducted. MTT (HiMedia) stock solution (5mg/ml) was prepared in PBS and added (10 µl) to each well after the intervals of 1, 4, 7 and 13 days. The plates were kept in CO_2 incubator for 3 h, after which the media along with MTT was removed and dimethyl sulfoxide (DMSO, Merck) was added (100 µl/ well) in order to allow the respiring cells to convert the water soluble MTT into insoluble formazan crystals. Later, the absorbance was determined using microplate reader (Multiskan Go, Thermo Fisher

Scientific) at 570 nm. The media was replaced on a day prior to determining the cell viability. The mean values of the absorbance were used to determine the survivability of cells on the polymers samples with control as a reference.

Cell staining

The cells on the surface of the samples (along with control) were stained with acridine orange (Thermo Fischer Scientific) in order to determine the adhesion of cells and thus the biocompatibility of the synthesized polymeric samples. The acridine orange stain (10 mg/ml) was diluted and used for staining the cells. The cell culture media was removed from the well plates containing samples followed by rinsing with PBS thrice. Acridine orange stain was then added to the samples and incubated for 30 min before analyzing the cells under Floid Cell Imaging Station (Thermo Fisher Scientific).

3.3 Results and Discussion

3.3.1 Synthesis of AB/AC and ABC type copolymers

The AB diblock copolymers consisting of PCL (A) and PLLA/PDLA (B/C) segments with varying block lengths are synthesized by two-step ROP. The resultant diblock copolymer is used as a prepolymer in the subsequent synthesis of ABC tri-sb copolymer. The results of the series of syntheses are summarized in **Table 3.1**. Mn (NMR) values of PCL are determined from the terminal to main chain ε-caprolactone signal ratios of the ^{1}H-NMR spectrum (**Figure 3.1-1**). These values are only slightly different from the theoretical values (Mn (th)) which may be due to the measurement error. The synthesized PCL is used as a macro-initiator used for the synthesis of PCL-PLLA and PCL-PDLA where the block length of PLLA and PDLA is varied from 10 kDa to 30 kDa.

^{1}H-NMR spectra of the synthesized polymers along with their structure are shown in **Figure 3.1-1**. The signals in the spectra are assigned by the alphabets as mentioned in the structures. The first step ROP of ε-caprolactone leads to the appearance of terminal group peak for PCL at 3.65 ppm which disappears on the second step ROP which is evident of the PDLA block being attached to the terminal group of PCL. Subsequently, a hydroxymethylene peak (terminal) at 4.36 ppm appears in case of both diblock and triblock copolymers which is also present in the mono hydroxyl- terminated PDLA shown in the spectra. Also, ^{13}C NMR spectra of the synthesized homopolymers/copolymers are shown in **Figure 3.1-2**.

Table 3.1: Synthesis of AB/AC Diblock and ABC Tri-sb copolymers.

	Comp. ratio (PLA)	Molar feeding ratio [M/I]	Conv. (%)	Mn (th) kDa	Mn (NMR) kDa	Mn (GPC) kDa	Mw (GPC) kDa	PDI (Mw/ Mn)	Mn (Block length) (NMR)
10CL		88.5	99.5	10.0	8.6	22.1	48.8	2.21	8.6CL
10CL-10D	50%D	77.0	99.5	19.0	20.2	48.6	71.8	1.47	9.6CL-10.6D
10CL		88.5	99.2	10.0	9.8	23.4	47.3	2.02	9.8CL
10CL-10L	50%L	77.0	94.3	20.9	19.7	45.5	69.8	1.53	9.8CL-9.9L
10CL-10L-10D	66.6%D/L	77.0	90.0	29.7	31.7	59.0	100.6	1.70	9.8CL-9.9L-9.9D
10CL		88.5	99.3	10.0	10.2	22.8	46.3	2.03	10.2CL
10CL-20D	66.6%D	154.1	93.8	31.1	33.8	64.0	107.2	1.67	10.9CL-22.9D
10CL		88.5	99.2	10.0	10.6	23.6	47.4	2.01	10.6CL
10CL-20L	66.6%L	154.1	93.3	31.3	29	59.1	105.2	1.78	9.9CL-19.1L
10CL		88.5	99.3	10.0	10.8	25.1	48.9	1.94	10.8CL
10CL-30D	75%D	231.2	75.5	30.7	43.2	69.8	160.5	2.3	10.8CL-32.4D
10CL		88.5	99.3	10.0	10.2	23.4	47.7	2.03	10.2CL
10CL-30L	75%L	231.2	80.5	31.4	40.4	77.3	141.0	1.82	9.7CL-30.7L

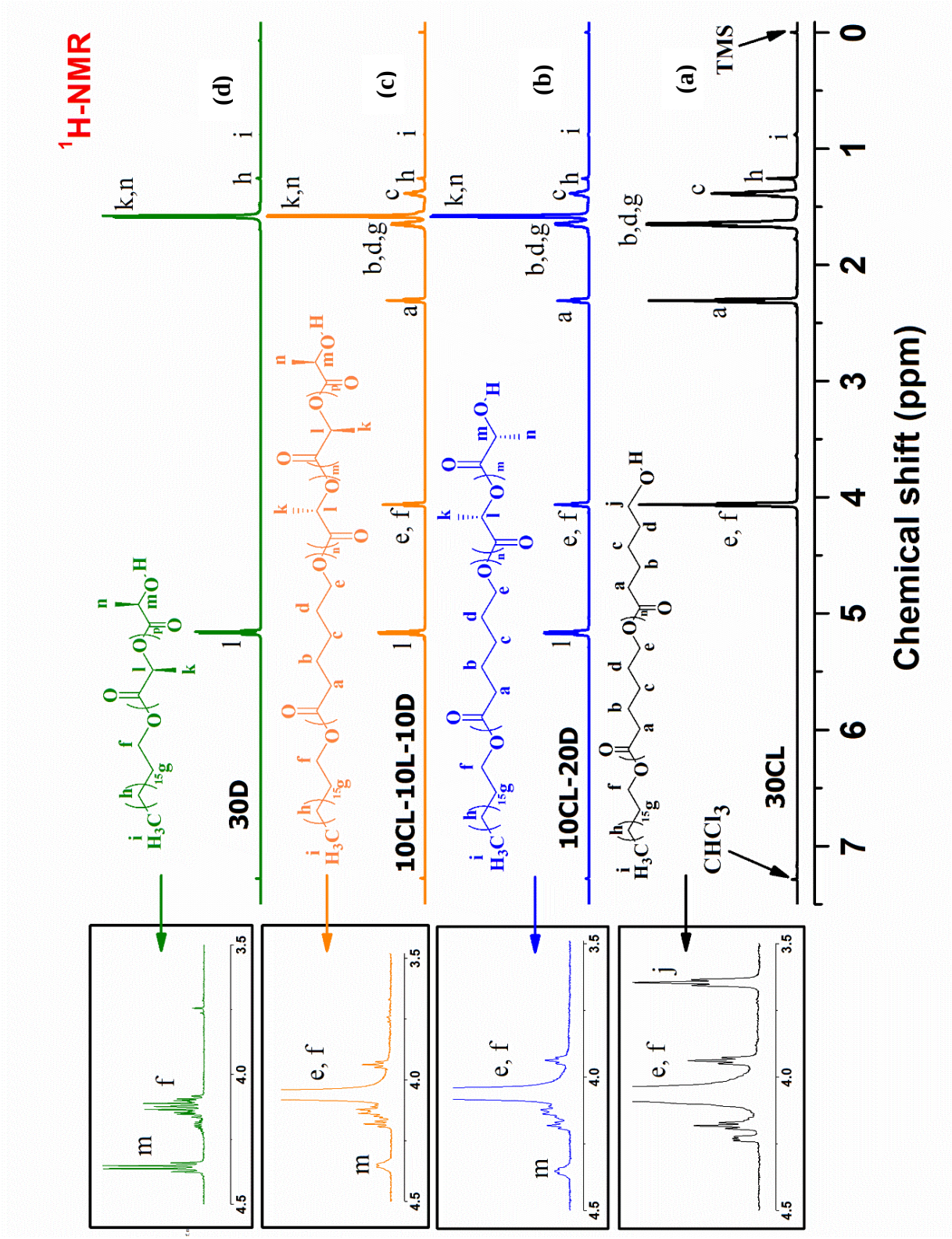

Figure 3.1-1: Representative ^{1}H NMR spectra of (a) PCL, (b) diblock copolymer, (c) tri-sb copolymer, and (d) PDLA along with their expanded regions (3.5-4.5 ppm).

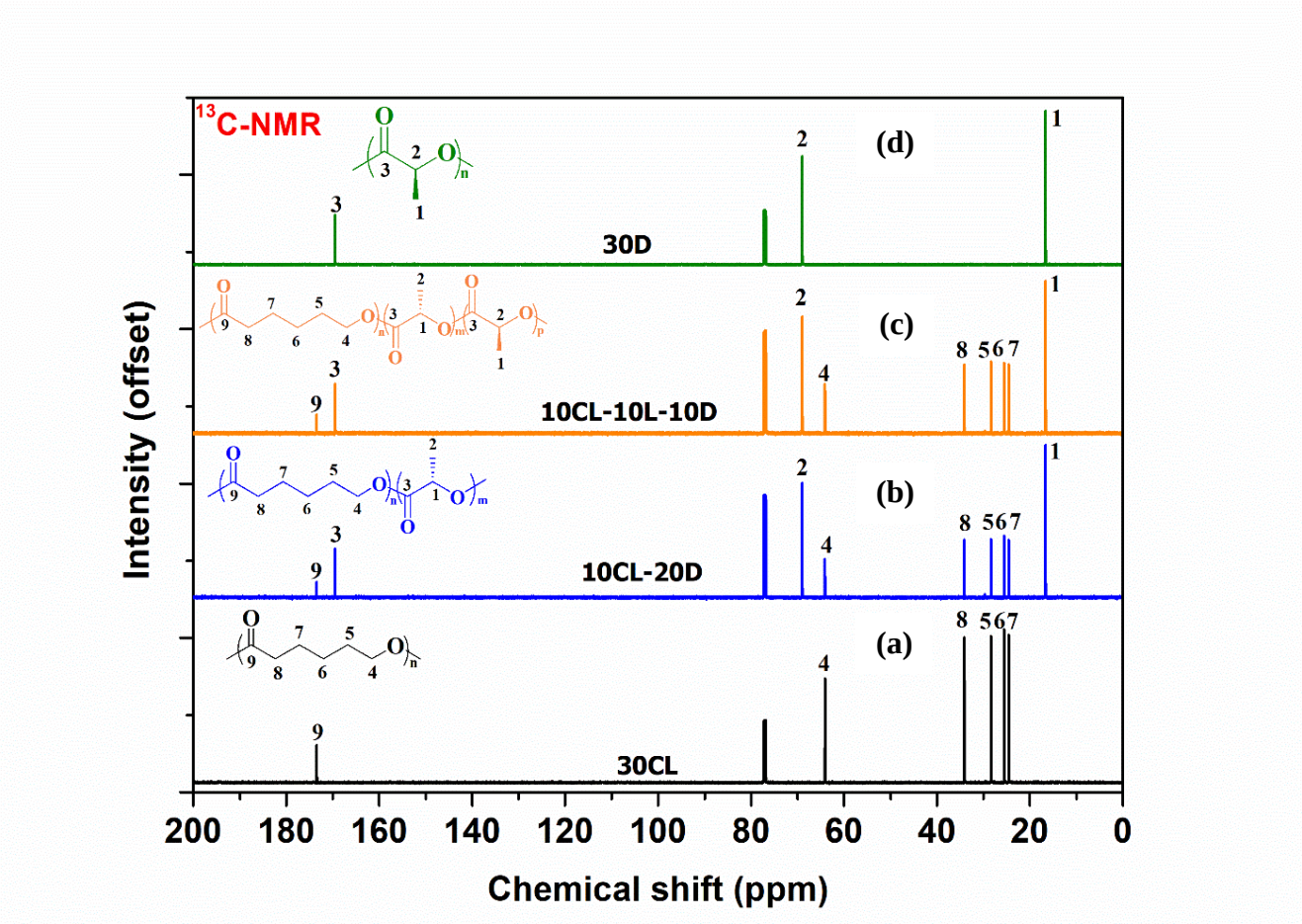

Figure 3.1-2: Representative ^{13}C NMR spectra of (a) PCL, (b) diblock copolymer, (c) tri-sb copolymer and (d) PDLA.

Figure 3.2 shows the GPC curves of a series of block copolymers from PCL to PCL-PLLA-PDLA via PCL-PLLA. The elution time of PCL (30CL) is 13.3 min, which is reduced to 12.9 min for the PCL-PLLA (10CL-20D) and further reduced to 12.6 min for the PCL-PLLA-PDLA (10CL-10L-10D). This clearly indicates the increasing molecular weight of the copolymers along with the absence of bimodal peaks, supporting the success in each step of ROP. Further the chromatograms of PCL-PDLA with different block lengths of PDLA revealed that the elution time decreased with the increasing block length of PDLA confirming the success of chain extension of PDLA (**Figure 3.2(b)**).

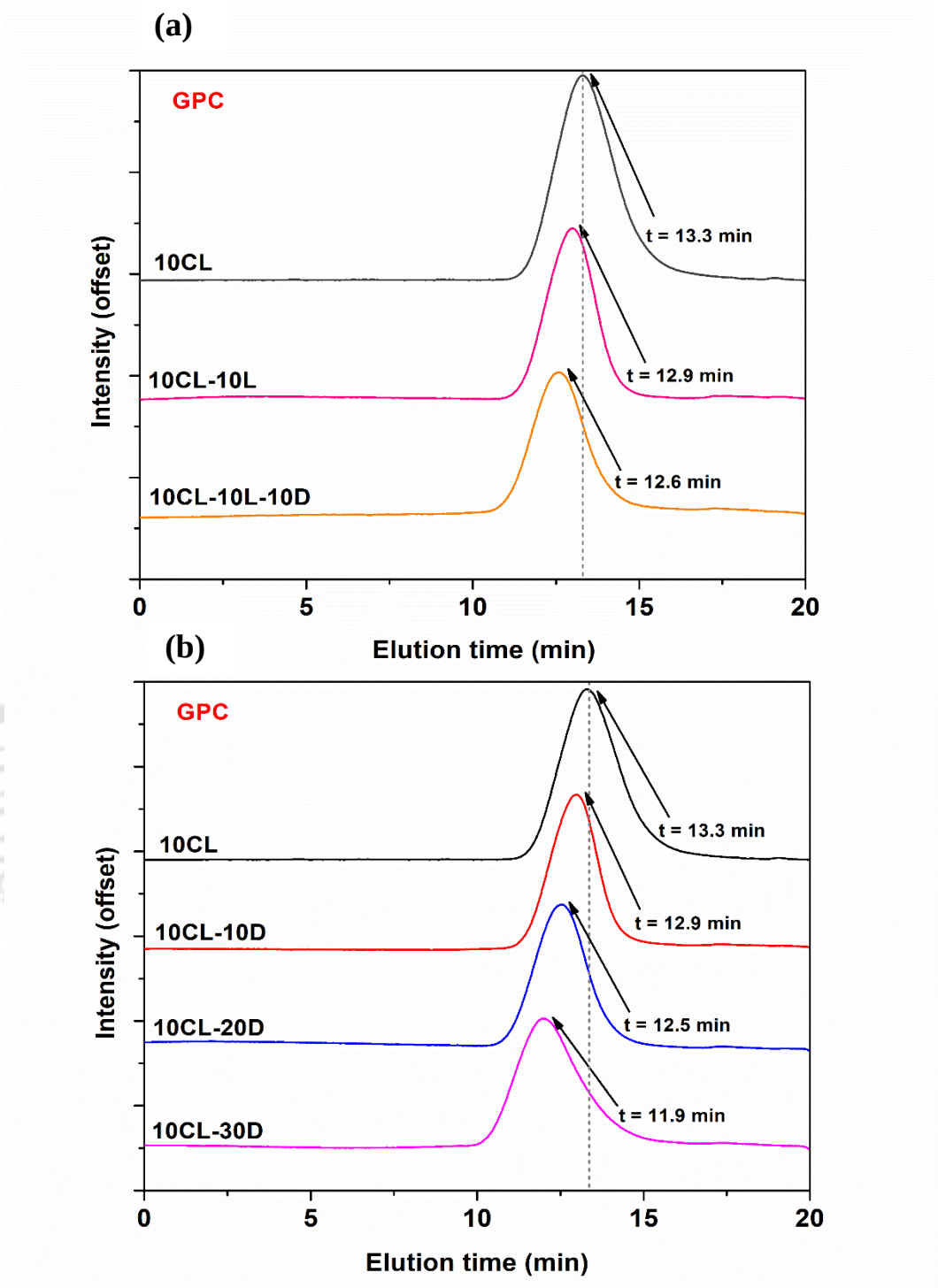

Figure 3.2: GPC curves of (a) series of block copolymers from PCL to PCL-PLLA-PDLA via PCL-PLLA and (b) chromatograms of PCL-PDLA with different block lengths of PDLA.

3.3.2 Thermal analysis

The DSC thermograms of the block copolymers compared with that of PCL and PDLA are shown in **Figure 3.3(a)**. The enthalpy of fusion (melting) (ΔH_m) of PCL decreases from 42.4 to 20.2 J/g with increasing the block length of PDLA whereas the ΔH_m of PDLA is increased from 36.8 to 43.4 J/g as indicated in **Table 3.2**. These changes in enthalpy correspond to the decreasing content of PCL and increasing content of PDLA in the copolymer system. A small exothermic peak (66 °C) is visible just above the T_m of PCL in case of 10CL-10D; and the crystallization temperature (T_{cc}) of PDLA is increased from 77.1 ºC to 84.0 ºC as the block length of PDLA is increased from 20 to 30 kDa. This indicates that the T_{cc} of the diblock copolymers is shifted towards that of PDLA homopolymer (98.2 ºC) as the PDLA content is increased, which in turn confirms separate crystallization of PCL and PDLA blocks of varying length.

Figure 3.3(b) shows the DSC thermograms of the enantiomeric diblock copolymer blends and the tri-sb copolymer. A bimodal distribution of stereocomplex T_m (221.8, 235.4) in case of B_10-10 is observed which is possibly due to the effect of quenching leading to the formation of relatively thinner and thicker lamellae of stereocomplex crystals. Due to the low molecular weight of the PDLA/PLLA, blocks of the B_10-10 form perfect stereocomplex crystals upon blending, without generating the homocrystals. The homocrystal formation in case of B_10-20 at 171 °C may be due to the increasing molecular weight of PLLA/PDLA blocks in the diblock copolymers that are blended. The peak at 222 °C indicates the formation of stereocomplex crystals of relatively smaller size. In case of B_10-30 sample, the T_m at 223.6 °C indicates the formation of stereocomplex crystals which are almost identical to that of B_10-20. Also, a large endothermic peak at 176.5 °C is due to the homo-crystal melting, corresponding

to the increased molecular weight of the PLLA/PDLA blocks. It is therefore indicated that the higher molecular weight of the block sequences increases the formation of homo-crystals instead of stereocomplex crystals. The formation of homocrystals is a well-known phenomenon which usually increases with the increasing molecular weight. In order to overcome the formation of homocrystals, Gupta et al. have reported the chemical modification of cellulose microcrsytals (CMC) which is grafted on the PDLA chains and the resulting material is melt mixed with PLLA in order to form the preferential stereocomplex biocomposite.[30] In the current investigation, in case of tri-sb copolymer, T_m is shown at 210 °C which is lower than that of the enantiomeric blend samples, but no T_m due to homocrystals is observed. It can be inferred that preferential formation of stereocomplex crystals is allowed although the crystals show a relatively lower T_m. This drop of T_m is favorable in reducing the processing temperature of the triblock copolymer. Further, the cold crystallization peak becomes prominent in B_10-20 and B_10-30, as the molecular weight is increased. Also, the enthalpy of cold crystallization (ΔH_{cc}) is increased with the molecular weight of the copolymer blend. The absence of exothermic peak (T_{cc}) in case of 10CL-10L-10D suggests much easier crystallization in 10CL-10L-10D. The thermal properties of diblock, triblock and pentablock copolymers based on PCL and PLA were reported by Rosen et al. where the two crystalline domains were observed along with very high crystallinities of about 60%.[160] Furthermore, the homocrystals were found to be absent in case of stereoblock copolymers which is also accordance with the current investigation.

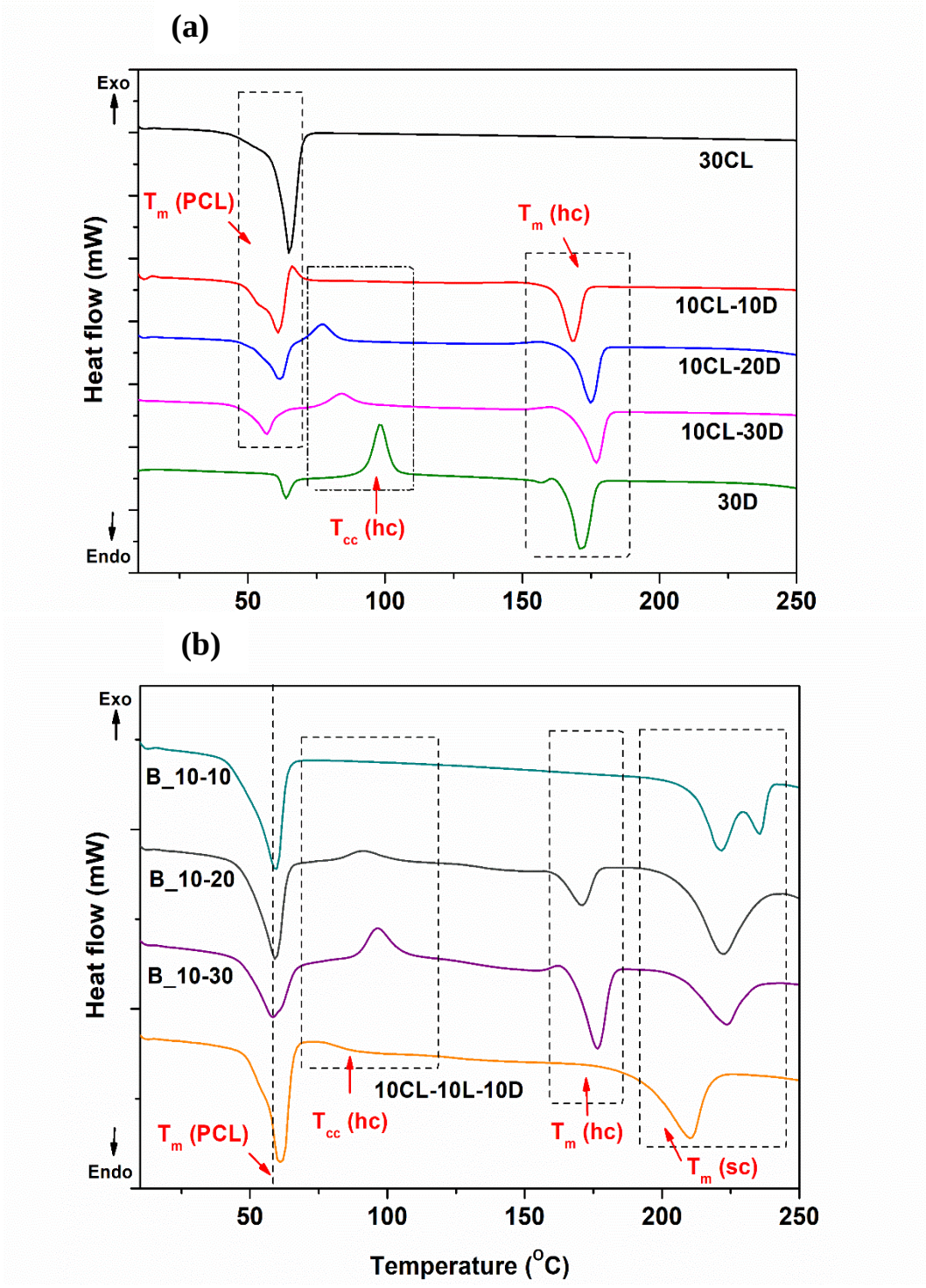

Figure 3.3: DSC thermograms of (a) PCL, PDLA and PCL-PDLA diblock copolymers, and (b) enantiomeric diblock copolymer blends and tri-sb copolymer.

Table 3.2: Thermal transitions in the homopolymers and block copolymers as determined from DSC.

Identity	**T_m (PCL,℃)**	**ΔH_m (PCL, J/g)**	**T_{cc} (PLA,℃)**	**ΔH_m (PLA, J/g)**	**T_m (hcPLA,℃)**	**ΔH_m (hcPLA, J/g)**	**T_m (scPLA, ℃)**	**ΔH_m (scPLA, J/g)**
30CL	65.0	91.8	-	-	-	-	-	-
10CL-10D	61.0	42.4	-	-	168.5	36.8	-	-
10CL-20D	61.1	31.4	77.1	14.2	174.9	39.5	-	-
10CL-30D	56.9	18.4	84.0	22.4	177.1	43.4	-	-
30D	-	-	98.2	49.2	171.0	49.7	-	-
B_10-10	59.3	38.4	-	-	-	-	221.8, 235.4	39.1
B_10-20	59.2	31.3	91.3	4.5	171.0	10.1	222.0	41.9
B_10-30	58.4	19.7	96.6	11.3	176.5	23	223.6	24.2
10CL-10L-10D	61.1	31.4	-	-	-	-	210.0	30.6

Figure 3.4-1(a) represents the TGA curves of the homopolymers and diblock copolymers. It is observed that PDLA (30D) and PCL (30CL) begin to degrade at 268.7 °C and 340.4 °C, respectively. The maximum degradation temperature of PCL is 435.8 °C whereas that of PDLA is 322.2 °C as displayed in **Figure 3.4-2(a)**. Further it is seen that degradation of PDLA takes place in a single step whereas in the thermal degradation of PCL, a shoulder is seen at 369.2 °C, suggesting two consecutive mechanisms involved. A similar phenomenon was reported by Persenaire et al. who confirmed the two-step degradation mechanism for PCL. The first step is accounted for the ester pyrolysis reaction leading to the cleavage of polyester chains; and the second step is thought to be driven by the back-biting reaction leading to the formation of ε-caprolactone.[161] In contrast, the di-block copolymers having the same molecular weight with PCL and PDLA showed the onset degradation temperature around 308.9 °C, which suggests that the thermal stability of PDLA is enhanced upon incorporation of a PCL block. The thermal stability is found to enhance with the increasing block length of PDLA or decreasing the PCL content. **Figure 3.4-1(b)** displays the TGA curves of the enantiomeric copolymer blends and triblock copolymer. The onset degradation temperatures of the enantiomeric diblock copolymer blends are found to be almost identical with those of their single copolymers. They seem to increase from 305.9 °C to 312.6 °C with increasing their molecular weight. The triblock copolymer is thermally stable till 313.5 °C which is slightly higher than that of B_10-30. However, the maximum degradation temperature of enantiomeric blends is found to reduce with the increasing the PLA content (**Figure 3.4-2(b)**) by which the stereocomplex formation is deceased.

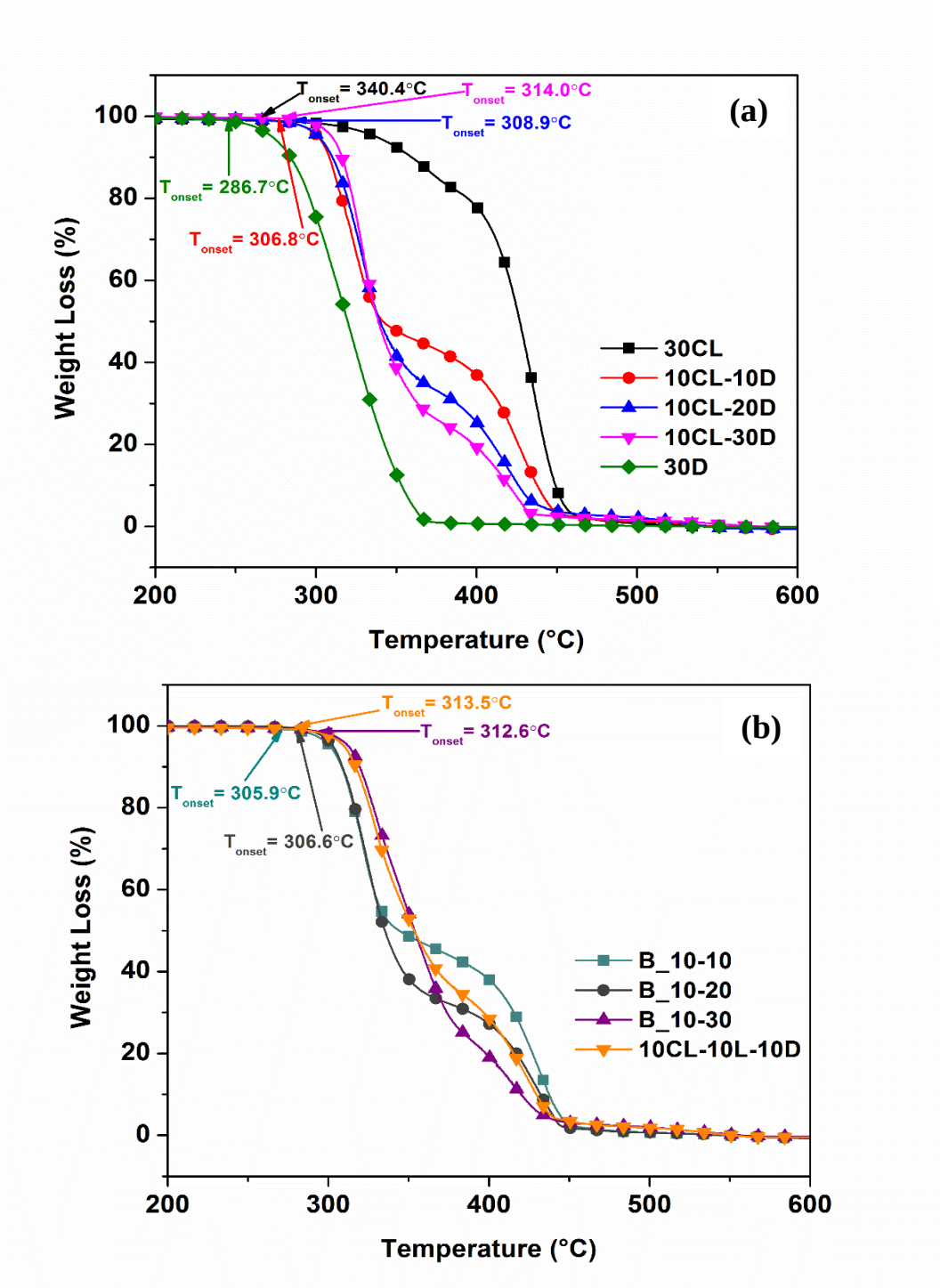

Figure 3.4-1: TGA curves of (a) diblock copolymers, and (b) tri-sb copolymer and the enantiomeric diblock copolymer blends.

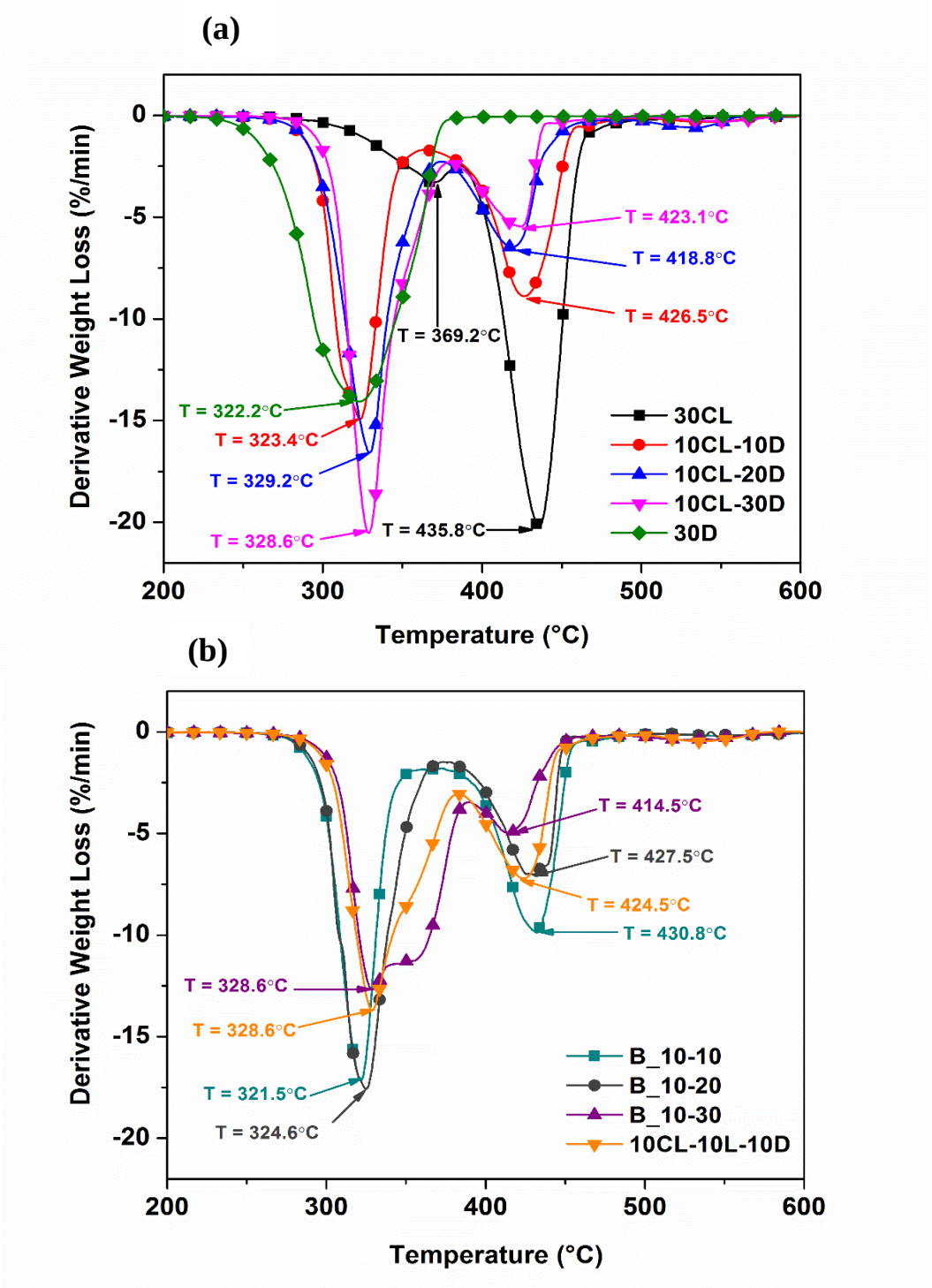

Figure 3.4-2: TGA curves for derivative weight loss (%) of (a) diblock copolymers, and (b) tri-sb copolymers and the enantiomeric diblock copolymer blends.

3.3.3 Mechanical properties

Figure 3.5-1 manifests the typical stress-strain (SS) curves of the polymer films of the block copolymers and their enantiomeric blends as well as of the tri-sb copolymer. The tensile strength and elongation (at break) are plotted as a function of PDLA or PDLA/PLLA content of the copolymers in **Figure 3.5-2(a)**. The tensile strength of PCL (control) is 13.1 MPa and elongation at break is 76.1%. The higher elongation of PCL is due to its soft and flexible nature as the test is performed at 25 ^{o}C (rubbery region of PCL). The tensile strength of PDLA is 16.6 MPa whereas its elongation is 2.7% which is attributed to its brittle nature. The lower value of tensile strength in comparison to that of ordinary PLLA and PCL films is possibly due to the lower molecular weight of the present samples. The tensile strength of diblock copolymers is found to increase from 14.8 to 28.9 MPa along with an increase in elongation at break ranging from 6.4% to 17.8% with the increasing the block length of PDLA. A similar phenomenon is seen in the case of the enantiomeric copolymer blends wherein the tensile elongation and stress are found to increase from 7.1 to 58.9% and 14.3 to 26.7 MPa respectively with increasing the PLA content (**Figure 3.5-2(a)**). On the other hand, in case of tri-sb copolymer film, the tensile elongation and stress are restricted to 12.6% and 25.1 MPa, respectively. The lower elongation could be attributed to the higher stereocomplex formation imparting higher brittleness. Further, the tensile toughness of PCL and PDLA are found to be 5 and 0.2 MJ/m^3, respectively. The tensile toughness of the diblock copolymers is found to increase from 0.8 to 2.2 MJ/m^3 with the increasing block length of PDLA which could be due to the increasing rubbery state in the system imparting toughness to the material. The modulus of PDLA is 1258.5 MPa or 1.258 GPa which is much higher than PCL (265 MPa or 0.265 GPa). The modulus of the diblock copolymers increases from 394 to 708 MPa

with the increasing block length of PDLA as shown in **Figure 3.5-2(b)**. Similarly, the tensile modulus and tensile toughness of the enantiomeric copolymer blends increase from 346 to 679 MPa and 0.6 to 11 MJ/m^3, respectively as shown in **Figure 3.5-3(b)**. The modulus of tri-sb copolymer is 670 MPa which is higher than that of the blend samples whereas the tensile toughness (1.7 MJ/m^3) is significantly lower than that of the enantiomeric diblock blend (B_10-20). This is because of the lower elongation at break for the tri-sb copolymer. In conclusion, tensile strength, modulus and the toughness of the diblock copolymers are enhanced with increasing the block length of PDLA. It can be inferred that involvement of PCL block in the mechanical properties of PLA materials, particularly improve the brittleness. Han et al. had synthesized PLA and PEG (polyethylene glycol) triblock copolymers i.e. PLLA-PEG-PLLA and PDLA-PEG-PDLA and blended them in equivalent ratios. They found that upon increasing the block length of PEG (middle segments) led to the improvement in elongation at break of both the triblock copolymers and the enantiomeric blends whereas their tensile strength was reported to be reduced.[162] However, in the current study, the stress-strain measurements at the ambient temperature show that both the tensile strength and elongation at break are increased in the order of 10D < 20D < 30D. It is reasonable that the tensile strength increased when the volume fraction of glassy PDLA is increased. On the other hand, an unusual increase in elongation at break is observed which may be due to the presence of PCL in the rubbery state because of its T_g being lower than room temperature. The stress-strain curves for the 10CL-20D and 10CL-30D specimens indicate the typical behavior of strain-induced plastic-to-rubber transition[163,164]. In this case, possibly the continuous hard domains (crystalline PCL, amorphous and crystalline PDLA phases) are fractured into smaller pieces upon stretching the specimen but the crack propagation is

terminated at the rubbery domain (the amorphous PCL phase), not resulting in the macroscopic breakdown of the specimen. Therefore, the specimen could be stretched more after the yield point.[164] Also, it is observed from the DSC results (**Figure 3.3(a)**) that, ΔH_m for PCL is lower and ΔH_m - ΔH_{cc} for PDLA is also lower for 10CL-20D and 10CL-30D specimens as compared to those for 10CL-10D specimen. This clearly indicates that the amount of amorphous PCL phase existing in the virgin specimen is larger in the 10CL-20D and 10CL-30D specimens as compared to that of 10CL-10D specimen. Since the termination of the crack propagation is due to the existence of rubbery domain, the specimen having the larger amount of the rubbery phase must exhibit clearer plastic-to-rubber transition upon stretching. Thus, the elongation at break is in the same order of the amount of rubbery phase, which is 10D < 20D < 30D rationalizing the experimental results.

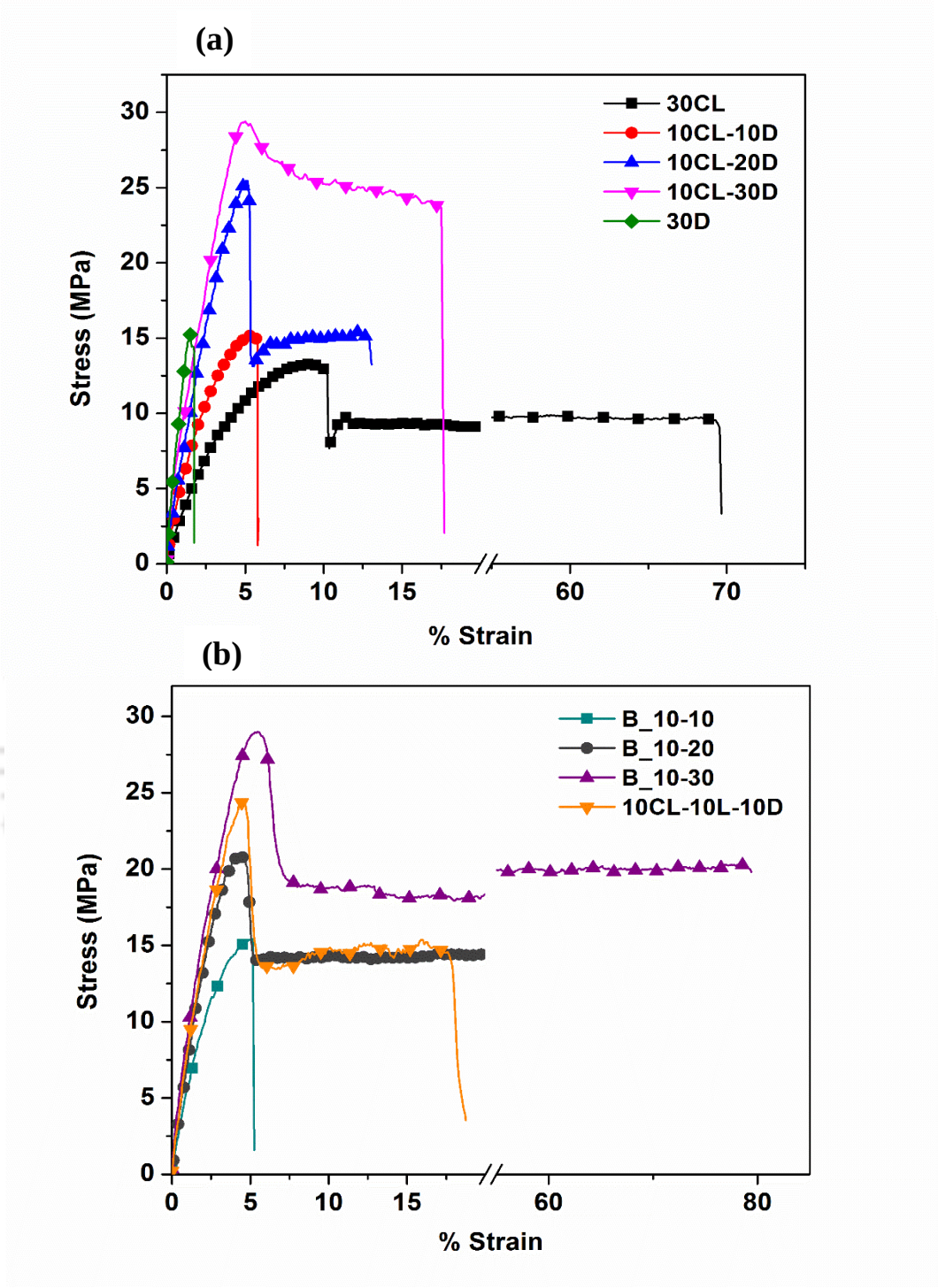

Figure 3.5-1: Representative data for stress vs (%) strain of (A) homopolymers and diblock copolymers; (B) diblock blends and tri-sb copolymer.

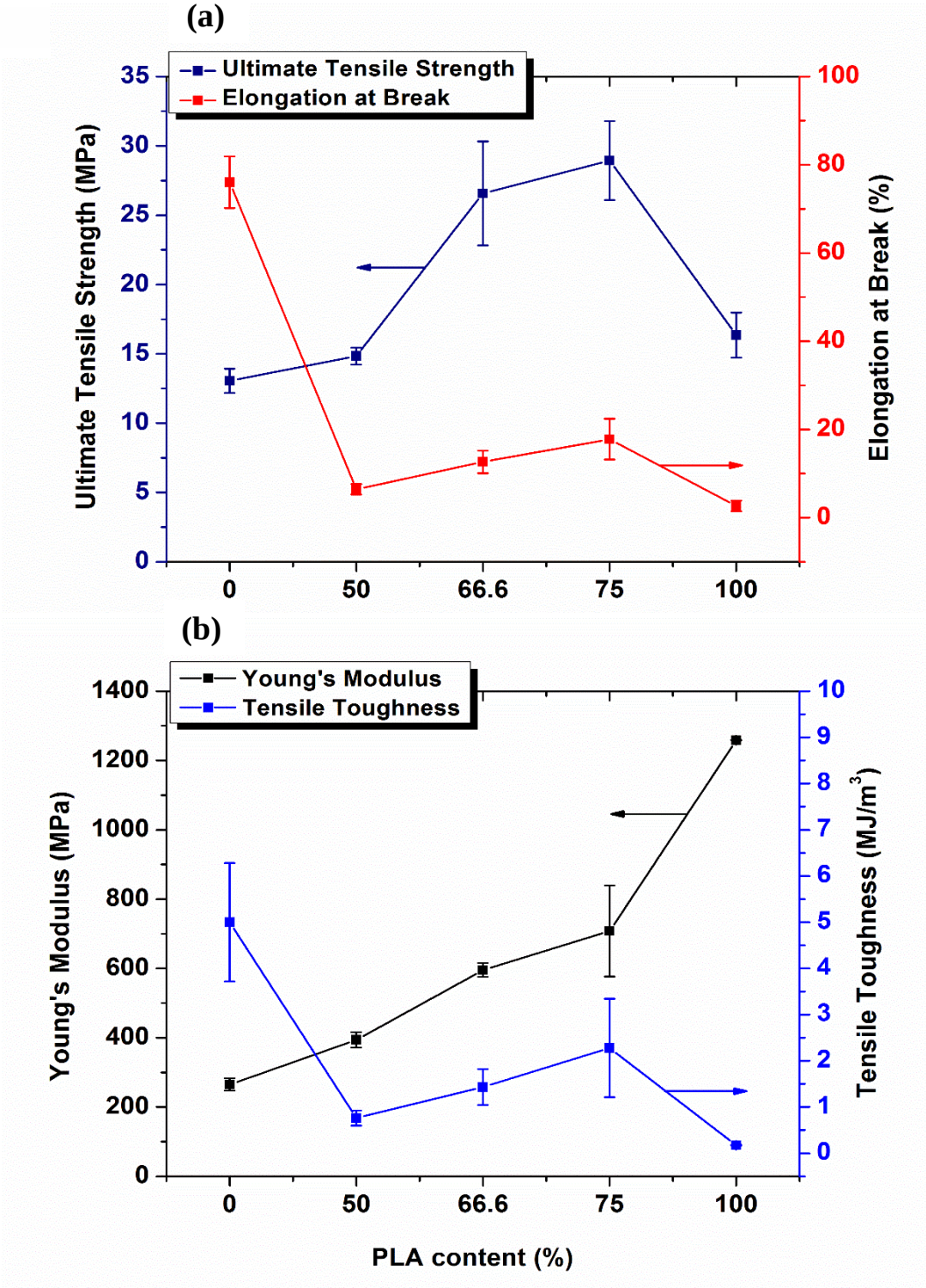

Figure 3.5-2: Representative data for (a) UTS and elongation at break, (b) Young's modulus and tensile toughness of homopolymers and diblock copolymers.

***0**=30CL
***100**=30D
***50**=10CL-10D
***66.6**=10CL-20D
***75**=10CL-30D

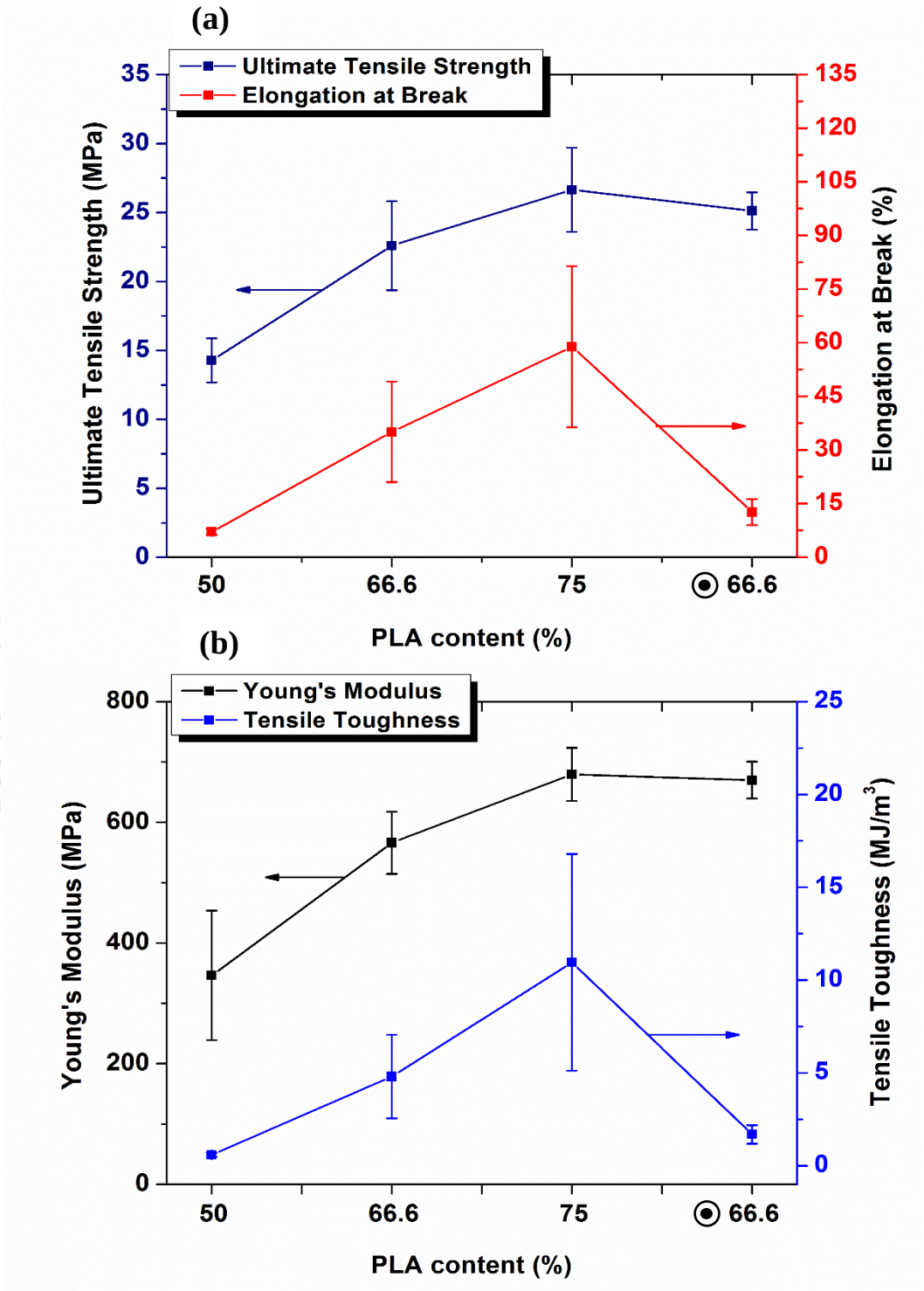

Figure 3.5-3: Representative data for a) UTS and elongation at break, b) Young's modulus and tensile toughness of diblock blends and tri-sb copolymer.

***100**=30D
*◉ **66.6**=10CL-10L-10D
* **50**=B_10-10
***66.6**=B_10-20
***75**=B_10-30

Table 3.3: Mechanical properties of synthesized homopolymers, diblock copolymers, enantiomeric blends and tri-sb copolymer.

Identity	**Sample code (PLA content, %)**	**Ultimate tensile strength (MPa)**	**Young's Modulus (MPa)**	**Elongation at break (%)**	**Tensile toughness (MJ/m^3)**
Homopolymers and Diblock copolymers					
30CL	0	13.1 ± 0.9	265.2 ± 17.9	76.1 ± 5.9	5 ± 1.3
10CL-10D	50	14.9 ± 0.6	394.1 ± 22.2	10.7 ± 2.1	0.8 ± 0.2
10CL-20D	66.6	26.6 ± 3.8	595.4 ± 20.2	12.7 ± 2.5	1.4 ± 0.4
10CL-30D	75	28.9 ± 2.8	707.9 ± 131.3	17.8 ± 4.6	2.3 ± 1.1
30D	100	16.6 ± 1.6	1258.5 ± 0.8	2.7 ± 1.2	0.2 ± 0.0
Block copolymers possessing Stereocomplexation					
B_10-10	50	14.3 ± 1.6	346.1 ± 107.2	7.1 ± 0.9	0.6 ± 0.1
B_10-20	66.6	22.6 ± 3.2	566.1 ± 51.6	35.1 ± 14.0	4.8 ± 2.3
B_10-30	75	26.7 ± 3.1	679.3 ± 44.1	58.9 ± 22.5	11.0 ± 5.9
10CL-10L-10D	⦿66.6	25.1 ± 1.3	670 ± 30.4	12.6 ± 3.6	1.7 ± 0.5

The temperature dependent storage modulus of the block copolymer films is shown in **Figure 3.6**. The samples of PDLA and B_10-10 were too brittle to be analysed. The storage modulus, tan δ and T_g for the remaining samples at 30 °C are outlined in **Table 3.4**. The storage modulus of PCL is as low as 380 MPa which is significantly enhanced upon copolymerization with PDLA. Further, as the block length of PDLA increases (in case of diblock copolymers), an evident increase in the storage modulus is found which is attributable to the increasing molecular weight of the copolymer. The same effect is observed in the case of blend samples. However, the storage modulus of the triblock

copolymer sample is found to be higher than that of 10CL-20D and B_10-20 having the same molecular weight. This may signify that stereocomplexation enhances the storage modulus of the film. The tanδ curves in **Figure 3.6(b)** indicate that T_g increases with increasing the block length. The storage modulus (at 30° C) of B_10-30 is slightly lower than that of 10CL-30D but it is found to increase with the temperature. A rapid decrease in storage modulus below the glass transition region of PDLA is observed due to the melting of PCL and its diffusion into the domain. Above T_g, PDLA chains tend to crystallize by themselves and this possibly leads to the increase in storage modulus up to a certain extent.

Table 3.4: Storage modulus, tan δ and glass transition temperature (T_g) determined from DMA.

Sample identity	**Storage modulus (MPa), at 30° C**	**Tan δ**	**T_g (° C)**
30CL	380 ± 91	-	-
10CL-10D	960 ± 95	0.84 ± 0.08	54.6
10CL-20D	1743 ± 81	0.53 ± 0.05	62.5
10CL-30D	2270 ± 127	0.44 ± 0.04	63.1
B_10-20	1685 ± 25	0.39 ± 0.04	63.4
B_10-30	1943 ± 133	0.47 ± 0.07	66.6
10CL-10L-10D	1854 ± 105	0.62 ± 0.11	65.5

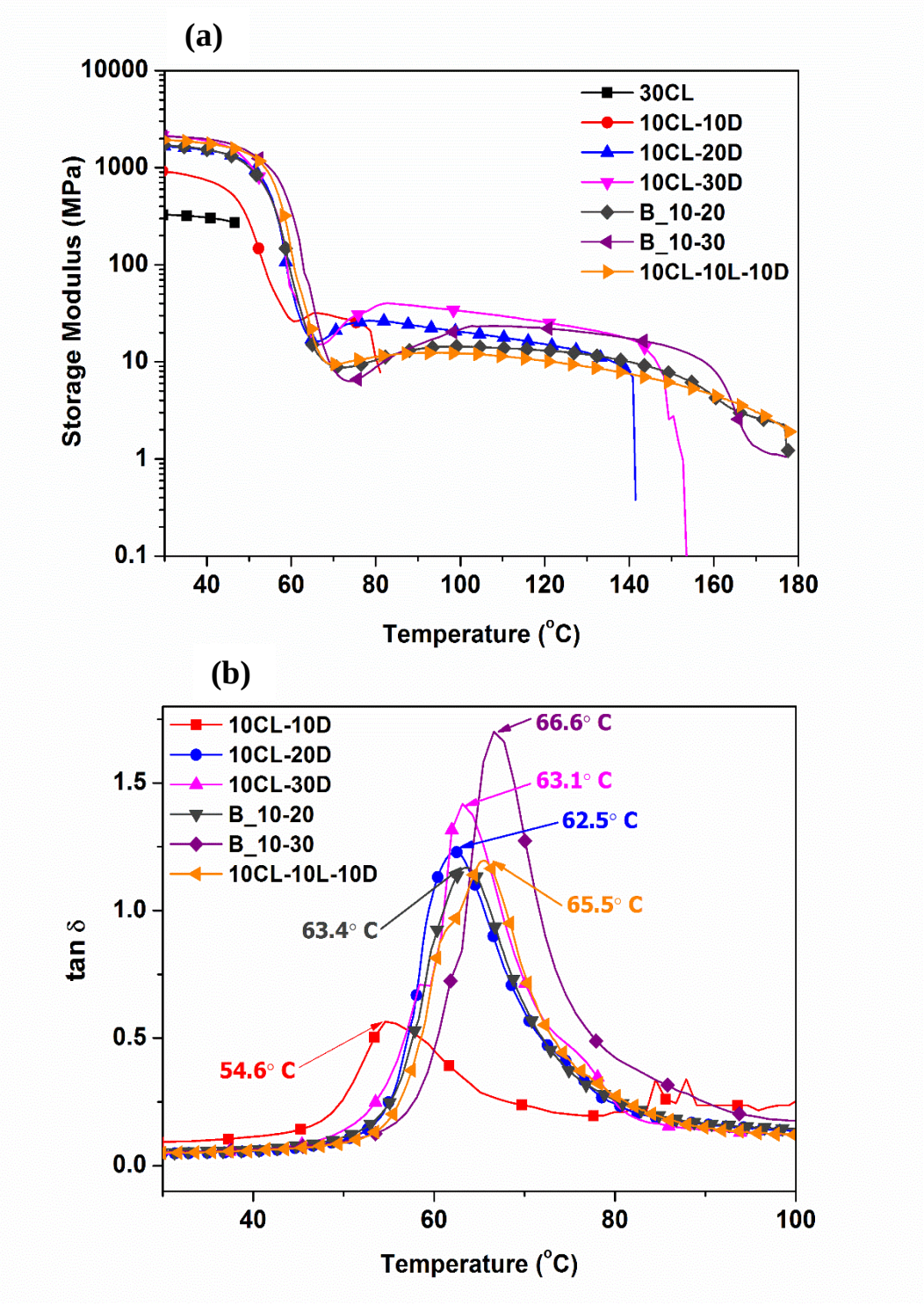

Figure 3.6: Temperature-dependent changes in (a) storage modulus of homopolymer, diblock copolymers, diblock copolymer blends and tri-sb copolymer; (b) tan δ.

3.3.4 Crystallization behavior

From the above discussion, it is observed that blending the diblock copolymers leads to the significant improvement in mechanical properties which is due to the stereocompelxation. In order to obtain insights into the stereocomplex crystallization in the enantiomeric blends and tri-sb copolymer, X-ray diffraction (XRD) studies are conducted. The representative XRD spectra are shown in **Figure 3.7**. The PLA homopolymers and stereocomplex polymers are known to crystallize in pseudo-orthorhombic unit cell and triclinic unit cell containing 10_3 and 3_1 helical structures respectively. The diffraction peaks at 11.8 º and 20.7 º in the spectra correspond to (110), (300/030)[36] crystal planes of stereocomplex crystallites whereas the peaks at 21.3º and 23.7º correspond to (110) and (200) lattice planes of PCL[165]. Additionally, the diffraction peak at 23.9º correspond to the (220) crystal plane of stereocomplex PLA which would have merged with that of PCL. It is evident from the spectra that the major diffraction peaks of PCL and stereocomplex PLA are present in the synthesized enantiomeric diblock blends and tri-sb copolymer indicating the presence of both moieties. Further, it is known that the diffraction peaks of PLA homopolymer are usually found at 14.7º, 16.5 º and 18.9 º corresponding to (010), (200) and (014)/(203) crystal planes[166] respectively. It is reported by Konishi et al. that the semicrystalline polymers (having a faster crystallization rate) often acquire an intermediate state between crystalline and amorphous states upon quenching which is known as "mesophase.[167] In line to this, Zhang et al. reported that PLLA attains a mesophase in the PLLA-PEG-PLLA block copolymer upon quenching due to its faster crystallization rate.[168] This effect was accounted for the lower T_g of PEG and lower molecular weight of PLLA block which was supported by WAXD. In the present case, a similar phenomenon is observed for the synthesized

copolymers as shown in **Figure 3.7-1**. The diffraction peaks of PCL and B_10-10 are evident of their crystalline nature even in the melt quenched state but the diffraction peak for PDLA is found to be absent. Also, relatively broad diffraction peaks for B_10-20, B_10-30 and 10CL-10L-10D are observed upon melt quenching which become intense on annealing at 120 ℃ for 1 h. This effect may be indicative of the mesophase of PDLA in the melt quenched state in the copolymer system. This would be because of the relatively lower molecular weight of PDLA in and the lower T_g of PCL which possibly enhances the molecular mobility of PDLA thereby enhancing the rate of crystallization of PDLA in the copolymer system. **Figure 3.7-2** shows the absence of the diffraction peaks for PDLA homocrystals in B_10-10 and 10CL-10L-10D which strongly supports the results obtained from DSC in the previous sections indicating the presence of only stereocomplex crystallites.

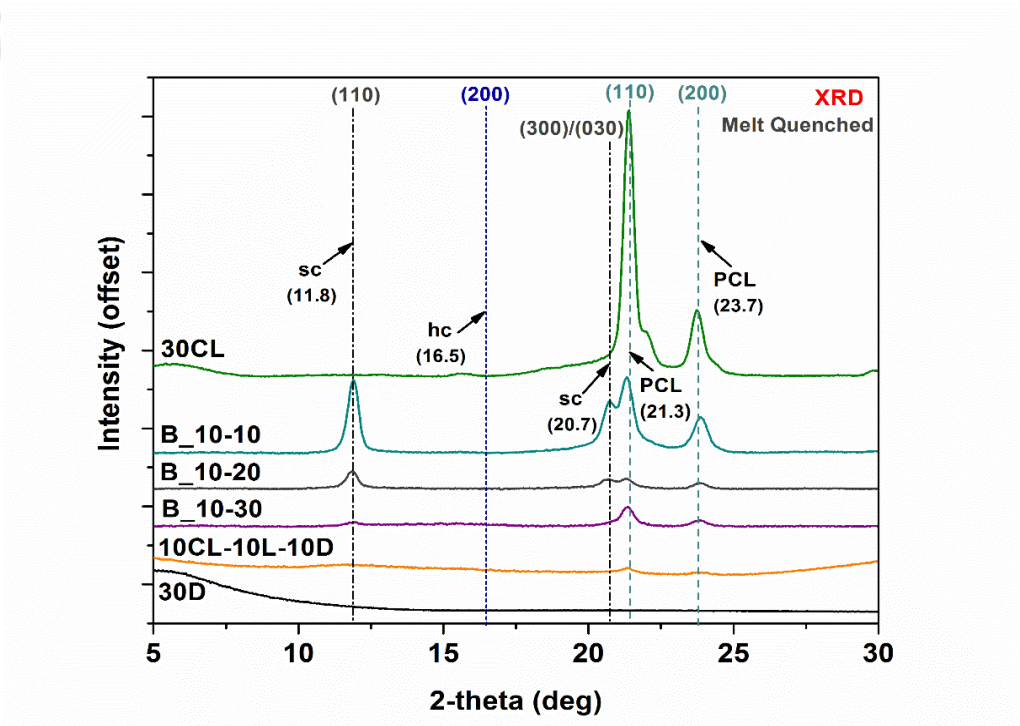

Figure 3.7-1: Intensity vs 2-theta of homopolymers, enantiomeric diblock blends and tri-sb copolymer.

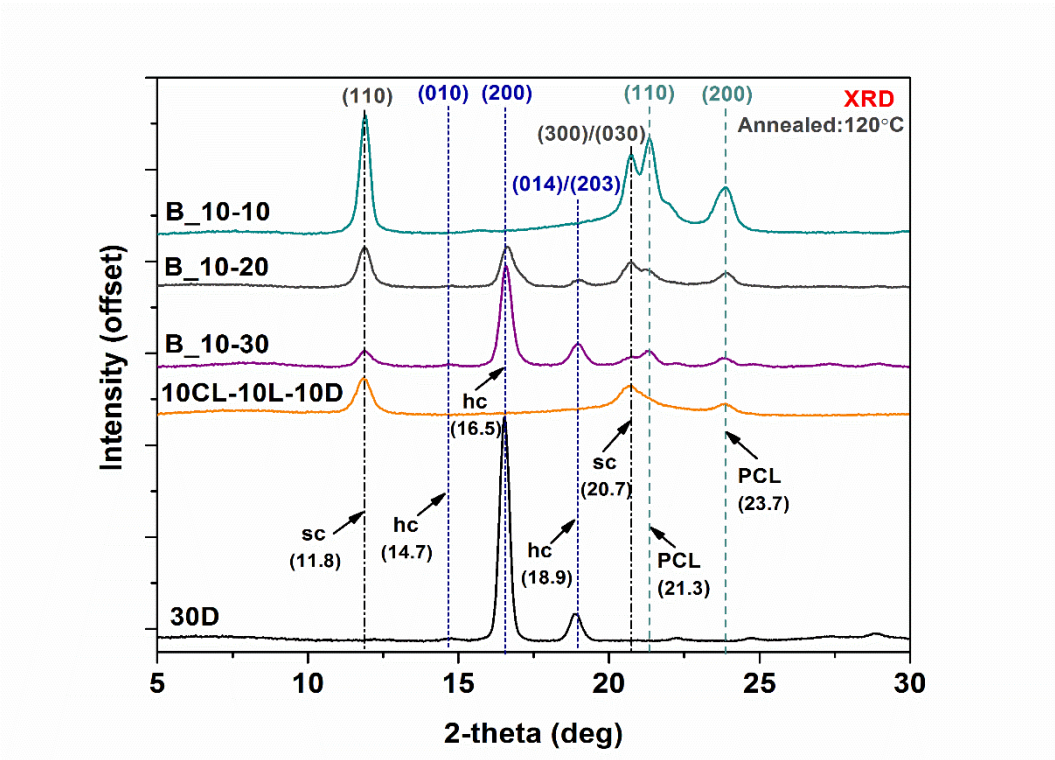

Figure 3.7-2: Intensity vs 2-theta of homopolymers, enantiomeric diblock blends and tri-sb copolymer after annealing at 120 °C for 1 h.

3.3.5 Thermal processability and thermomechanical stability

The processing of the biodegradable polymers using conventional techniques still remains a challenge and is often accompanied by the incorporation of several fillers/additives into the polymer matrix so as to enhance their thermal processability. However, the incorporation of fillers/additives into the polymers made for biomedical applications may impart toxic long/short term effects into the human body and thus may not be desirable.[169] In this regard, the direct processing of the biodegradable polymers would serve as an effective approach. In the current work, among all the synthesized materials, diblock copolymer (10CL-30D) and enantiomeric blend (B_10-30) are chosen pertaining to their relatively higher molecular weight for the direct thermal processing. The samples are successfully processed as shown in **Figure 3.8** in order to fabricate the cortical and

cancellous bone screws which are regarded as orthopaedic fixation devices. Additionally, the TGA analysis (in the above sections) indicate an enhancement in the thermal stability of PLA upon incorporation of PCL as a block segment.

Furthermore, the stereocomplexation in PLA has been reported to enhance the thermomechanical stability of the resulting material. In a study conducted by Srisuwan et al., heat-resistant stereocomplex PLA/poly(ε-caprolactone-co-L-lactide) blend films were made by *in situ* melt blending followed by compression molding wherein the stereocomplex PLA is reported to enhance the heat resistance while the copolyester fraction is accounted for reducing the brittleness of the film[170]. Similarly, in the present work, the stereocomplex crystallites as hard segments may be improving the heat stability of the system whereas the soft segments (PCL) may be imparting plasticization effect and thus reducing the brittleness of the polymer during processing. In this regard, a visual inspection of the thermomechanical stability of the cancellous bone screw made using the enantiomeric blend (B_10-30) possessing stereocomplexation has been conducted and compared with commercially available PLA (PLA 2003D, NatureWorks). The cancellous screw made using enantiomeric diblock blend (B_10-30) is found to be thermo-mechanically stable at 121 °C over a duration of 60 min whereas a deformation is observed in case of the cancellous screw made from commercial PLA over a period of 10 min **(Figure 3.9)**. The enhanced thermomechanical stability of the synthesized material renders it suitable for applications such as biomedical implants that require the steam sterilization which is usually conducted at 121 °C.

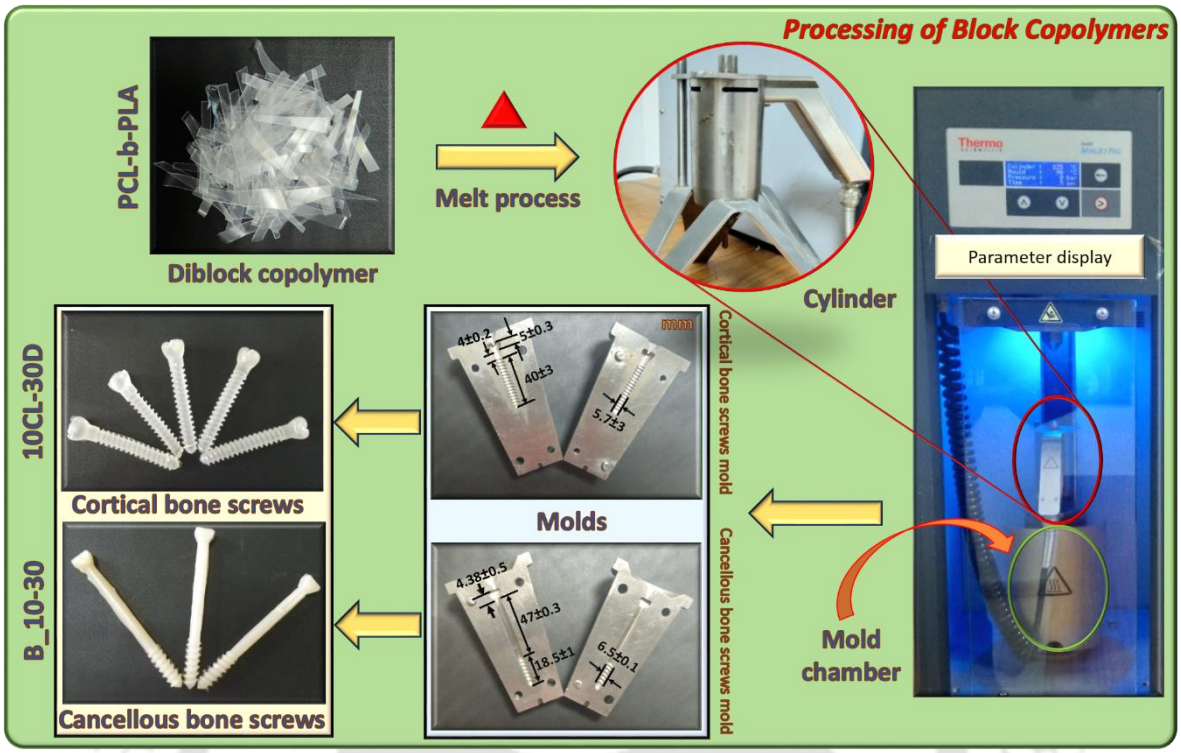

Figure 3.8: Thermal processing of diblock copolymer and enantiomeric diblock blend to yield representative orthopedic fixation devices.

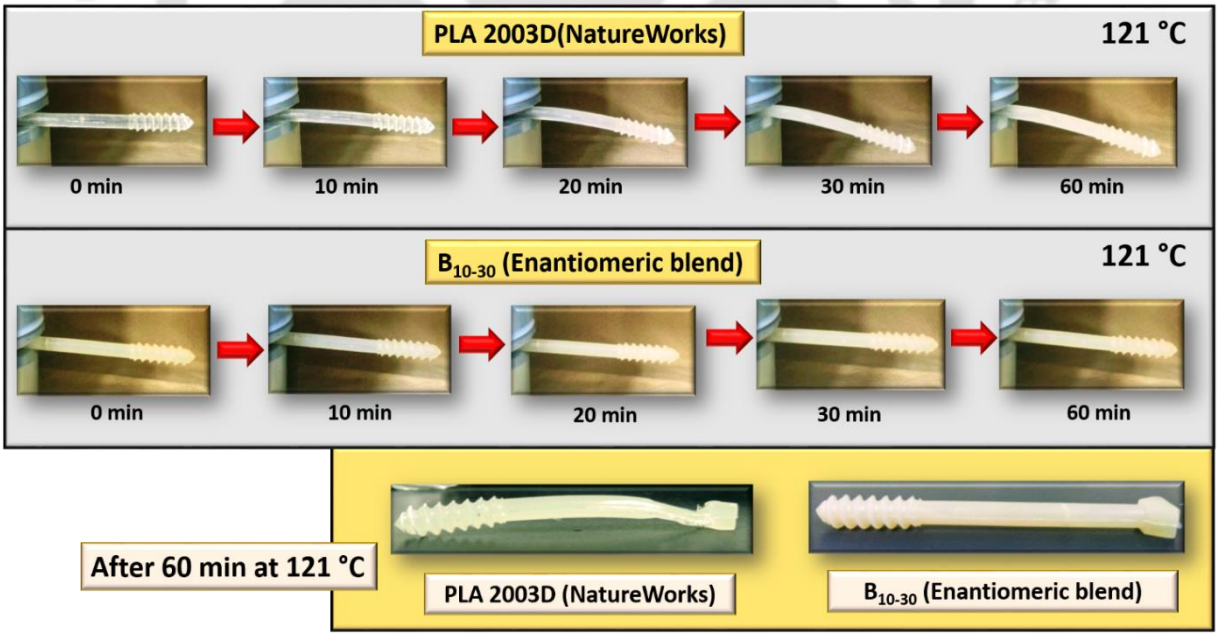

Figure 3.9: Thermo-mechanical stability of the cancellous bone screw made from enantiomeric diblock blend and commercial PLA 2003D (NatureWorks) at 121 °C.

3.3.6 Biocompatibility

Figure 3.10 shows MG-63 cell viability on PCL, PDLA, diblock copolymers, enantiomeric diblock copolymer blends and tri-sb copolymer. It is apparent from the results that MG-63 cells adhere and multiply on the surfaces of the synthesized materials up to 13 days indicating the biocompatible nature of the materials. Further, one-way ANOVA is used to determine the significance of the cell viability data and p-value (probability value) < 0.05 indicates that the results are statistically significant. Further, the representative images of MG-63 cell adhesion onto the surface of the synthesized samples after 1 day is shown in **Figure 3.11**. The green color indicates the cells stained with acridine orange which is evident of the cell adhesion on the surface of the synthesized homopolymers and block copolymers and thus their biocompatible nature.

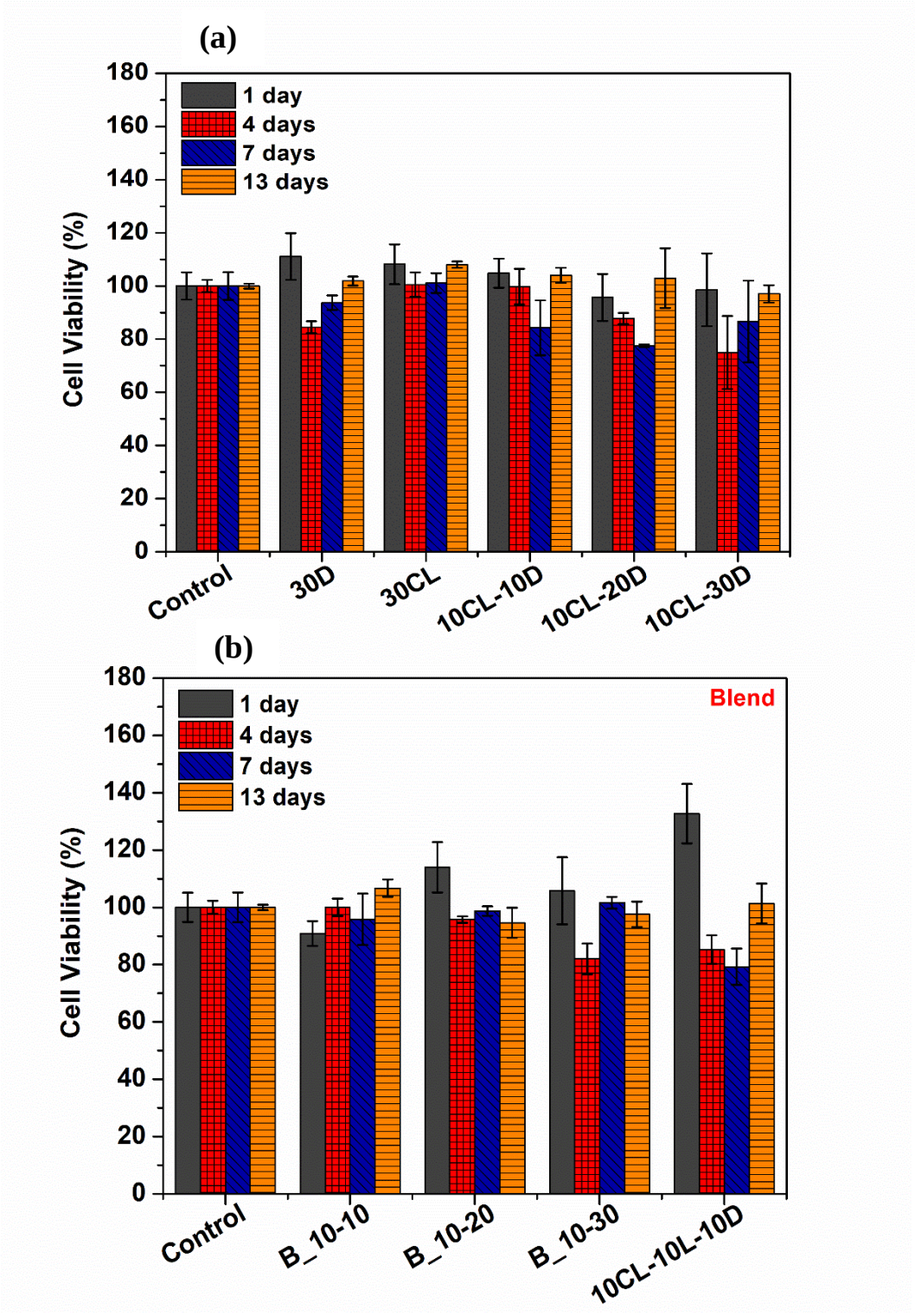

Figure 3.10: MG-63 cell viability on (a) homopolymers and diblock copolymers (b) diblock blends and tri-sb; along with control after 1, 4, 7 and 13 days.

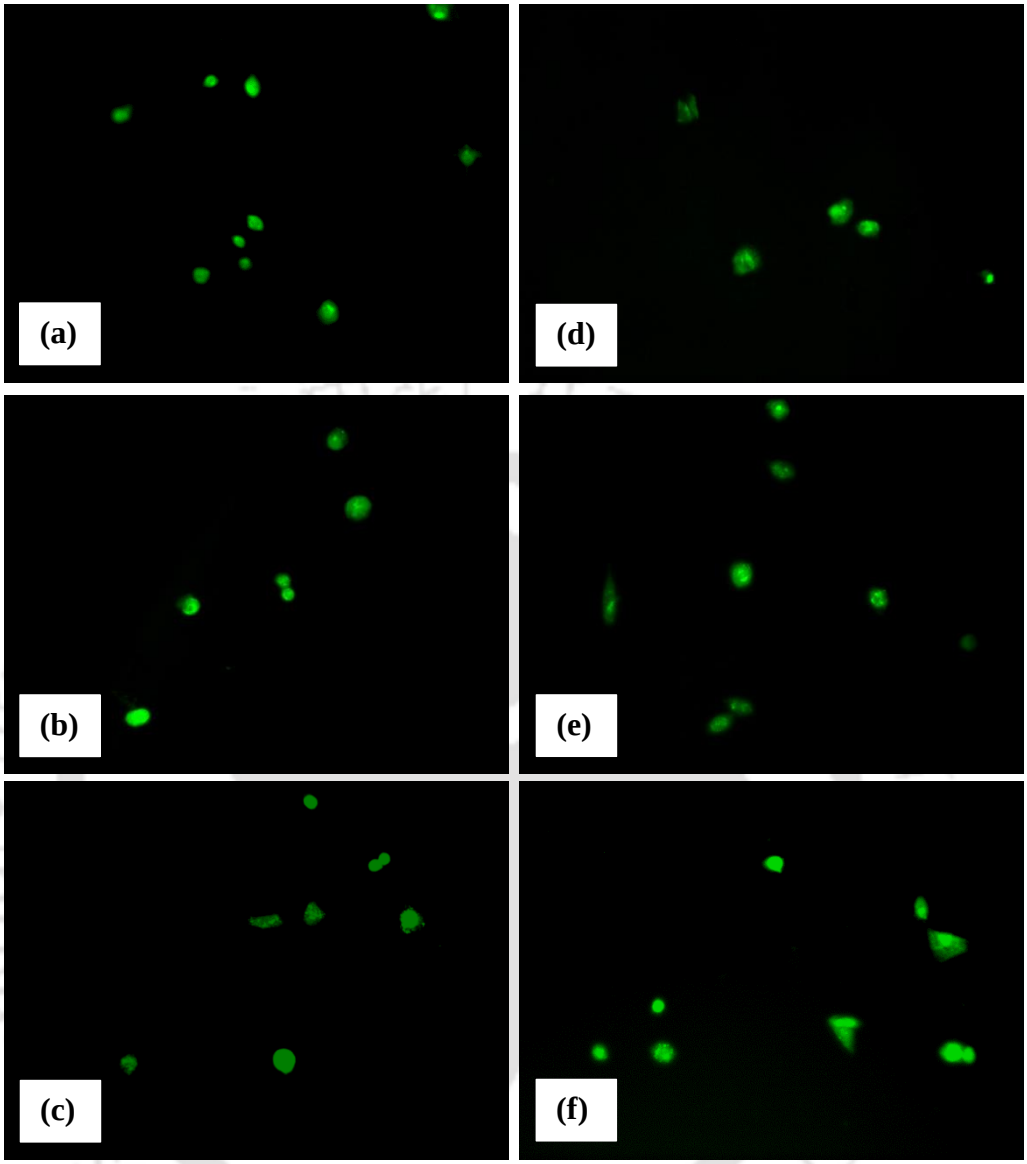

Figure 3.11: MG-63 cell adhesion on (a) control, (b) 30 CL, (c) 30D, (d) 10CL-30D, (e) B_10-30 and (f) 10CL-10L-10D after 1 day and staining with acridine orange.

3.4 Conclusion

In the current work, the diblock copolymers based on PCL and PDLA/PLLA and the enantiomeric blends thereof along with a stereo-triblock copolymer are successfully synthesized by targeting their molecular weight. The effect of block length on the thermal, mechanical and crystallization behavior of the synthesized materials have been illustrated in detail. Furthermore, the selected formulations of the diblock copolymer (10CL-30D) and the enantiomeric blend (B_10-30) are directly processed using injection molding process to fabricate the representative orthopedic fixation devices such as cortical and cancellous bone screws respectively. Also, the cancellous screws made from the enantiomeric blend are found to be thermo-mechanically stable at 121 °C as compared to the commercial PLA 2003D. The developed material may thus be considered as suitable for sterilization when used for applications *in vivo*. The biocompatibility of the synthesized homopolymers and block copolymers is determined from MTT assay using MG-63 (human bone osteosarcoma) cells and stained with acridine orange which is evident of the adhesion of cells on the surface of the synthesized materials. The current work is therefore a holistic approach towards developing biodegradable, biocompatible, thermally processable and potentially sterilizable materials for intended biomedical applications.

Chapter: 4

Triblock Copolymers based on PLA and PCL, and their Stereocomplex Blends

Graphical Abstract

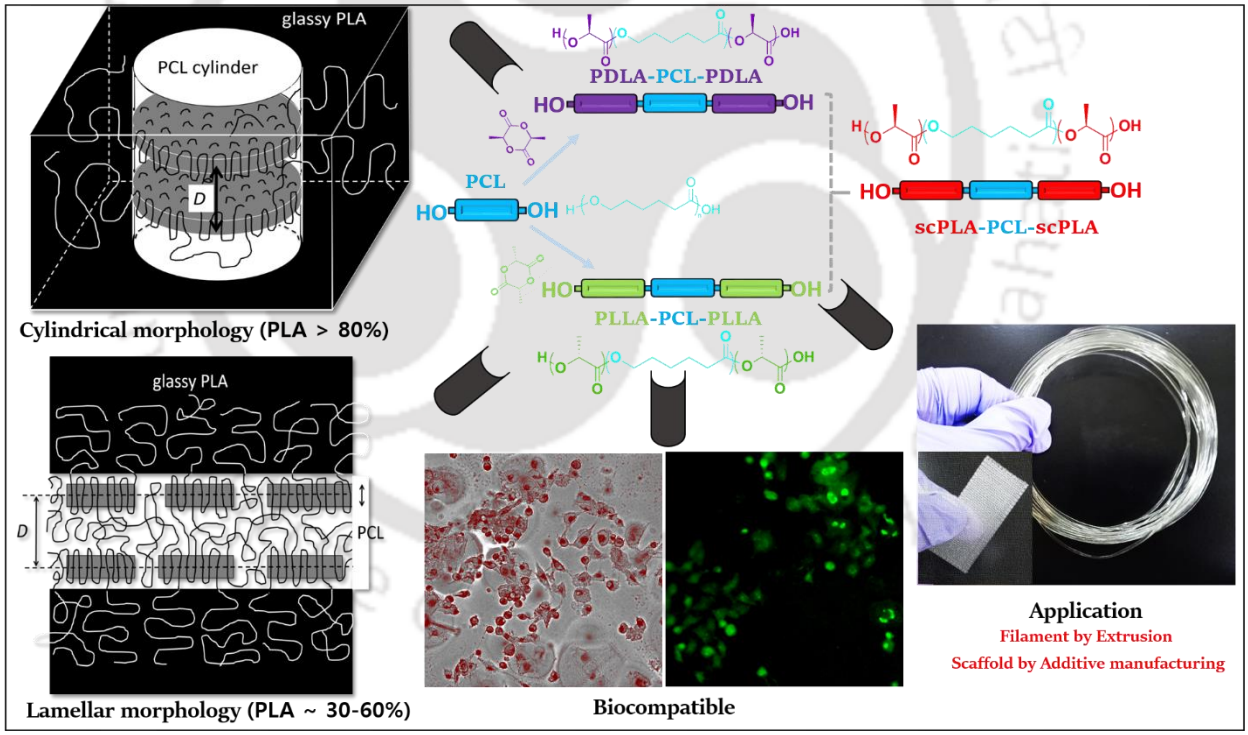

Outcome:

- *Toughened PLA-b-PCL-b-PLA Triblock Copolymer based Biomaterials: Effect of Self-Assembled Nanostrcuture and Stereocomplexation on the Mechanical Properties. Polymer Chemistry, 12 (2021): 3809-3824.*

Abstract

The current research unfolds the effect of the block lengths, microdomain morphology and stereocomplexation on the mechanical properties of the PLA-PCL-PLA triblock copolymers where PCL is involved to improve the poor extensibility of PLA. The linear triblock copolymers PLLA-PCL-PLLA and PDLA-PCL-PDLA (PLLA: poly (L-lactic acid) and PDLA: poly (D-lactic acid)) are made by two step ring opening polymerization and blended in 1:1 ratio to achieve the stereocomplex blends where the molecular weight of the terminal as well as the mid segment is tailored. The mechanical strength and elongation at break range from 13 MPa to 36 MPa and 540 to 950%, respectively, for the triblock copolymers with varied block lengths. Such wide-ranged mechanical properties are ascribed to the morphology of self-assembled-nanostructure of triblock copolymers as corroborated with the small angle X-ray scattering (SAXS) results. To render it industrially viable, the process of triblock copolymer synthesis is scaled up to ~500 g batch followed by its processing using the twin-screw extruder to make the filament which is used for 3D printing of a mesh-type scaffold. The synthesized materials are tested for their biocompatibility by performing MTT assay using the rat bone osteosarcoma (UMR-106) cells which renders them as potential biomaterial.

4.1 Introduction

Block copolymerization serves as an effective strategy for chemically connecting the immiscible polymers at the molecular level which prevents the macrophase separation between them[171,172]. More often, the block copolymerization has been adopted to develop materials with hybrid properties that are otherwise difficult to be achieved by a homopolymer alone or by random copolymerization[173,174]. The widely studied class of aliphatic polyesters viz. poly(lactic acid) (PLA)[175-177] and poly(ε-caprolactone) (PCL)[178] manifest interesting and complementary properties[179,180] which are often used in combination to obtain the copolymers with tailored properties[181]. PCL is known for its high toughness, however suffers from the drawbacks of lower yield strength and modulus. PLA on the other hand, has high strength and modulus with a very low elongation. Further, the lower glass transition temperature (T_g) and lower melting temperature (T_m) of PCL restricts its use in widespread applications. Additionally, PLA is a bio-derived material whereas PCL is derived from petroleum feedstock.

Block copolymers of PCL and PLA are made by adopting the simplest strategy of sequential ring opening polymerization[182] which allows the effective control of the molecular weight of the individual block segments[183,184]. Further, the existence of the enantiomers of PLA, i.e., poly(D-lactic acid) (PDLA) and poly(L-lactic acid) (PLLA), permits the exploitation of the stereocomplex crystals[185] which is formed by the enantiomeric PLA chains and completely different from the PLA homopolymer crystalline structure[65,186]. The melting temperature of the stereocomplex PLA (sc-PLA) is much higher ~50 °C as compared to the PLA homopolymers[73,37], due to the densely

packed crystalline chains, which is also reported to enhance the thermal stability of the materials[187,96].

PLA and PCL have been approved by FDA[188,189] for their use in the gene and drug delivery systems, rendering their safety and potential to be used for the biomedical/clinical[190] applications. The commercial biomedical applications of PLA and/or PCL include the contraceptives[191], sutures[192,193], nerve conduits[194], etc., which further extend their exploration in the bone tissue engineering applications[195,87]. Further, PCL has been effectively used for toughening the brittle materials by chemical modification[196], blending[197] or copolymerization[198]. Lately, efforts have also been made to develop the stereocomplex block copolymers based on PLA[199] for the applications such as hydrogels[200] drug delivery[201] and tissue engineering[202,203].

Taking advantage of the flexibility of PCL, high strength of PLA and thermal stability of sc-PLA, it is possible to develop biodegradable materials with tailored properties such as high strength and toughness along with thermal stability. Achieving a control over the block length of the individual segments further lead to the development of materials with desired mechanical properties[204,205] as the molecular weight remains to be the controlling factor[206,207]. Additionally, the backbone architecture significantly alters the mechanical properties[208,209] including the self-assembly[210,211] of block copolymers. Analogous to this, in the previous chapter, we reported the synthesis of linear diblock copolymers (PCL-PLA) and their stereocomplex blends wherein we achieved an increase in elongation (at break) up to 9 fold for the diblocks and 29 fold for the stereocomplex diblocks as compared to neat PLA[86]. However, the elongation (at break) was increased to several hundred folds when PCL was placed between the PLA terminals (linear triblock

copolymers) which has been elaborated in the present research. Jing et. al. reported the synthesis of PLA-PCL-PLA triblock copolymers followed by their terminal functionalization to develop shape memory polymers[212]. They reported the behavior of PLA-PCL-PLA as brittle solids whereas the multiblock copolymers were reported as thermoplastic elastomers. However, the maximum elongation achieved by the multiblock copolymers was ~500% with a compromise on the yield strength (~7 MPa). Furthermore, Jiao et. al. reported the synthesis of multiblock copolymers by chain extension of the PLA-PCL-PLA triblock copolymers[213]. The multiblock copolymers showed an increase in elongation with a compromise on the tensile strength as well as the storage and elastic modulus. The maximum elongation achieved was ~120% and the storage modulus was ~20 MPa when the PCL content was increased to 30%. In a study reported by Li et. al., sc-PLA was reinforced into PCL by solution blending and with the increasing content of sc-PLA, the tensile yield strength was found to increase to ~20 MPa whereas the elongation dropped to ~450% when the content of sc-PLA was increased to 30%. These studies indicate the potential of using PCL and PLA in developing toughened materials, however a trade-off is usually observed between the tensile strength and the elongation at break. Although, it is well-known that ABA triblock copolymers including PLA (or PLLA) side blocks are toughened, the resulting Young's modulus, yield strength and ultimate tensile strength have gradually been decreased [214]. Further, little attention has been paid on identifying the effect of block lengths on the mechanical properties of block copolymers and their correlation with the self-assembly.

Here, we report the synthesis of PLLA-PCL-PLLA and PDLA-PCL-PDLA triblock copolymers and their stereocomplex blends wherein the block lengths of both PCL and PLA moieties are varied and their effect on various properties are evaluated. The

molecular weight of the block copolymers as well as stereocomplexation are the governing parameters for controlling the macroscopic properties which may be explored for developing customized materials. Taking into consideration of the large-scale preparation and acceptance of block copolymers, we present the solvent-free scale-up synthesis process for the triblock copolymers with the controlled molecular weight, followed by its processing using the conventional twin-screw extruder in order to develop a filament for 3D printing of the representative scaffold. The synthesized materials are further tested for their biocompatibility using the rat bone osteosarcoma cells where the bone cells are found to adhere on the polymer surfaces, indicating their non-toxic nature.

4.2 Experimental section

4.2.1 Materials

ε-Caprolactone was purchased from Nacalai Tesque, Kyoto, Japan which was distilled and stored under an inert environment. D- and L-lactides (optical purities 99.9%) were purchased from Musashino Chemical Laboratories, Ltd. Tokyo, Japan. 1,12-Dodecanediol (DMG) was procured from Tokyo Chemical Industry Co., Ltd., Tokyo, Japan. Tin octoate ($Sn(Oct)_2$, 95%) was acquired from Sigma Aldrich, St. Louis, USA via Nacalai Tesque and distilled under high vacuum followed by dissolving in dried toluene (0.2 g/ml and 0.5 g/ml) and stored under an inert environment. 1,1,1,3,3,3-Hexafluoro-2-propanol was obtained from Central Glass Co. Ltd., Yamaguchi, Japan. Chloroform (HPLC grade) was obtained from Merck & Co., India. Dichloromethane and methanol were purchased from Nacalai Tesque and used without purification.

4.2.2 Step 1 ROP: Synthesis of macroinitiator

In the first step, di-hydroxyl terminated PCL was synthesized by ring opening polymerization (ROP) of ε-caprolactone in the presence of DMG as an initiator and $Sn(Oct)_2$ catalyst as shown in **Scheme 4.1**. Briefly (for the case of 20D-11CL-20D), the initiator (DMG, 0.495 mmol) was added to the polymerization apparatus fixed with a three-way connector and a magnetic stirrer, and evacuated at 10 Pa for 3h with intermittent N_2 purging followed by adding the pre-distilled monomer (ε-caprolactone, 43.8 mmol) and a catalyst solution (tin octoate, 0.175 mmol) with a syringe under N_2 atmosphere. The apparatus was sealed under N_2 atmosphere and immersed in an oil-bath at 180º C, and the polymerization reaction was conducted for 25 min. After the reaction, a part of product was withdrawn to determine the conversion by ^{1}H-NMR. As the conversion of PCL was higher than 99%, the product was directly subjected to next step without further purification. The macroinitiator was thus synthesized using a solvent-free route.

PCL, ^{1}H-NMR (600 MHz, $CDCl_3$): δ = 4.06 ($CH_2CH_2CH_2CH_2C\underline{H}_2O$-), 3.65 ($CH_2CH_2CH_2CH_2C\underline{H}_2OH$), 2.3 ($OC\underline{H}_2CH_2CH_2CH_2$-), 1.64 ($OCH_2C\underline{H}_2CH_2C\underline{H}_2CH_2O$-), 1.38 ($OCH_2CH_2C\underline{H}_2CH_2CH_2O$), 1.25 (-$OCH_2C\underline{H}_2(CH_2)_8C\underline{H}_2CH_2O$-), 0.88 (-$OCH_2CH_2(C\underline{H}_2)_8CH_2CH_2O$-) ppm

4.2.3 Step 2 ROP: Synthesis of ABA triblock copolymers

ABA type triblock copolymers were synthesized in the second step (ROP) where the monomer (D- or L-lactide, 143 mmol) was added to the synthesized macroinitiator (for the same case as above) and evacuated at 10 Pa. The monomer was kept for drying at room temperature for 1 h followed by drying at 40 ℃ for 12 h. After drying the

monomer, the system was filled with N_2 gas and immersed into the oil-bath at 180 °C where PCL and lactide were melted. After the complete solubilization of the monomer into the melt of macroinitiator, a catalyst solution (0.057 mmol) was added with a syringe and the reaction was continued for 25 min. After the reaction, a sample was withdrawn to determine the conversion by ^{1}H-NMR. The synthesized triblock copolymer was dissolved in dichloromethane and precipitated in excess methanol. The precipitates were filtered and dried under vacuum at 80 °C for 12 h. The block copolymers are designated as *X*D-*Y*CL-*X*D or *Z*L-*Y*CL-*Z*L where *X*, *Y* and *Z* represent the molecular weights (kDa) of the sequences PDLA (D), PCL (CL) and PLLA (L), respectively.

PDLA, ^{1}H NMR (600 MHz, $CDCl_3$): δ = 5.17 (OCC$\underline{H}_2$CH$_3$O), 4.36 (OCC$\underline{H}_2$CH$_3$OH), 4.12 (OC$\underline{H}_2$CH$_2$(CH$_2$)$_8$CH$_2$C$\underline{H}_2$O), 1.57 (OCCH$_2$C$\underline{H}_3$O), 1.25 (-OCH$_2$C$\underline{H}_2$(CH$_2$)$_8$C$\underline{H}_2$CH$_2$-O-), 0.88 (-OCH$_2$CH$_2$(C$\underline{H}_2$)$_8$CH$_2$CH$_2$O-) ppm.

Triblock copolymer, ^{1}H NMR (600 MHz, $CDCl_3$): δ = 5.17 (OCC$\underline{H}_2$CH$_3$O), 4.36 (OCC$\underline{H}_2$CH$_3$OH), 4.06 (CH$_2$CH$_2$CH$_2$CH$_2$C$\underline{H}_2$O-), 2.3 (C$\underline{H}_2$CH$_2$CH$_2$CH$_2$CH$_2$O-), 1.64 (OCH$_2$C$\underline{H}_2$CH$_2$C$\underline{H}_2$CH$_2$O-), 1.38 (OCH$_2$CH$_2$C$\underline{H}_2$CH$_2$CH$_2$O), 1.25 (-OCH$_2$C$\underline{H}_2$(CH$_2$)$_8$C$\underline{H}_2$CH$_2$O-), 0.88 (-OCH$_2$CH$_2$(C$\underline{H}_2$)$_8$CH$_2$CH$_2$O-) ppm

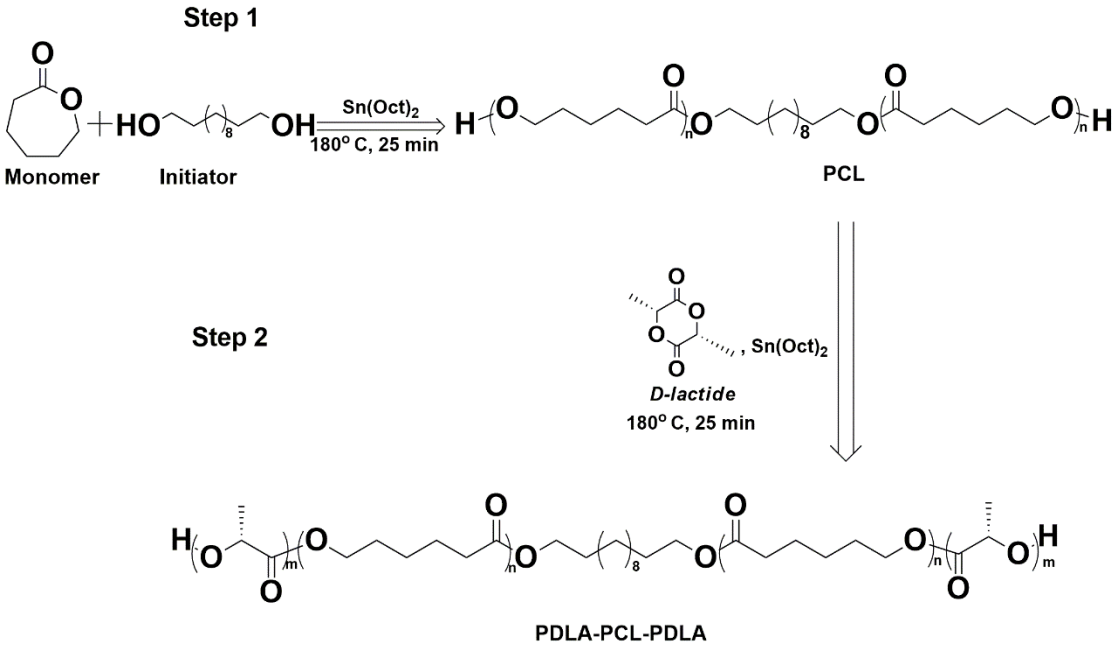

Scheme 4.1: Synthesis route to PDLA-PCL-PDLA triblock copolymers via two-step ring-opening polymerization (ROP).

4.2.4 Fabrication of enantiomeric blends of block copolymers

The enantiomeric triblock copolymers were blended in 1:1 ratio in order to achieve the stereocomplexation in the block copolymers. Typically, 2 g each of the triblock copolymers (20D-11CL-20D and 19L-18CL-19L) were added to a glass beaker with a mixture of dichloromethane (45 ml) + hexafluoroisopropanol (5 ml) and stirred until complete dissolution. The dissolved material was reprecipitated into excess methanol, and the obtained filtrates were dried under vacuum at 80 ℃ for 12 h.

4.2.5 Melt compression molding

The synthesized triblock copolymers and their blends were compression molded to make the films for evaluating their properties. For instance, the triblock copolymer 20D-11CL-20D was held between two Teflon sheets with an aluminum spacer having a window (5 cm × 5 cm) with the thickness of ~200 μm, which was compression molded

at 210 °C for 5 min at 1 MPa followed by quenching in ice-water. Similarly, the enantiomeric blend specimens were made with the molding temperature set to 235 °C.

4.2.6 Characterization

^{1}H and ^{13}C NMR measurements were performed using AV600 spectrometer (Bruker, Germany). The synthesized materials were dissolved in deuterated chloroform ($CDCl_3$) containing 0.03% tetramethylsilane (TMS) as an internal reference.

Gel permeation chromatography (Shimadzu, Japan) was used to determine the number- (Mn) and weight-average (Mw) molecular weights of the synthesized samples. The measurements were conducted at 40 °C by using the HPLC grade chloroform as an eluent with a flow rate of 1 ml/min. The equipment consisted of LC-20AD pump, RID-10A refractive index detector and SIL-20A HT auto sampler, and the polystyrene standards (370 Da to 500 kDa) were used for the calibration of columns. The sample solutions (20 mg/ml) were filtered by syringe filters (0.45 μm) prior to measurements.

Wide angle X-ray scattering (WAXS) measurements were conducted using a Powder X-ray Diffractometer (Rigaku, Miniflex) composed of HyPix-400 MF 2D hybrid pixel array detector along with X-ray source operating at 40 kV and 15 mA (CuKα radiation, λ = 0.154 nm). The measurements were performed at an angular scanning rate of 10°/min in the scanning (2theta/theta) range of 3-40° at ambient temperature. The crystallinity and the fractional crystallites of the synthesized materials is evaluated using equations 1-5.

$$X_{c,PCL}(\%) = \frac{I_{c,PCL}}{I_{c,PCL} + I_{amp,PCL}} \quad (1)$$

$$X_{c,sc}(\%) = \frac{I_{sc,PLA}}{I_{sc,PLA} + I_{amp,PLA}} \quad (2)$$

where, $X_{c,PCL}$ and $X_{c,SC}$ are the crystallinities of PCL and stereocomplex PLA crystallites, respectively. $I_{c,PCL}$ and $I_{SC,PLA}$ denote the total intensity of the crystalline reflection peaks for PCL and stereocomplex crystal of PLA, respectively. Furthermore, $I_{amp,PCL}$ and $I_{amp,PLA}$ denote the intensity of the amorphous halo peak for PCL and PLA (PDLA & PLLA), respectively. Here, it should be noted that the observed amorphous halo peak was appropriately decomposed into the contribution of PCL and PLA.

$$f_{c,PCL}(\%) = \frac{X_{c,PCL}}{X_{c,PCL} + X_{c,sc}} \quad (3)$$

$$f_{c,sc}(\%) = \frac{X_{c,sc}}{X_{c,PCL} + X_{c,sc}} \quad (4)$$

where, $f_{c,PCL}$ and $f_{c,SC}$ are the fraction of PCL and stereocomplex PLA crystallites, respectively.

The thermal transitions in the melt quenched samples were examined by differential scanning calorimetry using DSC 214 Polyma (NETZSCH, Germany) under a nitrogen environment. The triblock copolymer samples were heated from 0 ℃ to 190 ℃, whereas the blend samples were heated from 0 ℃ to 240 ℃ at a rate of 10 ℃/min.

The mechanical properties of the polymer films (5 mm width, 10 mm gauge length) were examined using a universal testing machine (UTS Orientec ST-1150) equipped with a load cell of 1000 N, and the cross head speed was set to 5 mm/min. The measurements were conducted under ambient conditions, and the results are reported as averages of five respective specimens.

The dynamic tensile viscoelastic measurements were conducted using dynamic mechanical analysis DMA 242 E (NETZSCH, Germany) under a nitrogen atmosphere.

The measurements were conducted for a rectangle specimen 15-mm long and 5-mm wide, at a heating rate of 2 ℃/min with a dynamic frequency of 1 Hz and a strain amplitude of 6.67×10^{-3}. The measurement range of temperature for the neat triblock copolymers was 25-160 ℃ and that for the triblock copolymer blends was 25-180 ℃.

The nanostructure of the synthesized materials were evaluated using small angle X-ray scattering (SAXS) at room temperature through a Nano Viewer (MicroMax-007HF; Rigaku, Japan) which consisted of a confocal flux mirror (CMF, Rigaku), an X-ray generator as well as three collimation slits (0.3, 0.25, 0.3 mm). The distance between the sample and the detector (PILATUS 100 K, Switzerland) was set to 1.0 m. The components other than CuKα radiation (λ=0.154 nm) were eliminated by Ni filter. The measurement resulted in the 2D SAXS patterns which were used to obtain 1d profiles (scattering intensity $I(q)$ vs the magnitude of the scattering vector (q)) by performing the circular average. The definition of q is given below, where θ is the scattering angle.

$$q = \left(\frac{4\pi}{\lambda}\right)\sin\frac{\theta}{2}$$

The Lorentz corrected profile [$q^2\ I(q)$ vs. q] was obtained by multiplying q^2 to the 1d-profile.

The water vapor transmission rate (WVTR) of the polymer film was evaluated using the ASTM standard E398-03 on a PERMATRAN-W Model 1/50 (Mocon, U.S.A.) where the relative humidity (RH) was fixed to 95%. The film samples (60 cm^2) were analyzed at 37.8 ± 0.1 ℃ and ambient pressure. The films for the WVTR analysis were prepared by solution casting method. Each of the synthesized polymers was dissolved in chloroform (2 wt% concentration), stirred until complete dissolution, and poured into a petri dish.

After allowing the solvent to evaporate at room temperature in 12 h, the solidified film was dried in a vacuum oven at 50 ℃ for 12 h. For a control WVTR measurement, a homopolymer (PLA) having Mn~30 kDa was used.

4.2.7 Scale-up synthesis

The triblock copolymer (20D-11CL-20D) was synthesized in a scale of ~500 g with the controlled molecular weight. Here, the monomer (ε-caprolactone, 8.76×10^2 mmol) was fed directly (without distillation) to the round bottom flask together with the initiator (DMG, 9.88 mmol) and the catalyst (tin octoate, 0.7 mmol). The polymerization was conducted for 30 min at 180 ℃, and after which a sample was taken out to determine the conversion by ^{1}H-NMR. To the synthesized polymer, D-lactide was added (2.87×10^3 mmol), and the flask was evacuated at 10 Pa at 40 ℃ for 12 h. This was followed by melting at 180 ℃ until the monomer was solubilized into the melt of PCL. To the homogenous melt, the catalyst (tin octoate, 1.15 mmol) was added, and the reaction was continued at 180 ℃ for 30 min. The resultant polymer was taken out into a flat tray and the conversion of lactide was determined by ^{1}H-NMR, which was found to be >95%. The polymer was kept in a vacuum oven at 110 ℃ for 36 h to remove the residual lactide by sublimation. After removing the monomer, the sample was subjected to ^{1}H-NMR to ensure that no residual peak of lactide was involved. The molecular weight of the product was determined as shown in equation 1-v. The solvent-free synthesis of triblock copolymer was thus achieved in a larger scale.

4.2.8 Processing of triblock copolymer by (twin-screw) extrusion:

The synthesized triblock copolymer (after crushing) was processed using a twin-screw extruder (Toyoseiki, Japan) where the barrel temperature was set to 180 ℃ and the screw

speed was set to 10 rpm. The filament (ϕ ~ 1.4-1.8 mm) was extruded through the die which was conveyed into a cold water bath and collected on a winder.

4.2.9 3D printing of the filament:

The extruded filament was further used for the 3D printing (Moth Mach S3DP333, Slab) of a mesh-type scaffold. The temperature to melt the filament was set to 190 ℃ and the scaffold was printed layer by layer at the printing bed which was fixed at room temperature.

4.2.10 *In vitro* studies

UMR-106 cell culture

UMR-106 (rat bone osteosarcoma) cells were cultured in T75 flasks using Dulbecco's modified eagle's medium (DMEM) supplemented with 10% fetal bovine serum (FBS) and 1% penicillin streptomycin. The cells were cultured and maintained in a CO_2 incubator at 37 ℃ under the humidified atmosphere. The circular polymer films were sterilized with ethanol (70%) followed by washing with phosphate buffer saline (PBS); and irradiated under UV light after placing in the 96 well plates. The cell count was determined using trypan blue stain (Sigma Aldrich) with an automated cell counter (Countess II FL, Thermo Fisher Scientific) and 2.88×10^3 cells/well were seeded (in triplicates) in 96 well plates containing samples along with control (polystyrene microplates) by adding 100 µl DMEM per well. In addition, the medium (without cells) was added to the samples (triplicates) to eliminate the background absorption.

MTT assay

The mitochondrial activity of UMR-106 cells seeded onto the developed materials was evaluated by the enzymatic conversion of MTT (3-(4,5-dimethylthiazol-2-yl)-2,5-

diphenyltetrazolium bromide) dye. The stock (5 mg/ml) of MTT (Sigma Aldrich) was prepared in PBS and added (10 µl) to each of the wells at the intervals of 8, 16, 24, 48, 72 and 96 h. The well-plates were incubated for 3 h and then the medium involving MTT was removed from the wells. Finally, dimethyl sulfoxide (DMSO, 100 µl/well) was added to the wells so as to allow the formation of Formazan crystals. The absorbance was then recorded at 570 nm using a microplate reader (Multiskan Go, Thermo Fisher Scientific). The mean absorbance of the control (polystyrene) was subtracted from that of the samples.

Cell staining and microscopy

The cells adhering onto the surface of the samples along with the control sample were stained with Nuc Red™ (Live 647 Ready Probes™, Thermo Fisher Scientific) and acridine orange (Thermo Fisher Scientific) stains after 48 h of culturing. The Nuc Red stain was added (2 drops) directly into the wells containing medium and incubated for 20 min. The acridine orange stain was diluted (in PBS) before adding into the wells. The cell culture media were removed from the wells followed by washing off the samples (and the control well) with PBS thrice. The acridine orange stain was then added to the wells and incubated for 30 min. The plates were removed and the cells were analyzed with the fluorescence microscope (Floid Cell Imaging Station, Thermo Fisher Scientific).

4.3 Results and Discussion

4.3.1 Block copolymer synthesis

The triblock copolymers (PLLA-PCL-PLLA and PDLA-PCL-PDLA) are synthesized by two-step ROP[79,215] where the block length of both PCL and PLA segments is varied from 10 kDa to 20 kDa. **Table 4.1** shows the characterization of the series of the synthesized polymers. The molecular weights of the synthesized block copolymers are evaluated from ^{1}H-NMR spectroscopy. The molecular weight (M_n) of PCL and the triblock copolymers determined from NMR are slightly different than the theoretical molecular weight which may be due to the measurement error. The ^{1}H-NMR spectra of PCL, PLA and triblock copolymer (20D-11CL-20D) are shown in **Figure 4.1-1** along with their structures where the proton signals are assigned.[216,145] It is observed that the terminal group signal of PCL is present at 3.65 ppm which is no longer present in the triblock copolymer (second step ROP). Instead, a new signal at 4.36 ppm (hydroxymethine) appears in the triblock copolymer, suggesting the growth of the PLA chains at the ends of the PCL chains (terminal groups), confirming the complete synthesis of a triblock copolymer. Further, the ^{13}C NMR spectra are shown in **Figure 4.1-2** together with the structures and assignments of the respective carbon signals. The GPC curves of the triblock copolymers are shown in **Figure 4.2**. The elution time for the triblock copolymer 10D-11CL-10D is 12.5 min which is reduced to 12.3 min for 9D-23CL-9D, 11.9 min for 20D-11CL-20D and 11.6 min for 19D-18CL-19D. The decrease in the elution time is observed with the increasing molecular weight of the block copolymers. Further, each of the GPC curves of triblock copolymers showed a unimodal peak which confirmed that the triblock

copolymers were synthesized successfully by ROP of lactide using PCL diol as an initiator.

Table 4.1: Sample characterization.

Specimen code name	Molar feeding ratio [M/I]	Conv. (%)	Mn (theoretical) kDa	Mn (NMR) kDa	Mw/Mn (GPC)
11CL	88.5	99.4	10.1	11.0	1.97
10D-11CL-10D	154.1	93.2	31.7	31.5	2.13
11CL	88.5	99.4	10.1	10.9	1.88
10L-11CL-10L	154.0	93.6	31.7	31.5	1.94
11CL	88.5	99.2	10.0	10.6	1.88
20D-11CL-20D	308.3	93	51.9	50.1	2.48
10CL	88.5	99.3	10.0	10.4	1.93
20L-10CL-20L	308.3	94.3	52.3	49.7	2.65
23CL	185.6	99.3	21.0	22.9	1.97
9D-23CL-9D	145.8	87.5	40.9	40.2	2.05
20CL	177.1	98.5	19.9	19.6	2.18
8L-20CL-8L	154.1	90.2	39.9	35.2	2.33
18CL	179.0	99.5	20.3	18.3	1.96
19D-18CL-19D	307.5	85.4	56.1	56.5	3.1
22CL	177.3	99.1	20.1	21.9	2.13
16L-22CL-16L	308.3	93.9	61.8	53	2.28

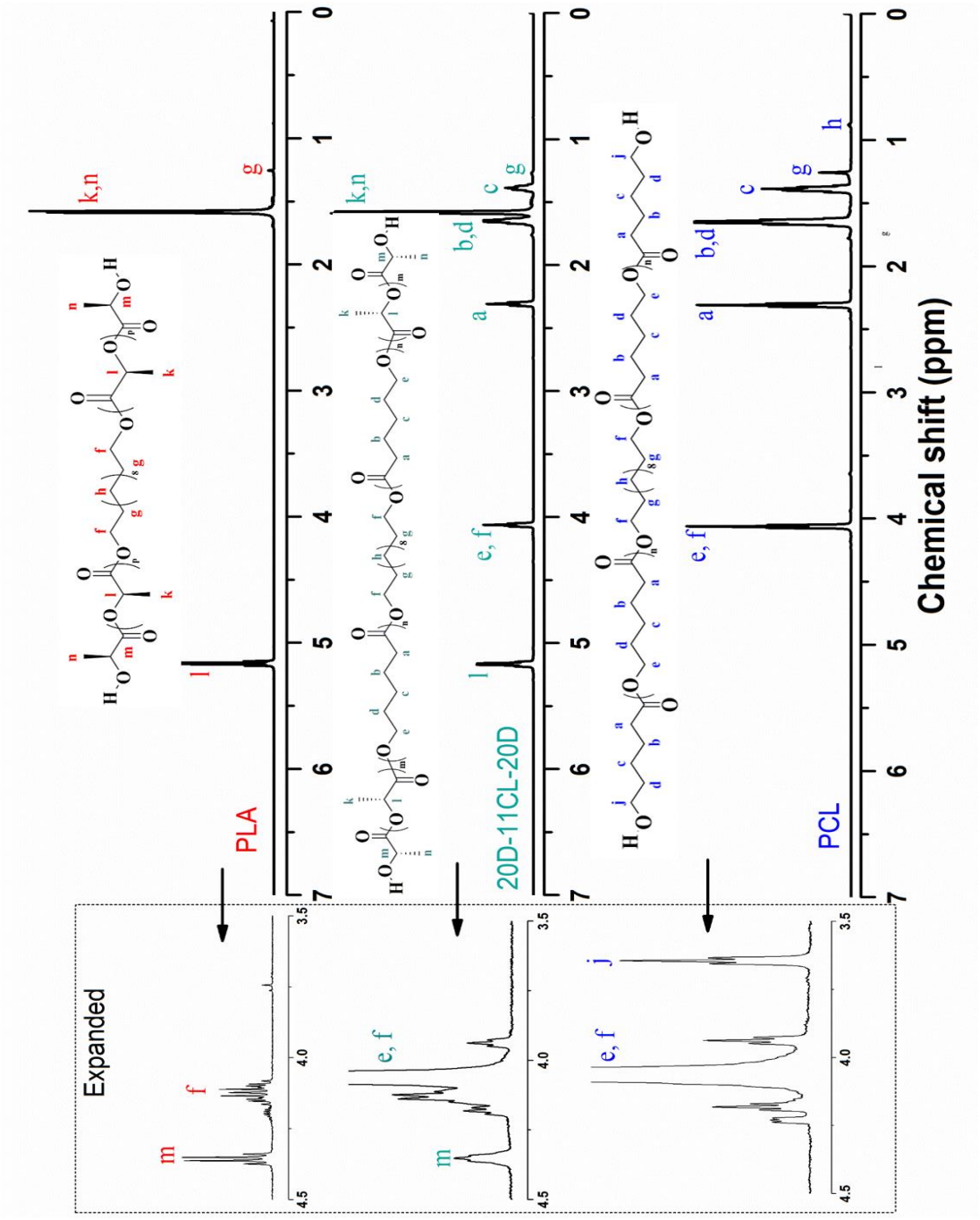

Figure 4.1-1: ^{1}H-NMR spectra of homopolymers and the 20D-11CL-20D triblock copolymer.

*The number average molecular weight (Mn) of the homopolymers/block copolymers is determined from ^{1}H-NMR (Figure S1) by using the following equations (S1-I to S1-v):

Degree of polymerization of dihydroxyl terminated PCL, $DP_{PCL} = \frac{e}{j} + 2$ (1-i)

Degree of polymerization of dihydroxyl terminated PLA, $DP_{PLA} = \frac{l}{m} + 2$ (1-ii)

Number average molecular weight of dihydroxyl terminated PCL,

$$Mn_{PCL} = (Mo_{PCL} \times DP_{PCL} \times 2) + Mo_{DMG}$$
$$= [114.14 \times \left(\frac{e}{j} + 2\right) \times 2] + 202.34 \quad \text{(1-iii)}$$

Number average molecular weight of dihydroxyl terminated PLA,

$$Mn_{PLA} = (Mo_{PLA} \times DP_{PLA} \times 2) + Mo_{DMG}$$
$$= [72 \times \left(\frac{l}{m} + 2\right) \times 2] + 202.34 \quad \text{(1-iv)}$$

Number average molecular weight of triblock copolymer (PLA-PCL-PLA)

$$Mn_{triblock} = [(Mo_{PCL} \times DP_{PCL}) + Mo_{DMG}] + [(Mo_{PLA} \times DP_{PLA} \times 2) + Mo_{DMG}]$$
$$= [\{114.14 \times \left(\frac{e}{j} + 2\right) \times 2\}\textbf{\textit{Err}}\text{or! Bookmark not defined.}173 + 202.34]$$
$$+ [\{72 \times \left(\frac{l}{m} + 2\right) \times 2\} + 202.34] \quad \text{(1-v)}$$

where, Mo = molar mass of repeating unit

M_{DMG} = molar mass of initiator

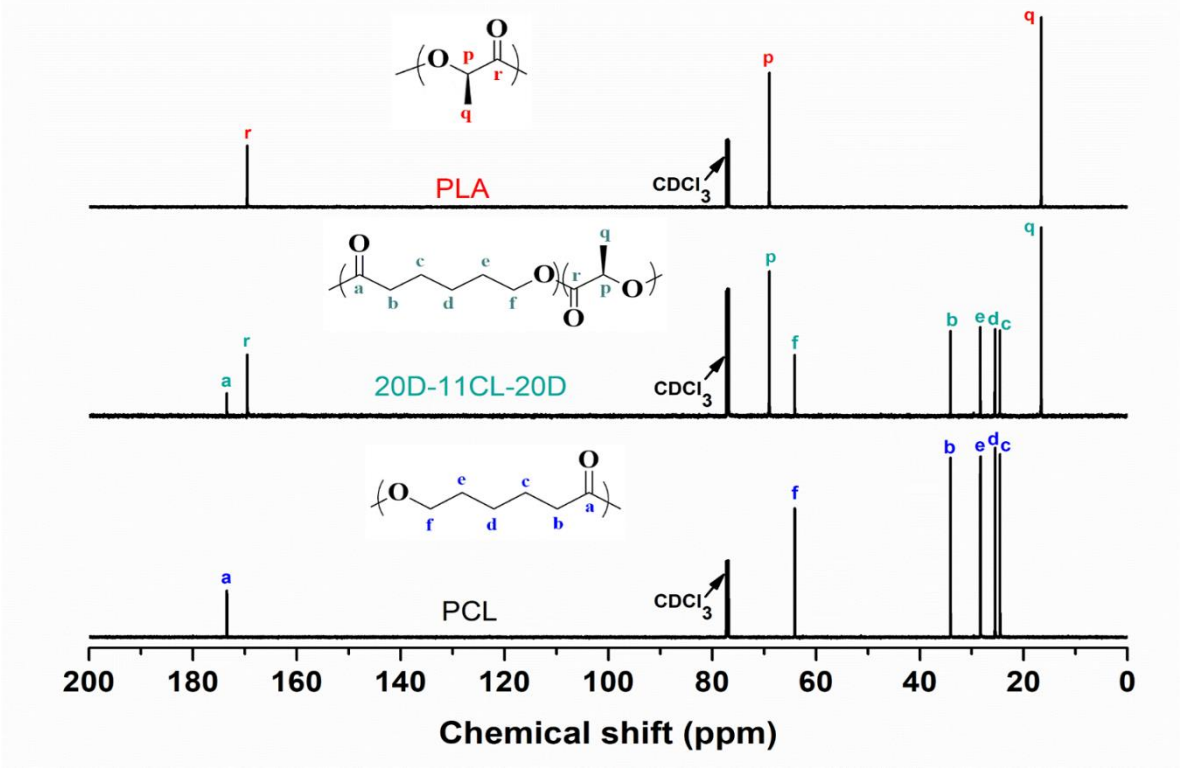

Figure 4.1-2: ^{13}C-NMR spectra of homopolymers and the 20D-11CL-20D triblock copolymer.

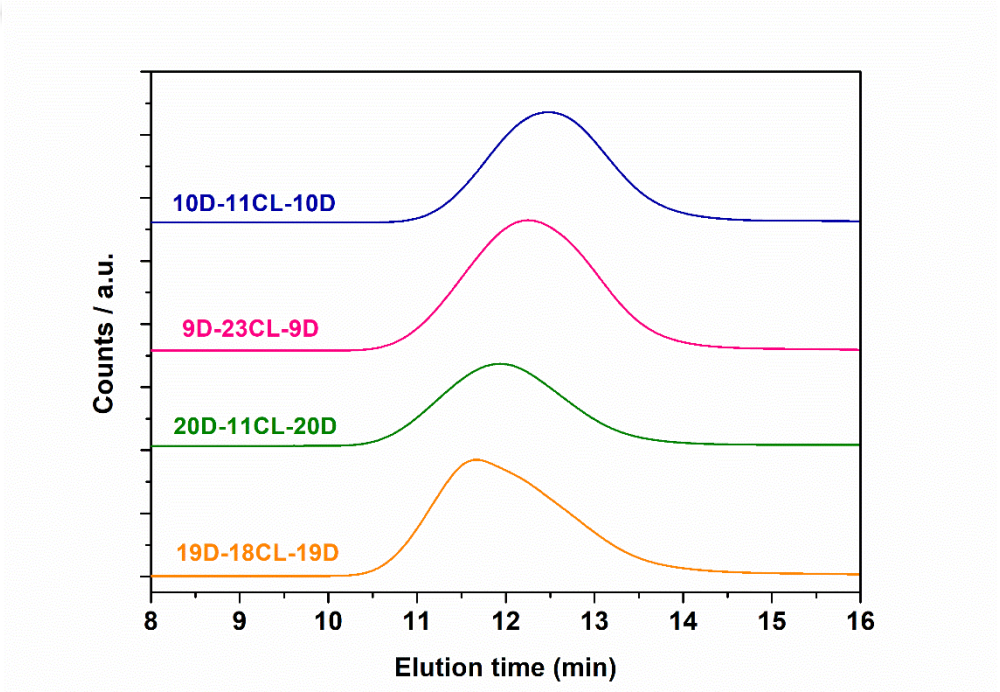

Figure 4.2: GPC curves of triblock copolymers.

4.3.2. Crystallinity of block copolymers

In order to ascertain the crystallization behavior of the synthesized polymers, WAXS measurements are conducted. It is known that PLA crystallizes into different crystal forms[217,218], namely α, α′ (δ), β, γ which depend on the conditions of the sample preparation[219,220]. For instance, the α-form is known to have a pseudo hexagonal (orthorhombic) unit cell with the packing of 10/3 helical chains, whereas the crystallite size of α′ form is substantially smaller than α form[221]. The major scattering peaks of PLA are observed at q = 11.6 and 13.3 nm^{-1} corresponding to (200)/(110) and (203) crystal planes, respectively[222]. PCL is known to crystallize in an orthorhombic unit cell with the major scattering peaks at 11.0, 14.9, 15.3, 16.6 and 20.7 nm^{-1} corresponding to (102), (110), (111), (200) and (210) lattice planes, respectively [223]. The regular packing of a pair of PLLA and PDLA chains in the triclinic unit cell with the 3/1 helical confirmation results in the formation of stereocomplex (sc) crystals. The scattering peaks of the sc crystals corresponding to (110) and (030/300) crystal planes are observed at q = 8.3 and 14.5 nm^{-1}, respectively[224].

The WAXS profiles of the homopolymers and triblock copolymers are shown in **Figure 4.3(a)**, whereas those of equimolar enantiomeric triblock copolymer blends are shown in **Figure 4.3(b)**, which are plotted as a function of q (nm^{-1}). As shown in **Figure 4.3(a)**, no scattering peak is visible for PDLA (50D specimen) whereas clear and distinct peaks are visible for PCL (50CL). The scattering peaks for the PCL constituent are evident in case of the triblock copolymers whereas those for the PDLA constituents are absent. The absence of the WAXS peaks of PLA in the triblock copolymers may be attributed to the melt-quenching technique adopted to prepare the film specimens, where the PLA constituent may be retaining its amorphous nature (due to its higher T_g and

slower crystallization) whereas the PCL chains still acquire the mobility to crystallize to some extent (due to its lower T_g and rapid crystallization), thus giving rise to the WAXS peaks of PCL. Further, as shown in **Figure 4.3(b)** for the triblock copolymer blends (B1, B2, B3 and B4), the scattering peaks from PCL crystals are evident along with the presence of relatively weaker scattering peaks for the stereocomplex (sc) crystals. Furthermore, PCL (50CL) is observed to have a relatively higher crystallinity (62.8%) in the melt quenched state as shown in **Table 4.2**. The total crystallinity is found to be the lowest for 20D-11CL-20D (18.2%) which is the specimen with the lowest PCL content (~21%). As discussed later, the cylindrical microdomain morphology is expected to be formed for this specimen from the lower PCL composition (~21%). The crystallinity is found to increase to 33.2, 31.8 and 33.9% for the specimens 19D-18CL-19D (~32% PCL content), 10D-11CL-10D (~35% PCL content) and 9D-23CL-9D (~56% PCL content), respectively. For those specimens, the lamellar microdomain morphology is expected so that the effect of the space confinement due to the PLA lamellar microdomains on the PCL crystallization is considered to be lesser than that for the case of 20D-11CL-20D specimen. However, almost half the crystallinity of PCL for those specimens as compared to that of the neat PCL implies the space confinement due to the PLA lamellar microdomains. The blend specimen B2 (20D-11CL-20D/20L-10CL-20L) has the lowest degree of crystallinity (37.2%), accounting to PCL constituent (18.2%), which is increased to 59.5% with increasing PCL content (~56%) for B3 (9D-23CL-9D/8L-20CL-8L) specimen. The sc crystallinity is lower for the specimens having longer PLA block chains (B2 and B4) whereas, higher sc crystallinity is found in the specimens comprising shorter PLA block chains (B1 and B3) due to the higher mobility of the PLA chains with lighter extent of the polymer chain entanglement. Further, the specimens B2 and B4 are

homocrystal (hc) rich ($\Delta H_{m,\ PDLA}$ is higher than B1 and B3 in **Figure 4.2**) whereas B1 and B3 are sc rich, which in turn suggests that the lower molecular weight PLA chains lead to the well-formed sc crystallites and retard the formation of hc. The lowest crystallinity in the specimens 20D-11CL-20D and B2 may be due to the confined crystallization of PCL in the PCL cylindrical microdomains in the matrix of the glassy PLA[225-232]. Additionally, it is remarked that the crystallinity of the triblock copolymer blends is higher than their respective enantiomers which is also discussed in the subsequent sections.

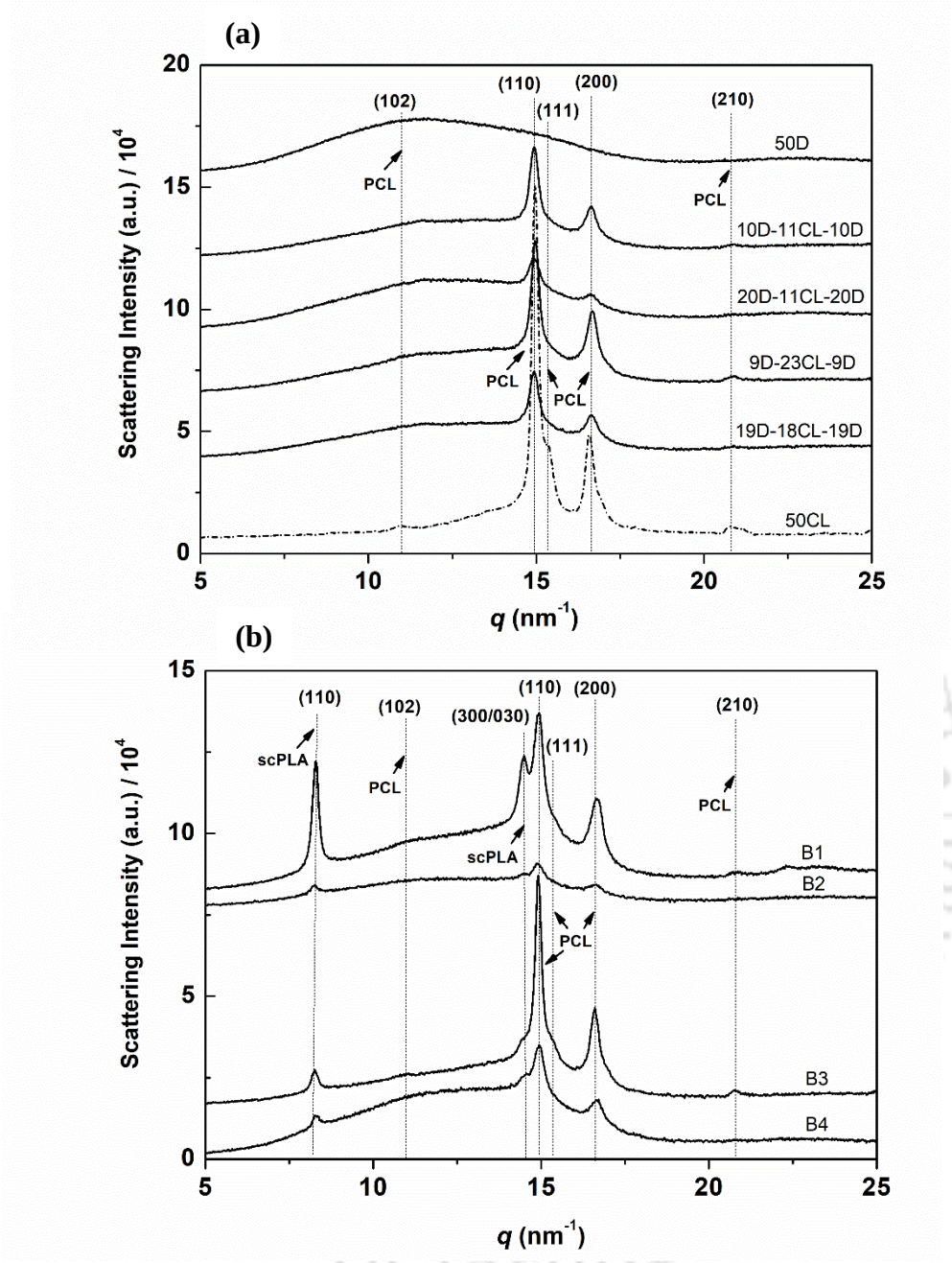

Figure 4.3: WAXS profiles of (a) PCL and PLA homopolymers, and neat triblock copolymers, and (b) triblock copolymer blends (as-prepared specimens). B1:10D-11CL-10D/10L-11CL-10L (50/50), B2: 20D-11CL-20D/20L-10CL-20L (50/50), B3:9D-23CL-9D/8L-20CL-8L (50/50) and B4:19D-18CL-19D/16L-22CL-16L (50/50) blend specimens.

Table 4.2: Crystallinities determined by WAXS results.

Specimen code name	$X_{c,PCL}$ (%) [1]	$X_{c,PLA}$ (%) [2]	$X_{c,sc}$ (%) [3]	$X_{c,PCL}$ (%) [4]	$X_{c,PLA}$ (%) [5]	f_{PCL} (%) [6]	f_{sc} (%) [7]
50CL	62.8	0	0	56.5	-	100	-
10D-11CL-10D	31.8	0	0	69.5	39.4	100	-
20D-11CL-20D	18.2	0	0	39.7	41.8	100	-
9D-23CL-9D	33.9	0	0	55.0	29.6	100	-
19D-18CL-19D	33.2	0	0	74.8	40.9	100	-
B1 [8]	54.6	0	8.7	47.6	36.1	86.3	13.7
B2 [9]	37.2	0	1.9	57.4	47.6	95.1	4.9
B3 [10]	59.5	0	6.7	67.6	24.7	89.9	10.1
B4 [11]	47.4	0	1.2	87.7	39.7	97.5	2.5

[1] Crystallinity of PCL at room temperature (WAXS)

[2] Crystallinity of PLA at room temperature (WAXS)

[3] Crystallinity of the stereocomplex PLA at room temperature (WAXS)

[4] Crystallinity of PCL ($X_{c,PCL}$, DSC),

where, $X_{c,PCL} = \Delta H_m/(\Delta H°_m \times W_{PCL})$

$\Delta H°_m$ = enthalpy of fusion for 100% crystal of PCL (139.5 J/g)[233] and

W_{PCL} = weight fraction of PCL

[5] Apparent crystallinity of PLA ($X_{c,PLA}$, DSC) at 110 °C

where, $X_{c,PLA} = \Delta H_{m,hc}/\Delta H°_{m,hc} + \Delta H_{m,sc}/\Delta H°_{m,sc}$

$\Delta H°_{m,hc}$ = enthalpy of fusion for 100% homocrystal of PLA (93 J/g)[234]

$\Delta H°_{m,sc}$ = enthalpy of fusion for 100% stereo-complex crystal of PLA (142 J/g)[36]

[6] Fraction of PCL crystallites

[7] Fraction of stereocomplex PLA crystallites

[8] 10D-11CL-10D/10L-11CL-10L (50/50) blend specimen

[9] 20D-11CL-20D/20L-10CL-20L (50/50) blend specimen

[10] 9D-23CL-9D/8L-20CL-8L (50/50) blend specimen

[11] 19D-18CL-19D/16L-22CL-16L (50/50) blend specimen

4.3.3 Thermal properties

The DSC curves (1st heating cycles) of the synthesized materials are shown in **Figure 4.4**. Exothermic peaks are observed in the range of 70 ℃ to 110 ℃, followed by their melting in the form of hc PLA and sc-PLA. The melting temperature of PCL is 64.2 ℃ which is reduced to 59.5 ℃ for 9D-23CL-9D (~56% PCL), 56.6 ℃ for 19D-18CL-19D (~32% PCL), 54.5℃ for 10D-11CL-10D (~35% PCL) and 53.8 ℃ for 20D-11CL-20D (~21% PCL) specimen (**Table 4.3**). The melting point (T_m) of PCL in the case of triblock copolymers is found to be reduced by ~10 ℃ when the content of PCL is reduced to 21% (or content of PLA is increased to 79%). The enthalpy of cold crystallization of PLA ($\Delta H_{cc,PLA}$) is the lowest for 9D-23CL-9D (4.5 J/g) which is increased to 13.8 J/g for 10D-11CL-10D, 21.8 J/g for 19D-18CL-19D and 24.7 J/g for 20D-11CL-20D. Furthermore, the melting point of hc PLA in the blend sample is in the range of 167-173 ℃ whereas the melting point of sc-PLA is 218-222 ℃, which is ~50 ℃ higher than that of hc PLA. Further, it is remarked that the enthalpy of melting ($\Delta H_{m,PCL}$) is lowest for the 20D-11CL-20D (11.9 J/g) and B2 (17.3 J/g), which are the specimens having the lowest content of PCL (~21%).

The melting peaks of PCL and PDLA constituents for the triblock copolymers (**Figure 4.4(a)**) may be attributed to the presence of two crystalline domains. This is also true in the case of triblock copolymer blends (**Figure 4.4(b)**) where the melting peaks for the sc-PLA are also present along with those of hc PLA. On the other hand, as seen in the subsequent (WAXS) section, the scattering peaks for the sc-PLA (relatively weaker) and PCL are evident in the melt quenched state whereas no scattering peak is observed for hc PLA, suggesting that the PLA amorphous chains frozen in the melt-quenched specimen crystallize upon heating above the T_g to form homocrystals and sc crystals (for the blend

specimens). The reduction in T_m for the triblock copolymers (other than 19D-18CL-19D) as compared to T_m of the PDLA homopolymer (50D) indicates that the crystalline lamellae are thin, implying the confined crystallization within the PLA lamellar microdomains. As a matter of fact, $\Delta H_{cc,PLA}$ is smaller as compared to that of 50D, although PCL is melt at $T_{cc,PLA}$. The crystallizability of PLA is improved ($T_{cc,PLA}$ is lowered) with increasing the PCL content for the neat block, while the order of $\Delta H_{cc,PLA}$ is opposite (**Table 4.3**). This may indicate that the faster crystallization results in lower crystallinity[235]. Since the PLA/PCL blend is reported to exhibit the lower critical solution temperature (LCST) phase behavior[236], it is considered that PCL can be solubilized in the PLA phase so that the T_g of the mixed PLA amorphous phase is decreased and the mobility of PLA chains is increased. Thus, the crystallizability is considered to be improved. The lowered T_g also accounts for the lowering of $T_{cc,PLA}$. As for the enantiomeric blends, there would be no difference in $T_{cc,PLA}$ while it is clearly recognized that there is a strong correlation of $\Delta H_{cc,PLA}$ with $X_{SC,PLA}$. Namely, $\Delta H_{cc,PLA}$ is larger when $X_{SC,PLA}$ is lower. This implies that the cold crystallization of PLA is suppressed by this preformed sc crystallite through the suppression of the molecular mobility.

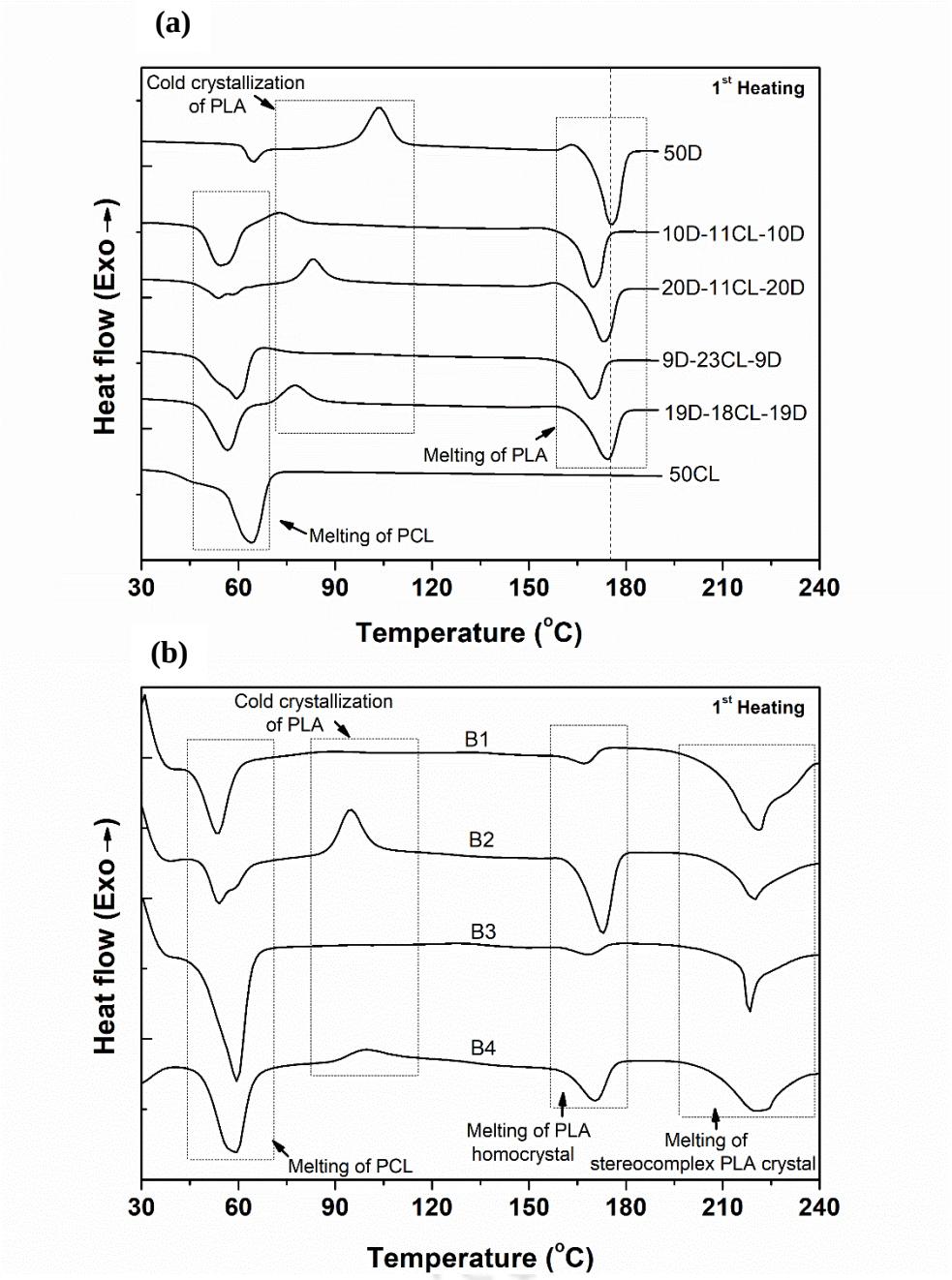

Figure 4.4: DSC curves of the first heating cycles for the melt-quenched samples of (a) homopolymers and triblock copolymers, and for (b) triblock copolymer blend specimens. The heating rate was 10 °C/min.

Table 4.3: Summaries of the DSC results.

Specimen code name	$T_{m,\ PCL}$ (ºC)	$\Delta H_{m,\ PCL}$ (J/g)	$T_{cc,\ PDLA}$ (ºC)	$\Delta H_{cc,\ PDLA}$ (J/g)	$T_{m,\ PDLA}$ (ºC)	$\Delta H_{m,\ PDLA}$ (J/g)	$T_{m,\ scPLA}$ (ºC)	$\Delta H_{m,\ scPLA}$ (J/g)
50D	-	-	103.6	41.3	175.4	49.8	-	-
10D-11CL-10D	54.5	34.3	72.8	13.8	169.8	36.6	-	-
20D-11CL-20D	53.8	11.9	83.3	24.7	173.2	38.9	-	-
9D-23CL-9D	59.5	43.0	68.1	4.5	169.4	27.5	-	-
19D-18CL-19D	56.6	33.5	77.6	21.8	174.5	38.0	-	-
50CL	64.2	78.8	-	-	-	-	-	-
B1 [1)]	53.5	23.5	-	-	167.2	3.9	221.5	45.3
B2 [2)]	54.0	17.3	94.7	18.8	172.8	27.7	222.0	25.3
B3 [3)]	59.5	52.9	-	-	168.3	8.6	218.2	22.0
B4 [4)]	59.2	39.3	99.8	17.3	170.4	15.6	219.8	32.5

[1)] 10D-11CL-10D/10L-11CL-10L (50/50) blend specimen
[2)] 20D-11CL-20D/20L-10CL-20L (50/50) blend specimen
[3)] 9D-23CL-9D/8L-20CL-8L (50/50) blend specimen
[4)] 19D-18CL-19D/16L-22CL-16L (50/50) blend specimen

Crystallinity of PCL from DSC:

$$X_{c,PCL}\,(\%) = \frac{\Delta H_{m,PCL}}{\Delta H^{\circ}_{m,PCL} \times W_{PCL}} \times 100 \qquad (4\text{-i})$$

wherse, $\Delta H^{\circ}_{m,PCL}$ = 139.5 J/g and

W_{PCL}= weight fraction of PCL

4.3.4 Dynamic mechanical properties

The plot of the tensile modulus *E′* as a function of temperature for (a) triblock copolymers and (b) enantiomeric blends of the block copolymers is shown in **Figure 4.5-1**. The temperature dependence of *E′* for all the specimens including blends clearly exhibited abrupt drop with more than two decades of magnitude around 55 ºC, which is ascribed to the transition from glassy to rubbery states of PLA. Further, it is interesting to note the behavior of E′ over a temperature range of 60 ℃ to 90 ℃. As a matter of fact, the T_{cc} of triblock copolymers is observed beyond 60 ℃ (as shown in DSC results) which can be correlated to the increasing values of storage modulus due to the crystallization of PLA. A rise in the storage modulus is observed after 73 ºC, 71 ºC, 64 ºC and 62 ºC for the triblock copolymers 20D-11CL-20D, 19D-18CL-19D, 10D-11CL-10D and 9D-23Cl-9D respectively, which is in line with the decreasing order of their T_{cc} being 83.3 ºC, 77.6 ºC, 72.8 ºC and 68.1 ºC respectively. Similarly, it is observed that the storage modulus increases after 70 ºC and 68 ºC for the blends B4 and B2 which have their T_{cc} at 99.8 ºC and 94.7 ºC respectively. It is also noteworthy that the 9D-23CL-9D specimen, B1 and B3 blend specimens did not exhibit such retrieving behaviors of *E′* in the temperature range of 60 ºC to 90 ºC. For these specimens, the exothermic peak due to the cold crystallization of PLA is not discernible in the DSC curve in **Figure 4.4**. For other specimens, a strong correlation between the extent of the *E′* retrieving and the enthalpy of exothermic peak due to the cold crystallization of PLA can be confirmed. Nevertheless, the fact that the exothermic peak was not observed in the DSC curve does not mean that the PLA did not crystallize during the heating process. It is because the endothermic peak was clearly observed for these specimens. Rather the fact that there was no undershoot in *E′* in the temperature range of 60 ℃ to 90 ℃ may indicate that the cold crystallization of

PLA already completed below 60 ℃. Also the lack of the exothermic peak in the DSC curve can be recognized as a result of the overlap with the endothermic peak of the PCL melting.

The value of E' at 30 ℃ of the specimen 20D-11CL-20D is 2130 MPa which is reduced to 1864 MPa, 1543 MPa and 1172 MPa for 19D-18CL-19D, 10D-11CL-10D and 9D-23CL-9D specimens, respectively. In principle, it is considered that E' is dependent on the content of the hard PLA. Therefore, the values of E' at 30 ℃ are plotted as a function of the PLA content in **Figure 4.5-1**. The representative plots of the storage modulus as a function of PLA content are shown together in **Figure 4.5-1(a)** for the B1-B4 specimens which show the same tendencies as those for the neat block copolymers. It is further found in that the enantiomeric blending slightly reduces the value of E' with almost the same extent (300-500 MPa) other than B2 at room temperature (**Figure 4.5-1(a)**) or other than B1 at 110 ℃ (**Figure 4.5-1(b)**).

Since the strain amplitude is as little as 6.67×10^{-3} for the dynamic mechanical measurement, the resulted storage Young's modulus E' can reflect the structure in a virgin material without nay deformation or breakage. This is in contrast with the stress-strain (SS) measurement where the mechanical response reflects the structure in the material which already suffer from the preceded deformation of the material in the former stage of the elongation of the SS measurement. Namely, the structure in the material changed from that in the virgin material. Thus, the resulted Young's modulus from the SS measurement does not reflect the structure in the virgin material. In this regard, the E' of the dynamic mechanical measurement is more suitable and sensitive to the morphology and the degree of crystallinity.

Overall, *E′* increases with an increase in the PLA content for all of the neat triblock copolymers and for all of the blend specimens at 30 ºC, as shown in **Figure 4.5-1(a)**. This is simply because the PLA is in the glassy state. The same tendency can be confirmed for all the neat triblock copolymers in **Figure 4.5-1(b)** at 110 ºC where the PLA is in the rubbery state and the crystalline PCL phase is completely melted. However, the PLA phase partly crystallizes in the heating process to 110 ºC. Therefore, the *E′* at 110 ºC depends on the apparent degree of crystallinity of PLA at 110 ºC, which can be estimated by $\Delta H_{m,PLA}/\Delta H^{o}_{m,PLA}$ where $\Delta H_{m,PLA}$ denotes the enthalpy of fusion of PLA appearing at its T_m (around 170 ºC) and $\Delta H^{o}_{m,PLA}$ is that of 100% PLA crystal and taken as 93 J/g. The values of $\Delta H_{m,PLA}/\Delta H^{o}_{m,PLA}$ are tabulated in **Table 4.2**. As for the blend specimens (B1-B4), their complex behavior of *E′* at 110 ºC with respect to the PLA content in **Figure 4.5-2b** can be reasonably recognized in terms of apparent degree of PLA (homocrystal + sc crystal) crystallinity at 110 ºC. The values of $\Delta H_{m,PLA}/\Delta H^{o}_{m,PLA}$ are also tabulated in **Table 4.2**, where $\Delta H_{m,PLA}$ is the summation of the enthalpy of fusion of homocrystal and sc crystal for the case of blend specimens.

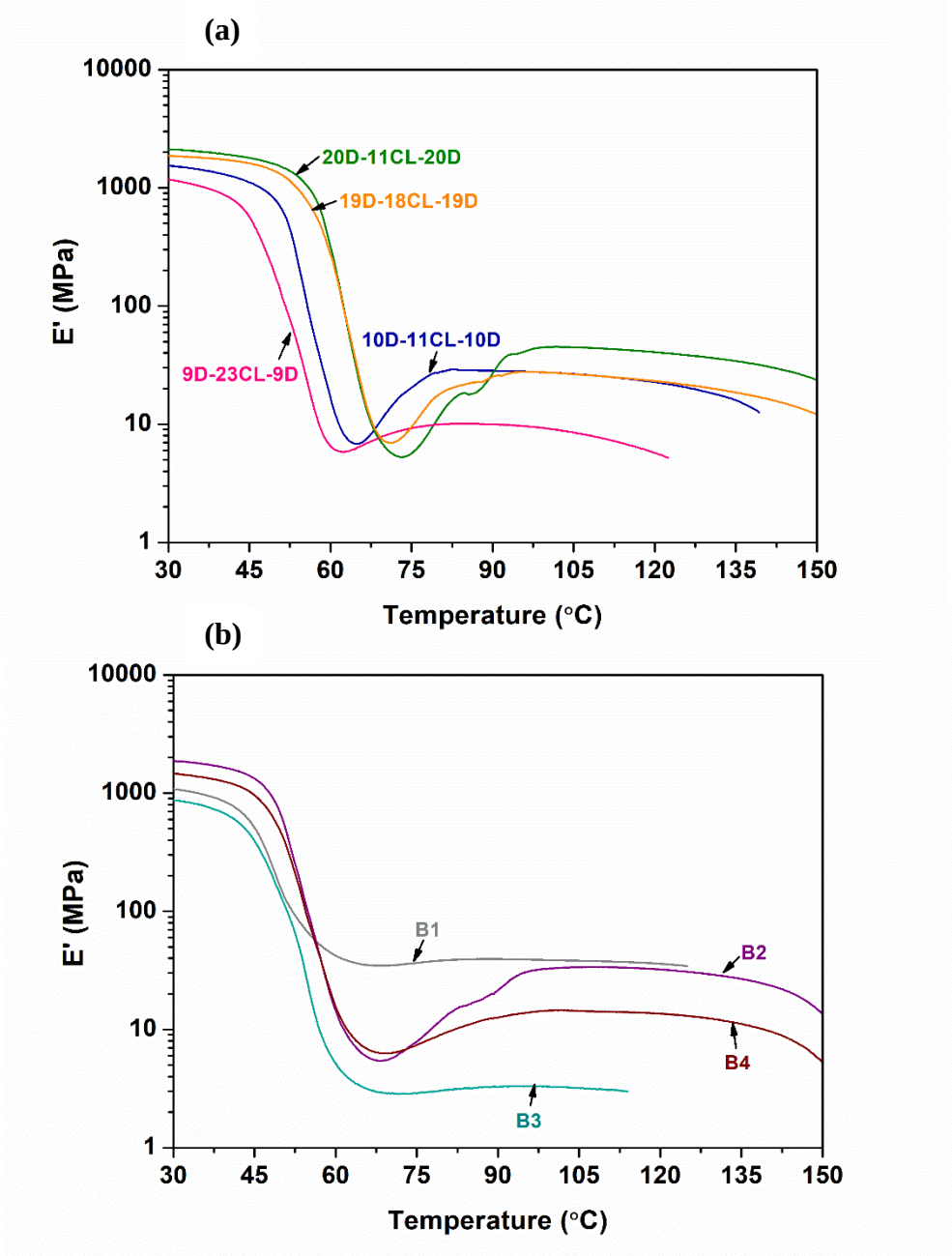

Figure 4.5-1: Changes in storage modulus (*E′*) as a function of temperature for (a) triblock copolymers and (b) triblock copolymer blends obtained by the dynamic tensile viscoelastic measurements at the dynamic frequency of 1 Hz (as-prepared specimens).

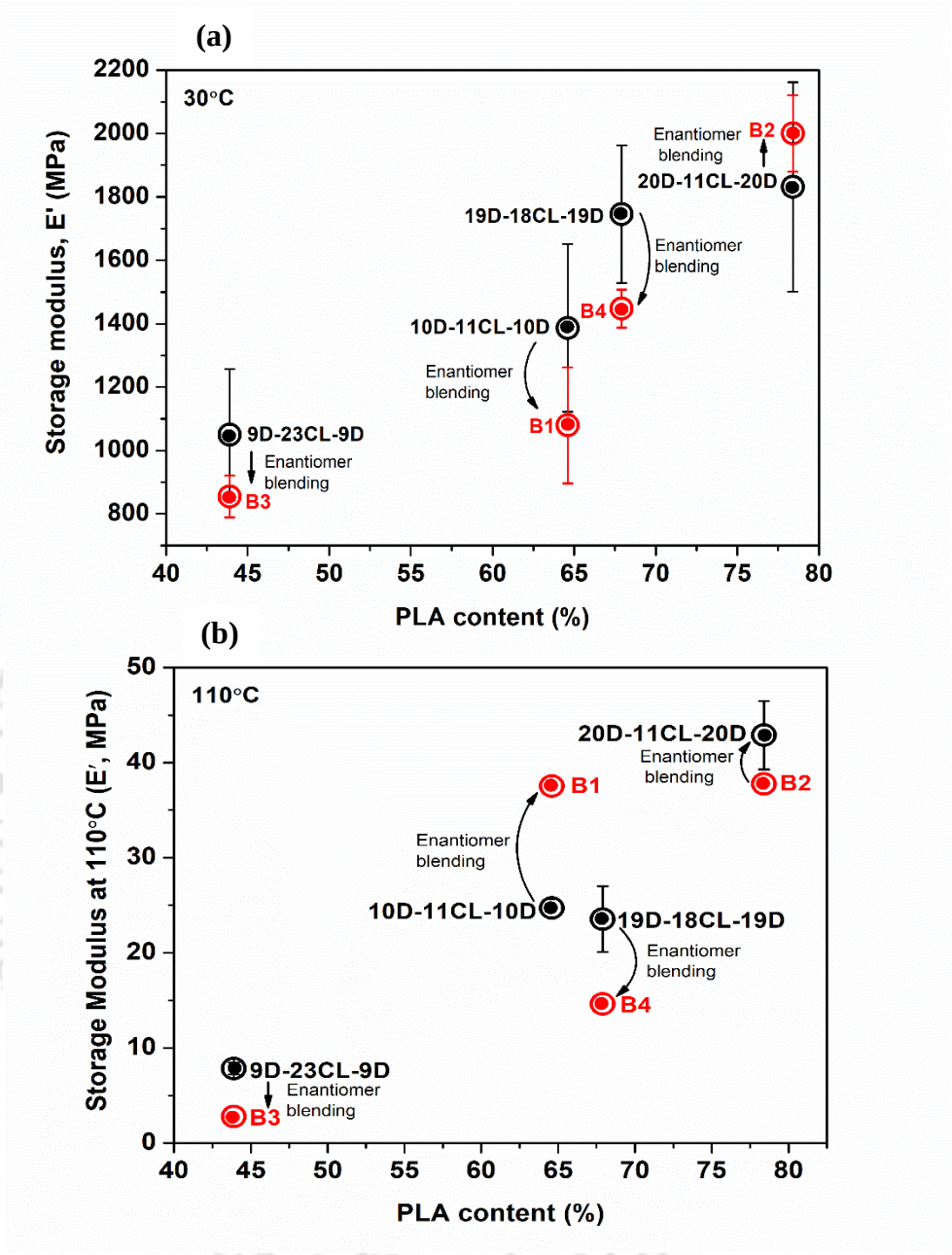

Figure 4.5-2: Representative plots of storage modulus (*E′*) at 30 °C (a) at room temperature and (b) at 110 °C, for the neat block copolymers and their blends as a function of the PLA content, as determined from the dynamic mechanical analysis.

4.3.5 Stress-strain behavior

Figure 4.6 shows the representative stress-strain (SS) curves where the homopolymer PDLA (50D) is observed to have a yield strength of ~40 MPa with a low elongation at break of ~6.8%, whereas PCL (50CL) has a yield strength of 13.1 MPa with a very high elongation at break of 1683%, giving a toughness of 273 MJ/m^3 (**Table 4.4)**. The ultimate tensile strength of PCL is ~27 MPa.

The triblock copolymer (20D-11CL-20D) with the maximum content of PLA (79%) is found to have the ultimate tensile strength of ~36 MPa, and an elongation at break of ~700%, whereas the triblock copolymer (9D-23CL-9D) with the maximum content of PCL (55%) has a strength of ~16 MPa and an elongation of ~600%. Although the block length of the flexible segment (PCL) is higher in the latter case, its elongation at break is inferior. Furthermore, it is found that 10D-11CL-10D specimen shows a lower yield strength (~13 MPa) and the elongation at break of ~550%, whereas the ultimate tensile strength of 19D-18CL-19D specimen is ~21MPa and the elongation at break is ~950%.

The SS curves of the triblock copolymers (**Figure 4.6(a)**) are observed to have relatively higher tensile strength (than the neat PCL) and higher elongation (than the neat PLA) due to the presence of both the hard (PLA) and soft (PCL) segments in the backbone. Although PCL has a very high elongation at break as compared to the triblock copolymers, its lower yield may restrict its use for load bearing applications. Further, the elongation of PCL is also dependent on its molecular weight [86]. Additionally, PCL has a lower modulus (140 MPa) as compared to the triblock copolymers (500 – 800 MPa) which may serve as an essential factor for the mechanical integrity of the material or implant. The

triblock copolymers thus offer possibilities of synthesizing materials having the advantages of both PLA and PCL which may be desired for targeted applications.

A significant difference in the elongation at break between the triblock copolymers with the nearly same PCL and PLA content (comparison between 10D-11CL-10D and 19D-18CL-19D) is attributed to the higher molecular weight of the soft PCL block chain. Note here that it has been reported that the elongation at break is increased with increasing the molecular weight of PDLA in case of homopolymer[237]. Further, as observed for the blend samples where the yield strength and elongation of B1 (10D-11CL-10D/10L-11CL-10L) and B4 (19D-18CL-19D/16L-22CL-16L) having nearly the same content of PCL and PLA are compared. B4 is found to have the ultimate tensile strength of 20 MPa and an elongation of ~450 % whereas B1 has the ultimate tensile strength of ~15 MPa and an elongation of ~540 %. The significant increase in the ultimate tensile strength of B1 as compared to that for the neat block (10D-11CL-10D) is attributed to the stereocomplexation (as observed by the DSC and WAXS, where $X_{c,sc}$ = 8.7%, which is the best among all the blends).

Overall, the mechanical properties (the stress level of the SS curves) of the triblock copolymer blends are similar to, or slightly lower than those of their corresponding enantiomeric triblock copolymers. It is noteworthy that there is no yield peak in the SS curve for specimen B1 which also shows the largest strain hardening among the four specimens. For this specimen (B1), the SAXS profile shown in **Figure 4.7** did not indicate a clear peak corresponding to the long period of the stacks of the crystalline PCL lamellae, although $X_{c,PCL}$ (**Table 4.2**) is larger than that of the neat block. Thus, it can be expected that the PCL crystallites are small and dispersed in the PCL lamellar microdomain. These

dispersed crystallites may play a role of the physical crosslinking points so that the elastomeric properties such as no yield peak and the strain hardening show steep increase in the late stage of elongation. As for the higher stress level for B1 in the range of 20 ~ 100% strain as compared to that of the neat triblock 10D-11CL-10D specimen, it may be ascribed to the much higher $X_{c,PCL}$ of the B1 specimen (**Table 4.2**).

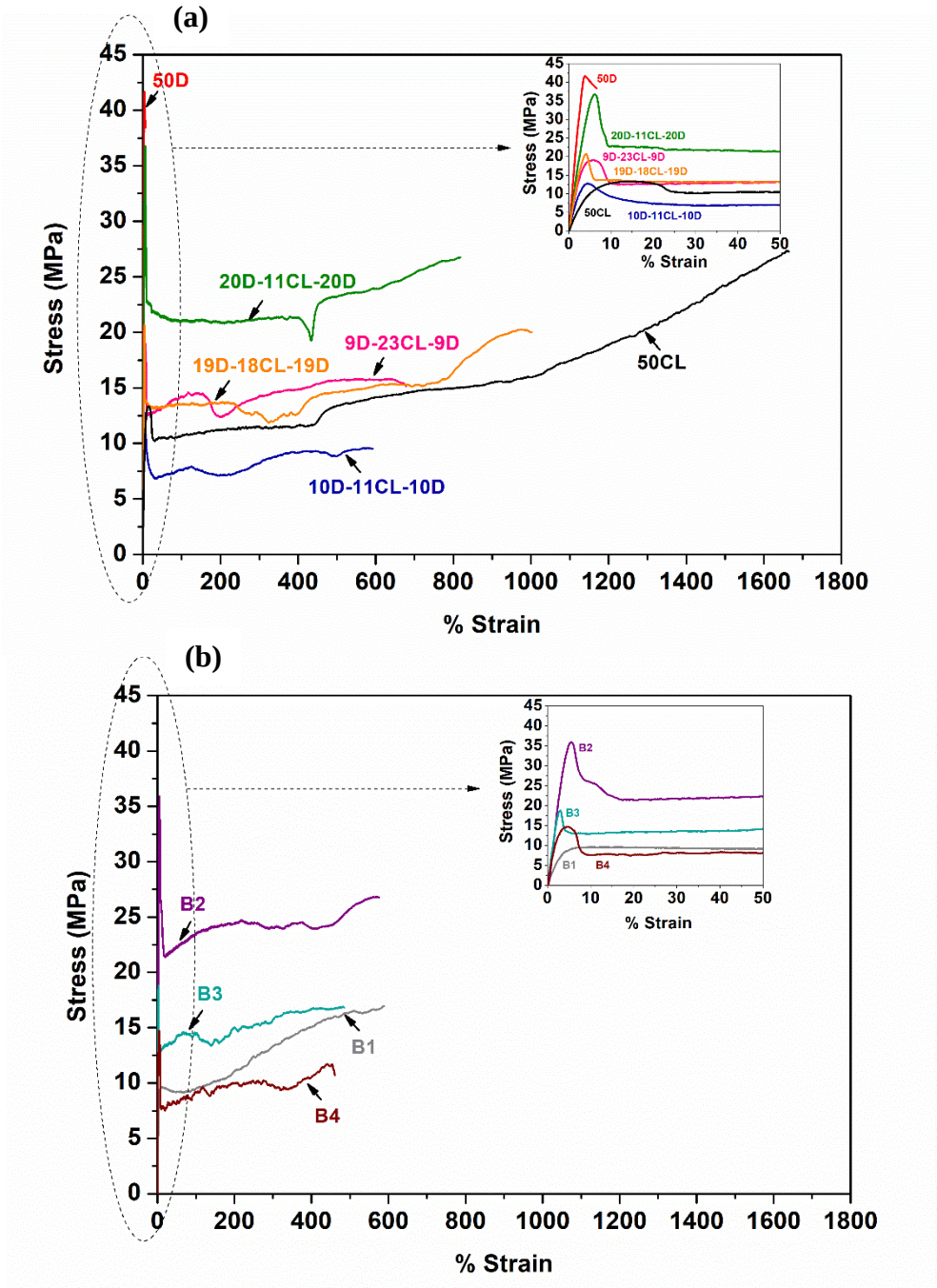

Figure 4.6: Stress-strain curves measured at room temperature for (a) homopolymers and triblock copolymers and (b) triblock copolymer blends (as-prepared specimens).

Table 4.4: Summaries of the stress-strain results.

Specimen code name	Yield strength (MPa)	Ultimate tensile strength (MPa)	Elongation at break (%)	Young's modulus (MPa)	Tensile toughness (MJ/m^3)
50D	39.7 ± 1.9	39.7 ± 1.9	6.8 ± 2.0	1387.2 ± 83.4	2.0 ± 0.7
10D-11CL-10D	12.9 ± 0.8	12.9 ± 0.8	544.7 ± 91.2	508.2 ± 91.9	51.5 ± 12.3
20D-11CL-20D	36.2 ± 1.4	36.2 ± 1.4	708.3 ± 199	792.7 ± 74.4	160.3 ± 19.9
9D-23CL-9D	15.9 ± 3.2	15.9 ± 3.2	598.5 ± 151	677.5 ± 62	69.3 ± 29.4
19D-18CL-19D	21.1 ± 0.6	21.3 ± 0.8	949.6 ± 70.9	580.2 ± 57.9	147.3 ± 16.3
B1 [1)]	9.9 ± 0.8	15.6 ± 1.4	540.6 ± 58	345.6 ± 54	65.4 ± 11.6
B2 [2)]	32.5 ± 3.1	32.5 ± 3.1	661.2 ± 121.5	830.1 ± 56.1	152.9 ± 22.3
B3 [3)]	13.8 ± 1.3	13.8 ± 1.3	430.5 ± 42	602.5 ± 72	38.5 ± 8.7
B4 [4)]	20.1 ± 2.4	20.1 ± 2.4	455.3 ± 37.3	813.3 ± 130.8	70.4 ± 7.8
50CL	13.1 ± 0.8	26.9 ± 1.6	1683 ± 79.4	143.6 ± 19.7	273.4 ± 19.7

4.3.6 Nanostructure of block copolymers

To understand the effect of microdomain structures on the properties of the block copolymers, small-angle X-ray scattering (SAXS) measurements are conducted. The SAXS profiles of the triblock copolymers and their blends at room temperature are shown in **Figure 4.7-1(a)** and **4.7-1(b)**, respectively, whereas the Lorentz-corrected SAXS profiles are shown in **Figure 4.7-2**. The long period is determined from the q position of the first order peak in the Lorentz-corrected profile in the q range of $0.09 < q < 0.15$ nm^{-1}, which is found to be 45.9, 52.5, 63.9 and 61.3 nm for the specimens 10D-11CL-10D, 20D-11CL-20D, 19D-18CL-19D and 9D-23CL-9D, respectively. Further, a broad peak is observed in the Lorentz corrected profile in the q range of $0.3 < q < 0.5$ nm^{-1}. This broad peak is ascribed to the long period (D) of the crystalline lamellae sandwiching the amorphous layers which are 15.5, 19.6, 19.6 and 22.6 nm for the specimens 10D-11CL-10D, 20D-11CL-20D, 19D-18CL-19D and 9D-23CL-9D, respectively.

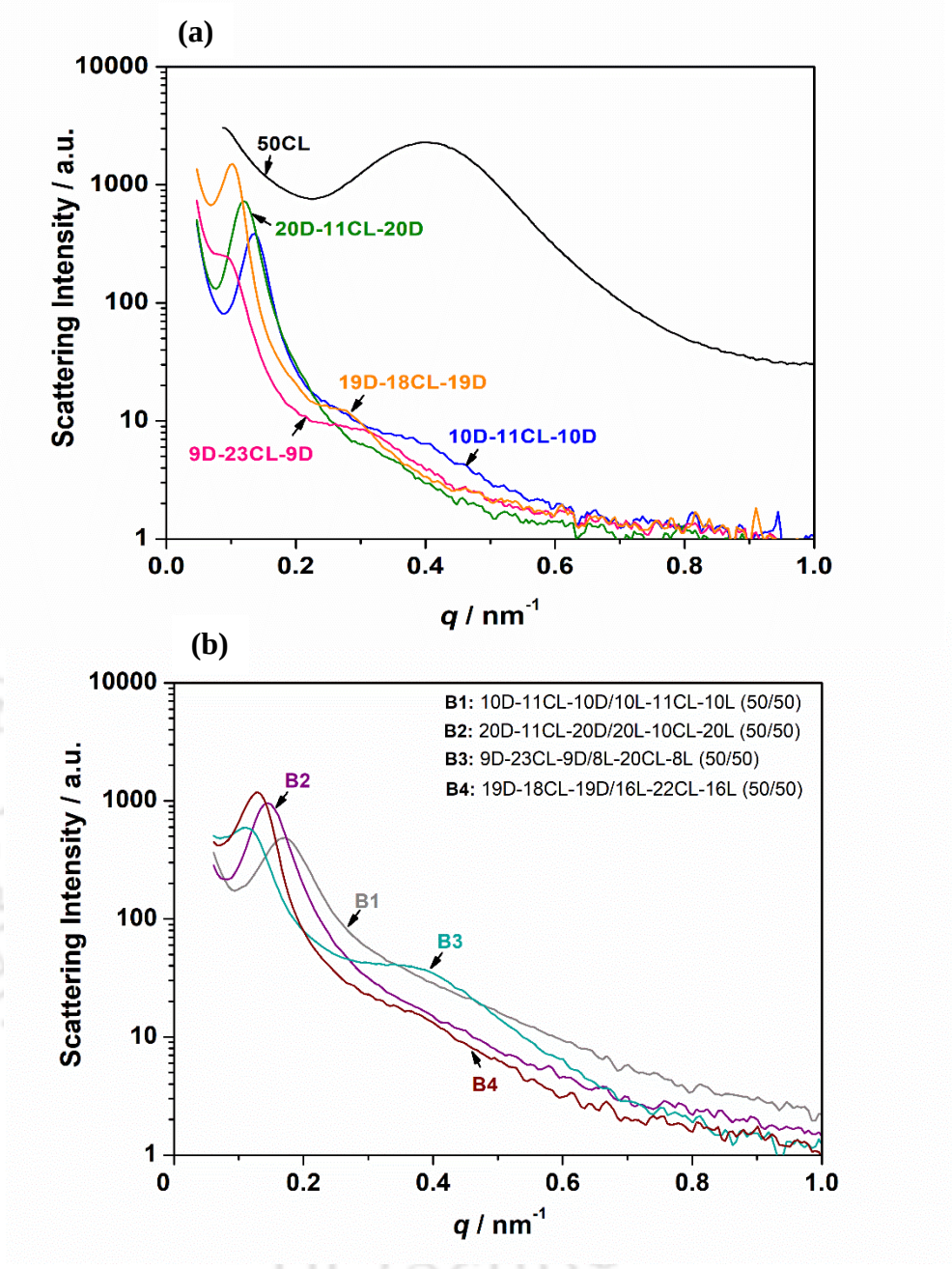

Figure 4.7-1: 1d SAXS profiles of (a) neat triblock copolymers and (b) triblock copolymer blends (as-prepared specimens).

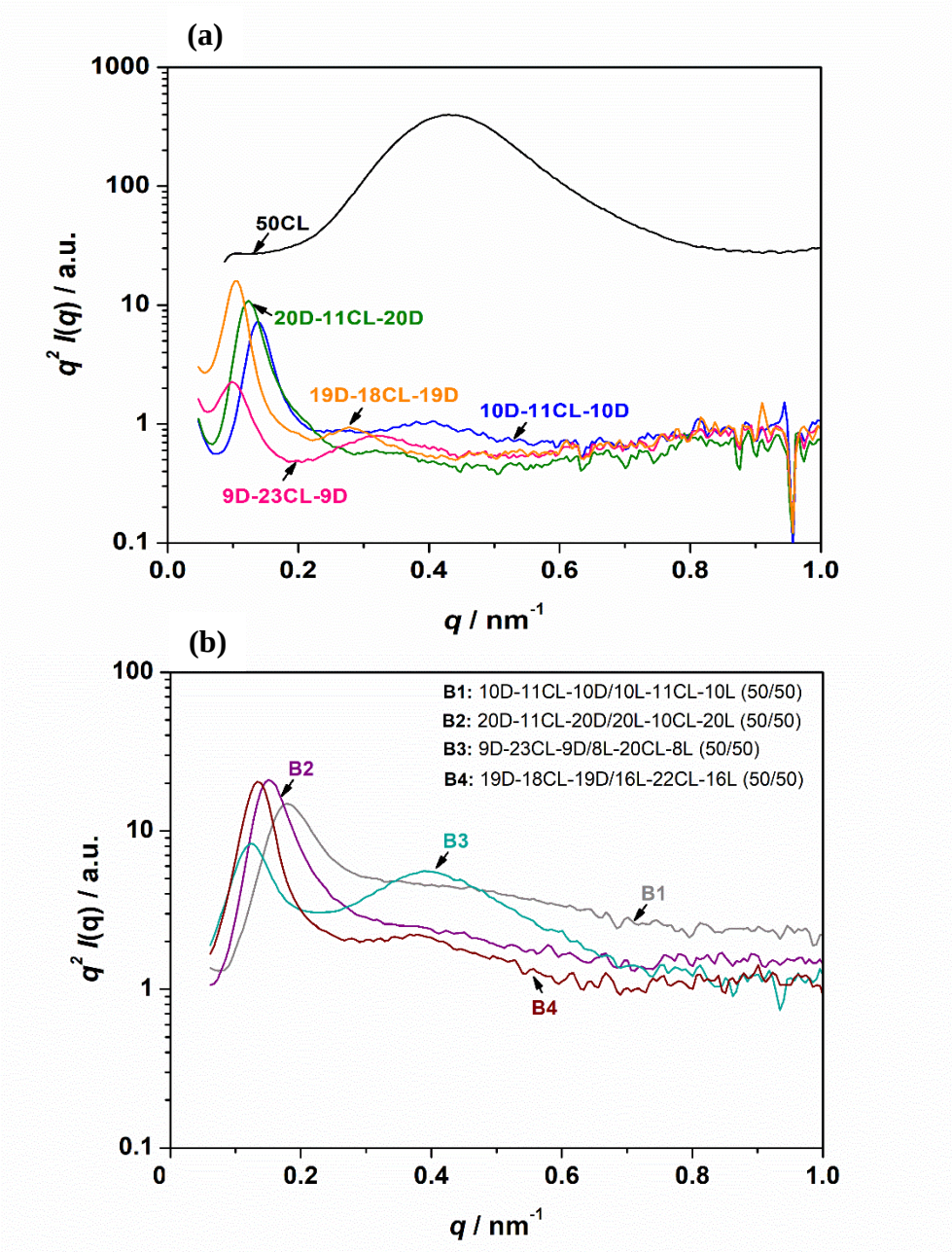

Figure 4.7-2: Lorentz-corrected SAXS profiles of (a) neat triblock copolymers, and (b) triblock copolymer blends (as-prepared specimens).

The LCST (lower critical solution temperature) phase behavior for PCL/PDLA blends was reported by Meredith et al.,[236] where the critical point is observed at 86 °C when the mass fraction of PCL is 36% ($M_{w,PCL}$= 114000 and $M_{w,PDLA}$= 127000). Since the

specimens in the present study were prepared by melting the triblock copolymers at 210 ℃ and enantiomeric blends at 235 ℃ followed by quenching them in ice-water, the specimens may contain the frozen structure at 210 ℃ which may be in the microphase-separated region in the LCST phase diagram. To account for the microphase-separated structure, the SAXS measurements were conducted at higher temperature (above T_m of PLA and PCL) for the triblock copolymers, as shown in **Figure 4.8**. The first-order peaks were clearly visible even at the higher temperature (~210 ℃), indicating the existence of a microphase-separated domain. Based on this knowledge, we constructed nanostructure models by considering that PCL started to crystallize in the PCL microdomain space, which is confined by the glassy PLA phase, upon T-jump from melt at 210 ºC to 0 ºC (ice-water).

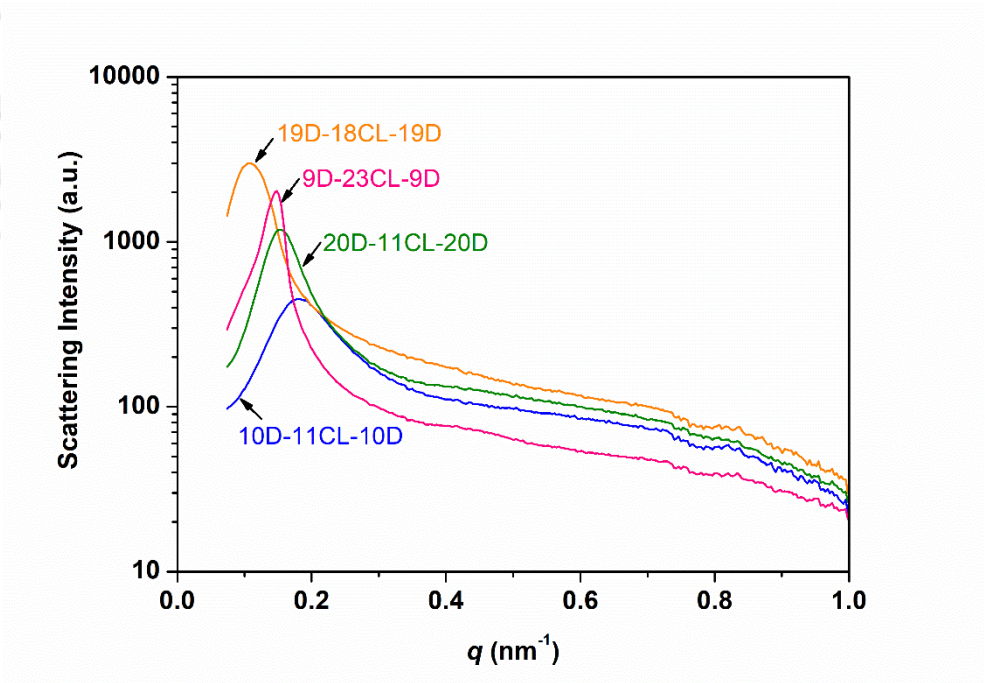

Figure 4.8: 1d SAXS profiles of the triblock copolymers measured at 210 ℃.

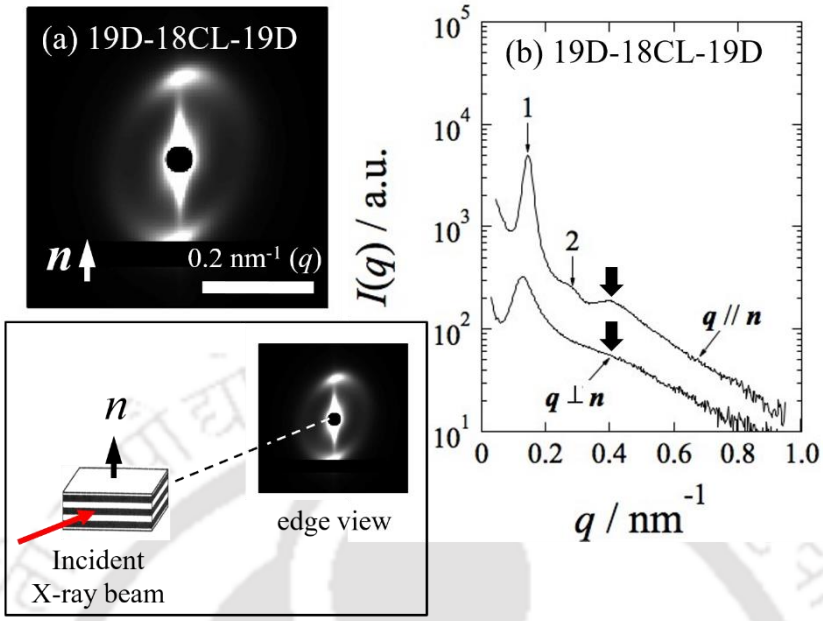

Figure 4.9: (a) 2D-SAXS pattern of the oriented 19D-18CL-19D specimen along with the (b) sector averaged 1d-profiles in the perpendicular and parallel directions with respect to the film normal (*n*) of the specimen.

In order to construct a structure model, it is important to examine the orientation of the crystalline PCL lamellae in the PCL lamellar microdomain. For this purpose, we conducted the 2D-SAXS measurement of the oriented 19D-18CL-19D specimen. Note that the specimen was compressed with the compression rate of 2.0 (= t_0/t) where t_0 and t denote the thickness of the initial specimen and that of the compressed specimen, respectively) at 210 ºC and then the compressed specimen was quenched to ice-water temperature to induce the crystallization of PCL.

Figure 4.9(a) shows the 2d-SAXS pattern of the compressed 19D-18CL-19D specimen, exhibiting two clear spots in the direction of *n* (the direction parallel to the film normal of the specimen). This clearly indicates that the lamellar microdomains were oriented preferentially parallel to the substrate surface upon the application of the compressional force. **Figure 4.9(b)** shows the 1d-SAXS profiles parallel and perpendicular to ***n***. In the

former profile, there observed a second-order peak of which *q* position is exactly twice of that for the first-order peak. This fact ensures that the lamellar microdomains order regularly in the direction of $\boldsymbol{q}$ // **n**. Furth700%ermore, the relatively broad peak (specified by the thick arrow around $\boldsymbol{q}$ = 0.40 nm^{-1}) is also clearly discernible. Since this peak is very broad as compared to the others and its *q* position is not relatively three-fold of the *q* value for the first-order peak, we cannot assign this peak as the third-order peak due to the lamellar microdomains. Rather, it should be considered that this broad peak is ascribed to the long period of the crystalline PCL lamellae. It should be noted that such a broad peak was hardly discernible (at the position specified with the thick arrow) in the 1d-SAXS profile in the perpendicular direction ($\boldsymbol{q} \perp$ **n**). If the direction of the stacking of the PCL crystalline lamellae in the PCL microdomain would be perpendicular to the microdomain interface between PLA and PCL, then the broad peak appearing in the 1d-SAXS profile in the perpendicular direction ($\boldsymbol{q} \perp$ **n**) should be much clearer with higher intensity. Therefore, the results shown in **Figure 4.9(b)** indicate that the direction of stacking of the PCL crystalline lamellae in the PCL microdomain is more or less parallel to the microdomain interface between PLA and PCL. Based on this experimental result, the nanostructure models shown in **Figure 4.10** were constructed, where a set of the glassy PLA, crystalline PCL, amorphous PCL and crystalline PCL is alternating. According to the model (the flat-on orientation of the crystalline lamellae with respect to the interface), it can be further speculated that the nucleation of the PCL crystallization is easily triggered on the interface of the microdomain, because the PCL block chains are tethered to the interface which is a solid wall of the glassy PLA lamellar microdomain so that the PCL chains in the vicinity of the wall can easily start forming a nucleus. The reason of drawing of only a pair of the PCL crystalline lamellae is because of the

confinement of the stacks in the PCL microdomain in its thickness direction. Namely, this is to accommodate the stack of the crystalline lamellae with a given long period, which is almost similar to the thickness of the PCL lamellar microdomain, into the PCL lamellar microdomain.

Although the structure model illustrated in the **Figure 4.10** represents the general feature, the individual models corresponding to the specimens can be considered. It should be noted here that the microdomain repeating period (the alternating period of the set of glassy PLA/crystalline PCL/amorphous PCL/crystalline PCL), *d*, is evaluated from the *q* position of the first-order peak (q_1) in **Figure 4.7-2** by $d = 2\pi/q_1$, while the long period (*D*) of the PCL lamellar stacking is evaluated from the *q* position of the broad peak (q^*) in **Figure 4.7-2** by $D = 2\pi/q^*$.

Using the following relations,

$$d = l_{PLA} + l_{c,PCL} + l_{a,PCL} + l_{c,PCL}$$

$$D = l_{c,PCL} + l_{a,PCL}$$

The fraction of the PCL phase (f_{PCL}) can be evaluated, as:

$$f_{PCL} = (D + l_{c,PCL})/d$$

where, l_{PLA}, $l_{c,PCL}$ and $l_{a,PCL}$ denote the thickness of the glassy PLA phase, that of the crystalline PCL lamella, and that of the amorphous PCL layer, respectively. Using the value of the crystallinity ($X_{c,PCL}$), $l_{c,PCL}$ can be estimated as:

$$l_{c,PCL} = D \times X_{cPCL}$$

Thus,

$$f_{PCL} = (1 + X_{c,PCL})\, D/d$$

is formulated. The values of f_{PCL} estimated by using this equation were all overestimated for 9D-23CL-9D, 10D-11CL-10D and 19D-18CL-19D specimens. In order to compensate this overestimation, the schematic shown in **Figure 4.11** is considered, where grains with short width are dispersed in the matrix of glassy PLA phase. Thus, the total amount of white PCL phase (including its crystalline and rubbery amorphous phases) can be reduced. Furthermore, the reason why the stack of the crystalline lamellae was only partly described in the PCL lamellar microdomain is to set the total crystallinity of PCL at the same value evaluated from the WAXS result, as well as by the consideration that the chain folding of the PCL chains cannot be continued in a long distance in the lateral direction (parallel to the microdomain interface).

As for the 20D-11CL-20D specimen, cylindrical morphology should be considered (**Figure 4.12**) because of the smaller fraction of the minor component (PCL) (21 wt%) as compared to the broader value between the lamellar and cylindrical morphology[238]. This is the reason why the structure model indicates the cylindrical microdomain. However, the stacking of the crystalline lamellae illustrated in the cylindrical microdomains repeat in the direction parallel to the cylindrical axis is just a speculation because it seems no other possibility to construct the crystalline lamellae inside the cylindrical microdomains. This model also meets the similar expectation of triggering the nucleation at the microdomain interface. Nevertheless, the disc-shape of the crystalline lamellae is just the speculation. It may be better to consider, for example, an incomplete disc having many holes.

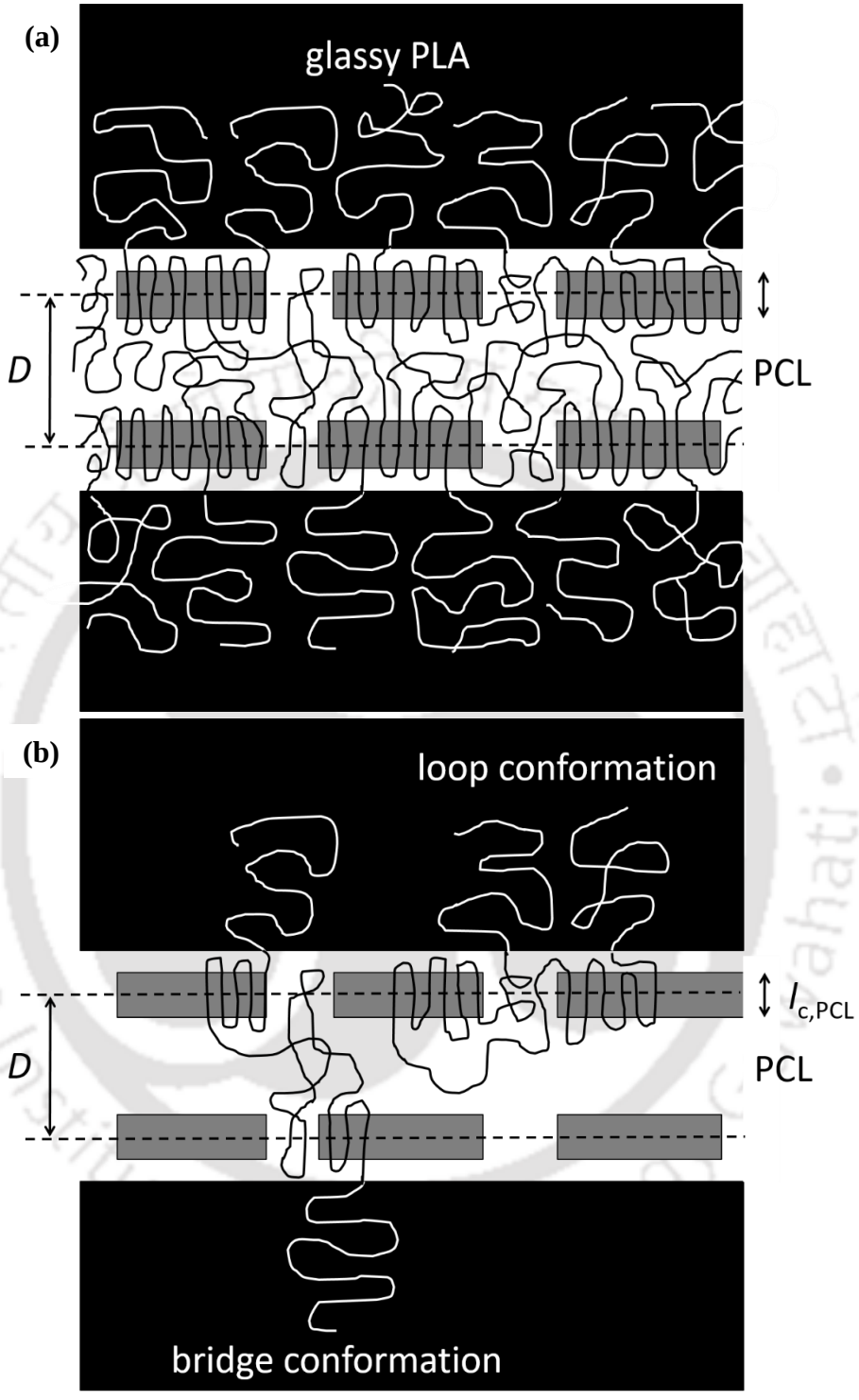

Figure 4.10: (a) Plausible nanostructure model for the 10D-11CL-10D, 19D-18CL-19D and 9D-23CL-9D specimens. Panel (b) highlights two typical conformations of the triblock copolymer chains in the nanostructure model in the panel (a).

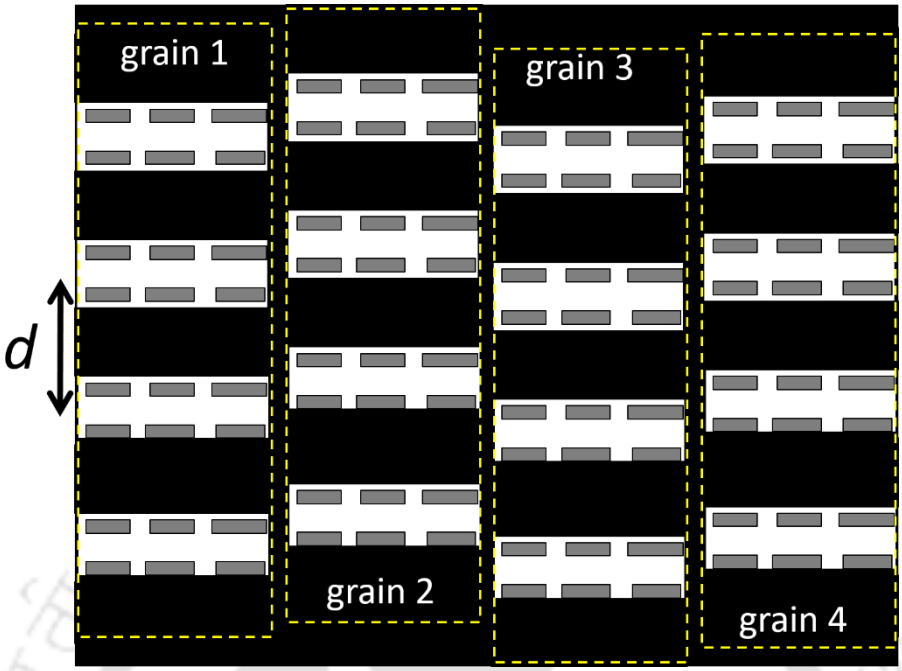

Figure 4.11: Illustration of the grains comprising some sets of repeating glassy PLA (black) + crystalline PCL (grey) + amorphous PCL (white) layers in the matrix of the glassy PLA (black). Note here that such glassy PLA matrix comprises also the PLA block chains so the distance between two neighboring grains should be quite short.

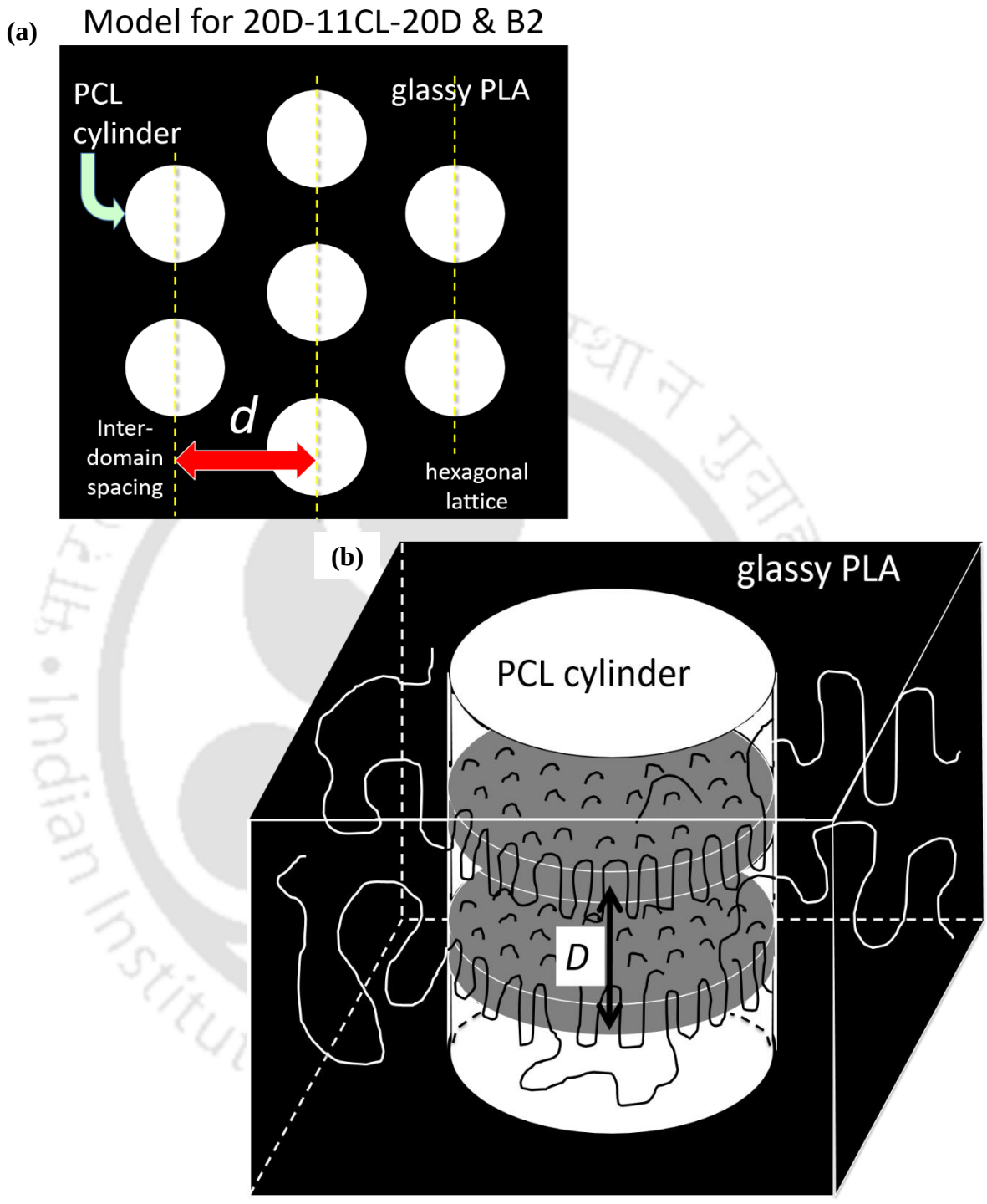

Figure 4.12: Plausible nanostructure model for the 20D-11CL-20D and B2 specimens. (a) Top view and (b) perspective view.

4.3.7. Correlation of Mechanical Properties with Nanostructure

The physical properties of the block copolymers depend strongly on their nano-structures. The block copolymers form the lamellar morphology[239] when the fraction is in a range of 0.33 ~ 0.67 in case of three triblock copolymer specimens other than 20D-11CL-20D. As for the 20D-11CL-20D specimen consisting of ~21% PCL, it possibly forms the cylindrical morphology. An increased extensibility of this specimen (~700%) may be due to the confinement of PCL phase in the cylindrical microdomain thereby resulting lower crystallinity (~18.2%). As for the ultimate tensile strength, its higher value for the 19D-18CL-19D specimen may be ascribed to the higher extent of the continuity of the PDLA glassy amorphous microdomains as well as its higher thickness. The thicker PDLA lamellar microdomain in 19D-18CL-19D (as shown in the structure model, **Figure 4.10**) may result in the higher yield strength and the higher ultimate tensile strength as well as the longer soft PCL chains which prevent the macroscopic breakage of the specimen in the early stage of elongation.

As for the mechanical behavior of the B4 specimen showing the lower yielding stress and the lower ultimate stress with the lower ultimate elongation as compared to those of the neat triblock copolymer specimen (19D-18CL-19D), the $X_{c,PCL}$ value of B4 is much larger than 19D-18Cl-19D (**Table 4.2**). Nevertheless, B4 exhibited the lower mechanical properties which may be attributed to the much shorter grain length (in the directions of the microdomains repeat, **Figure 4.11**) as the first-order peak in the SAXS profile was found to be wider for B4 as compared to that for the neat 19D-18CL-19D specimen (**Figures 4.7-1 & 4.7-2**). Since this peak-width is inversely proportional to the grain length, the results of SAXS possibly indicate the existence of the shorter grains in the B4 specimen which in turn may be responsible for the lower mechanical properties. On the

contrary, it may be opposite for the case of B3 possibly resulting in the mechanical properties of B3 being slightly higher than those of the neat 9D-23CL-9D. However, for the B2 specimen, a similar argument may not be true as the microdomain morphology is presumed to be cylindrical due to the lower weight fraction of PCL (~21%).

The specimen 20D-11CL-20D is found to exhibit the maximum stress, which may be ascribed to the higher content of PLA forming a glassy matrix phase with the PCL. However, the specimens 19D-18CL-19D and 9D-23CL-9D exhibit almost similar SS curves while their PCL fractions differ which may be corroborated to the difference of their nano-structures. The regularly ordered nano-structure with the relatively longer grains may be considered for the specimen 19D-18CL-19D due to the sharp first order peak. For the specimen 9D-23CL-9D, the first order peak is very broad which may result in a nanostructure with shorter grains (**Figures 4.7-1 & 4.7-2**). Further, the first-order peak was much broader for 10D-11CL-10D as compared to that of the 19D-18CL-19D specimen, indicating the shorter grains with poorer ordering regularity of the nanostructures in the 10D-11CL-10D specimen. This character may account for the lower mechanical properties of this specimen as compared to 19D-18CL-19D, although the PLA fractions are similar to each other. Although the mechanism of the formation of such nano-structures should be perfectly understood with respect to the microscopic analysis and molecular structure (molecular weight and composition of the triblock copolymer) along with the PCL crystallization upon melt quenching, this is beyond the scope of the current study. Studies by simultaneous time-resolved SAXS/WAXS experiments are currently ongoing for the elucidation of the process of the nanostructure formation upon melt quench to the isothermal crystallization temperatures.

4.3.8. Water vapor permeability

The water vapor permeability signifies the ability of a material to allow the passage of water vapor through it, where the higher value of permeability implies the rapid passage of water vapor and vice versa. It is observed from **Figure 4.13** that PLA has the lowest value of water vapor transmission rate (WVTR) (~3.7 g·mm·m^{-2}·day^{-1}) while the value of WVTR of PCL is not detected by the instrument under the given parameters (95% RH) which may correspond to the very high permeability of PCL. The value of WVTR was found to increase to 9.5 and 10.4 g·mm·m^{-2}·day^{-1} for the specimens 10D-11CL-10D and 19D-18CL-19D, respectively, upon the involvement of the PCL segment in the matrix of PLA. These are the specimens with the nearly same content of PCL and PLA and the close values of WVTR of these specimens suggest the role of PCL in increasing the permeability of the triblock copolymers. Furthermore, the WVTR of the specimen 20D-11CL-20D is found to be reduced to 5.8 g·mm·m^{-2}· day^{-1} with the decreasing content of PCL (20%) which further confirms the effect of PCL leading to the improved water vapor permeability of the materials. The reason behind the increased permeability of the block copolymers may correspond to the lower T_g of PCL (-60 °C) leading to the increased of vapor. On the other hand, PLA exists at a temperature lower than its T_g where the polymer chains are frozen (glassy state) and the segmental motion of the chains is restricted, to make the permeability of vapor difficult. For the blend specimen B2 (20D-11CL-20D/20L-20CL-20L), the value of WVTR is further reduced to 4.6 g·mm·m^{-2}·day^{-1} which may be due to the increased crystallinity of PCL (**Table 4.2**) leading to a much lower segmental mobility and molecular diffusion which further restricts the passage of water vapor.

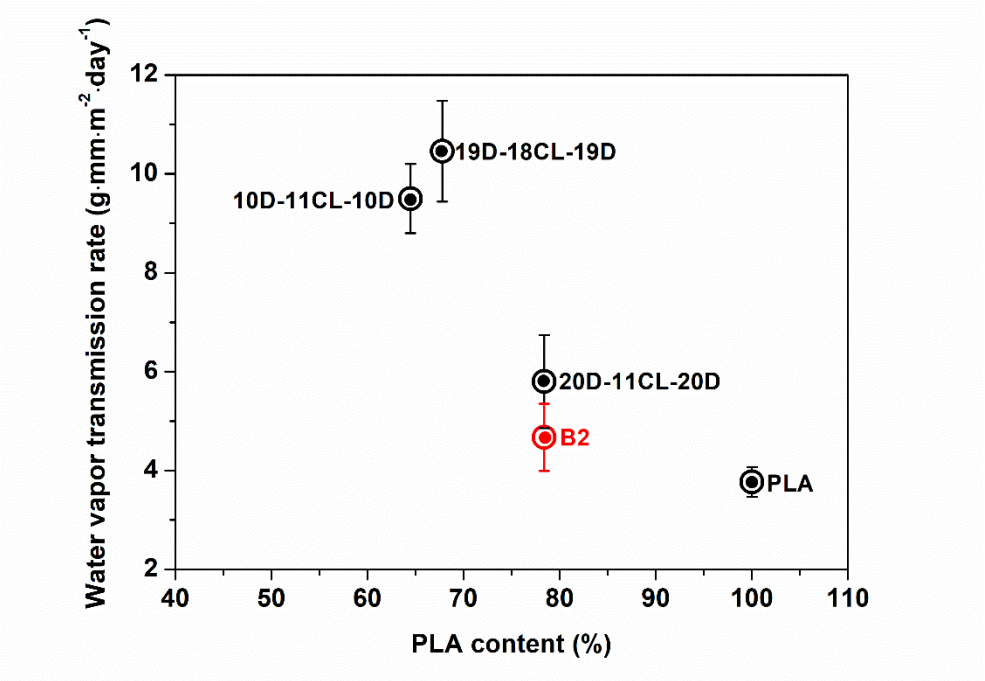

Figure 4.13: Water vapor transmission rate as a function of the PLA content.

4.3.9. Scale-up Synthesis

The use of solvent in synthesizing polymers is not favorable for the industrial production as well as for the solvent-specific harmful effects rendering on the biomedical devices. Therefore, efforts have been paid on developing solvent-free routes for synthesizing polymers in large-scale. The solvent free synthesis of PLA block copolymers was reported by Lee et. al. where they used the high-speed ball milling to mix the macroinitiator, monomer and the catalyst to obtain high molecular weight block copolymers.[240] The bulk polymerization strategy does not involve the use of any solvent during the synthesis process and allows the easy control of molecular weight. However, the purification step usually incorporates the use of harsh solvents, rendering the process industrially unviable. For the triblock copolymer (PLA-PCL-PLA), PCL is made in the first step ROP which gives the conversion >99%, and it directly subjected to the second step ROP where lactide is used as the monomer. The conversion achieved in the second step is >95% in which the removal of

residual monomer is required. Here, we adopted the sublimation technique for removing the residual lactide from the triblock copolymer in order to circumvent the used solvent, rendering it industrially viable. We succeeded the synthesis with the batch of 500 g.

4.3.10 Processing of Triblock Copolymer via Twin-screw Extrusion and 3D printing

Biobased/biodegradable polymers usually experience a difficulty in processing by using the established processing techniques such as injection molding, extrusion, etc. where the limiting factors may be the molecular weight, low thermal stability, extreme brittleness, etc. This often requires special processing designs[241], or the use of stabilizers which further affect their degradation rate and modify their properties for end-use applications[242]. However, it is intended to show that we successfully synthesized a triblock copolymer (with tailored properties) which was processed by using the conventional twin-screw extruder without incorporating any stabilizers to produce filaments. The filaments were further used for 3D printing of a representative mesh-type scaffold (**Figure 4.14**), which suggests the processability of these triblock copolymers for making intended materials for targeted applications.

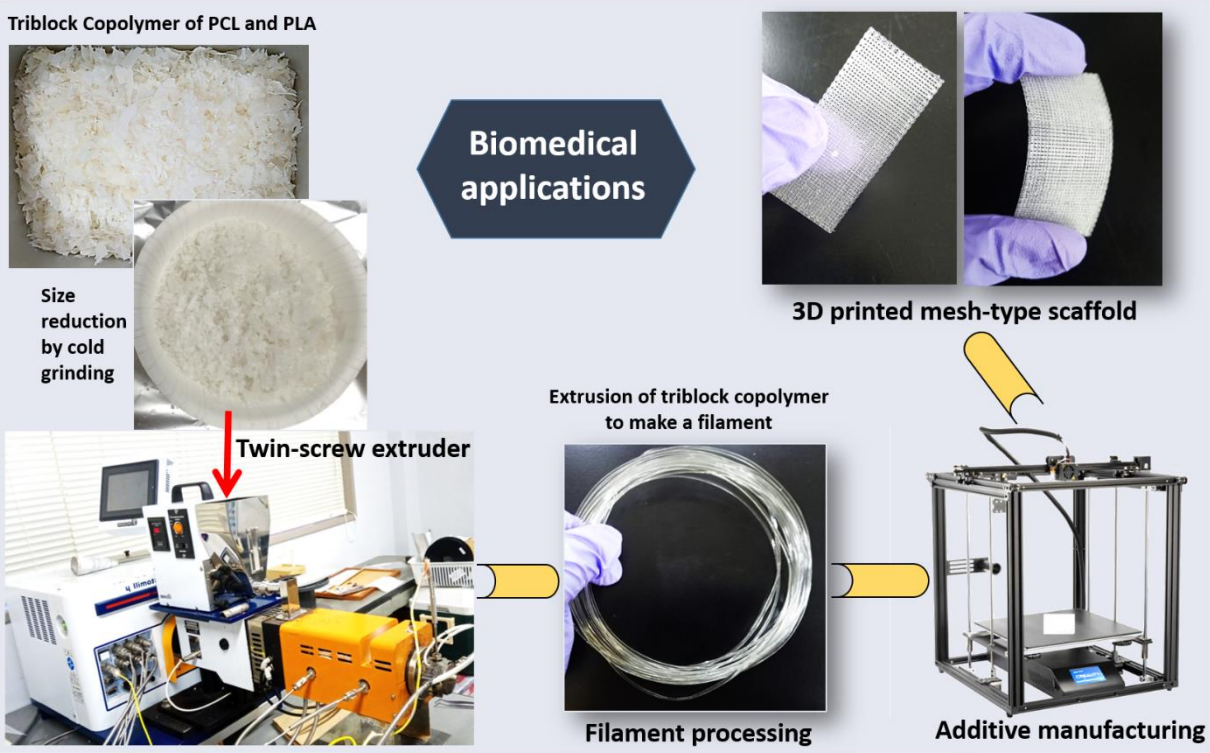

Figure 4.14: Melt processing of triblock copolymer (synthesized by the scale-up method) to fabricate the filament which was successfully used for 3D printing of a mesh-type scaffold.

4.3.11. Biocompatibility

The triblock copolymer and the blend were tested by the ordinary MTT assay in order to inspect the viability of cells. The UMR-106 cell viability (%) is determined as a function of time (as compared to control, 100 % viability) and shown in **Figure 4.15**. The results show that the rat bone cells adhere and grow on the surfaces of the homopolymers and block copolymers over a duration of 72 h, indicating the non-toxic nature of the synthesized materials. The pattern of the time-dependent change in the cell-viability is similar between PLA and B2 (blend specimen), and between PCL and the triblock copolymer. This behavior may be ascribed to the top surface of B2 specimen having PLA rich in composition whereas that of the triblock copolymer having PCL rich in composition. Further, the cells adhered

to the surface of the materials (after 42h) are shown in **Figure 4.16**. The images observed in the bright field and under fluorescence differentiate the effect of the fluorescent dyes. The Nuc Red^{TM} Live stain (cell permeant) emits red fluorescence when bound to the nucleus of living cells[243], which is observed for all the specimens. Further, acridine orange is a cell permeable and nucleic acid binding stain which emits green fluorescence[244] when it binds to dsDNA as observed. The adhesion of rat bone osteosarcoma cells is evident upon staining the specimen surfaces, indicating their non-toxic nature.

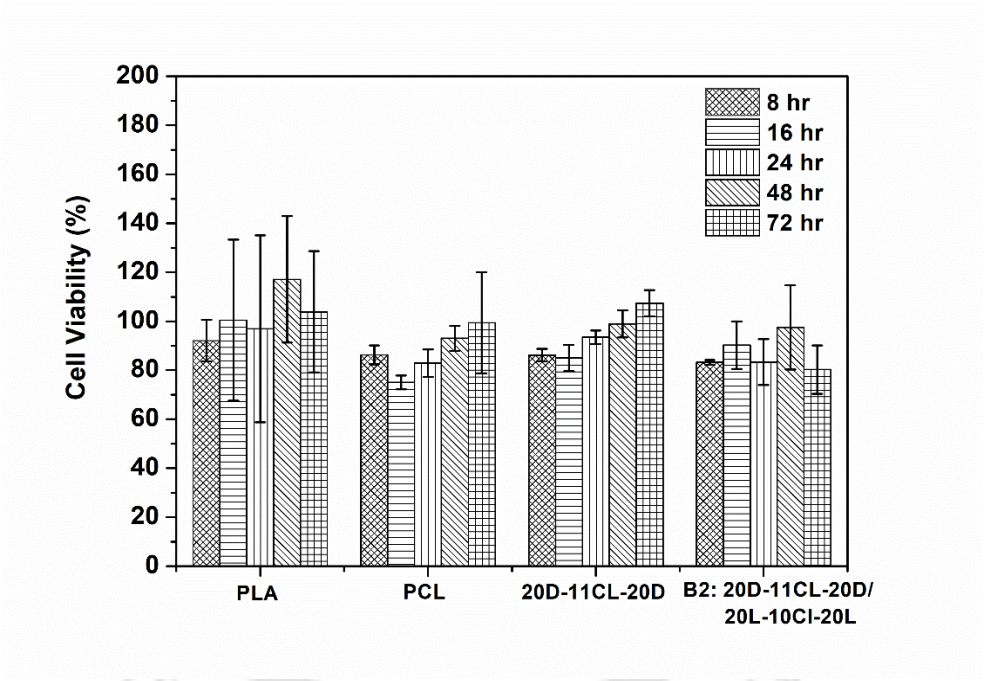

Figure 4.15: Viability of rat bone osteosarcoma cells determined by MTT assay.

Specimen code name	**Stain:** NucRed™ Live		**Stain:** Acridine orange	
	(a) Bright field images	**(b) Fluorescence images**	**(a) Bright field images**	**(b) Fluorescence images**
Control (Polystyrene)	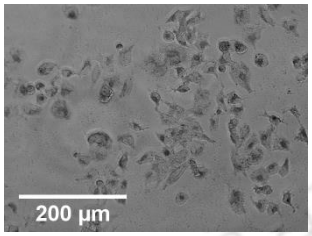	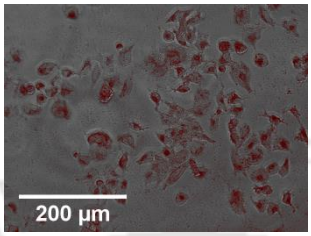	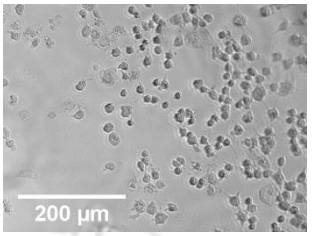	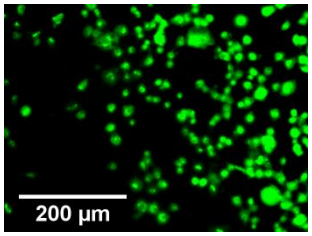
PLA	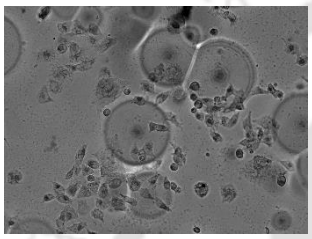	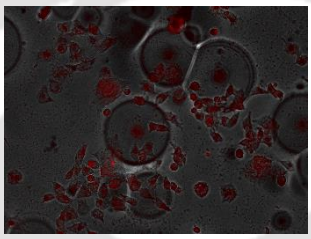	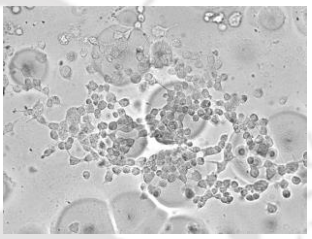	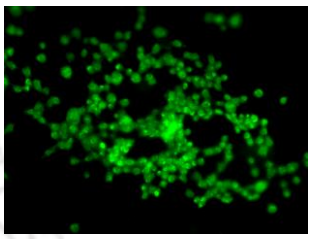
PCL	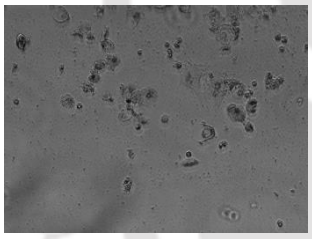	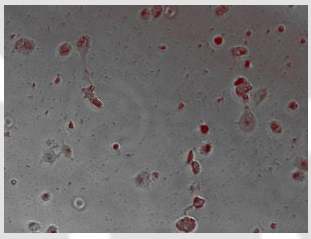	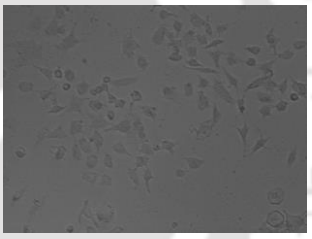	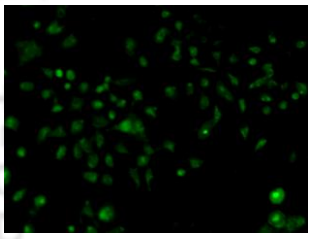
20D-11CL-20D	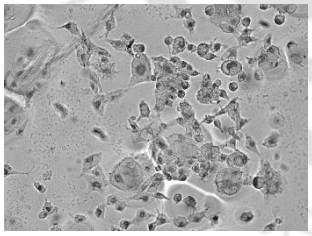	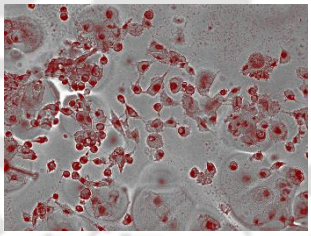	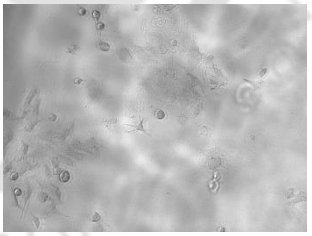	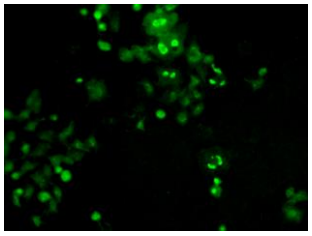
B2: 20D-11CL-20D/ 20L-10CL-20L (50/50)	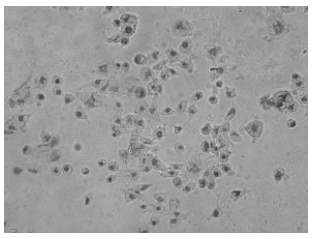	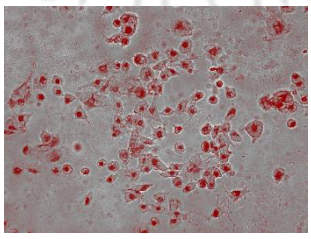	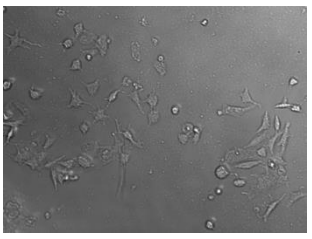	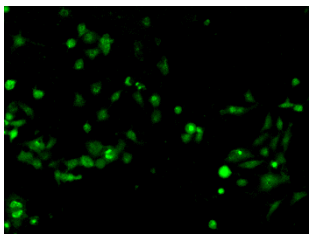

Figure 4.16: Representative images of rat bone osteosarcoma cells adhering on the specimen surface after 48h of culturing, being stained with NucRed™ Live and acridine orange.

4.4. Conclusion

The triblock copolymers (PLA-PCL-PLA) were synthesized with varying block lengths of PCL and PLA. Their enantiomeric blends were also prepared. The effects of the composition and the block length on the macroscopic properties of the specimens were examined where the significant improvement in the mechanical properties is found for the triblock copolymer (20D-11CL-20D) having ultimate tensile strength of ~36 MPa and an elongation at break of ~700% with a high toughness of ~160 MJ/m^3. The tensile strength of the block copolymers range from 13 MPa to 36 MPa whereas the extensibility range from ~540% to 950% upon tailoring their block length. Such wide-ranged mechanical properties were correlated with the morphology of the self-assembled nanostructure of triblock copolymers where the specimens 9D-23CL-9D (~56% PCL), 10D-11CL-10D (~35% PCL) and 19D-18CL-19D (~32% PCL) were found to have the lamellar morphology whereas the specimen 20D-11CL-20D (~21% PCL) had a cylindrical microdomain structure as remarked from the SAXS analysis. The significant changes in mechanical properties with the varying composition of the block copolymers and their total molecular weight revealed the possibilities of developing customized materials with controlled properties which can be targeted for specific applications. The mesh-type scaffold was prepared by 3D-prinitng of the filament obtained by processing the triblock copolymer 20D-11CL-20D using an industrially viable approach. The adherence and multiplication of the rat bone osteosarcoma cells on the surfaces of synthesized materials suggested non-toxic nature of the 3D printed scaffold.

Chapter: 5

Stereoblock Terpolymers based on PLA and PCL with Preferential Stereocompelxation

Graphical Abstract

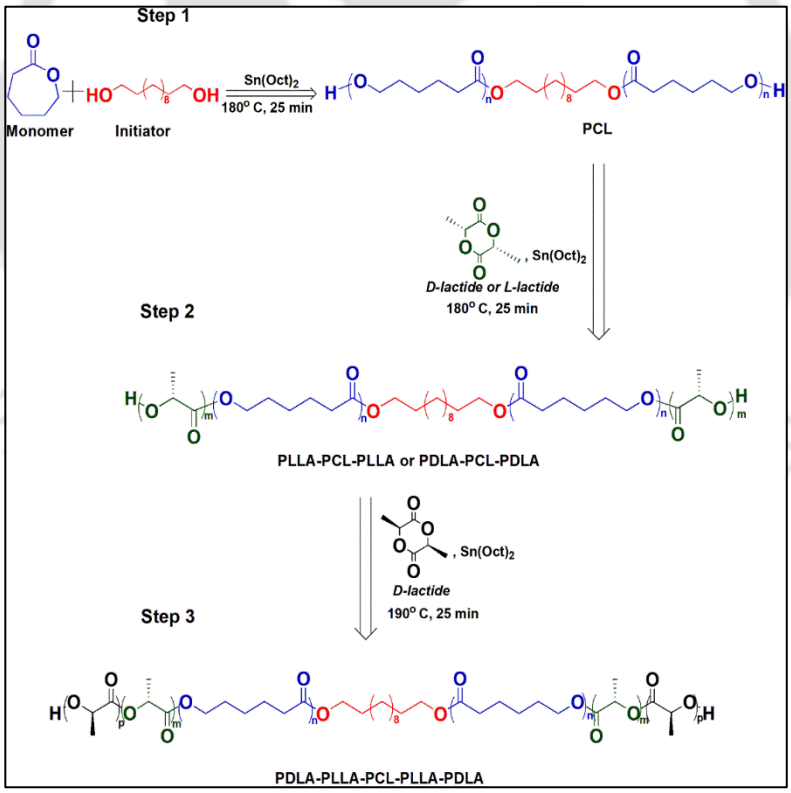

Outcome:

- *Patent filed: Stereocomplex Terpolymers and Composites of PLA and PCL, and a Method of Preparation Thereof (Application No: 202131013736)*

Abstract

The current chapter unfolds the synthesis of stereoblock terpolymers having preferential stereocomplexation by three-step ring opening polymerization. The stereoblock terpolymers are synthesized by bulk melt polymerization where PCL is incorporated as a mid-segment. The enantiomeric stereoblock terpolymers are blended to obtain the enantiomeric blend. The effect of heating rate on stereocomplexation is manifested for the terpolymer and its blend. The mechanical properties and crystallization behavior are also determined. The viability of rat bone osteosarcoma cells (UMR-106) on the surface of synthesized materials is also established.

5.1 Introduction

In the recent years, stereocomplexation in PLA has attracted significant attention of the scientific community due to its ability to improve the properties of PLA. Stereocomplex crystallites are a result of the hydrogen bonding between the methyl and carboxyl groups of PLLA and PDLA during melt and solution blending[245]. Formation of stereocomplex in the polymeric matrix leads to the higher melting temperature, improved tensile strength, resistance to hydrolytic degradation etc. However, stereocomplexation in PLA is highly depended on its molecular weight and efficient molecular interaction. Generally, stereocomplex crystallites are formed well upon blending low molecular weight PLLA and PDLA. On the other hand, high molecular weight PLA is desired for the mechanical stability of the end product and blending of high molecular weight PLLA and PDLA results in the formation of stereocomplex crystallites along with homocrystallites which leads to the inferior overall properties. In order to enhance the stereocomplexation and molecular interaction between PLLA and PDLA chains, several techniques such as

development of block copolymers[86], in situ biocomposite fabrication[97], use of low molecular weight species of PLA in enantiomeric PLA[246], selective laser sintering[247], oil-water emulsion blending[245], microwave irradiation[248], use of supercritical fluid[249], thermally induced technique[250], etc. are developed by different researchers worldwide.

Among the above mentioned techniques, block copolymerization has shown promising results to obtain polymers with the high content of stereocomplexation along with improved mechanical properties[251, 252]. In case of the block copolymers, two or more different types of polymers can be used for developing polymeric system with tailored properties. In the context of current work, the presence of aliphatic polyester sequence makes poly (lactic acid) (PLA) and poly (ε-caprolactone) (PCL) biodegradable under suitable conditions which is useful for the biomedical applications. The products of hydrolytic and/or enzymatic degradation i.e. lactic acid and caproic acid of these polymers are found to be eliminated through metabolic pathways[188, 253]. Being a thermoplastic material with relatively higher strength, PLA can be a suitable candidate for biomedical applications, however, lower elongation at break hinders its use. Blending of soft and hard materials can be translated to materials having collective properties of both, however macrophase separation turns out to be a limiting factor. Addition of soft segment in the backbone chain of PLA can lead to the achievement of enhanced mechanical properties and stereocomplexation in the PLA system due to the improved molecular interaction and reduced phase separation[254]. Lately, significant attention has been laid on developing diblock[252], triblock[252], pentablock copolymers incorporating soft segments along with PLA in the backbone.

Pentablock copolymers can attain minimum three different polymer blocks having different tacticity and properties in a single polymeric chain. Pentablock copolymers consisting of PLA have been synthesized by several research groups for different purposes which include polyethylene oxide (PEO), polypropylene oxide[255], poly(methyl methacrylate), polyimide, and PCL[256] along with PLA in the backbone chain. Further, pentablock copolymers containing the blocks of PLA, acrylamide, polyethylene glycol (PEG)[257]; PLA, PCL, PEG[258-261]; propylacrylamide, PCL, PEG[262], polydecalactone, PLA, PCL[263], PEO, polyvinylpyridine, PCL[264] have been developed to achieve tailored properties for intended applications. However, little has been studied about pentablock copolymers for enhancing the stereocomplexation in PLA.

Hirata et. al. have synthesized pentablock copolymer using poly(3-methy-1,5-pentylene succinate), an aliphatic polyester as soft segment in PLLA and PDLA stereoblock chains by three step polymerization process[79]. They developed pentablock polymer showed a preferential stereocomplexation due to the improved molecular mixing of enantiomeric PLA segments while exhibiting elastomeric nature due to presence of soft segment. The elastomeric nature of developed pentablock polymer was limited to (~470%) for 40 kDa molecular weight that reduced to less than 6 % in the case of higher molecular weight (95 kDa). In another study, Gardella et. al.[265] have attempted to synthesize pentablock PLA using polytetrahydrofuran (PTHF) as a soft segment between the hard segments of PLLA and PDLA blocks (PDLA-PLLA-PTHF-PLLA-PDLA) by two step synthesis route. The low molecular weight block copolymer was synthesized in the first step followed by incorporating the chain extender 1,6-hexamethylene diisocyanate (HDI) to increase the molecular weight. Further, Mao et. al. have synthesized pentablock polymer utilizing PEG as mid segment between enantiomeric PLLA and PDLA blocks for developing a

thermoresponsive physical hydrogel[266]. They found that the stereocomplex formation promoted the physical bridging between copolymer micelles and wider gelation temperature region and control drug release rate. However, the molecular weight of these materials was inadequate for the mechanical integrity of the material and use of PEG made this material particularly suitable for hydrogel applications. Additionally, Lee et. al. have utilized polybutylene succinate (PBS) as central soft segment between enantiomeric PLLA and PDLA segments to synthesize pentablock copolymer (PLLA-PDLA-PBS-PDLA-PLLA) by two step reaction[267]. They have shown that the direct connection of the PLLA and PDLA blocks in same chains facilitate the formation of stereocomplex crystals and utilization of PBS affected the crystallization kinetics and impart an elastic property. However, the elongation at break of the developed materials was found to be relatively lower along with the formation of hc PLA. The use of PCL as mid soft segment in pentablock copolymer was done by Rosen et. al.[160] using a magnesium complex catalyst. However, the process adopted was solution polymerization which was mainly focused on the effectiveness of catalyst used. The literature however does not report the use of PCL as a mid-segment along with PLLA and PDLA side blocks for development of pentablock copolymer using bulk melt polymerization technique.

It was noted in the earlier chapters, the blending of enantiomeric diblock or triblock copolymers led to the formation of sc-PLA crystals along with hc PLA crystals. Therefore this work aims at developing preferential sc crystals by means of stereoblock formation by three-step ROP. The mechanical, thermal and thermomechanical properties of the stereoblock terpolymer (pentablock copolymer) is done along with the cell viability studies for intended biomedical applications.

5.2 Experimental

5.2.1 Materials

L- and D-lactides (ee 99.9%) were acquired from Musashino Chemical Laboratories, Ltd. Tokyo, Japan. ε-Caprolactone was purchased from Nacalai Tesque, Kyoto, Japan, distilled and stored under N_2 environment. Dodecamethyleneglycol (DMG) or 1,12-Dodecanediol was purchased from Tokyo Chemical Industry Co., Ltd., Tokyo, Japan. Tin octoate ($Sn(Oct)_2$, 95%) was acquired from Sigma Aldrich, St. Louis, USA via Nacalai Tesque and distilled under high vacuum, dissolved in dried toluene (0.2 g/ml) and stored under an inert environment. 1,1,1,3,3,3-Hexafluoro-2-propanol was obtained from Central Glass Co. Ltd., Yamaguchi, Japan. Chloroform (HPLC grade) was obtained from Merck & Co., India. Methanol and dichloromethane were purchased from Nacalai Tesque and used without purification.

5.2.2 Synthesis of dihydroxyl terminated PCL

In the first step, ring opening polymerization (ROP) of ε-caprolactone was performed in the presence of DMG as an initiator and $Sn(Oct)_2$ catalyst to synthesize di-hydroxyl terminated PCL. The initiator (0.495 mmol) along with a magnetic stirring bar was added to a flask fixed with a three-way connector which was evacuated at 10 – 20 Pa for 3h. Thereafter, pre-distilled monomer (ε-caprolactone, 43.8 mmol) and a catalyst solution (tin octoate, 0.175 mmol) were added to the flask under N_2 atmosphere. The flask was sealed under N_2 atmosphere and the polymerization reaction was continued for 25 min at 180 °C. The conversion of the product was determined by ^{1}H-NMR. The conversion of PCL was higher than 99% and so it was used for the next step (as a prepolymer) without purification.

PCL, ^{1}H-NMR (600 MHz, $CDCl_3$): δ = 4.06 ($CH_2CH_2CH_2CH_2C\underline{H}_2O$-), 3.65 ($CH_2CH_2CH_2CH_2C\underline{H}_2OH$), 2.3 ($OC\underline{H}_2CH_2CH_2CH_2$-), 1.64 ($OCH_2C\underline{H}_2CH_2C\underline{H}_2CH_2O$-), 1.38 ($OCH_2CH_2C\underline{H}_2CH_2CH_2O$), 1.25 (-$OCH_2C\underline{H}_2(CH_2)_8C\underline{H}_2CH_2O$-), 0.88 (-$OCH_2CH_2(C\underline{H}_2)_8CH_2CH_2O$-) ppm

5.2.3 Synthesis of BCB/ACA triblock copolymers

The monomer (L- or D-lactide, 143 mmol) was added to the synthesized prepolymer (dihydroxyl terminated PCL) under N_2 atmosphere and evacuated at 10 Pa and 40 ℃ for 12 h. After this, the system was filled with N_2 gas and the flask was immersed into the oil-bath at 180 ℃ in order to melt PCL and lactide and solubilize the monomer into the melt of macroinitiator. After complete solubilisation, a catalyst solution (0.057 mmol) was added and the reaction was conducted for 25 min to synthesize BCB/ACA triblock copolymer by two-step ROP. The conversion of the product was determined by ^{1}H-NMR and found to be >90%. In order to remove the residual monomer, the synthesized triblock copolymer was dissolved in dichloromethane and purified using excess methanol. The precipitated product was filtered and dried in a vacuum oven 80 ℃ for 12 h. The triblock copolymers were ***A***L-***C***CL-***A***L or ***B***D-***C***CL-***B***D where ***A***, ***B*** and ***C*** represent the molecular weights (kDa) of the sequences PLLA (L), PDLA (B) and PCL (CL), respectively. The synthesized triblock copolymers was used as a prepolymer for the next ROP.

PLLA/PDLA, ^{1}H NMR (600 MHz, $CDCl_3$): δ = 5.17 ($OCC\underline{H}_2CH_3O$), 4.36 ($OCC\underline{H}_2CH_3OH$), 4.12 ($OC\underline{H}_2CH_2(CH_2)_8CH_2C\underline{H}_2O$), 1.57 ($OCCH_2C\underline{H}_3O$), 1.25 (-$OCH_2C\underline{H}_2(CH_2)_8C\underline{H}_2CH_2$-O-), 0.88 (-$OCH_2CH_2(C\underline{H}_2)_8CH_2CH_2O$-) ppm.

BCB/ACA Triblock copolymer, ^{1}H NMR (600 MHz, $CDCl_3$): δ = 5.17 ($OCC\underline{H}_2CH_3O$), 4.36 ($OCC\underline{H}_2CH_3OH$), 4.06 ($CH_2CH_2CH_2CH_2C\underline{H}_2O$-), 2.3 ($C\underline{H}_2CH_2CH_2CH_2CH_2O$-),

1.64 ($OCH_2C\underline{H}_2CH_2C\underline{H}_2CH_2O$-), 1.38 ($OCH_2CH_2C\underline{H}_2CH_2CH_2O$), 1.25 (-$OCH_2C\underline{H}_2(CH_2)_8C\underline{H}_2CH_2O$-), 0.88 (-$OCH_2CH_2(C\underline{H}_2)_8CH_2CH_2O$-) ppm

5.2.4 Synthesis of ABCBA/BACAB stereoblock terpolymers

To the purified BCB/ACA triblock copolymer, the monomer (L- or D-lactide) was added (mmol) and evacuated at 10 Pa at 40 ℃ for 12h. The system was filled with N_2 gas and the flask was immerse in an oil-bath at 180 ℃. The monomer and the prepolymer were allowed to melt completely until the monomer solubilized into the melt of the prepolymer. A solution of catalyst (mmol) was then added to the melt under N_2 atmosphere and the reaction was conducted for 25 min. After the reaction, the flask was brought to the room temperature and the conversion of the product was determined by ^{1}H-NMR. The product was dissolved in a mixture of dichloromethane and HFIP (10%) followed by precipitation in excess methanol. The precipitates after filtering were dried in a vacuum oven at 80 ℃ for 12h. The obtained products were ***B***D-***A***L-***C***CL-***A***L-***B***D or ***A***D-***B***D-***C***CL-***B***D-***A***D where ***A***, ***B*** and ***C*** represent the molecular weights (kDa) of the sequences PLLA (L), PDLA (B) and PCL (CL), respectively and designated as “penta” hereafter.

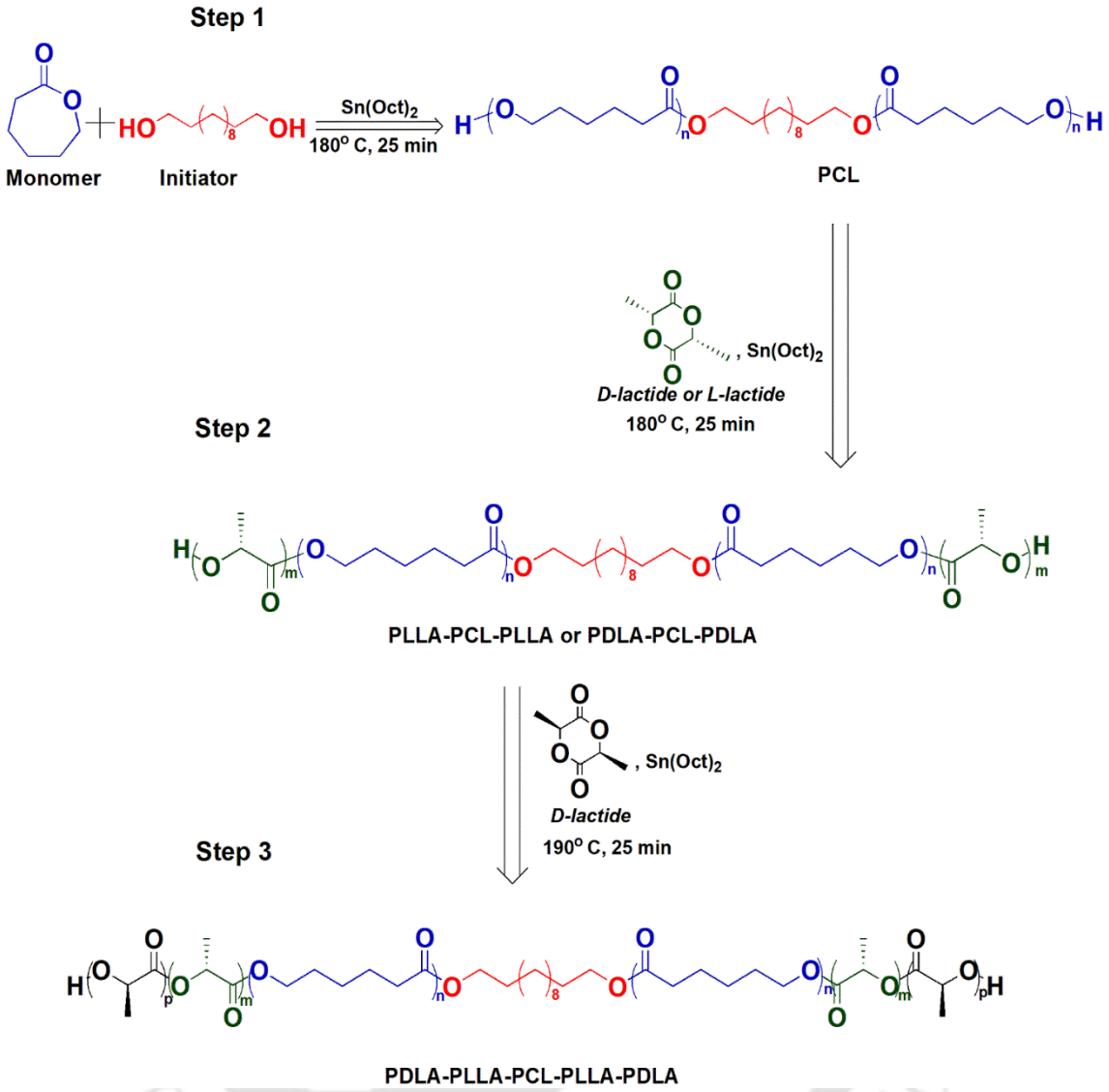

Scheme 5.1: Synthesis of stereoblock terpolymer via three step ring opening polymerization (ROP).

5.2.5 Blending of stereoblock terpolymers

The enantiomeric stereo-pentablock terpolymers were blended in 1:1 ratio, where 2 g each of the terpolymers (10L-10D-10CL-10D-10L and 10D-10L-10CL-10L-10D) were added to a flask with a mixture of dichloromethane (45 ml) + hexafluoroisopropanol (5 ml) and stirred until complete dissolution. The dissolved products were reprecipitated into excess methanol, and the precipitated filtrates were dried in a vacuum oven 80 °C for 12 h. The obtained blend was designated as “B_penta”.

5.2.6 Melt compression molding

Compression molding was used to fabricate the melt-quenched films of the stereo-pentablock terpolymers and its blend for further characterization. As for example, the terpolymer 10D-10L-10CL-10L-10D was held between two Teflon sheets with an aluminum spacer having a window (4 cm × 4 cm) and a thickness of ~200 μm, which was compression molded at 225-235 °C for 5 min at ~1 MPa followed by quenching in ice-water.

5.2.7 Characterization

The nuclear magnetic resonance (NMR) spectrometer (AV600 Bruker, Germany) was used to conduct ^{1}H and ^{13}C-NMR measurements where the synthesized materials were dissolved in deuterated chloroform ($CDCl_3$) containing 0.03% tetramethylsilane (TMS) as an internal reference.

The number (Mn) and weight average (Mw) molecular weight of the synthesized materials was determined using gel permeation chromatography (GPC Shimadzu, Japan). The eluent used was Chloroform and the measurement was conducted at a flow rate of 1 ml/min and the column temperature of 40 ℃.

The X-ray diffraction (XRD) measurements were conducted on a Powder X-ray Diffractometer (Rigaku, Miniflex) at an angular scanning rate of 10 °/min and the scanning range set to 3 – 30°. The X-ray source was operating at 40 kV and 15 mA (CuKα radiation, λ = 0.154 nm).

Differential scanning calorimetric measurements were conducted using DSC 214 Polyma (NETZSCH, Germany). The synthesized samples were heated from RT to 245 °C at the rate of 10°/min in the first heating scan, quenched to -100 °C by liquid nitrogen (in 3-5

min) and reheated from -100°C to 245 °C (second heating) at the heating rate of 10°/min to record the temperature profile of the as-synthesized samples. Further, the melt-quenched film samples were heated from RT to 245 °C at the rate of 10°/min to record the first heating scan.

The universal testing machine (Kalpak Instruments Ltd, India) was used to determine the tensile properties of the film specimens, which was equipped with a load cell of 500 N and the cross-head speed set to 5 mm/min. The results were reported as an average of five specimens.

The dynamic mechanical analyser DMS 242 E (NETZSCH, Germany) was employed to perform the dynamic tensile measurements where the specimen (15 mm length × 5 mm width) was heated at the rate of 2°/min under N_2 atmosphere and the frequency of 1 Hz. The heating range of the specimens was 25-180 °C.

5.2.8. *In vitro* studies

UMR-106 cell culture

UMR-106 (rat bone osteosarcoma) cells were cultured in T75 flasks using Dulbecco's modified eagle's medium (DMEM) supplemented with 10% fetal bovine serum (FBS) and 1% penicillin streptomycin. The cells were cultured and maintained in a CO_2 incubator at 37 ℃ under the humidified atmosphere. The circular polymer films were sterilized with ethanol (70%) followed by washing with phosphate buffer saline (PBS); and irradiated under UV light after placing in the 96 well plates. The cell count was determined using trypan blue stain (Sigma Aldrich) with an automated cell counter (Countess II FL, Thermo Fisher Scientific) and 2.88×10^3 cells/well were seeded (in triplicates) in 96 well plates containing samples along with control (polystyrene

microplates) by adding 100 µl DMEM per well. In addition, the medium (without cells) was added to the samples (triplicates) to eliminate the background absorption.

MTT assay

The mitochondrial activity of UMR-106 cells seeded onto the developed materials was evaluated by the enzymatic conversion of MTT (3-(4,5-dimethylthiazol-2-yl)-2,5-diphenyltetrazolium bromide) dye. The stock (5 mg/ml) of MTT (Sigma Aldrich) was prepared in PBS and added (10 µl) to each of the wells at the intervals of 8, 16, 24, 48, 72 and 96 h. The well-plates were incubated for 3 h and then the medium involving MTT was removed from the wells. Finally, dimethyl sulfoxide (DMSO, 100 µl/well) was added to the wells so as to allow the formation of Formazan crystals. The absorbance was then recorded at 570 nm using a microplate reader (Multiskan Go, Thermo Fisher Scientific). The mean absorbance of the control (polystyrene) was subtracted from that of the samples.

Cell staining and microscopy

The cells adhering onto the surface of the samples along with the control sample were stained with Nuc Red™ (Live 647 Ready Probes™, Thermo Fisher Scientific) and acridine orange (Thermo Fisher Scientific) stains after 48 h of culturing. The Nuc Red™ stain was added (2 drops) directly into the wells containing medium and incubated for 20 min. The acridine orange stain was diluted (in PBS) before adding into the wells. The cell culture media were removed from the wells followed by washing off the samples (and the control well) with PBS thrice. The acridine orange stain was then added to the wells and incubated for 30 min. The plates were removed and the cells were analysed with the fluorescence microscope (Floid Cell Imaging Station, Thermo Fisher Scientific).

5.3 Results and Discussion

5.3.1 Synthesis of stereoblock terpolymer

Stereoblock terpolymers with the sequences PLLA-PDLA-PCL-PDLA-PLLA and PDLA-PLLA-PCL-PLLA-PDLA are synthesized by three step bulk melt ROP. PCL-diol is used as macroinitiator for synthesis of PLLA-PCL-PLLA and PDLA-PCL-PDLA triblock copolymers. Further, PLLA-PCL-PLLA and PDLA-PCL-PDLA are used to fabricate enantiomeric stereoblock terpolymers PDLA-PLLA-PCL-PLLA-PDLA and PLLA-PDLA-PCL-PDLA-PLLA. The feeding ratio, conversion and molecular weight are condensed in **Table 1**. The theoretical and experimental values for the number average molecular weights (M_n) measured using NMR are found to be different insignificantly. The targeted molecular weight of PCL macroinitiator was ~10 kDa which was increased to ~30 kDa after ROP of PDLA or PLLA and further increased to ~50 kDa for stereoblock terpolymers.

The ^{1}H-NMR spectra of stereoblock terpolymers are shown in **Figure 5.1** with the structure of stereoblock terpolymer assigned. The value of PDI obtained from GPC (**Table 5.1**) is found to increase with the increasing molecular weight which may be attributed to the higher molecular weight of the macroinitiator working as a limiting factor for the mixing of monomer and macroinitiator. This may further be attributed to the bulk melt polymerization technique utilized to synthesize stereoblock terpolymers.

Table 5.1: Characterization of stereoblock terpolymers.

Polymer/ Copolymer	Molar feeding ratio [M/I]	Conv. (%)	Mn (th) kDa	Mn NMR kDa	Mn GPC kDa	Mw GPC kDa	PDI (Mw/Mn)
11CL	88.5	99.4	10.1	11.0	24.1	47.5	1.97
10D-11CL-10D	154.1	93.2	31.7	31.5	55.9	119	2.13
9L-10D-11CL-10D-9L	163.2	92.6	53.3	48.3	79.7	197	2.48
11CL	88.5	99.4	10.1	10.9	22.6	42.5	1.88
10L-11CL-10L	154.0	93.6	31.7	31.5	60.2	117	1.94
8D-10L-11CL-10L-8D	163.2	93.6	54.2	46.4	69.4	191	2.76

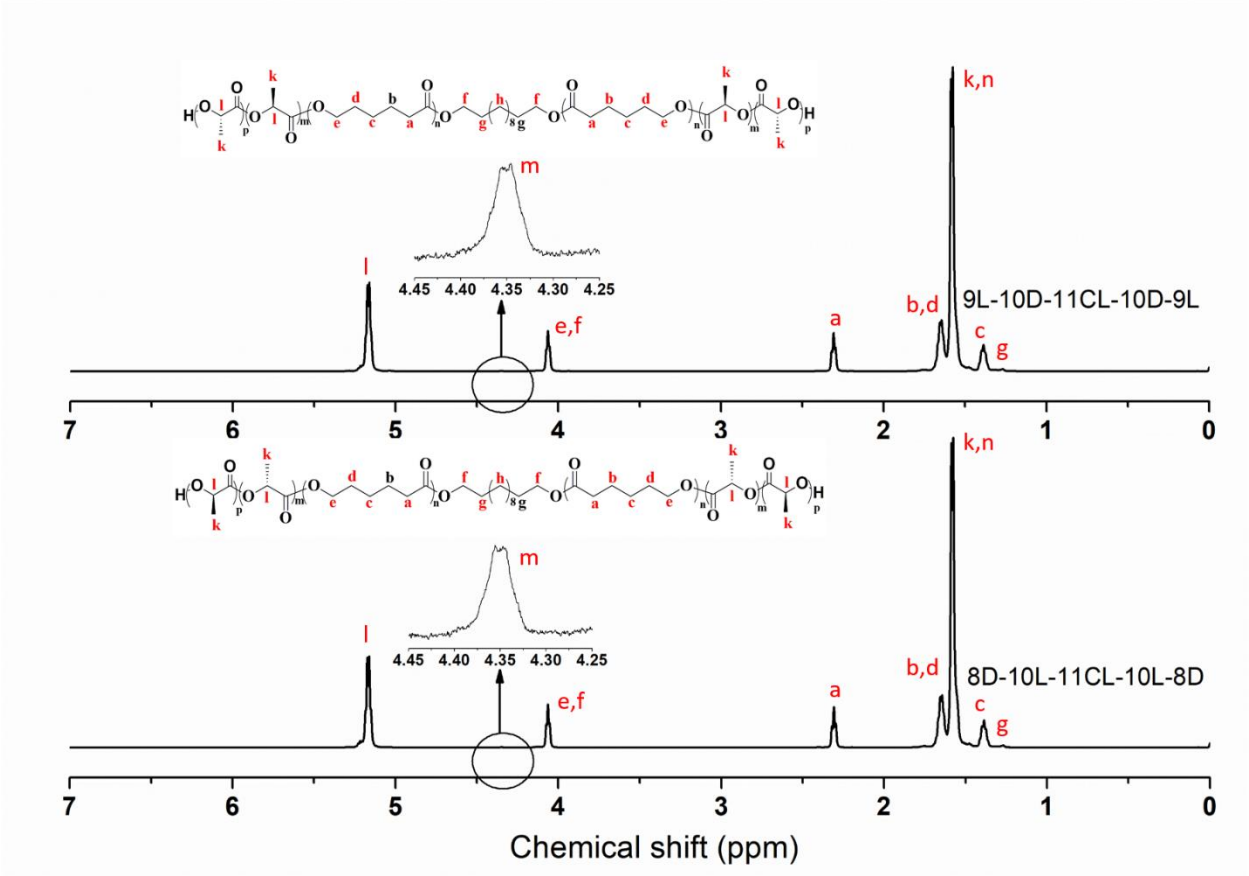

Figure 5.1: ^{1}H-NMR spectra of the stereoblock terpolymers.

5.3.2 Thermal properties of stereoblock terpolymers

Figure 5.2 shows the thermal transitions in stereoblock terpolymer and its enantiomeric blend. In the first heating cycle, the melting temperature of terpolymer and its enantiomeric blend is found to be around 193°C without any significant other endotherm which confirms the preferential stereocomplexation the polymer system. The melting temperature is relatively less than normal stereocomplex crystallites which may be the due to the formation of thinner lamellae. In the second heating cycle, melting endotherm for PCL is revealed around 46°C and exothermic transition related to the stereocomplex PLA crystallization at 85°C. The absence of any melting transition relating to hc suggests that the cold crystallization at 85°C is related to crystallization of sc-PLA. The lower cold crystallization temperature may be anticipated to the presence of PCL block in the polymeric chains. Further, the PCL crystals are melt over the temperature of 46°C and the molten PCL may work as a diluent that to facilitate the PLLA and PDLA chain movement. It also enhances the entropy of the PLA chains which allow them (PLLA and PDLA chains) to arrange and form preferential stereocomplex crystallites. This inherent mechanism can help during the melt processing and injection molding of sc-PLA. Normally, it has been seen that the injection molded articles of enantiomeric PLA cannot be crystallized even at higher mold temperature which also make them brittle. However, in the case of stereoblock terpolymers, the melt processing and injection molding can easily be done at higher mold temperature to get crystalline stereocomplex PLA with required toughness. The thermal transitions in the enantiomeric blend are found to be similar to that of stereoblock terpolymers.

Further, it is very important to understand the effect of heating rate on the formation of sc crystallites. It has been reported that the heating rates may affect the development of

sc crystallites in the polymer system after melt processing. The melt transitions of the stereoblock terpolymer and its enantiomeric blend at different heating rates are shown in the **Figure 5.3** and **Figure 5.4**. These results suggest that the heating rates (5, 10 and 20°C/min) do not affect the preferential formation of sc crystallites in the stereoblock terpolymer and its blend. The preferential sc crystallization is attributed to the presence of PLLA and PDLA in the same chain which facilitates the interaction between PLLA and PDLA block at the microscopic scale. Moreover, the presence of PCL soft segment as mid-block in the terpolymer provides an environment in which PLLA and PDLA can freely diffuse through the polymer to the crystallization site and develop sc crystallites preferentially.

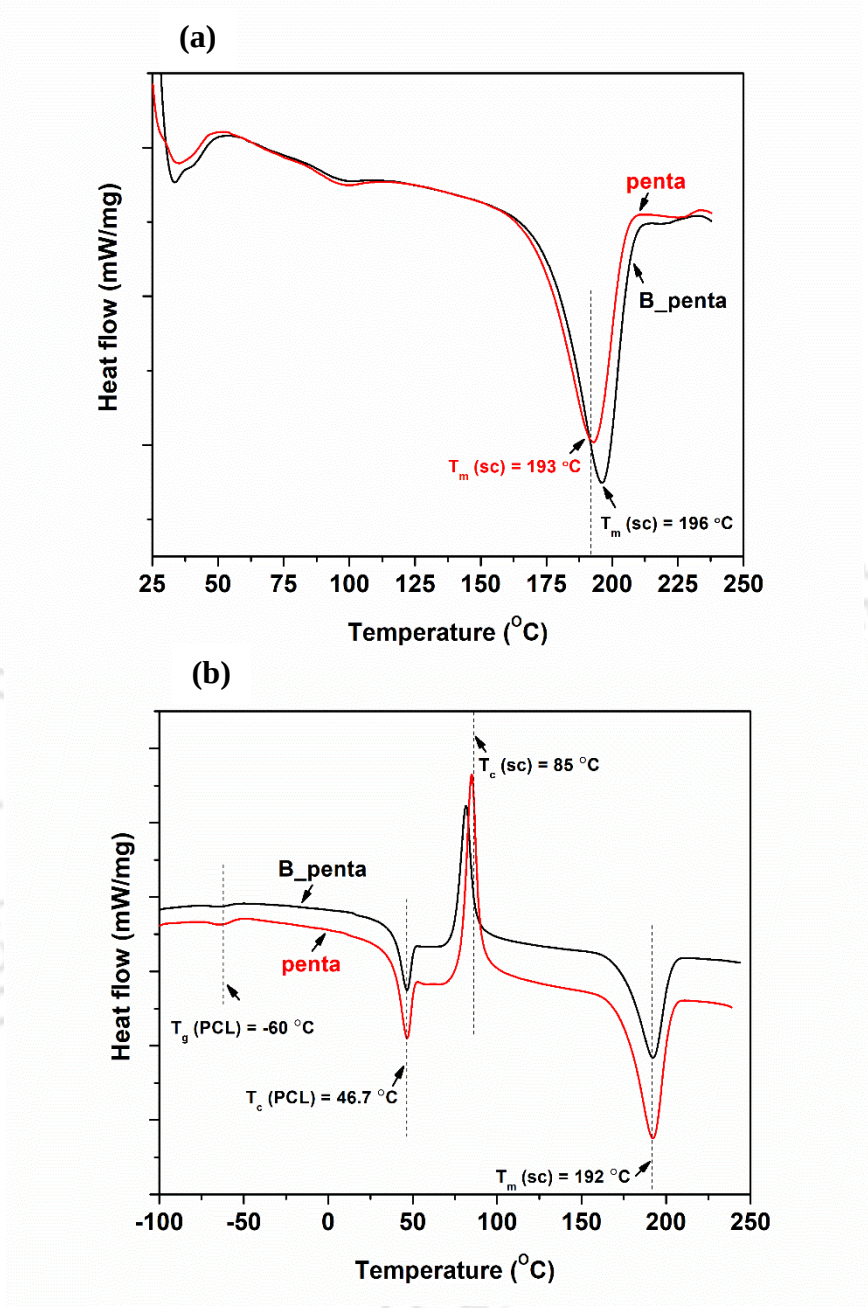

Figure 5.2: DSC curves of the stereoblock terpolymers (a) first heating, (b) second heating.

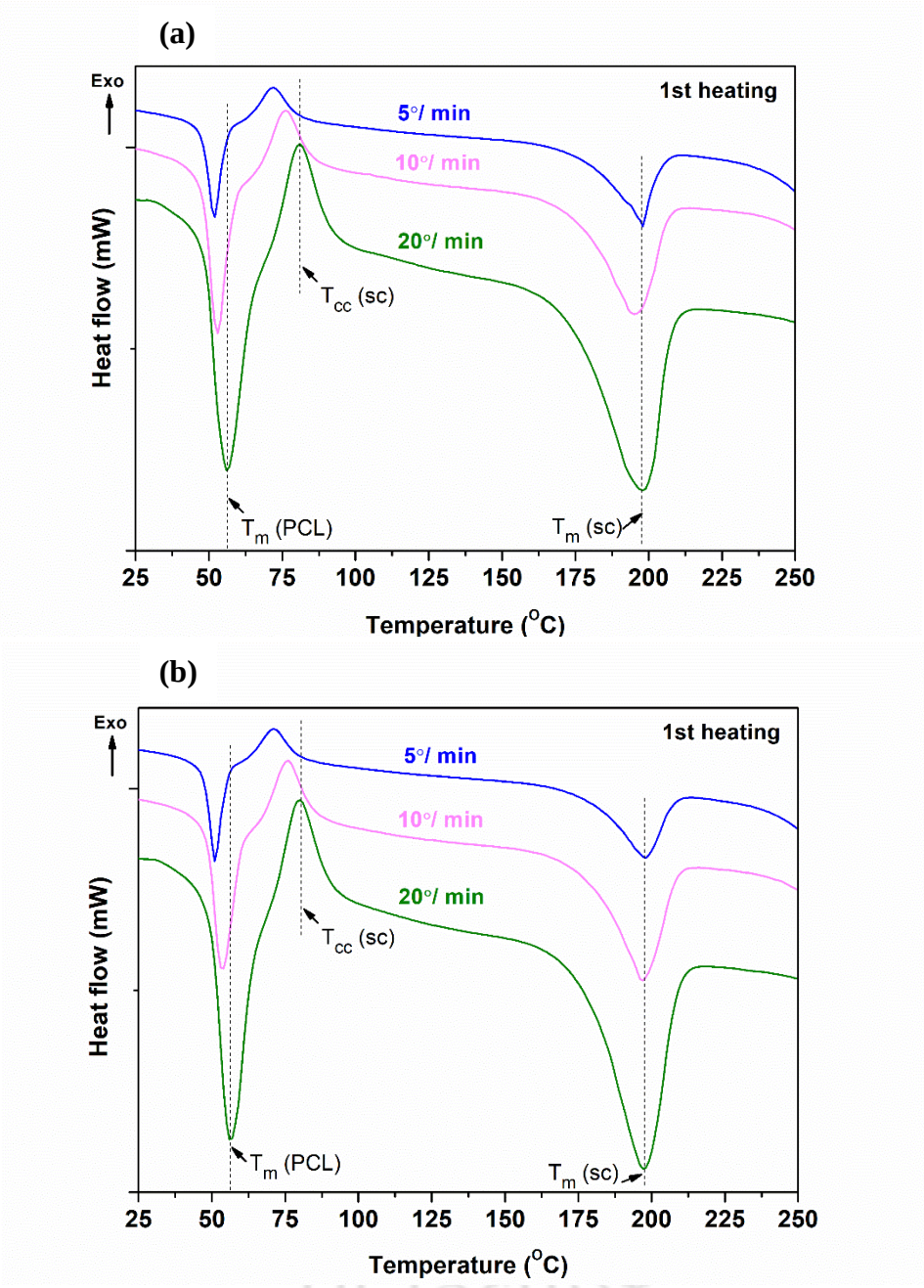

Figure 5.3: DSC curves (1st heating cycle) at different heating rates of (a) penta (b) B_penta specimens.

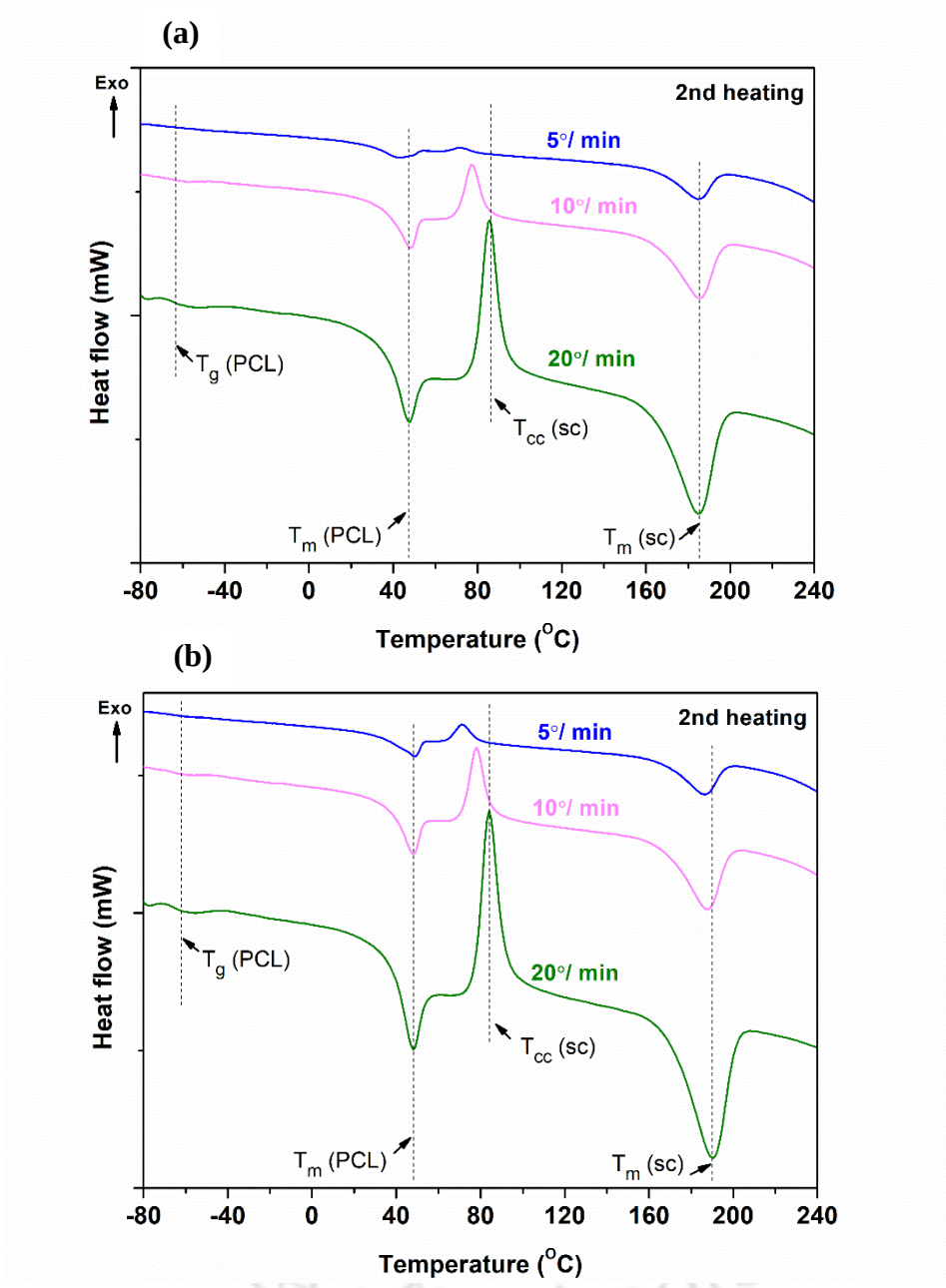

Figure 5.4: DSC curves (2nd heating cycle) at different heating rates of (a) penta (b) B_penta specimens.

Further, it is necessary to estimate the temperature up to with the polymer can sustain and does not undergo thermally induced degradation when subjecting materials to melt processing. **Figure 5.5** shows the weight loss of the developed stereoblock terpolymer and its blend against temperature. No significant difference in weight loss is found

between the terpolymer and its blend. The onset degradation temperature is observed at 314°C whereas the degradation temperature with maximum rate is found to be 333°C. The different steps in the degradation are attributed to the molecular architecture of the stereoblock terpolymer consisting of different species. PCL is known to have a higher degradation temperature as compared to PLLA or PDLA as seen in the previous chapters. PCL chains contain hydrocarbon chains which are stable at higher temperature in comparison to carbonyl groups in PLLA and PDLA. Overall, the synthesized materials can easily sustain the processing temperature below 314°C which is significantly higher than the normal processing temperature (200°C).

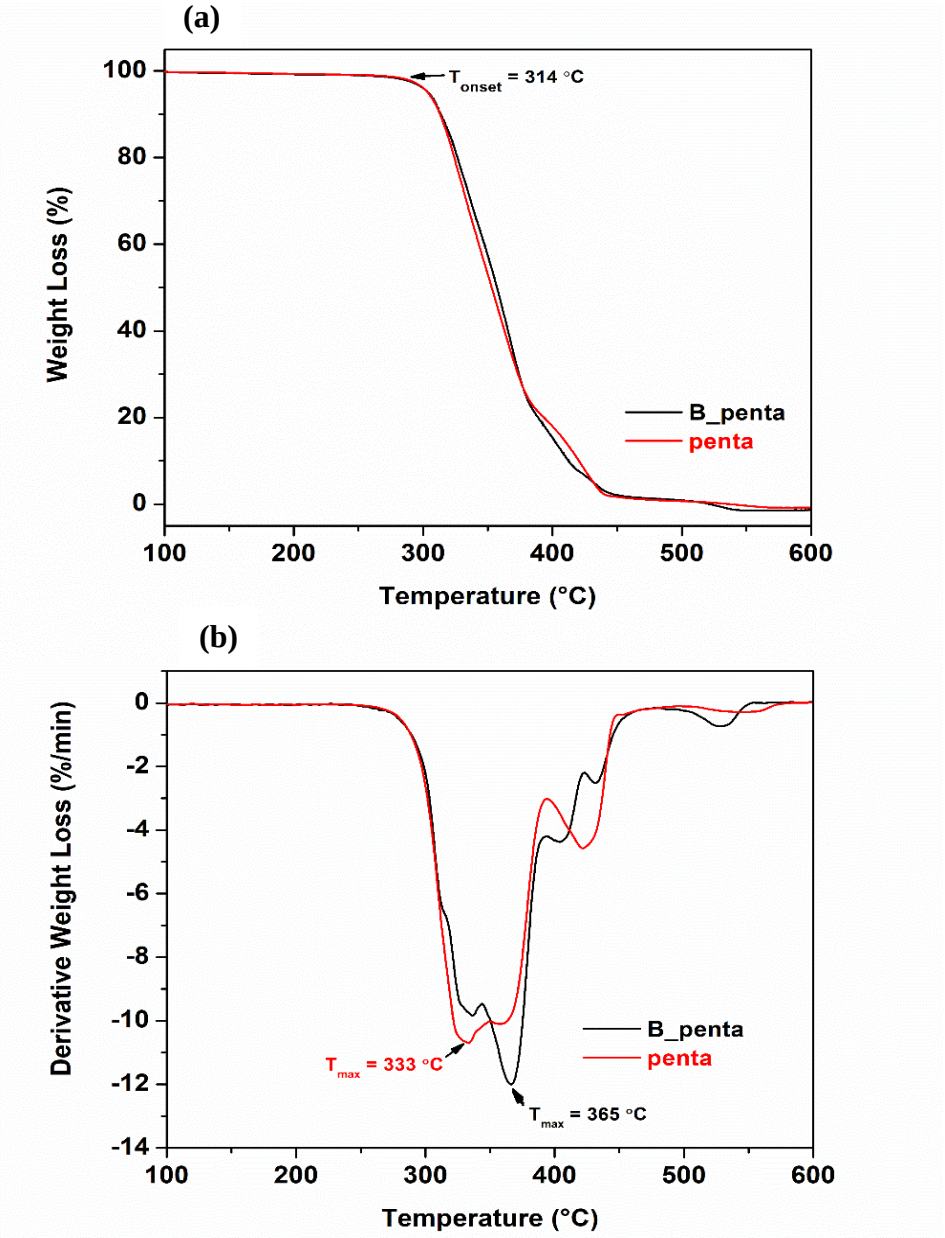

Figure 5.5: (a) % Weight loss and (b) Derivative weight loss of the penta and B_penta specimens.

5.3.3 Crystallization behavior

The formation of preferential sc crystallites is also confirmed by XRD analysis and shown in the **Figure 5.6**. From the above discussion, it is observed that stereoblock terpolymer and its blend demonstrated the preferential formation of sc crystallites. As discussed in the previous chapters, the pseudo-orthorhombic unit cells contains 10_3 (hc crystallites) helical chains and the triclinic unit cell contains 3_1 helical structure (sc crystallites). The dense packing of sc crystallites is responsible for the higher melting crystalline domain in the polymer system. In the figure, the diffraction peaks at 11.3° and 20.7° correspond to (110) and (300)/(030) crystal planes of stereocomplex crystallites whereas peaks at 21.3° and 23.8° belong to (110) and (200) lattice planes of PCL crystallites, respectively. No noticeable peaks are found for the hc crystals, which in turn confirm the formation of preferential sc crystallites. The intensities of the diffraction peaks of the annealed specimens are much higher than the melt-quenched specimens. This suggests that the sc crystallites forms even after cold crystallization at 120°C without any trace of hc crystallites. Overall, this analysis suggest that stereoblock terpolymer and it blend can easily form sc crystals with any hc crystal formation, and PCL facilitates the interaction of enantiomeric PLLA and PDLA chains. Such a formation of preferential sc crystallite further leads to the enhancement in mechanical properties which will be discussed in the subsequent sections.

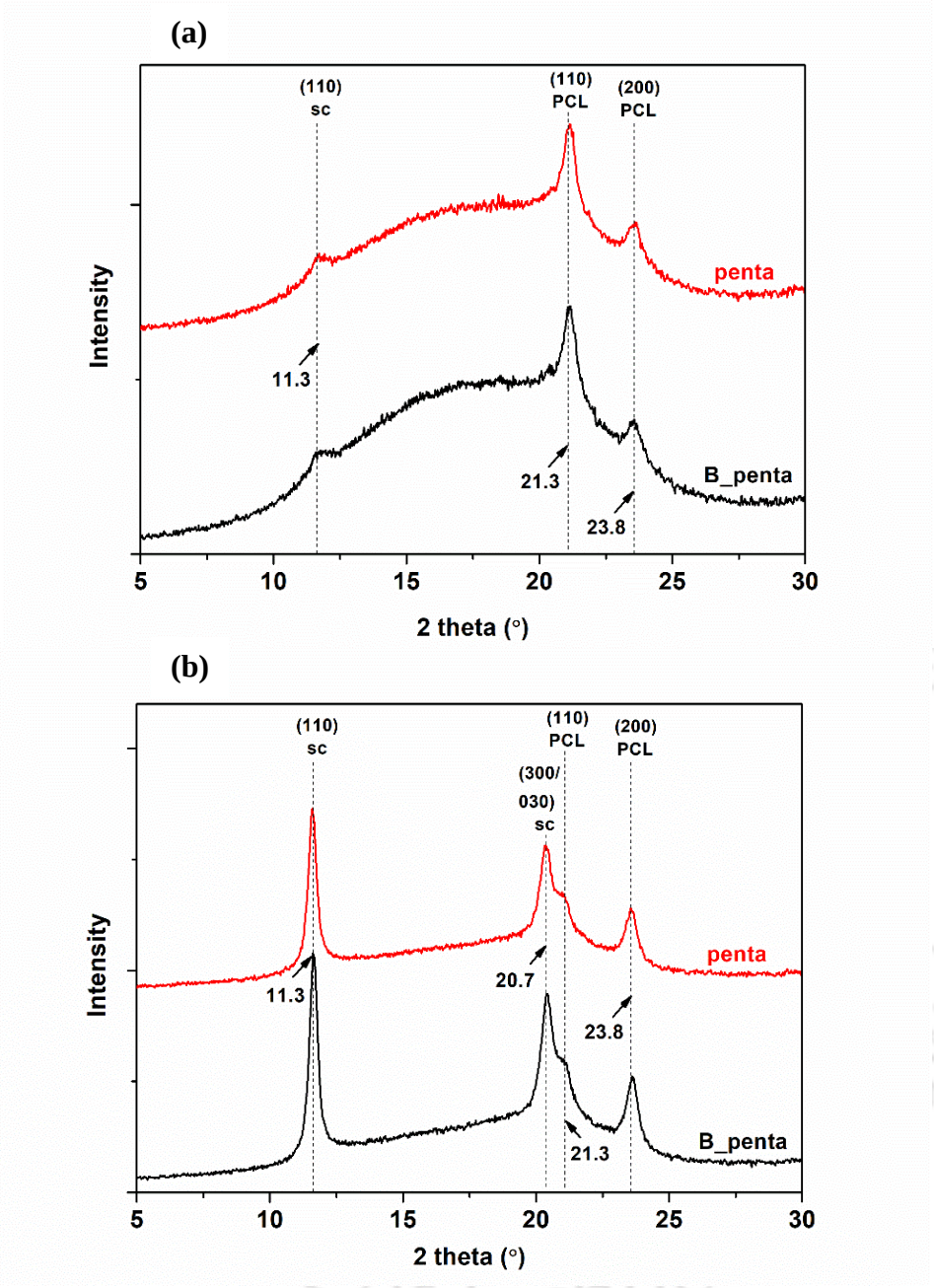

Figure 5.6: X-ray diffraction spectra of the penta and B_penta specimens after (a) melt quenching and (b) annealing at 120 °C.

5.3.4 Mechanical and thermo-mechanical properties of stereoblock terpolymers

From the previous chapters, it is confirmed that stereocomplexation in PLA plays a vital role in improving its mechanical and thermal properties. A typical stress-strain curve is shown in **Figure 5.7** and its results are summarized in **Table 5.2**. The tensile strength of the stereoblock terpolymer is found to be around 25 MPa which is enhanced to around 32 MPa for its enantiomeric blend. In case of the stereoblock terpolymer, the elongation at break is around 90% which is the result of presence of PCL block as mid segment. However, the elongation at break is lower in the case of enantiomeric blend. The formation of thicker lamellae of stereocomplex crystallites may be responsible for early breakage of the specimen. In the case of highly crystallite materials, the chain sliding and movement is restricted which may reduce the elongation effect of PCL.

Dynamic mechanical analysis of the stereoblock terpolymer and its blend are shown in **Figure 5.8**. DMA analysis was conducted to measure the change in storage modulus with increasing temperature. No significant difference is found in the storage modulus for the stereoblock terpolymer and its blend. The storage modulus is found to be around 1960 MPa at 30°C which was reduced to less than 10 MPa after heating to 60°C. This dip at around 55°C in the storage modulus is the result of melting of PCL crystallites in the specimens. The storage modulus is further increased with the temperature that corresponds to crystallization. As discussed in the previous sections, the molten PCL chains facilitate the preferential formation stereocomplex crystallites resulting from increased interaction of PLLA and PDLA chains.

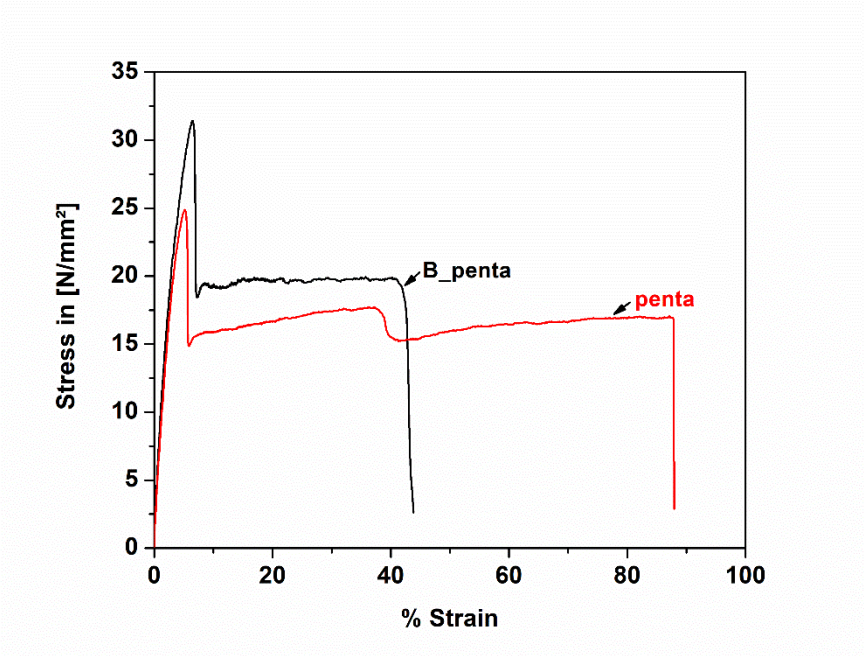

Figure 5.7: Stress vs strain curves of the penta and B_penta specimens.

Table 5.2: Results obtained from the Stress-strain analysis

Identity	Ultimate tensile strength (MPa)		Elongation at break (%)		Young's modulus (MPa)		Tensile toughness (MPa)	
penta	26.4	± 1.5	70	± 32.1	733.5	± 17.1	12.5	± 5.8
B_penta	29.8	± 1.3	34.3	± 10.9	757.7	± 2.0	6.28	± 51.9

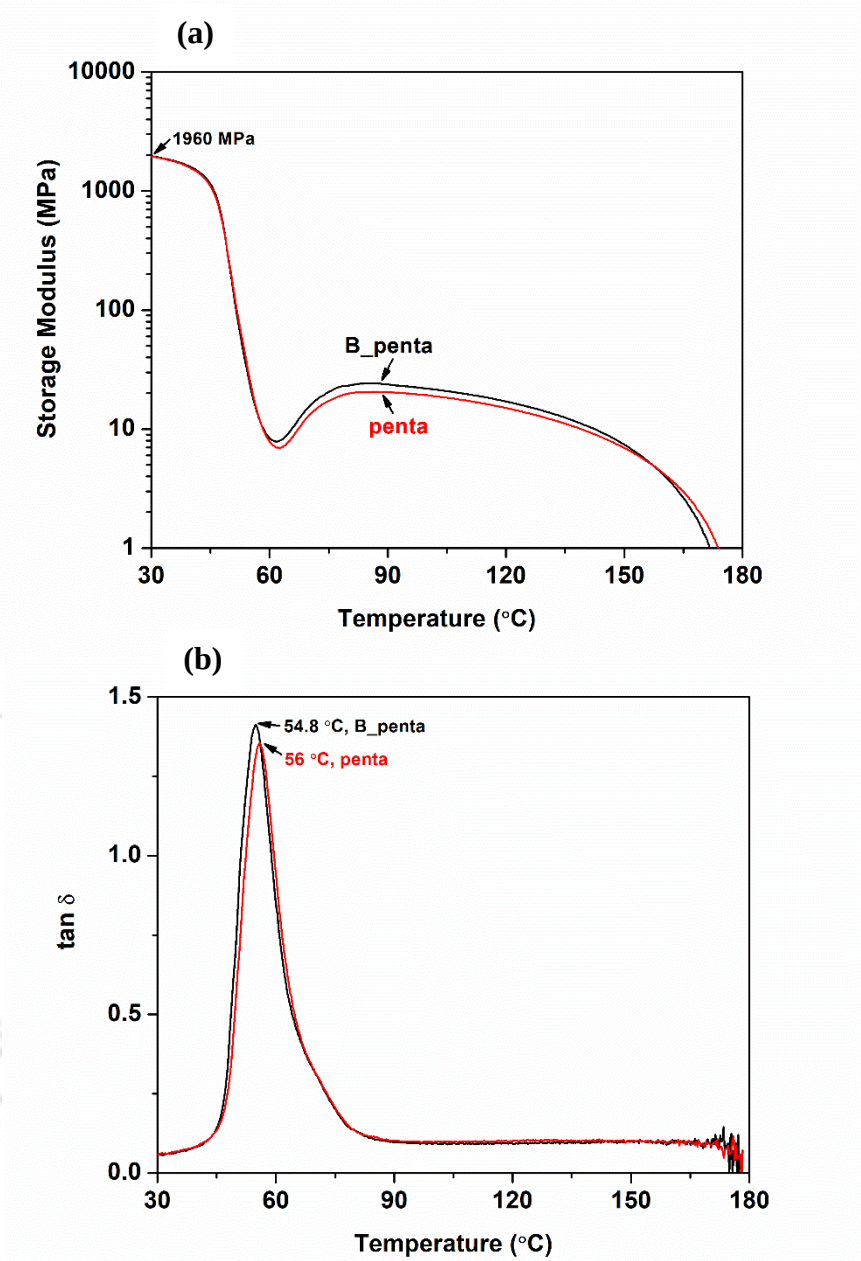

Figure 5.8: (a) Storage modulus and (b) tan δ as a function of temperature for the penta and B_penta specimens.

5.3.5 Biocompatibility

The cell viability of rat bone osteosarcoma cells (UMR-106) on the stereoblock terpolymer and its blend are shown in **Figure 5.9**. From the figure, it is apparent the rat bone osteosarcoma cells are adhering and multiplying on the surface of the developed materials over a period of 48h. The adhesion and multiplication of the rat bone osteosarcoma cells show that the produced materials are biocompatible and can employed in biomedical applications. The comparison with control suggests the favorable environment provided by the synthesized materials for the cells to grow and multiply. This indicates that the materials impose no adverse effect on survival of these cells. Furthermore, the representative images of the rat bone osteosarcoma cells adhered on the surface and stained using Nuc Red™ Live and Acridine orange stains are shown in **Figure 5.10**. Overall, cell viability studies suggest that the fabricated materials can be used as biomaterials for the potential applications.

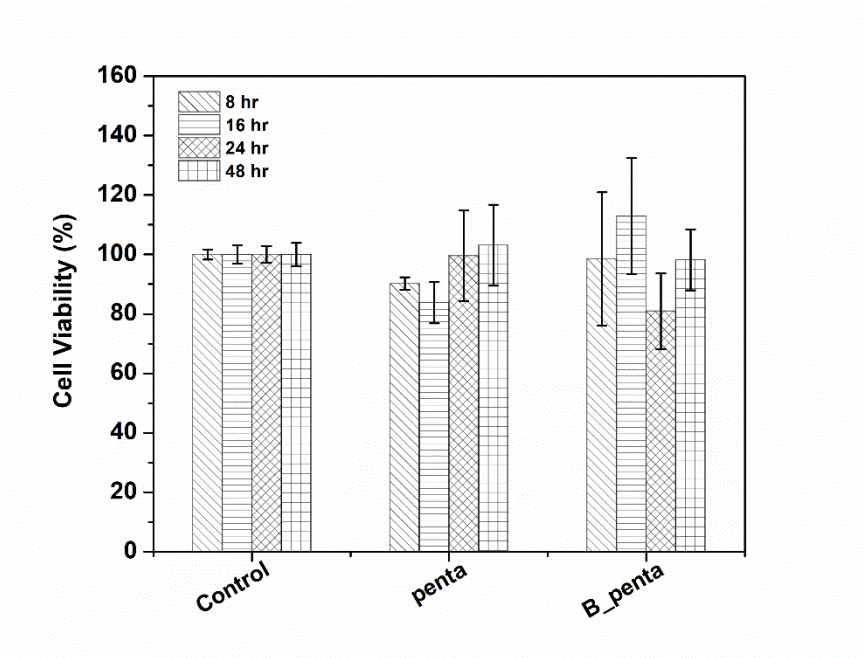

Figure 5.9: Cell viability (%) of the penta and B_penta specimens by performing MTT assay.

Specimen	*Stain:* ***NucRed™ Live***		*Stain:* ***Acridine orange***	
	Bright field images	**Fluorescence images**	**Bright field images**	**Fluorescence images**
Control	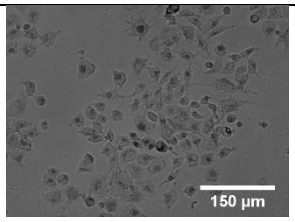	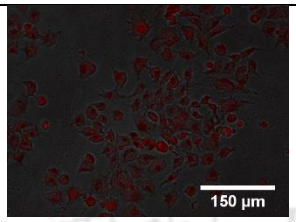	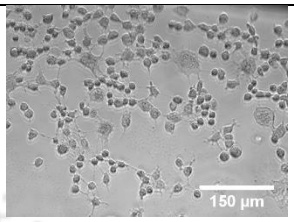	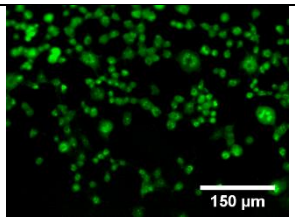
penta	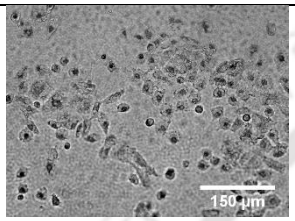	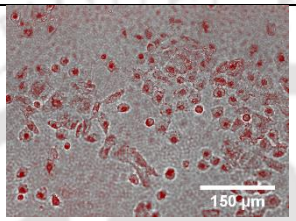	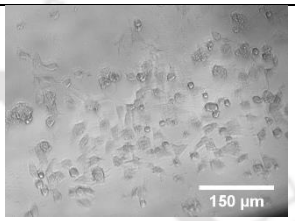	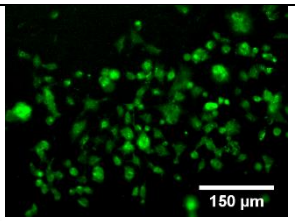
B_penta	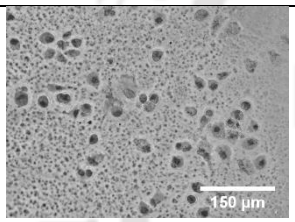	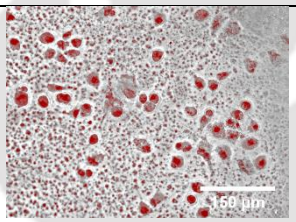	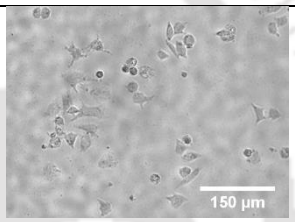	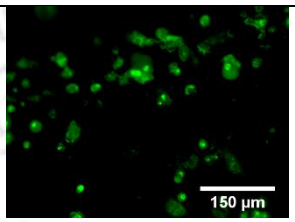

Figure 5.10: Adhesion of rat bone osteosarcoma cells on the surfaces of penta and B_penta specimens after 48h of culturing, and staining with NucRed™ Live and acridine orange stains.

5.4 Conclusions

The stereoblock terpolymers were successfully synthesized by three-step ROP leading to preferential sc formation. The preferential formation of sc crystals was confirmed from the DSC and XRD analysis. The formation of sc crystals was independent of the heating rate. The enantiomeric blend of stereoblock terpolymer led to the achievement of improved tensile strength and reduced elongation at break. It may be said that the molten PCL chains facilitate the preferential formation stereocomplex crystallites resulting from increased interaction of PLLA and PDLA chains. The adherence of rat bone osteosarcoma cells on the surfaces of synthesized materials indicated their biocompatible nature.

Chapter: 6

Random Copolymers based on L-lactide and ε-caprolactone, and its Composites

Graphical Abstract

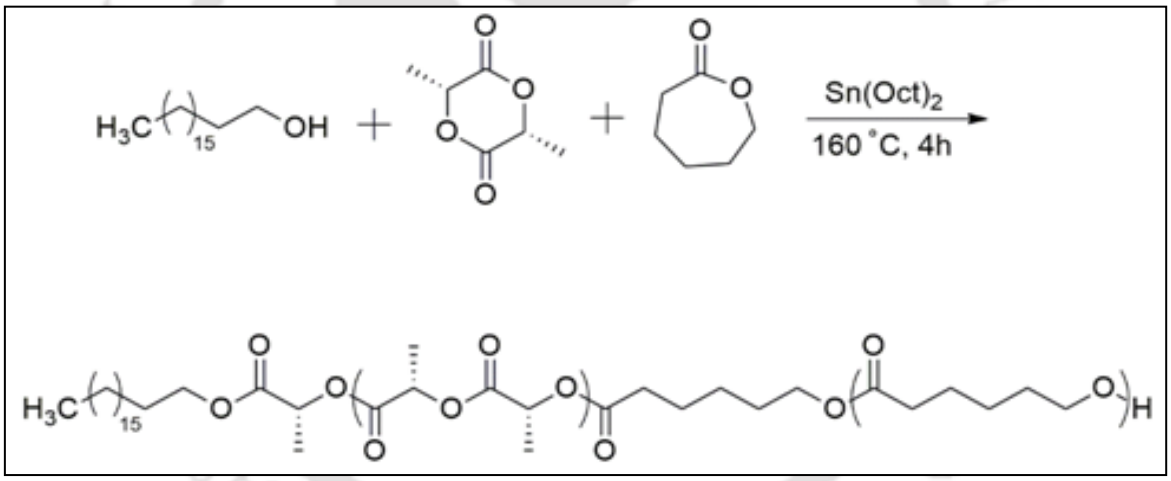

Outcome:

- *Patent filed: PLA-r-PCL based Shape Memory, Elastomeric Composites and Method of Preparation Thereof (Application No: 202131013652).*

Abstract

The current chapter manifests one-pot melt polymerization process for the synthesis of random copolymers of PLA and PCL with the varying content of lactyl and caproyl units. The random copolymerization is an affordable strategy to tailor the thermal and mechanical properties of the copolymers and design materials for customized applications. The shape memory and elastomeric properties of the random copolymers are underlined. Bioglass is incorporated as a filler into the matrix of elastomeric composites which further lead to the tailored thermal and mechanical behavior. The developed copolymers and composites may be employed for soft tissue applications.

6.1 Introduction

The present research employs copolymerization as an effective strategy for using these polymers in combination as it usually leads to the homogenous mixture upon interaction of PCL and PLA chains at the molecular level. The bulk polymerization of polymers usually requires no solvent during the polymerization and is relatively facile and an industrially viable technique for synthesizing the polymers. Bulk ring opening polymerization of these aliphatic polyesters by employing suitable catalysts has gained widespread acceptance. As discussed in previous chapters, caprolactone moiety contributes for chain flexibility, extensibility, with the ability to tailor the bulk modulus whereas lactide moiety provides tensile strength, relatively higher glass transition temperature (T_g), etc. The biomedical applications require materials with tailored properties. In this context, it is essential to design a strategy to tailor the properties of the copolymer matrix as per the requirement. Incorporation of lactide and ε-caprolactone

monomers into the same backbone chain can lead to the achievement of homogenous mixture of the hydrophobic polymers i.e. PLA and PCL, which is usually not possible by simple blending of them. The strategies of reducing macrophase separation between PLA and PCL include block copolymerization (as discussed in previous chapters), random copolymerization and formation of biocomposites.

Random copolymerization of lactide and ε-caprolactone may lead to a matrix system with tunable properties which can be employed for biomedical applications such as sutures, wound healing patches and soft tissue implants. Several researches have tried to develop random copolymer of lactide and caprolactone till date. Tsutsumi et. al.[268] have developed random copolymers with varying ratios of ε-caprolactone and lactide followed by employing them for controlled release of d-limonene in super critical conditions. However, the molecular weight of the copolymers achieved by them was 30 kDa. Further, several researchers have used different catalyst systems such as zinc based catalyst[269], homosalen aluminum (Al) complex[270], pyrrolylpyridylamido aluminum complexes[271], titanium complex derived from aminodiol ligand[272], N-heterocyclic carbenes[273], molybdenum complexes[274], mono-and dinuclear salen aluminum complexes[275], phenoxyimine Al complexes[276], aluminum alkoxide complexes[277], to develop random copolymers of lactide and ε-caprolactone. In another work, Dalmora et. al.[278] have developed random copolymers and used them for drug tocopherol encapsulation and release studies. Further, the random copolymers have also been exploited as toughening agents for improving the toughness of polylactic acid[279]. Random copolymers of lactide and ε-caprolactone can also be used as compatibilizers in the blend of PLA and PCL which affects their crystallization rate[280]. Further, little attention has been paid on

developing biocomposites using random copolymers of lactide and caprolactone as a matrix and inorganic fillers such as bioglass as a reinforcement.

Therefore, this chapter manifests the random copolymerization of lactide and ε-caprolactone using one pot ring opening polymerization to synthesize copolymers with varying molar ratios of the two monomers and evaluated the properties of resulting materials. The random copolymer having near elastomeric behavior is used as a matrix for the development of biocomposite incorporated with bioglass followed by their characterization.

6.2 Experimental

6.2.1 Materials

D-and L-lactides (optical purities 99.9%) were provided by Musashino Chemical Laboratories, Ltd. Tokyo, Japan. 1-octadecanol was procured from Tokyo Chemical Industry Co., Ltd., Tokyo, Japan. Tin octoate ($Sn(Oct)_2$, 95%) was obtained from Sigma Aldrich, St. Louis, USA via Nacalai Tesque which was distilled under high vacuum and dissolved in dried toluene (0.2 g/ml) and stored under inert environment. 1,1,1,3,3,3-Hexafluoro-2-propanol was obtained from Central Glass Co. Ltd., Yamaguchi, Japan. ε-caprolactone, dichloromethane and methanol were purchased from Nacalai Tesque and used without purification. Bioglass 45S5 particles were purchased from XL Sci Tech, Inc. USA (Average size 5 μm, Lot: XLS7352).

6.2.2 Synthesis of Poly(L-lactide-co- ε-caprolactone)

The random copolymers P(LA-r-CL) were synthesized in a single step using bulk ROP technique in presence of 1-octadecanol initiator and stannous octoate catalyst as shown in **Scheme 6.1**. Briefly (for the copolymer 1:1), the initiator (2.55×10^{-4} mol) along with

L-lactide (5×10^{-2} mol) was added to the polymerization tube and evacuated at 10 Pa for 6-8 h with intermittent N_2 purging to remove the residual moisture. The monomer (ε-caprolactone, 5×10^{-2} mol) was then added to the polymerization flask under N_2 atmosphere along with the catalyst solution (4×10^{-5} mol). The polymerization flask was then sealed under N_2 atmosphere and immersed in the oil bath pre-set at 160 °C. The reaction was carried out for 4h to form the copolymer. The conversion of monomers was determined by ^{1}H-NMR. The obtained copolymer was dissolved in chloroform and precipitated in excess methanol to obtain the precipitates of copolymer. The purified copolymer was dissolved in chloroform (2 wt %) and poured into a petri dish to form a copolymer film by evaporation of the solvent. The obtained copolymer film was dried in a vacuum oven at room temperature for 4-6 h followed by drying at 50°C for 24h. Thus obtained copolymer film was regarded 1:1.

6.2.3 Formation of composites

45S5 Bioglass particles were added to the synthesized random copolymer (1:1.5). For instance, the copolymer matrix (2.85 g) was dissolved in dichloromethane (50 ml) and 45S5 Bioglass particles (0.15g) were added to the matrix solution and sonicated for a specific time to enhance the dispersion of bioglass into the matrix of copolymer. The solution was further kept for stirring at room temperature until complete mixing. The obtained solution was poured into a petri dish and the solvent was allowed to evaporate at room temperature over a period of time. The obtained film was dried in a vacuum oven at 50 °C for 24h. The obtained composite film was regarded as 5%.

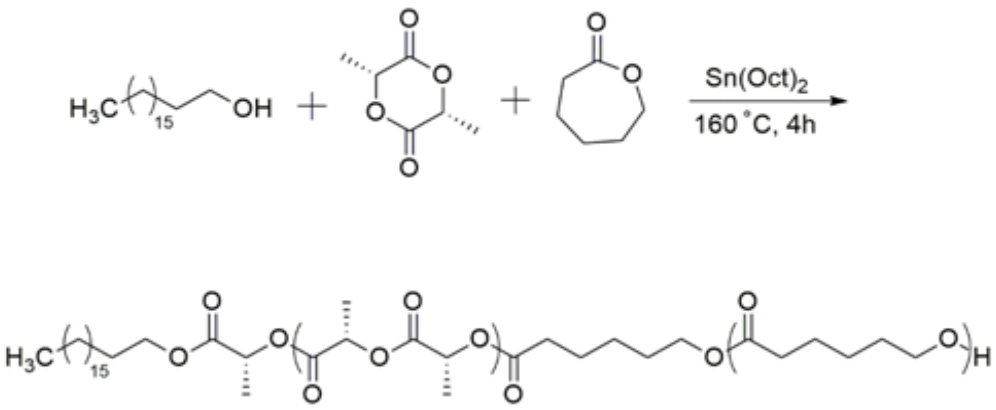

Scheme 6.1: Synthesis of random copolymer via single step ring opening copolymerization (ROP).

6.2.4 Characterization

^{1}H NMR and ^{13}C NMR measurements were done using AV600 spectrophotometer (Bruker, Germany). The materials after synthesis were dissolved in deuterated chloroform ($CDCl_3$) containing 0.03% tetramethylsilane (TMS) as an internal reference.

Gel permeation chromatography (Shimadzu, Japan) was used to determine the number- (Mn) and weight-average (Mw) molecular weights of the synthesized samples. The measurements were conducted at 40 ℃ by using the HPLC grade chloroform as an eluent with a flow rate of 1 ml/min. The equipment consisted LC-20AD pump, RID-10A refractive index detector and SIL-20A HT auto sampler and the polystyrene standards (370 Da to 500 kDa) were used for the system calibration. The sample solutions (20 mg/ml) were filtered by syringe filters (0.45 μm) prior to analysis.

The thermal transitions in the random copolymer films were observed by differential scanning calorimetry using DSC 204 F1 (NETZSCH, Germany) under nitrogen environment. The specimen (5-7 mg) were heated from 0 to 200 ℃ at the rate of

10 ℃/min, kept isothermal at 200 ℃ for 5 min followed by cooling at the rate of 10℃/min to -100 ℃.

Thermogravimetric analysis of the film samples was conducted on a TGA 4000 instrument (Perkin Elmer, USA) under inert (N_2) atmosphere, where the sample was heated from 30 ℃ to 700 ℃ at the heating rate of 10 ℃/min.

X-ray diffraction studies were conducted on a Powder X-ray Diffractometer (Rigaku, SmartLab) comprising of a 9KW rotating anode, operating at 45 kV and 112 mA (CuKα radiation, λ=0.154 nm). The analysis of composite films was carried out at the rate of 4°/min in the scanning (2θ) range of 3° - 40° at room temperature.

The mechanical properties of the polymer films (5 mm width, 10 mm gauge length) were determined using a universal testing machine (UTS Orientec ST-1150) equipped with a load cell of 500 N and the cross head speed was set to 5 mm/min. The measurements were conducted under ambient conditions and the results are reported as an average of five specimens along with standard deviation.

6.3 Results and discussion

6.3.1 Synthesis of Random Copolymers

The synthesized random copolymer was analyzed using ^{1}H NMR spectroscopy as shown in **Figure 6.1**. The corresponding chemical shifts are assigned to the structure which confirms the successful copolymerization reaction of ε-caprolactone and lactide in varying ratios as mentioned in **Table 6.1** in the presence of tin octoate catalyst. The conversion of corresponding lactyl and caproyl units is determined from ^{1}H-NMR. The molecular weights of the synthesized random copolymers are measured using GPC which are shown in **Table 6.2** and the corresponding GPC curves are shown in **Figure 6.2** which

suggest number average molecular weight found to around 45 kDa. The unimodal curve of GPC analysis confirms the success of ROP. However, the GPC curve shifts from unimodal to bimodal when the molar ratio of lactide and ε-caprolactone is 1:1. This suggests that the 50:50 ratio of two monomers lead to inhomogeneity. A variation in PDI of synthesized copolymers may be the result of monomer diffusion to the reaction site and its mixing in bulk.

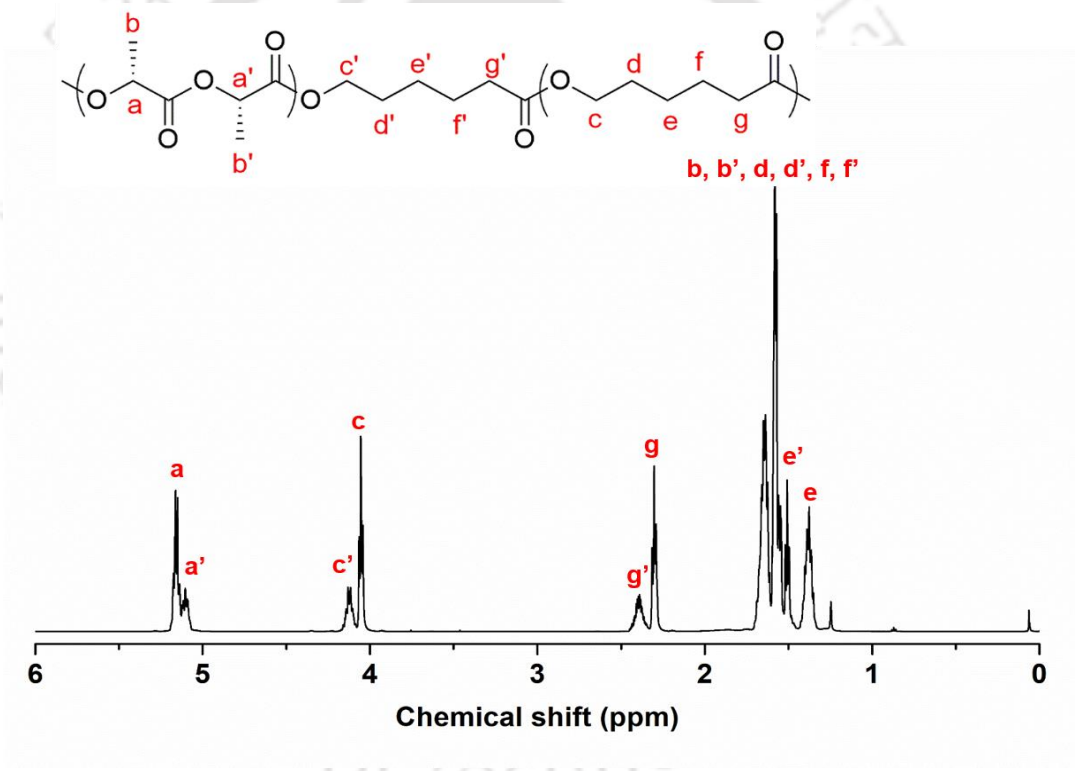

Figure 6.1: ^{1}H-NMR spectrum of the random copolymer.

Table 6.1: Molar ratio of the monomers for synthesizing random copolymers.

Molar ratio (PCL:PLLA)	Molar ratio (%)
1:0	100:0
1:1	50:50
1:1.5	40:60
1:2.333	30:70
1:4	20:80
1:9	10:90
0:1	0:100

Table 6.2: Mn (number average molecular weight) and Mw (weight average molecular weight) as determined from gel permeation chromatography.

Sample identity	Mn (kDa)	Mw (kDa)	PDI
1:1	43.1	81.8	1.89
1:1.5	46.4	96.9	2.09
1:2.333	42.6	93.4	2.18
1:4	47.9	91.1	1.89
1:9	44.2	101.9	2.30
PLLA	49.4	78.6	1.59

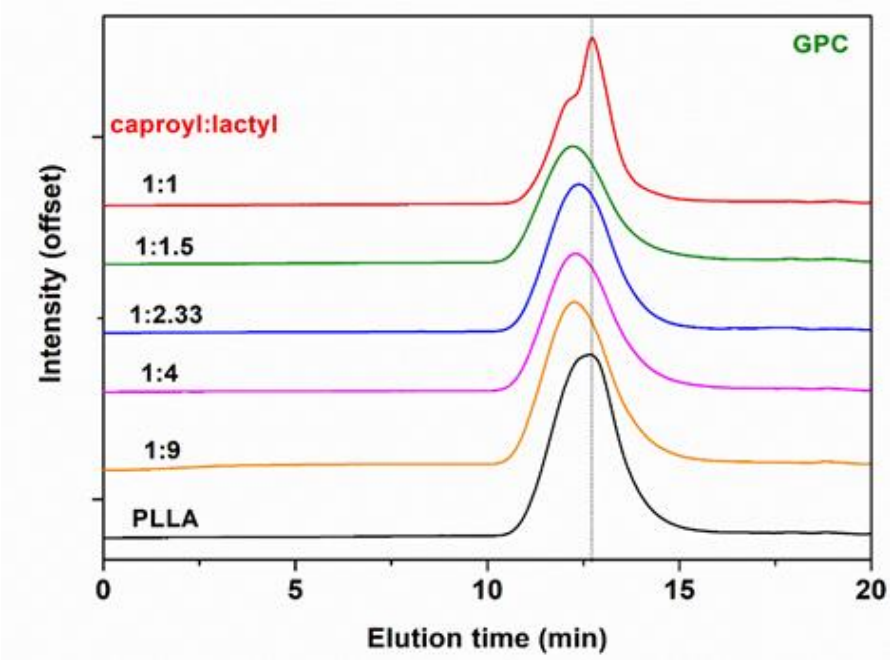

Figure 6.2: GPC curves of the synthesized random copolymers.

6.3.2 Thermal behavior

The thermal transitions in the random copolymers are analyzed using DSC and shown in **Figure 6.3**. It is found that the melting transition of the developed materials is highly dependent on ratio of lactyl and caproyl units. The melting transition of pure PLLA is observed around 177°C which is gradually reduced to 111.8°C as the content of lactide is decreased in the polymer system in the solution cast state. It is also confirmed that random polymerization leads to a single crystalline domain thereby resulting in single endothermic transition. The presence of higher amount of lactide (more than 50%) in the reaction system and its high reactivity due to the relatively higher steric hindrance may lead to the formation of PLLA chains with more than critical length. It is known that for the formation of crystallites, polymer chains should have a critical chain length. The PLLA chains having higher chain length may develop crystalline domains, resulting in melting transition in DSC analysis. The melting enthalpy corresponds to the presence of

crystalline domains and its amount. It can be seen that the enthalpy is reduced from 75.4 J/g to 4.6 J/g as the content of lactide in the reaction system is decreased. The amount of lactide governs the chain length of its homopolymers. It is already known that true random lactide and caprolactone polymer will not contain any crystallizable chains and deviation in its ratio leads to formation of homopolymers which can crystallize if they have critical chain length. On the other hand, the glass transition which is an indicator for the temperature at which polymer chains ends start to vibrate. The glass transition is found to be 59.7°C and decreased to -6.3°C with reduction in lactide content. The reduction of T_g also suggests the formation of soft materials which can be used for the soft tissue applications.

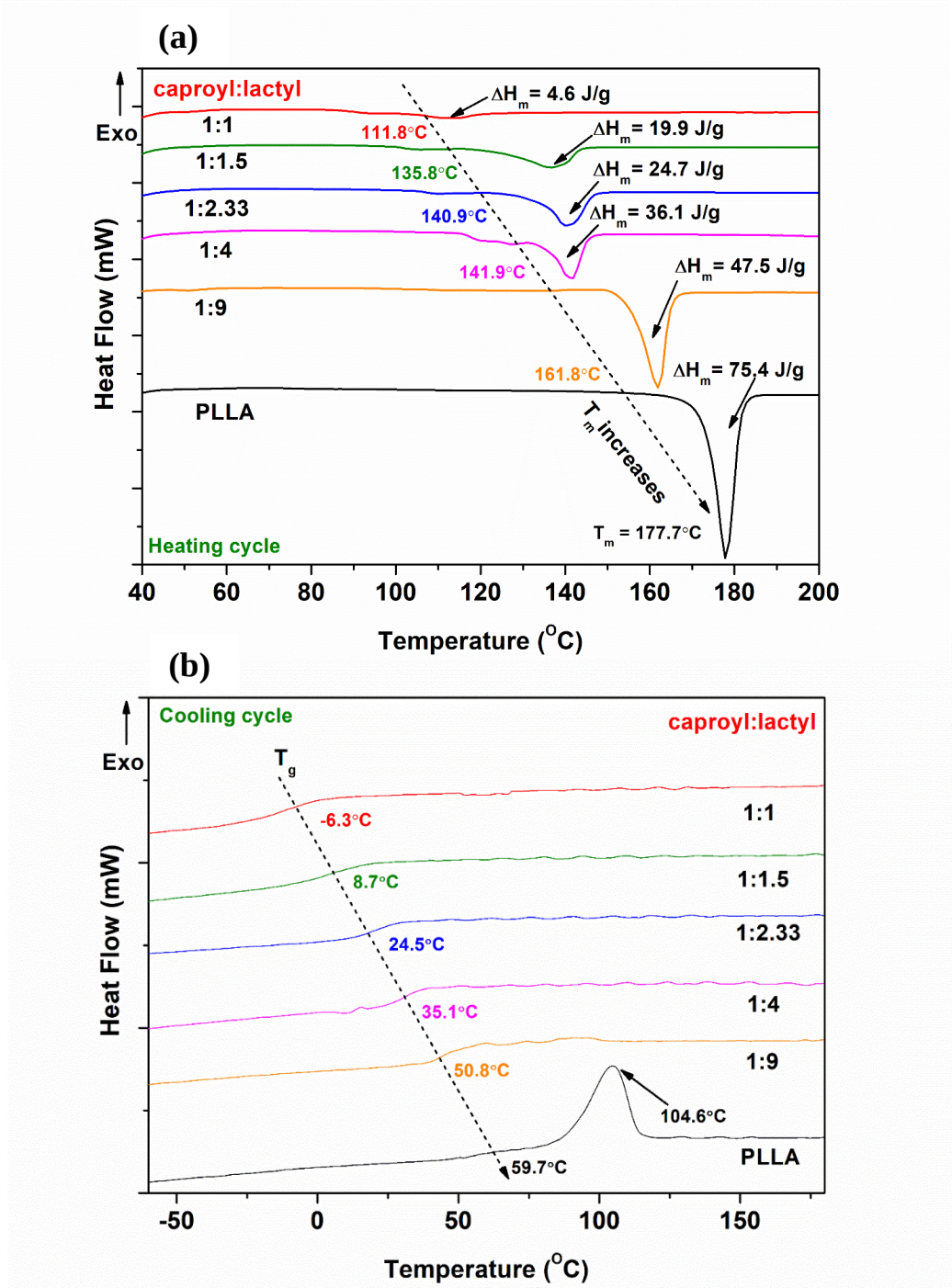

Figure 6.3: (a) First heating and (b) cooling cycles of the synthesized random copolymers.

With the information of thermal transitions acquired using DSC, it is also important to see the maximum temperature at which materials can survive without braking chemically. The chemical bonds in the synthesized materials can break during the melt processing. In order to study the stability of material at elevated temperature (beyond its melting) TGA is employed. The TGA results allow us to decide the processing temperature of the materials. The TGA curves of the synthesized random copolymers are shown in **Figure 6.4**. It is found that the PLLA shows a single step degradation profile at an elevated temperature. The compounds with carbonyl and methyl function groups in PLLA may degrade and evaporate all together at a higher temperature. However, increase in the content of caproyl content in the PLLA leads to the two step degradation profile as shown in **Figure 6.5**. PCL requires more energy to degrade chemically due to presence of relatively larger alkyl chain. The larger alkyl chains degrading at a higher temperature that may account for the two step degradation of copolymers.

Quantitatively, the onset degradation temperature for PLLA is found to be around 295°C which is increased to around 305°C. The presence of alkyl chains stabilize the polymer chains even at a higher temperature resulting in the elevated onset degradation temperature. Overall, the TGA analysis suggests that the synthesized copolymers can be melt processed below 295°C without chemical degradation.

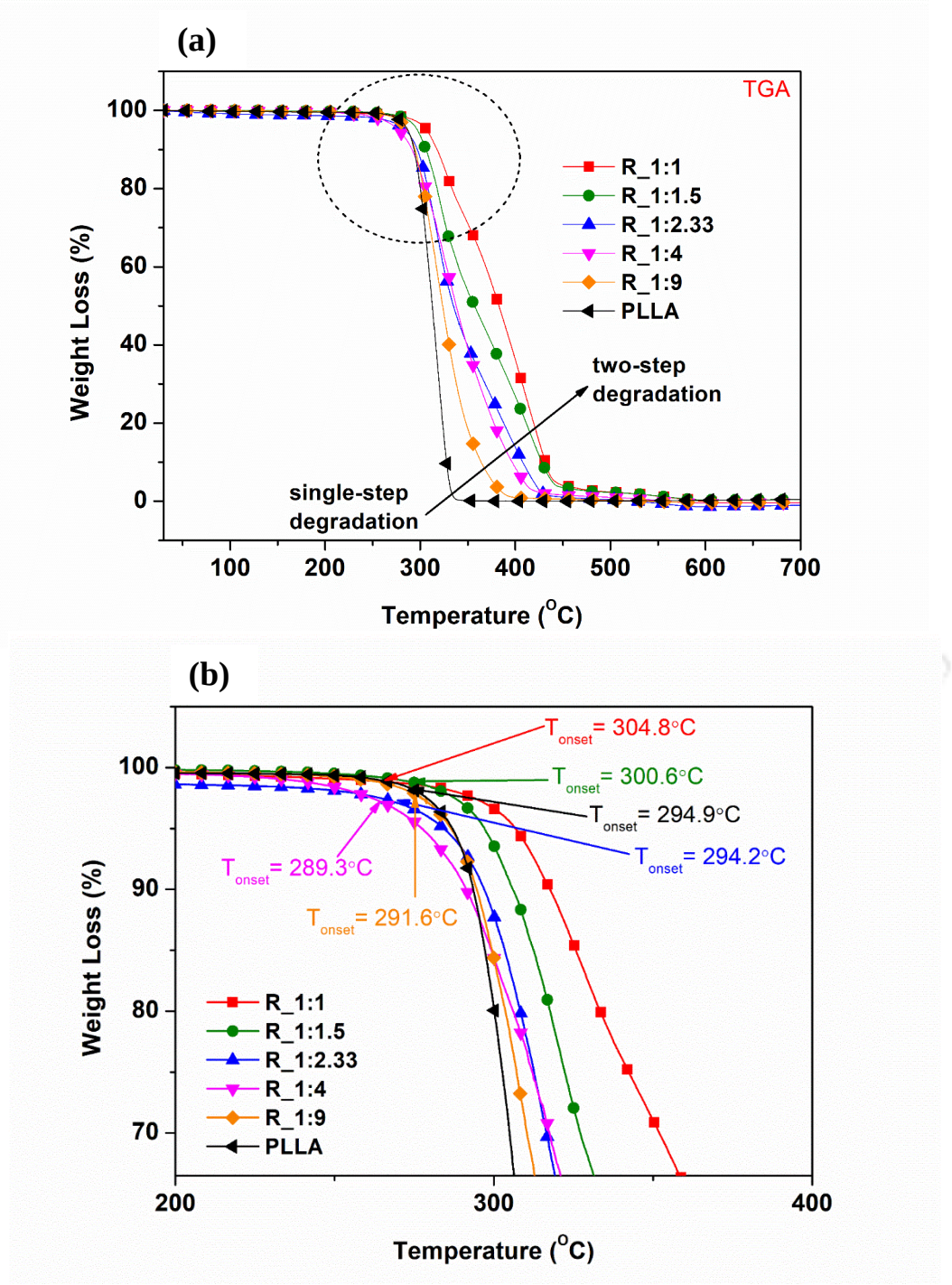

Figure 6.4: TGA curves of (a) the synthesized random copolymers and (b) the corresponding magnified image (200 – 400 ℃).

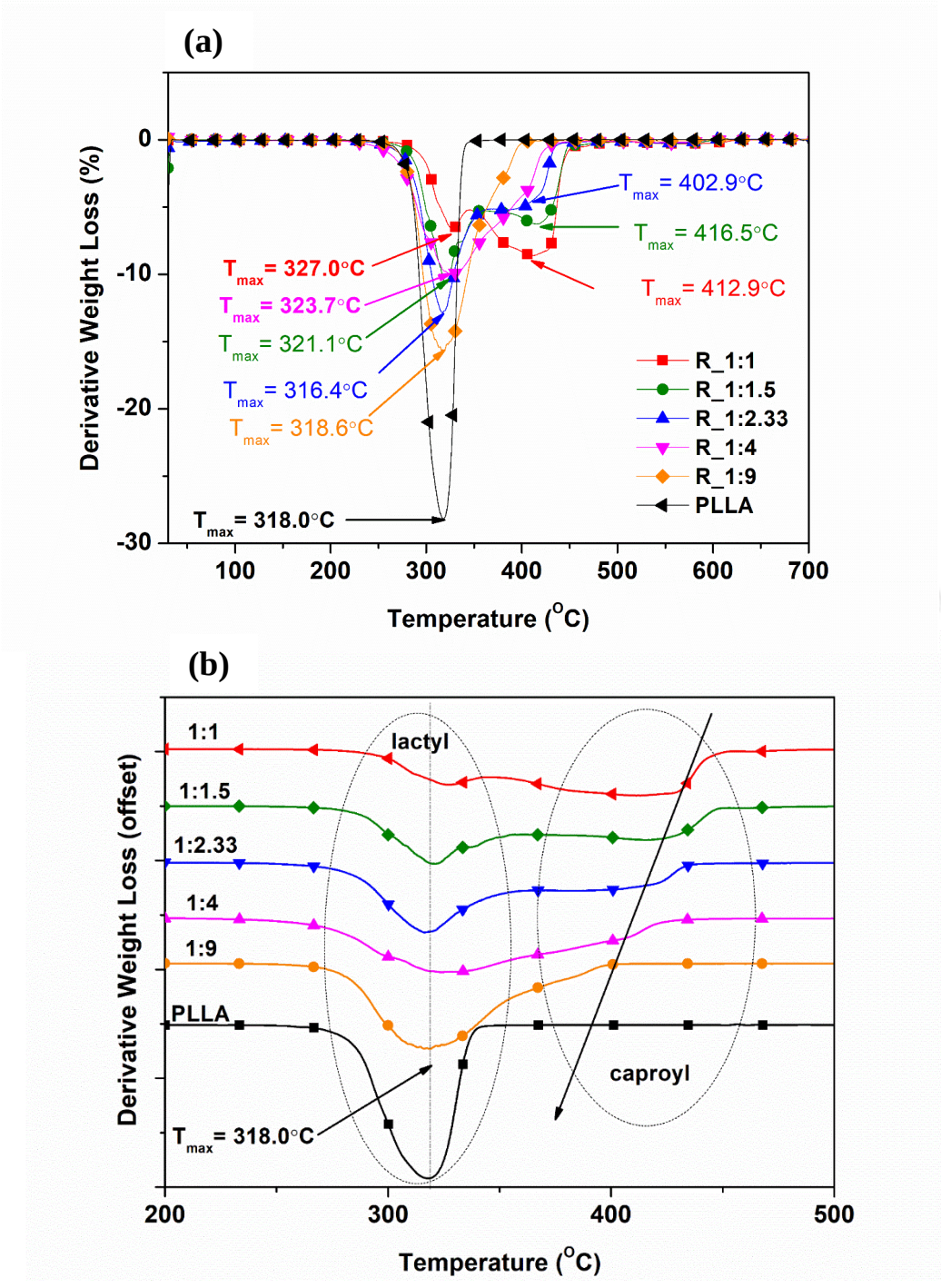

Figure 6.5: Derivative TGA curves of the synthesized random copolymers.

6.3.3 Mechanical properties

The intent of this work was to synthesize copolymers by single step melt processing in order to obtain materials with tunable mechanical properties. Random copolymerization is a one pot single step melt polymerization process and the ratio of lactyl and caproyl units affects the properties of the resulting copolymers. The copolymer films are tested using UTM and a typical strass-strain curve is shown in **Figure 6.6.** The corresponding data i.e. tensile strength, tensile modulus, toughness and elongation at break is shown in **Figure 6.7**. It is observed from the SS curve that as the tensile strength increases, its elongation at break decrease. Such a trade-off is observed for all the copolymer specimens which may be attributed to the content of soft ε-caprolactone units and hard lactide units, where the higher content of ε-caprolactone lead to the formation of materials with higher elongation at break whereas as higher lactide content relates to the higher tensile strength. The strain hardening phenomenon (1:2.22 and 1:1.5 specimens) may be due to presence of caproyl domains. Such a phenomenon was also observed in previous chapters.

In case of PLLA, tensile strength is found to be around 24 MPa which is significantly increased to around 55 MPa after addition of 10% caproyl units. The pristine PLLA having molecular weight of 50 kDa is considered as brittle material and an early fracture is detected before reaching its ultimate tensile strength upon the application of tensile pull. On the other hand, 10% incorporation of caproyl units maintain the strength of PLLA and provide mechanical support to the polymeric chains at the molecular level. Upon tensile pull, the brittle nature of PLLA is drastically reduced and the breakage is observed only after reaching its tensile strength (55 MPa). Further, increase in caproyl units leads to the reduction in tensile strength and enhancement in elongation at break.

The incorporation of caproyl units is also responsible for reduction in tensile modulus due to increased softness and reduced T_g of the copolymers. Elongation at break is found to be higher (~800%) in the case of copolymer containing 40% caproyl unit (60% lactyl unit). This specimen is further used as a matrix for the formation of biocomposites.

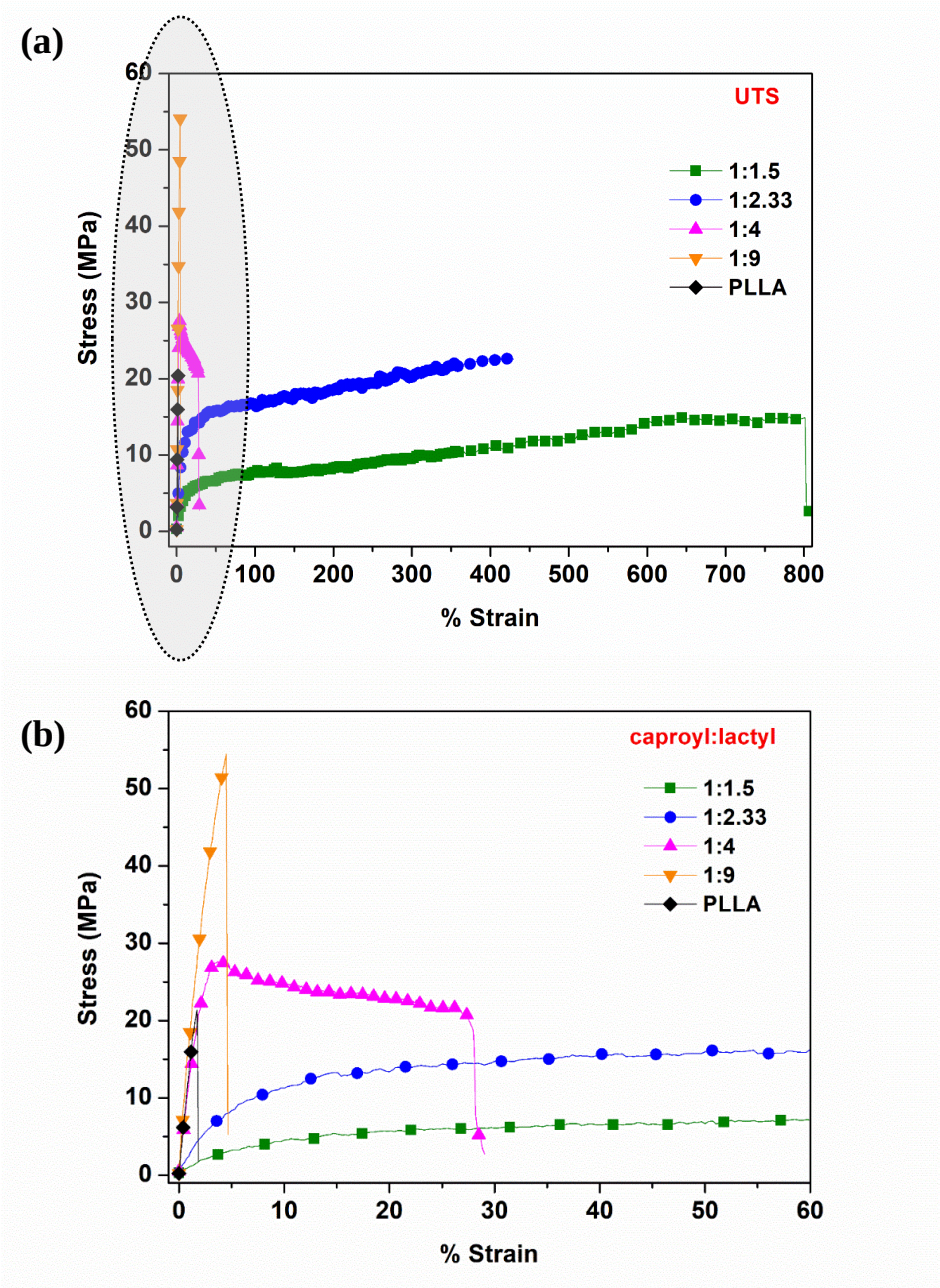

Figure 6.6: UTM curves of (a) the synthesized random copolymers and (b) the corresponding magnified image (0 - 60% strain).

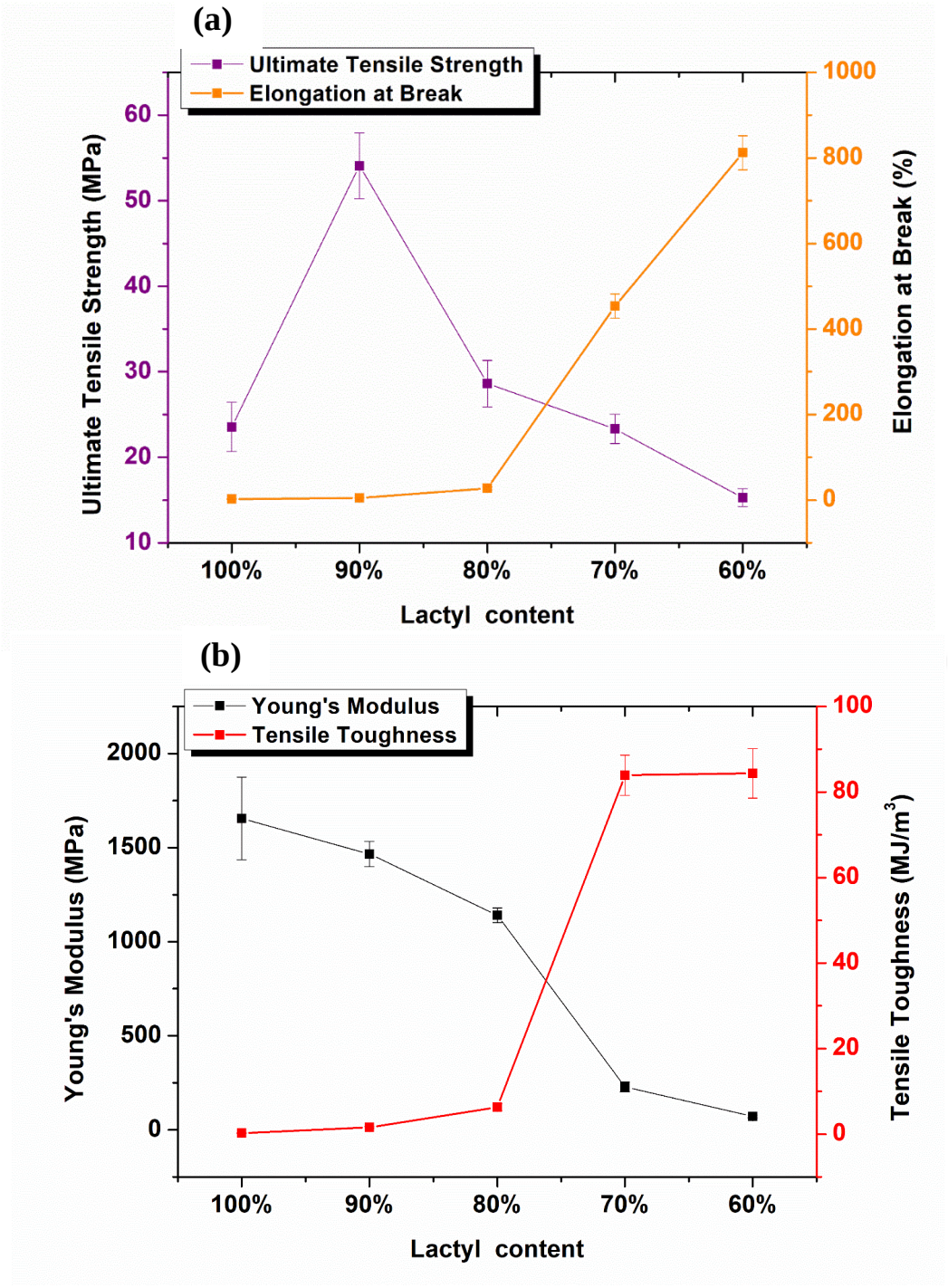

Figure 6.7: (a) Ultimate tensile strength and elongation at break; (b) Young's modulus and tensile toughness of the synthesized random copolymers.

6.3.4 Shape Memory and Elastomeric Effects

It is noteworthy to mention that a unique shape memory effect is found in the copolymer specimen (1:2.33). The presence of hard (lactyl units) and soft segment (caproyl units) make this copolymer a smart material. A qualitative study is conducted to understand the shape memory behavior of copolymers and shown **Figure 6.8**. It is found that tuning of content of caproyl and lactyl units may result in materials having different shape memory and elastomeric effects. In case of 30% caproyl unit in copolymer, shape memory effect is observed upon tensile pull. This is found to return back to its original state upon immersing in warm water (40 °C). The specimen (1:2.33) is found to retain its shape after mechanical stretching which suggests the ability of the material ability to fix its shape. The recovery of the specimen to its original shape when subjected to a warm water (40°C), shows the stimuli responsive nature of this material. The shape fixating may be the result of stress induced crystallization in the caproyl units which melts upon exposure to heat and the material returns back to its original shape.

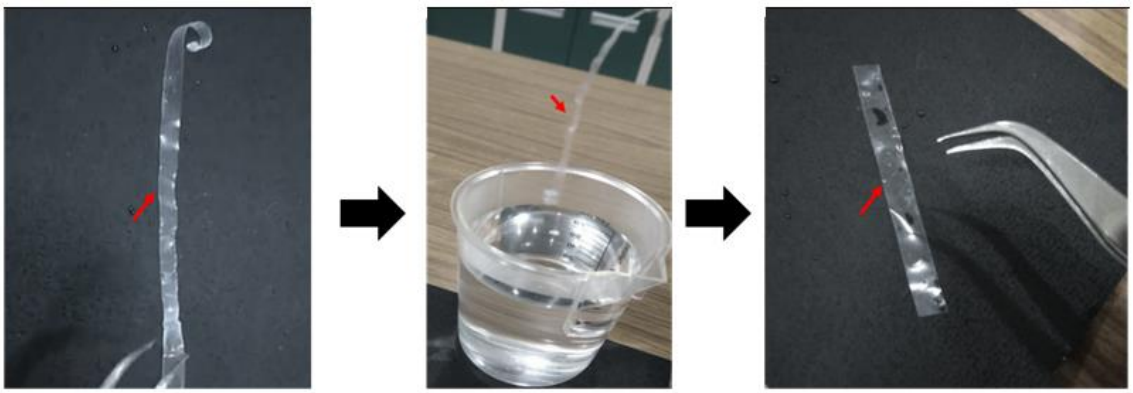

Figure 6.8: Shape memory effect observed in the copolymer specimen (1:2.33).

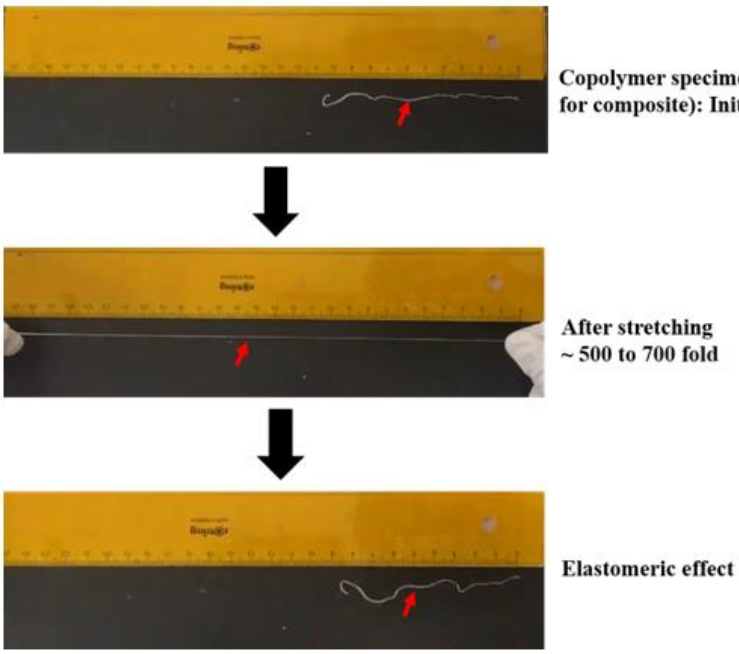

Figure 6.9: Elastomeric effect observed in the specimen (1:1.5).

Similarly, incorporation of 40% caproyl units into the copolymer specimen, leads to the achievement of elastomeric properties. The elastomeric effect of specimen (1:1.5) is shown in **Figure 6.9**. It can be seen from the figure that specimen act as an elastomer and recovers back even after stretching to 500-700%. These different types of applicability of such materials render the synthesis process an important one. It is possible to tailor the properties of by random copolymerization to obtain materials customized applications.

As the specimen (1:1.5) has highest elongation at break and can be employed in soft tissue engineering application, we have incorporated bioglass in it and evaluated different properties.

6.3.5 Random copolymer based Composites

It is known that bioglass is an inorganic biocompatible material and can be used for biomedical purposes. It also enhances the biocompatibility of the matrix and allowing the cells to adhere on its surface. The specimen 1:1.5 is chosen as a matrix for incorporating

bioglass and formation of composites. This choice of this specimen can be related to the soft tissue engineering applications requiring low modulus and higher toughness. Bioglass is loaded up to 50% in the copolymer specimen (1:1.5) by solution cast method. Incorporation of bioglass in random copolymer affect its crystallization behavior affecting thermal transitions of biocomposites. It is observed from **Figure 6.10** that the melting temperature of composites is reduced from 116°C to 95°C with the incorporation of 50% bioglass. Such a reduction in the melting temperature is most likely due to the formation of PLA crystallites having thinner lamellae. The presence of bioglass also affects the T_g of the biocomposites. T_g is found to reduce from 4.2°C to -16.4°C, suggesting that the bioglass hinders the PCL crystallization leaving behind an amorphous PCL domain. A microphase separation may be prevalent upon addition of bioglass into the copolymer matrix which particularly enhances the folding of PLA chains and hindering those of PCL chains.

The use of bioglass adversely affects the thermal degradation of biocomposites as shown in **Figure 6.11**. The biocomposites are found to be thermally stable up to 200 °C upon addition of 50% bioglass. This shows that the material can be melt processable to fabricate different articles for intended applications. It is already discussed in the previous sections that the two step thermal degradation of 1:1.5 random copolymer is attributed to the degradation of lactyl and caproyl units.

In order to understand the effect of bioglass content on the crystallization behavior of 1:1.5 random copolymer, XRD studies of the samples are conducted and shown in **Figure 6.12**. The peaks related to PLA crystallites are observed at 14.8°, 16.7°, 19.0°, 22.3° which may be accounted for (010), (200), (014)/ (203) and (015) crystal planes. The diffraction peaks for the PCL crystalline plans found at 21.3° and 23.8° which may be

accounted for (110) and (200) planes. The intensity of the diffraction peaks of PCL is found to be reduced whereas the intensity of peaks related to PLA is enhanced. This can be reasonably correlated with the discussion made for the thermal analysis.

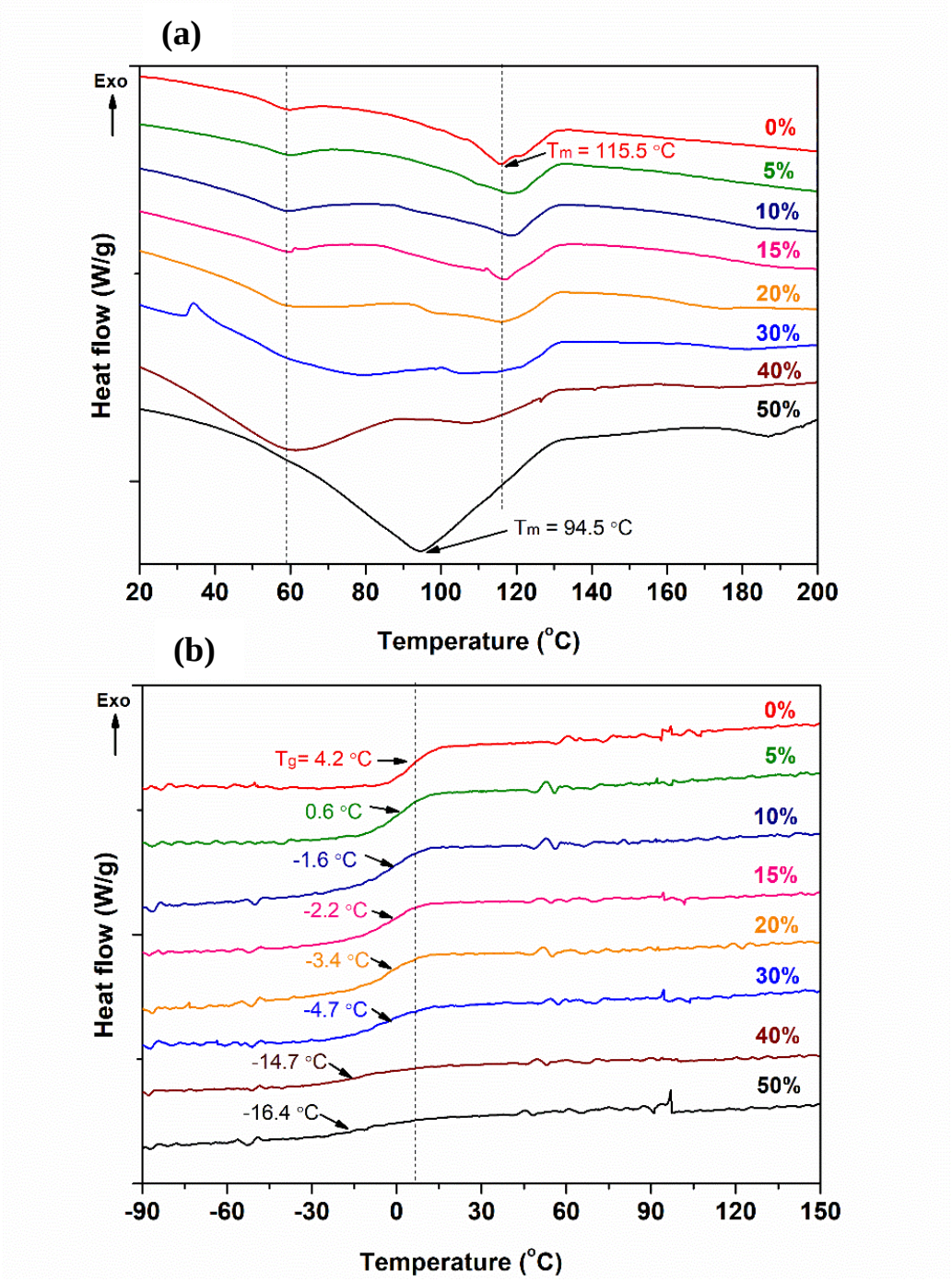

Figure 6.10: (a) First heating and (b) cooling cycle of the composites as determined from DSC.

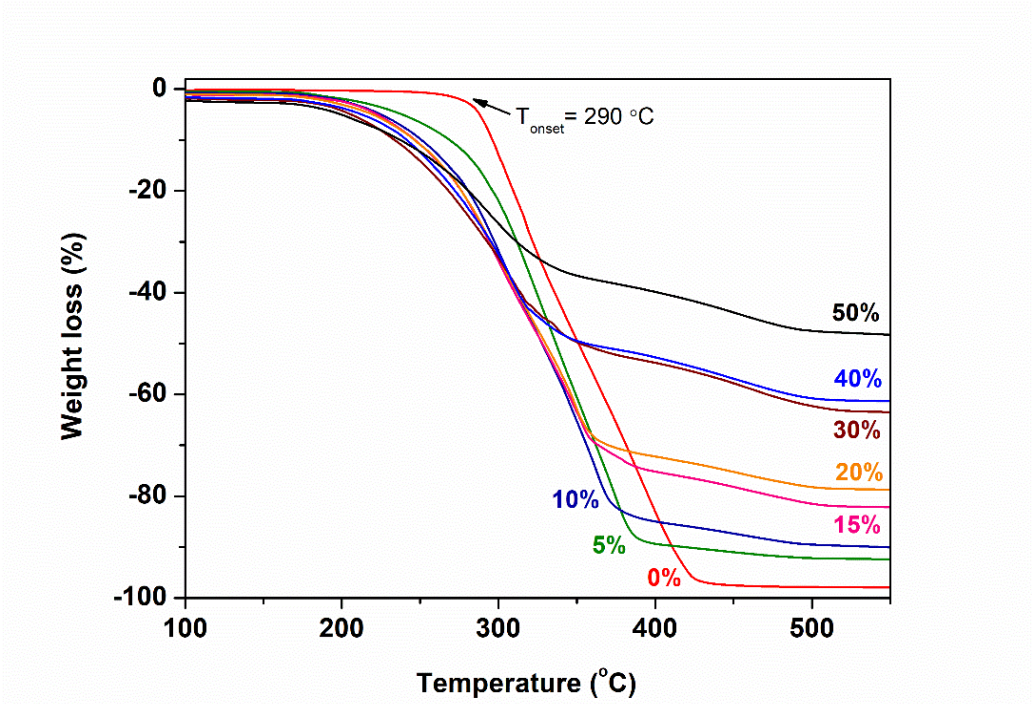

Figure 6.11: TGA curves of the composites.

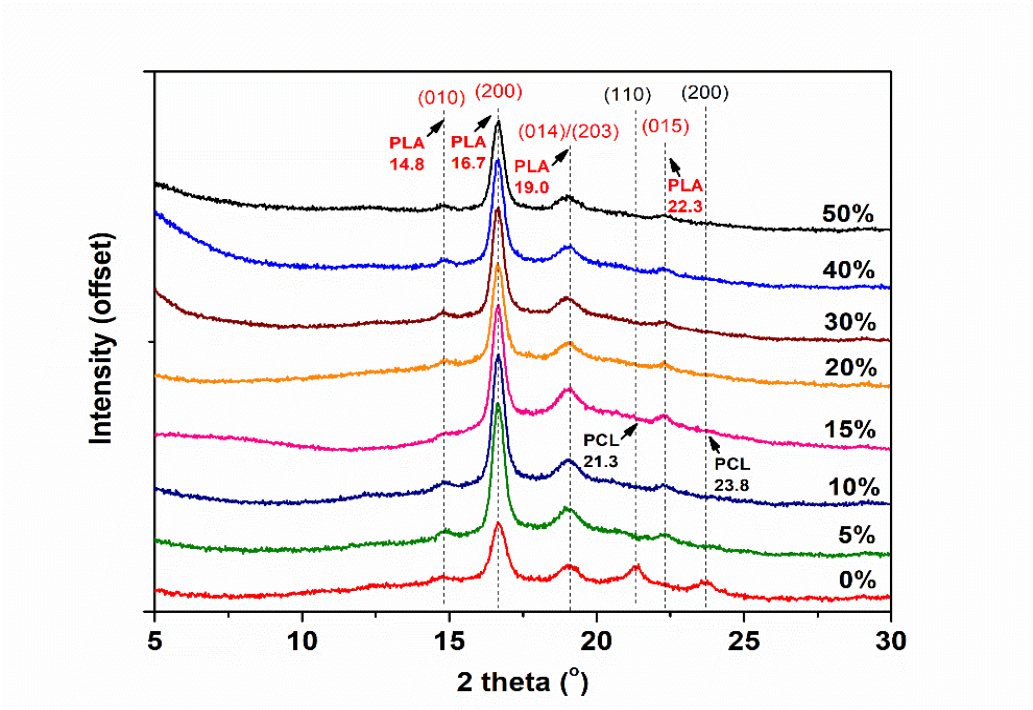

Figure 6.12: X-ray diffraction spectra of composites.

Integration of bioglass into the polymer matrix further affect its mechanical properties. A typical stress-strain curve is shown in **Figure 6.13** and the corresponding data are shown in **Table 6.3**. The polymer matrix (1:1.5) showed the tensile strength of ~9 MPa which was gradually reduced to ~1.7 MPa after incorporation of 50% bioglass. The elongation at break was maintained up to 200% upon loading 50% bioglass into the copolymer matrix. The tensile modulus of the biocomposite is also reduced from 19.7 MPa to 8.5 MPa after addition of 50% bioglass. The mechanical property evaluation confirms that reinforcing bioglass into the copolymer matrix leads to the stress concentration or discontinuous phase leading to the early breakage of the specimen. However, bioglass as a filler would improve the biocompatibility of biocomposites. Overall, relatively higher elongation at break (200-600%) and low modulus (8.5-24 MPa) render the composites suitable for soft tissue engineering applications.

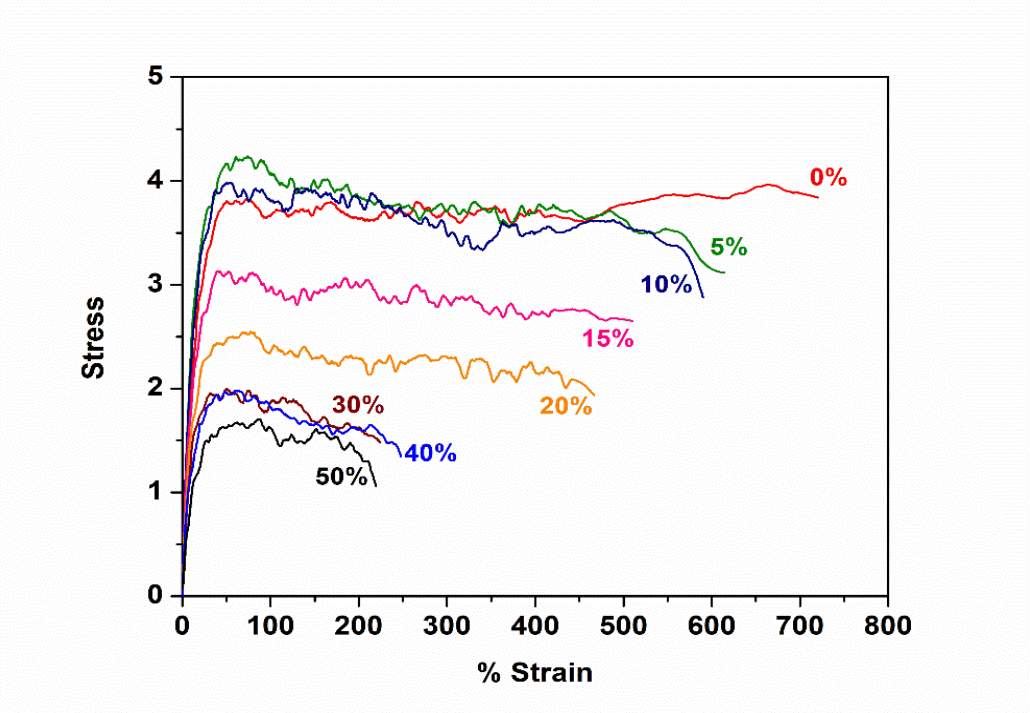

Figure 6.13: UTM curves of the composites.

Table 6.3: Ultimate tensile strength, elongation at break (%), toughness, Young's modulus and recovery ratio of the composites.

Sample (composite)	Ultimate tensile strength (MPa)	Elongation at break (%)	Toughness (MJ/m^3)	Young's modulus (MPa)	Recovery ratio (%)
0%	4.9 ± 0.9	885 ± 164	40 ± 13.5	19.7 ± 2.7	70 - 80
5%	4.2 ± 0.2	601 ± 28.3	21.6 ± 1.6	24 ± 0.5	85 - 90
10%	3.8 ± 0.4	594 ± 3.5	20.1 ± 1.8	20.5 ± 3.7	60
15%	3.3 ± 0.4	443 ± 58	12.9 ± 2.2	19.1 ± 2.5	50 - 60
20%	2.6 ± 0.1	464 ± 55	9.8 ± 1.2	13.9 ± 1.9	60
30%	2.4 ± 0.8	253 ± 10	4.6 ± 1.3	15.9 ± 5.5	60 – 70
40%	1.8 ± 0.2	255 ± 20	3.7 ± 0.7	11.5 ± 0.4	50 - 70
50%	1.7 ± 0	223 ± 24	3.2 ± 0.3	8.5 ± 0.3	60 - 70

6.4 Conclusions

This chapter underlines the synthesis of random copolymers of lactide and ε-caprolactone using single step one pot melt polymerization process. The variation in the content of caproyl and lactyl units result unique mechanical and thermal properties. Increase in the content of caproyl units led to the formation of random copolymer having the elongation at break of ~800%. Tailoring the ratios of lactyl and caproyl units also resulted in materials having shape memory and elastomeric properties. The incorporation of bioglass reduced the tensile strength of the matrix, however it maintained the elongation at break to ~200% even after addition of 50% bioglass. Such tailored properties of the random copolymers and its biocomposites render them suitable for the soft tissue engineering applications.

Chapter: 7

Metathesis Polymerization of a CO_2 Derived Lactone

Graphical Abstract

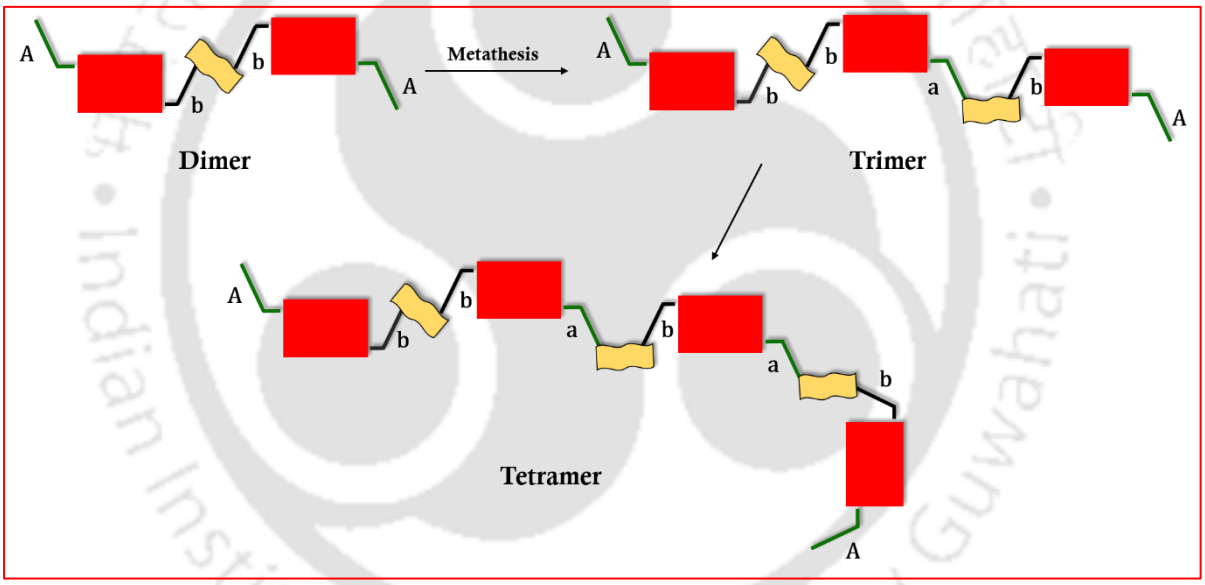

Outcome:

- *Patent (in process): Method of Utilizing CO_2 based Monomer and Polymerization Thereof*
- *Valorization of a CO_2 Derived Lactone by Acyclic Diene Metathesis Polymerization (to be submitted)*

Abstract

The exploitation of carbon dioxide (CO_2) as a feedstock for the chemical processes has been an evasive venture due to its thermodynamic stability. The synthesis of highly functionalized metastable δ-lactone (3-ethylidene-6-vinyltetrahydro-2H-pyran-2-one) was reported in 1970s which is formed by the condensation of CO_2 and 1,3-butadiene in the presence of palladium catalyst. Several attempts have been made to utilize the intermediate for the polymerization processes, however, only a few have been successful. Here, we report a novel mechanism of metathesis polymerization of the metastable monomer by the action of a transition metal carbene complex (Hoveyda Grubb's II generation catalyst) to yield a new class of materials. The reaction mechanism for the polymerization has been proposed and substantiated by nuclear magnetic spectroscopic analysis. The obtained polymeric species consist of a complex unit structure where the cyclic lactone groups are connected by the olefin groups in different combinations.

7.1 Introduction

The use of carbon dioxide (CO_2) in the synthesis of new molecules[281,282] has been a subject of interest[25] ever since its successful conversion to cyclic lactones by Inoue and co-workers[15], which is largely extended by Behr et al.[283]. Among various CO_2 derived lactones[284], the six-membered lactone (3-ethylidene-6-vinyltetrahydro-2H-pyran-2-one or α-ethylidene-δ-vinylvalerolactone: EVV) (**1**) is the most acknowledged[16] and investigated precursor[19,285] owing to its high yield and selectivity[286]. The quantum leap made by Nozaki and co-workers[20] in achieving the free radical polymerization of (**1**) served as a benchmark for the scientific community in developing

functionalizable materials[21]. Subsequently, the controlled polymerization of a trivinyl monomer derived from (**1**) was attempted by Chen et al. to yield linear and hyperbranched polymers[287]. Although a breakthrough has been achieved in polymerizing EVV (**1**), yet it is regarded as poorly polymerizable by common means due to the six-membered ring structure and the presence of high substitution on the ring[288]. Here, we take the advantage of substitution on the six-membered ring in order to redistribute the olefinic groups by means of a metathesis catalyst and develop a new class of materials. The well-known ruthenium based transition metal carbene complexes have witnessed an enormous utilization in catalysing olefin metathesis reactions[289,290]. In this regard, the current work reports the state-of-the-art metathesis polymerization of (**1**) in the presence of a phosphine free Hoveyda-Grubb's II generation catalyst, where the Hoveyda chelate (ortho-isopropoxy group) coordinates to the olefinic ends of the monomer generating the initiating species (**3** & **4**) and leading to the formation of the dimers (**5** & **6**) which may further react to form the oligomers (**9**, **10**, **12**, **13**) by different possible olefinic connections. The reaction mechanism for the contemporary metathesis polymerization has been proposed and elucidated by ^{13}C-NMR and ^{1}H-NMR spectroscopic analysis.

7.2 Experimental section

7.2.1 Materials

Palladium (II) acetylacetonate, triphenylphosphine (PPh_3), acetonitrile (99.8%) and diethyl ether were purchased from Nacalai Tesque, Kyoto, Japan. Carbon dioxide (>99.99%) and Argon (Ar, >99.99%) were purchased from KaindGas Co. Kyoto, Japan. 1,3-Butadiene (>93% GC) was obtained from Tokyo Chemical Industry Co. Ltd via Nacalai Tesque. Hoveyda-Grubb's II generation catalyst, Quadrasil® methyl thiourea

(MTU) were purchased from Sigma Aldrich via Nacalai Tesque. Toluene-d_8, Chloroform-D ($CDCl_3$) were purchased from Eurisotop via Nacalai Tesque.

7.2.2 Characterization

^{1}H-NMR and ^{13}C-NMR spectra were recorded on AV600 spectrometer (Bruker, Germany).

Field emission transmission electron microscope (FETEM, JEOL 200F) was used to determine the shape and size of the reaction product along with simultaneous EDAX (energy dispersive X-ray analysis) to determine the removal of Ru metal catalyst from the product. The sample for analysis was prepared by dispersing in acetone followed by placing a drop of it on the carbon coated TEM grid.

Further, the morphology of the reaction product (powder form) was characterized by using field emission scanning electron microscope (FESEM, Sigma Zeiss USA) at an acceleration voltage of 5kV. The powder sample was coated by gold sputtering prior to analysis.

The FTIR (Fourier transform infrared) spectroscopy was used to determine the structure of the Metathesis reaction product. The analysis was done on an FTIR spectrometer (Perkin Elmer, Spectrum two) and the sample was scanned from 4000 to 400 cm^{-1} with the accumulation of 16 scans.

Differential scanning calorimetry (DSC) was performed on DSC Polyma 214 (NETZSCH, Germany) where the sample (1-2 mg) was heated from room temperature to 200 ℃ at the rate of 10°/min and kept isothermal for 5min. It was further cooled

to -100 ℃ at the rate of 10°/min, kept isothermal for 5min and reheated to 330 ℃ at the rate of 10°/min.

7.2.3 Synthesis of α-ethylidene-δ-vinylvalerolactone:

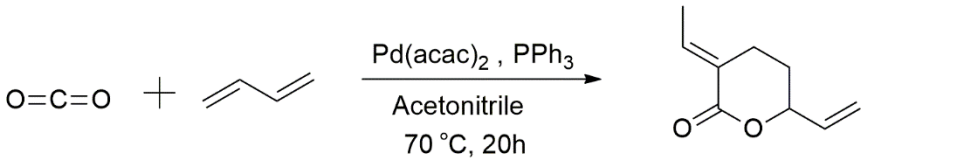

α-ethylidene-δ-vinylvalerolactone

(EVV)

Scheme 7.1: Reaction scheme for the synthesis of α-ethylidene-δ-vinylvalerolactone.

The monomer was synthesized by a reported procedure [283] with some modifications as shown in **Scheme 7.1**. Briefly, the catalyst palladium (II) acetylacetonate (40 mg, 0.13 mmol) and triphenylphosphine (120 mg, 0.458 mmol) were charged to a 50 ml stainless steel autoclave along with a magnetic stirring bar. The reagents were dried over vacuum followed by purging with N_2 gas several times. This was followed by the addition of acetonitrile (dried over 3Å molecular sieves). 1,3-butadiene (21.3 g, 394 mmol) was collected in a flask precooled at -40 ℃ which was transferred to the autoclave (held at -40℃) by a syringe. The autoclave was then pressurized with CO_2 until the pressure reached 7.6 MPa. The reaction was continued at 70 ℃ for 20h followed by quenching the autoclave in ice-water. The residual gas was vented by releasing the pressure followed by filtering the crude product and evaporating the volatile materials by using a rotavapor. The crude product (20.34 g, 95% yield) was subjected to distillation (70-80℃; 0.6-0.8 mmHg) to obtain the purified monomer. The ^{1}H-NMR and ^{13}C-NMR of the purified monomer are shown in **Figures 7.1 and 7.2** respectively.

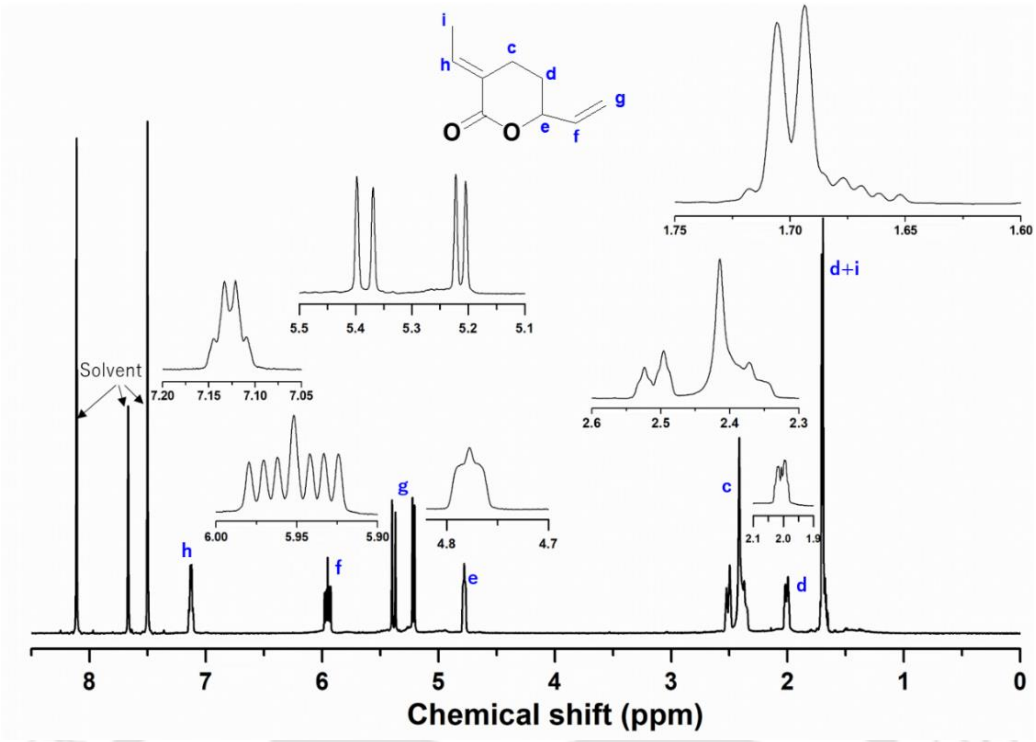

Figure 7.1: ^{1}H-NMR spectra of the monomer (EVV) in Nitrobenzene-d_5.

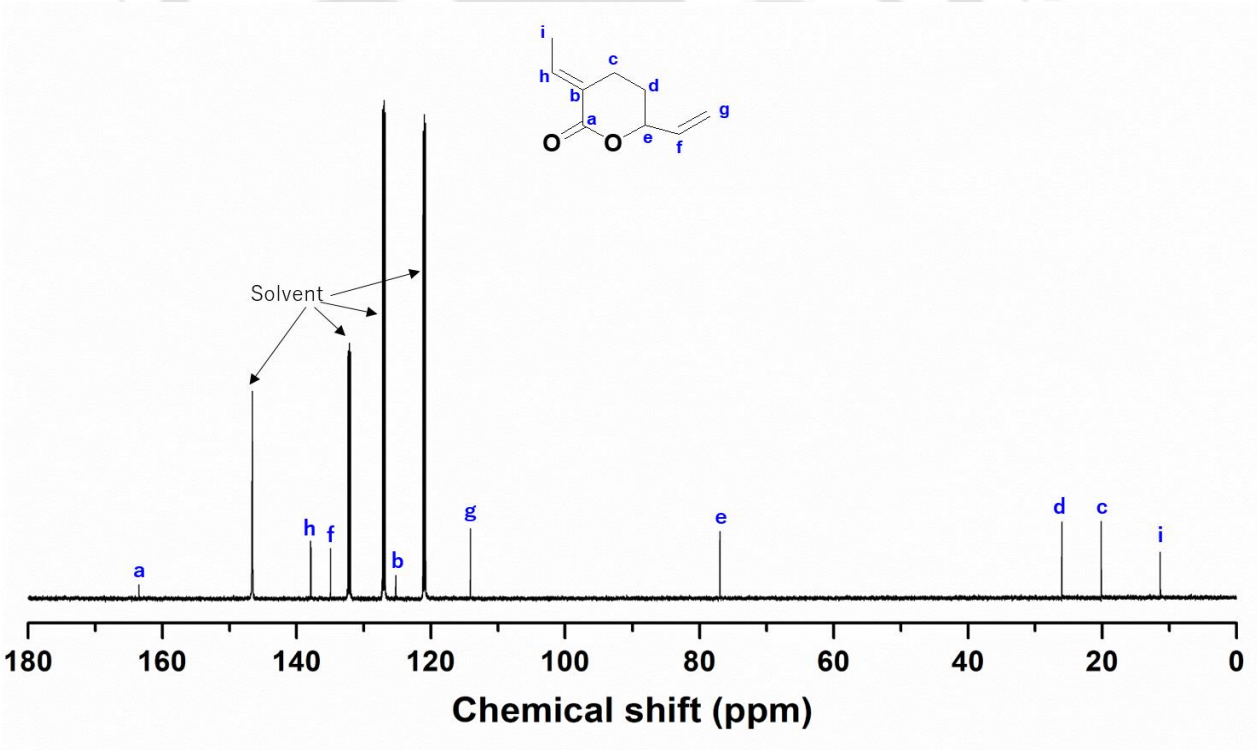

Figure 7.2: ^{13}C-NMR spectra of the monomer (EVV) in Nitrobenzene-d_5.

7.2.4 Procedure for Metathesis polymerization

Hoveyda-Grubb's II generation catalyst (33 mg, 5.27×10^{-2} mmol) was charged into a flask followed by drying over vacuum and purging with N_2 gas. This was followed by the addition of toluene-d_8 (0.5 ml) to the flask and mixing the catalyst with the solvent. The purified monomer (230 mg, 1.5 mmol) was fed to a NMR tube, to which the solvent-catalyst mixture was added under inert environment. The NMR tube was placed in an oil-bath at 100 ℃ under Ar atmosphere. The reaction was continued for 7 days and NMR was measured intermittently to ensure the consumption of the monomer. A color change was observed (dark brown) during the reaction.

7.2.5 Purification of the product

The obtained product was precipitated in excess of diethyl ether followed by filtering and drying in a vacuum oven for 24 h at 45 ℃. The NMR spectra showed the presence of free ligand which was removed by treating the product with a metal scavenger (Quadrasil® MTU, pre-washed with chloroform). Briefly, the obtained product was dissolved in $CDCl_3$, to which the metal scavenger was added and allowed to react for ~1h followed by filtering the scavenger by a filter paper. The filtrate (product) was used to measure NMR and the removal of scavenger was confirmed.

(a) Schematic of the reaction sequences

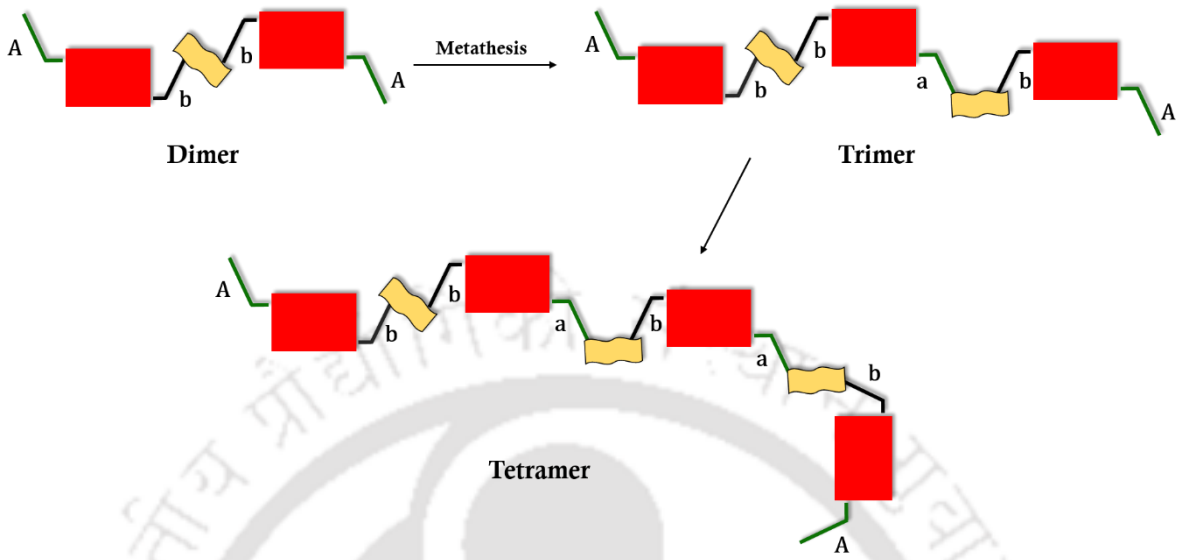

(b) Three-dimensional structure of the products

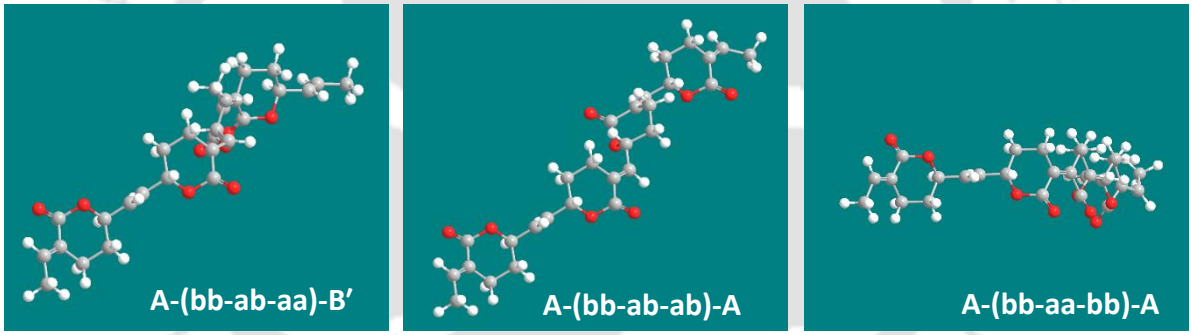

Scheme 7.2: Schematic representation of the product obtained by metathesis reaction.

7.3 Results and Discussion

A schematic representation of the metathesis product is shown in **Scheme 7.2** which indicate the redistribution of the olefinic groups (of the monomer) and their possible connections to form oligomeric products by the action of a metathesis catalyst. The mechanism of the metathesis polymerization is shown in **Scheme 7.3**, where the monomer (**1**) undergoes reaction with the Hoveyda-Grubb's II generation catalyst (**2**)

where the sterically less hindered vinyl group coordinates to the metathesis catalyst (**2**) serving as an initiating species (**3** & **4**), thereby leading to the formation of cis (**5**) and trans (**6**) dimers having the prominent connections of *A-(bb)-A* type. This may be accompanied by the formation of the minor intermediates having the connections of the type *B-(aa)-B* (**7**) and *A-(ba)-B* (**8**) due to the steric hindrance of the olefinic groups. As shown in **Scheme 7.4**, the dimer (**5**) easily enters the next step of polymerization due to the lower steric hindrance of its olefinic groups. The 1,2-disubstituted ethylenic group may readily undergo reaction with the metathesis catalyst as compared to the trisubstituted ethylenic group, which leads to the formation of *A-(bb-ab)-A* (**9**) type units with the liberation of a methylated monomer (**11**). Largely, the trimeric unit *A-(bb-ab)-A* (**9**) is involved in the reaction with the dimer in order to form a tetramer such as *A-(bb-ab-ab)-A* (**12**) where the methylated monomer (**9**) may be reproduced. The methylated monomer (**9**) owing to the higher reactivity of the vinyl group (disubstituted) may further react with the terminal species of the dimer in order to form minor units of *A-(bb-ab-aa)-B′* (**13**) type. In case the trisubstituted ethylenic group of (cis) dimer (**6**) is involved in the reaction, it can lead to the formation of *A-(bb-aa-bb)-A* unit (**10**), where the *aa* type connections are devoid of the olefinic protons.

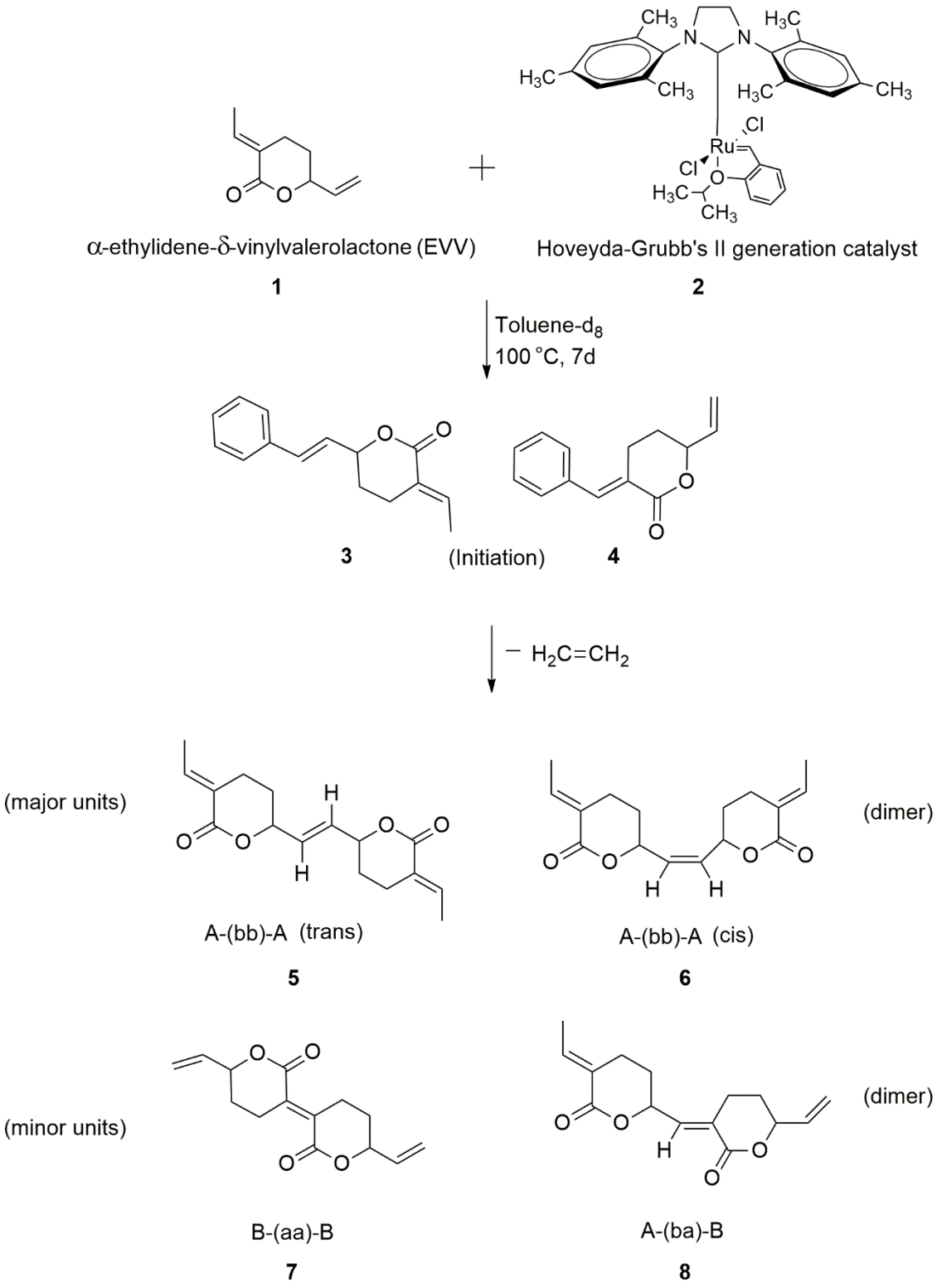

Scheme 7.3: Reaction mechanism of Metathesis polymerization to form the dimeric units.

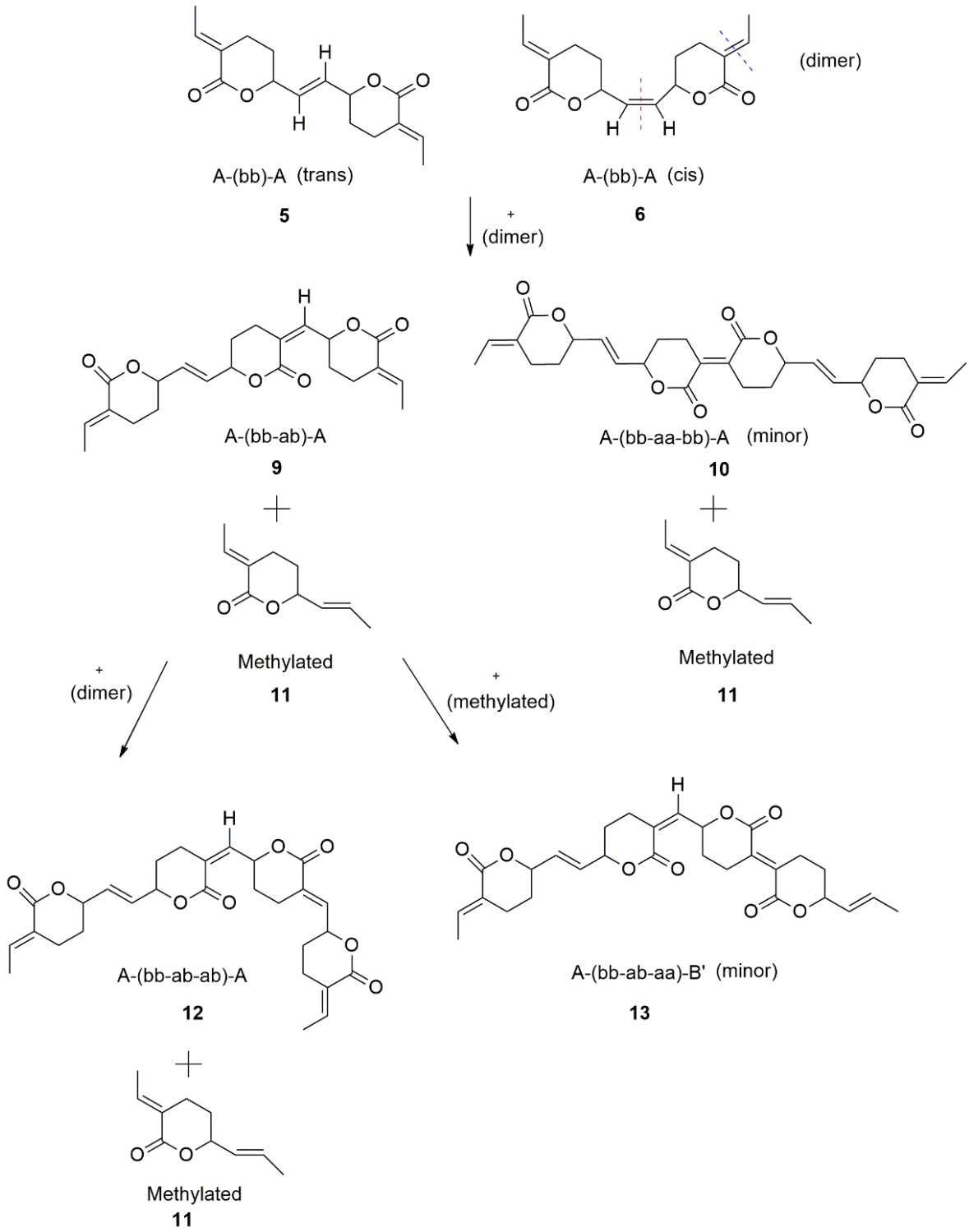

Scheme 7.4: Reaction mechanism of Metathesis polymerization to form the polymer.

After carrying out the metathesis reaction at 100 ºC in toluene-d_8 for 7d (as per the procedure given in supporting information), the obtained product is purified, and the free ligand is removed by scavenging. The transmission electron microscopic (TEM) analysis shows the spherical particles with the size of ~160 - 200 nm (**Figure 7.3(a)**). Upon closely examining the TEM image of the reaction product (**Figure 7.3(b)**), its surface shows the presence of holes (indicated by arrows) which may correspond to the sites of the removal of free ligand by scavenging. This may further be substantiated by the corresponding EDAX (energy dispersive X-ray analysis) spectrum (**Figure 7.3(f)**) which shows the residual content of Ru metal as 0.24 wt. % (or 0.03 at. %) thereby suggesting nearly complete removal of the metal catalyst. Further, the HR-TEM (high resolution TEM) images (**Figure 7.3(c) & (d)**) show the lattice fringes with the interplanar spacing of 1.2 Å and 2.07 Å which may be corroborated with the corresponding SAED (selected area electron diffraction) pattern showing the weak rings with the interplanar spacing of 1.19 Å and 2.12 Å (**Figure 7.3(e)**). The weak ring diffraction pattern suggests the presence of atomic lattices with no long range order. In other words, the reaction product is said to have a very low crystallinity.

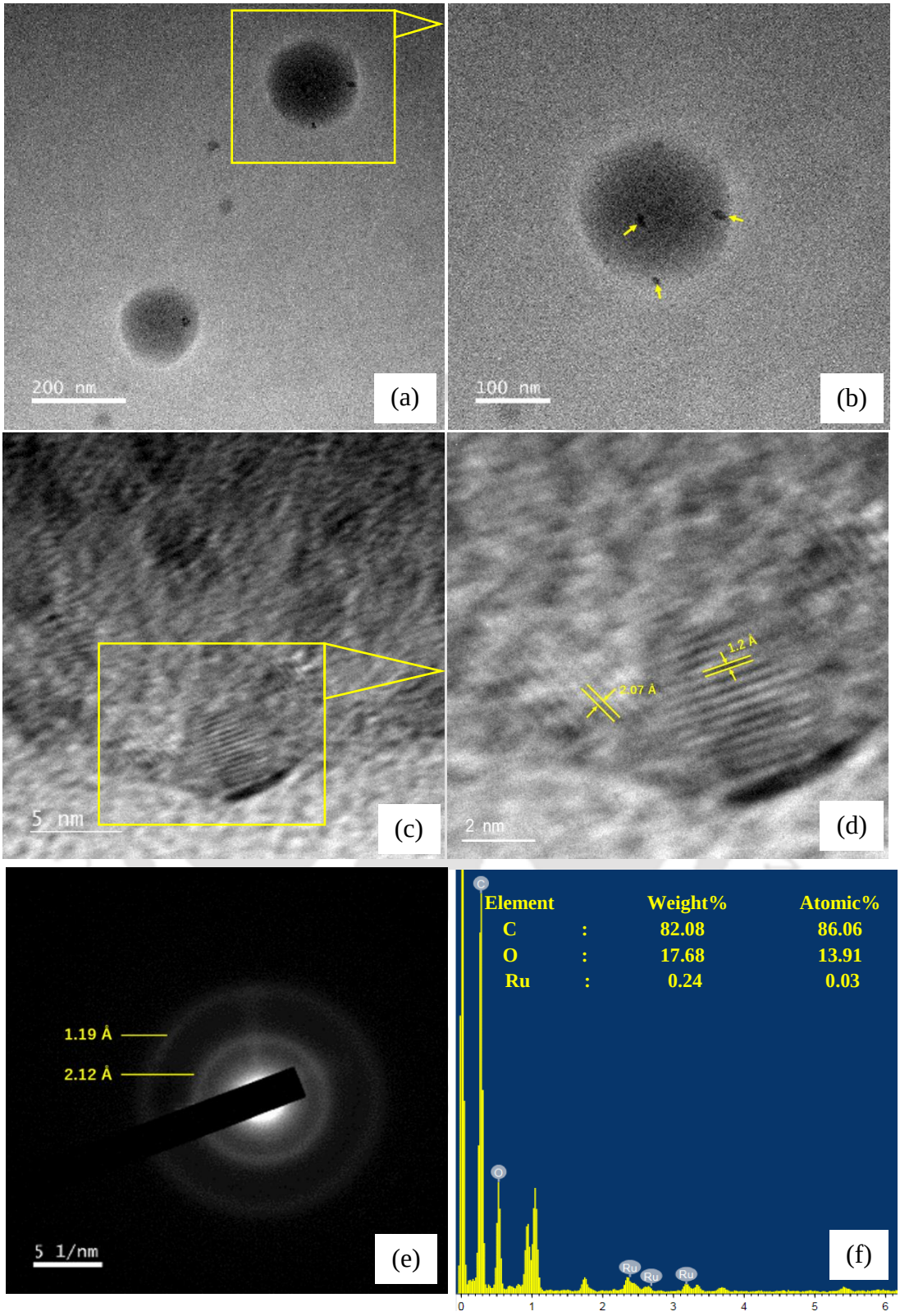

Figure 7.3: (a-b) Transmission electron microscopic images of the Metathesis reaction product, (c-d) HR-TEM images of the product and their corresponding (e) SAED pattern along with (f) EDAX spectrum.

The reaction mechanism of the synthesized product is elucidated upon analyzing its structure by ^{13}C-NMR spectroscopy as shown in **Figure 7.4.** It may be distinctly observed that the ring and the olefinic configuration is preserved. The signals observed in ^{13}C-NMR may be correlated with the predicted structures shown in **Figure 7.5** having three aliphatic carbons (δ ~ 15.6; 26.7; 34.3 ppm), several olefinic carbons (δ ~ 127.2; 125.8; 128.8; 136, 137.6, 141.5 ppm) along with two ether carbons (δ ~ 83.6, 76.8 ppm) and a carbonyl carbon (δ ~ 164.4 ppm). The oligomeric structure is preserved, and the presence of two ether carbons may strongly be attributed to the polymeric species and the terminals (the ratio of the terminal signals being larger than the polymeric signals in ^{1}H-NMR). The unit structure of the polymer may retain the ring structure, giving rise to the polymer signals similar to those of the terminals. The weaker aliphatic peaks are observed in ^{13}C-NMR spectrum (δ ~ 16 – 32 ppm) as the polymer may contain a mixture of three types of structures. However, due to the similar structure of the olefinic carbons, they are detected in the same magnetic field (C_K, C_H, C_J). The lower strength of the olefinic carbon C_J is due to the loss of nuclear overhauser effect (NOE).

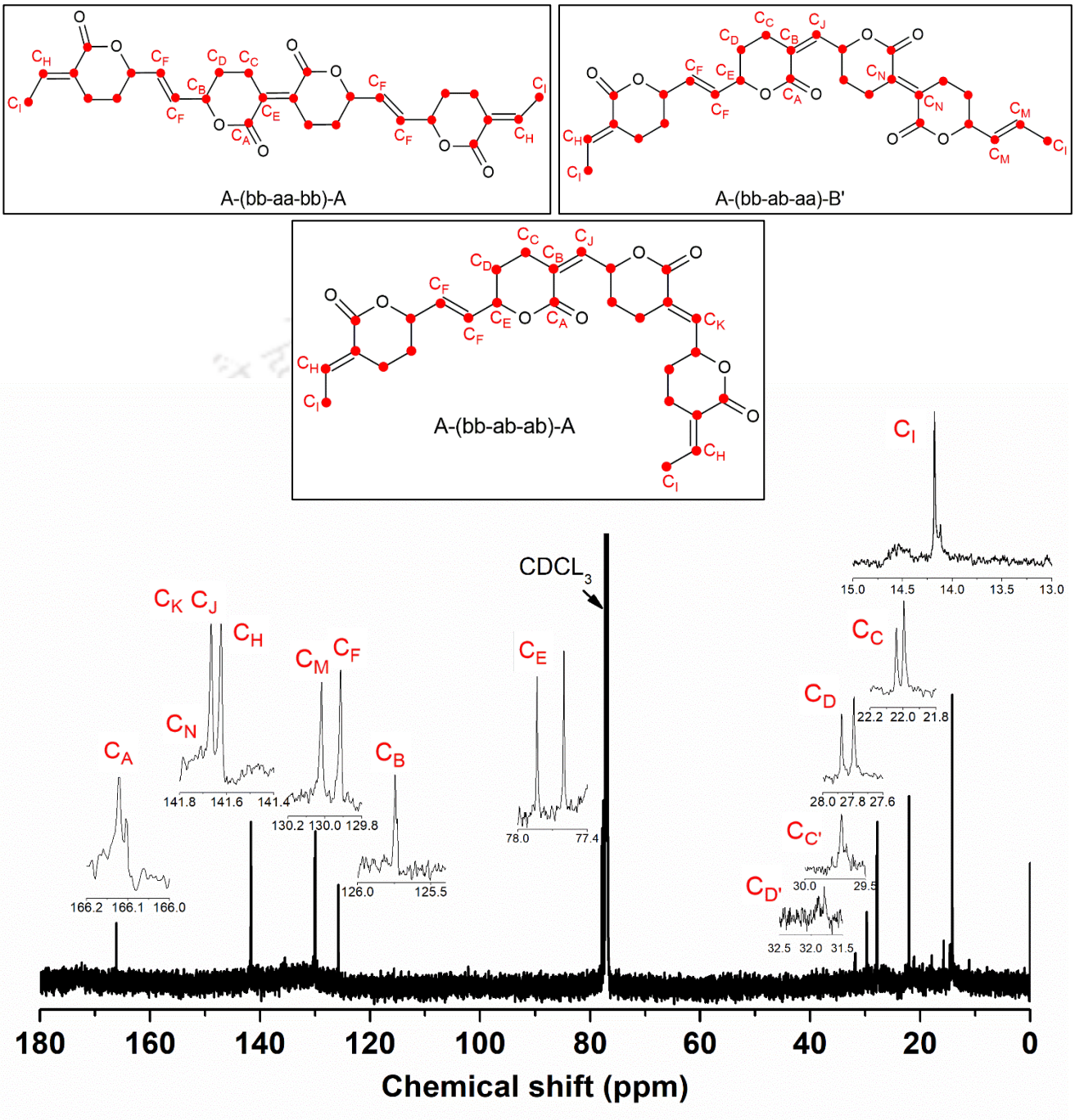

Figure 7.4: ^{13}C-NMR spectra of the Metathesis reaction product.

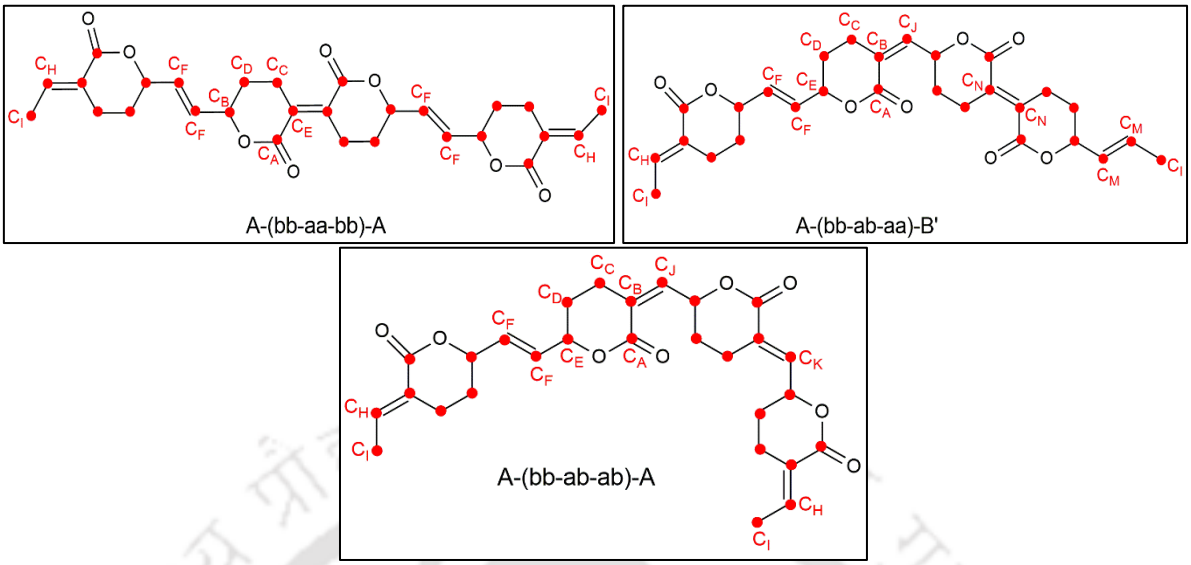

Group	Assignment	Chemical shift			
		A-(bb-ab-ab)-A	*A-(bb-ab-aa)-B'*	*A-(bb-aa-bb)-A*	*mixture*
CH_2	C_C	26.7; 27; 33	26.7; 27; 33	26.7; 27; 33	C_C : 26.7; 27; 33
	C_D	34.3	34.3	34.3	C_D : 34.3
C=CH	C_H	136	136	136	C_N : 141.5
	C_J ; C_K	137.6	137.6	-	C_J ; C_K : 137.6
	C_B	127.2; 125.8	127.2; 125.8	127.2	C_H : 136
					C_B : 127.2
C=C	C_N	-	141.5	141.5	$C_{B'}$:125.8
CH=CH	C_F	128.8	128.8	128.8	C_F : 128.8
	C_M	-	128.6; 128.1	-	C_M : 128.6; 128.1
C=O	C_A	164.4	164.4	164.4	C_A : 164.4
CH_3	C_I	15.6	15.6	15.6	C_I : 15.6
-COO-CH	C_E	83.6; 76.8	83.6; 76.8	83.6; 76.8	C_E : 83.6; 76.8

Figure 7.5: The prediction of the chemical structure (^{13}C-NMR) of the metathesis product (mixture of oligomers).

The reaction mechanism and the plausible structure of the synthesized product is further supported by ^{1}H-NMR spectroscopic analysis (**Figure 7.6).** The spectrum shows the evident broad signals together with the sharp signals which may be assigned to the ring/main chain protons and the terminal groups, respectively. Further, examining the ^{1}H-NMR spectrum of the polymer, it is known that the olefinic signals due to the H_H, H_K and H_J protons are observed at a lower magnetic field ($\delta \sim 6.5$ to 7 ppm). Further, the H_F proton is observed around $\delta \sim 5.5$ ppm, and a broad signal at $\delta \sim 4.5$ ppm can be ascribed to H_E proton. The signals of the ring protons involve several multiplets in the range of $\delta \sim 0.5 - 3$ ppm (H_D, H_C, H_I), which should be due to the different diads or the terminal units. The signal ratio of the aliphatic and olefinic protons is quite different from that of the predicted tetrameric structure *A-(bb-ab-ab)-A* (**12**) which may be due to the presence of mixture of tetrameric units (**10** & **13**) and a relatively large ratio of terminal groups.

The structural analysis of the metathesis product may thus be substantiated by ^{1}H-NMR and ^{13}C-NMR spectra where the obtained product may contain a mixture of oligomers having different olefin connections and thus giving rise to a complex unit structure. The predicted NMR spectra closely match the obtained spectra of the product further indicating the success of the ruthenium catalysed olefin metathesis reaction of EVV.

The FTIR spectrum (**Figure 7.8**) also reveals the presence of carbonyl peaks around 1362 cm^{-1} and 1702 cm^{-1} which may be attributed to the ring carbonyl stretching. Additionally, the peaks corresponding to hydroxyl (OH) and carboxylic acid (COOH) groups are absent which further supports the proposed structure of the metathesis reaction product. The glass transition of the reaction product is obtained from DSC analysis and shown in **Figure 7.9** and its morphology is shown in **Figure 7.10**.

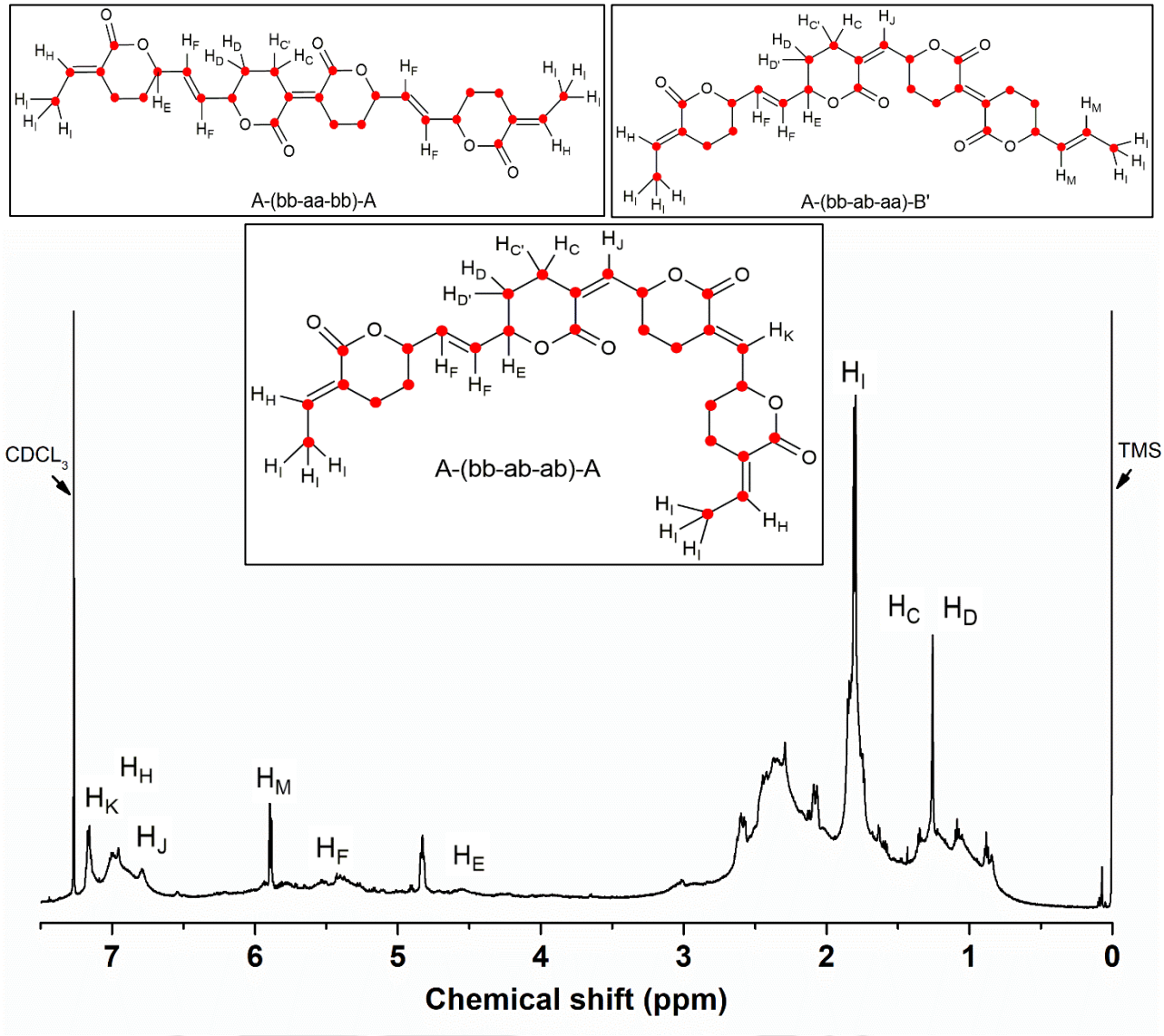

Figure 7.6: ^{1}H-NMR spectra of the Metathesis reaction product.

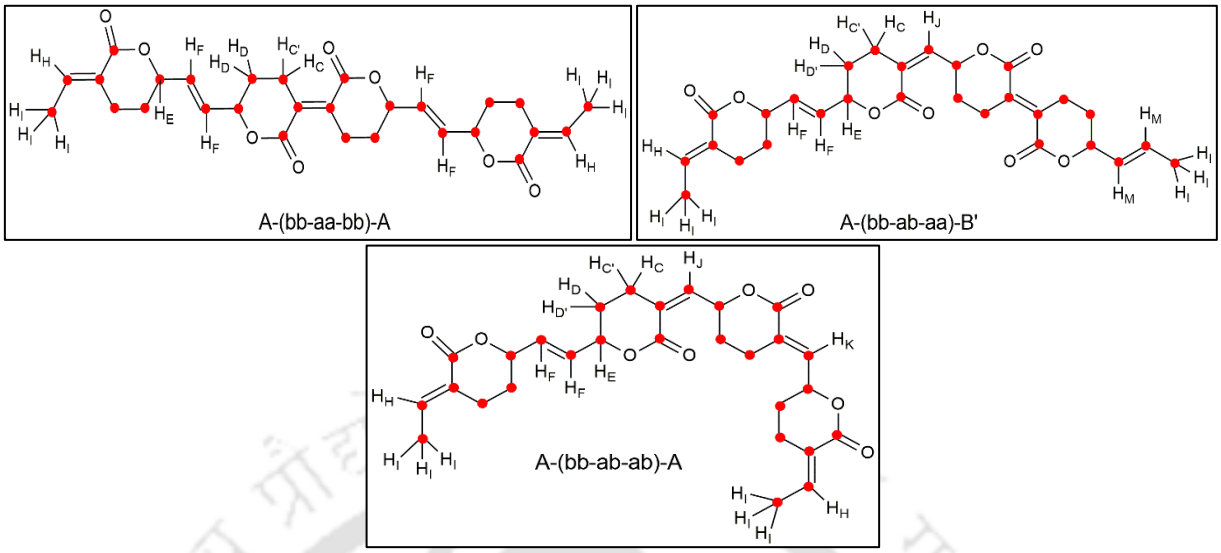

Group	*Assignment*	*Chemical shift*			
		A-(bb-ab-ab)-A	***A-(bb-ab-aa)-B'***	***A-(bb-aa-bb)-A***	***mixture***
CH_2	**H_C**	2.01; 1.91	2.01; 1.91	2.01; 1.91	**H_C** : 2.01; 1.91
	H_D	1.74; 1.49	1.74; 1.49	1.74; 1.49	**H_D** : 1.49; 1.74
C=C**H**	**H_H**	6.6	6.6	6.6	**H_H** : 6.6
	H_J	6.22	6.22	-	**H_J** : 6.22
	H_K	6.79	-	-	**H_K** : 6.79
CH=CH	**H_F**	5.88	5.88	5.88	**H_F** : 5.88
	H_M	-	5.67; 5.69	-	**H_M** : 5.67; 5.69
CH_3	**H_I**	2.05	2.05	2.05	**H_I** : 2.05
-COO-CH	**H_E**	4.64	4.64	4.64	**H_E** : 4.64

Figure 7.7: The prediction of the chemical structure (^{1}H-NMR) of the metathesis product (mixture of oligomers).

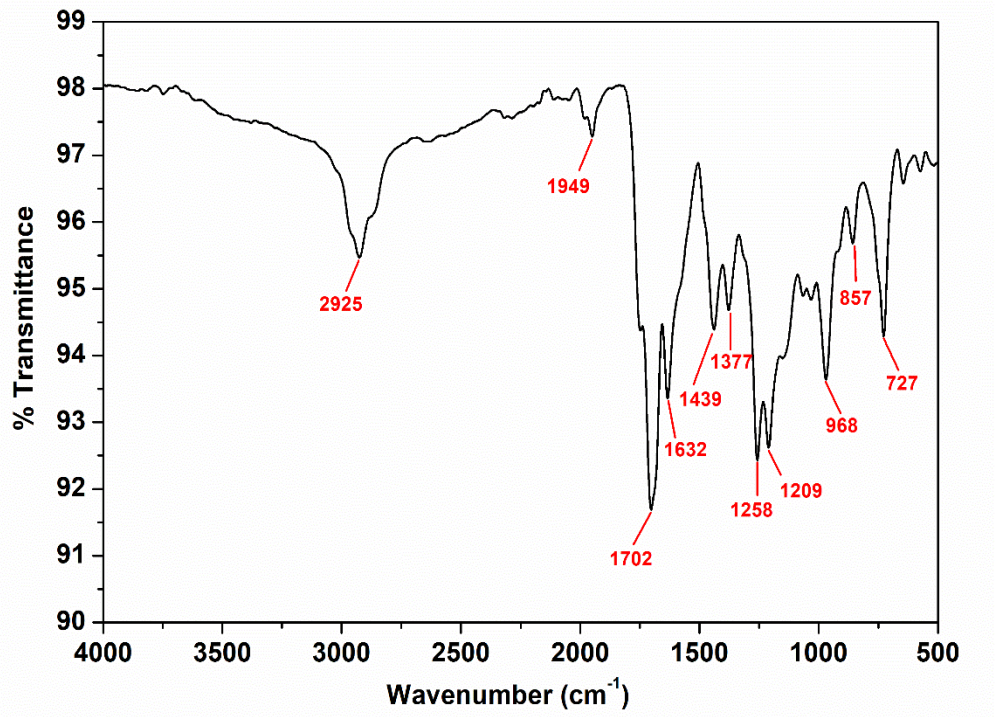

Figure 7.8: FTIR spectra of the metathesis product.

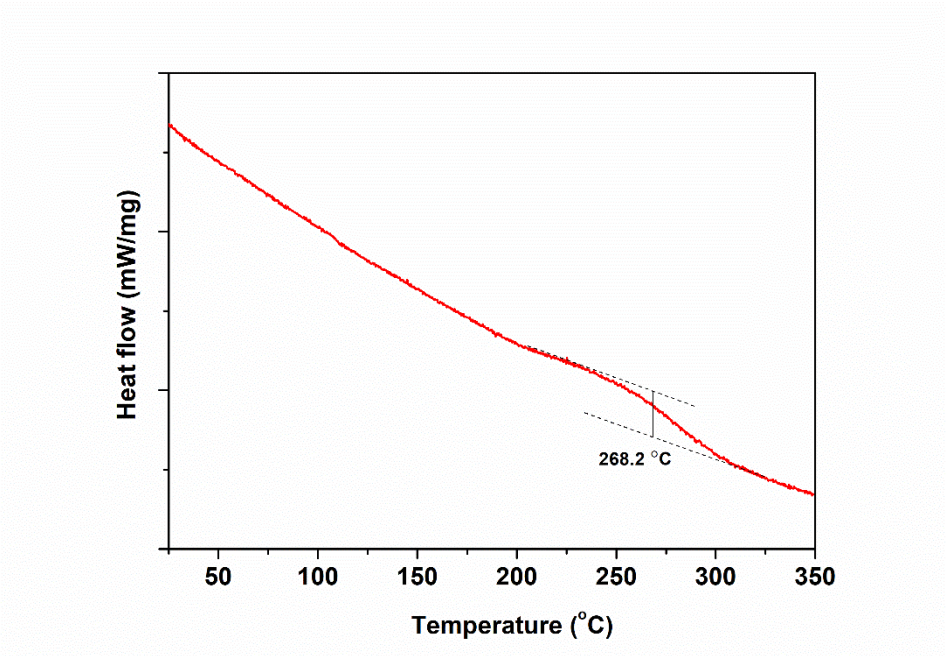

Figure 7.9: DSC curve of the metathesis product (second heating).

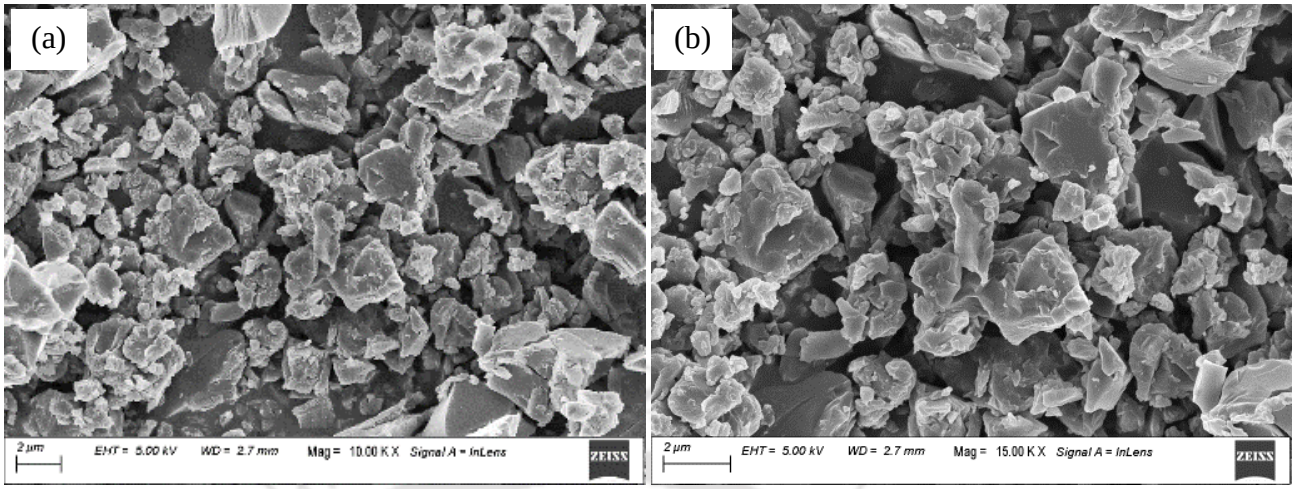

Figure 7.10: Field emission scanning electron microscopic (FESEM) images of the metathesis product at (a) 10 KX and (b) 15 KX magnifications.

7.4 Conclusion

The use of CO_2 as a precursor in synthesizing the substituted-lactone opened a new pathway for the researchers to further look into the possibilities of polymerizing the monomer (EVV). In this regard, the metathesis polymerization was conducted by using Hoveyda-Grubb's II generation catalyst to obtain a complex unit structure containing a mixture of oligomers. The structure of the obtained product was elucidated by ^{13}C- and ^{1}H-NMR analysis. The TEM analysis further revealed the absence of long range order in the product and the efficient removal of metal catalyst (Ru) by scavenging. The novel aspect of the olefin metathesis presented in this research thus remarks the application of greenhouse gas CO_2 as a precursor in developing a new class of polymers which may serve as an essential landmark for developing sustainable future materials.

Chapter: 8

Cationic Polymerization of a CO_2 Derived Lactone

Graphical Abstract

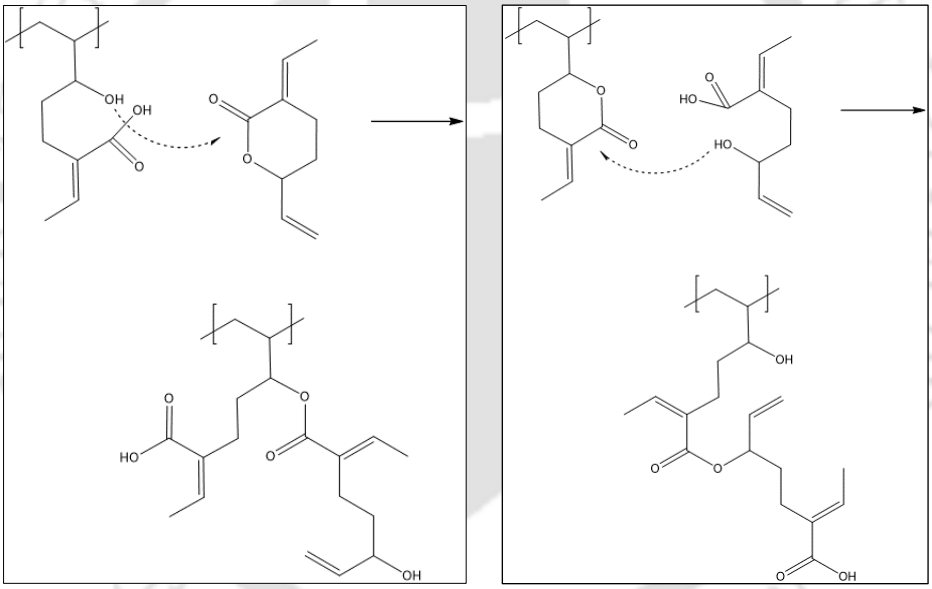

Outcome:

- *Patent (in process): Method of Utilizing CO_2 based Monomer and Polymerization Thereof*
- *Cationic Polymerization of a CO_2 Derived Lactone (to be submitted)*

Abstract

The exploitation of carbon dioxide as a feedstock for the synthesis of substituted lactones has witnessed an enormous recognition lately. The cationic ring opening polymerization of the carbon dioxide derived olefinic substituted valerolactone (α-ethylidene, δ-vinylvalerolactone) is attempted in the presence of highly reactive protic acid and the reaction has been monitored via nuclear magnetic resonance experiments. The product of the cationic polymerization is isolated and its structure determined.

8.1 Introduction

Much of the global industrial advancements are a result of the processes that are inspired from nature. Although the inception of research in the organic synthesis lasts back to centuries, there has been a perpetual exploration and application of novel processes to develop a new class of materials. While nature has unfolded a number of its components/sources to the scientific society, it still retains infinite things which are yet to be explored. One such natural source is carbon dioxide which is present in abundance in the environment and has an immense potential to be utilized for the chemical processes accounting to its renewability, non-toxicity and economic efficiency. The utilization of carbon dioxide as a building block in the organic synthesis has been explored by attempting the transition metal catalyzed reactions of carbon dioxide, which has attracted a significant attention of the scientific society[291]. For instance, the palladium catalyzed reaction of carbon dioxide and 1,3-butadiene was first attempted by Inoue and co-workers[15] to yield "α-ethylidene, δ-vinylvalerolactone" (EVV), which became the premier material for the researchers. However, the process was accompanied by the

formation of several by-products and significant efforts were made to overcome the constraints. Following this discovery, Behr et al. optimized the reaction conditions to yield selectively the monomer[283] (Scheme 1a). The process of telomerization was later applied to a continuous scale to optimize the development of a miniplant[292]. Gaining insights form the Behr's process, several researchers attempted to further optimize the yield and selectivity of EVV,[16,293] while others laid their efforts in developing alternative routes to synthesize possible lactones as intermediates to develop novel polymers[282]. Upon investigating the homopolymerization of EVV, Dinjus and coworkers reported that the reaction did not proceed in the presence of free radical, cationic or anionic initiators indicating the presence of high substitution on the ring which would lead to the decreased tendency of such (substituted) lactones to polymerize via ring opening mechanism[288]. Subsequently, a breakthrough in the free radical polymerization of EVV was achieved by Nozaki's group by overcoming the existing kinetic and thermodynamic barriers associated with the reaction[20]. Here, we report a distinctive approach for the cationic ring opening polymerization of EVV in presence of a highly reactive protic acid. The reaction product may consist of open chain units along with vinyl polymerization, which is determined by ^{1}H-NMR spectroscopic analysis.

8.2 Experimental section

8.2.1 Materials

Trifluoromethanesulfonic acid was purchased from Sigma Aldrich via Nacalai Tesque. Nitromethane-d_3, Chloroform-D ($CDCl_3$) were purchased from Eurisotop via Nacalai Tesque.

8.2.2 Characterization

^{1}H-NMR spectra were recorded on AV600 spectrometer (Bruker, Germany).

The morphology of the reaction product (powder form) was characterized by using field emission scanning electron microscope (FESEM, Sigma Zeiss USA) at an acceleration voltage of 5kV. The powder sample was coated by gold sputtering prior to analysis.

Differential scanning calorimetry (DSC) was performed on DSC Polyma 214 (NETZSCH, Germany) where the sample (1-2 mg) was heated from room temperature to 200 ℃ at the rate of 10°/min and kept isothermal for 5min. It was further cooled to -100 ℃ at the rate of 10°/min, kept isothermal for 5min and reheated to 330 ℃ at the rate of 10°/min.

8.2.3 Procedure for Cationic polymerization

The monomer α-ethylidene, δ-vinylvalerolactone (EVV) was synthesized according to the procedure reported in previous chapter. To the synthesized monomer (300 mg, 1.97 mmol), trifluoromethanesulfonic acid (1 mg, 6.66 $\times 10^{-3}$ mmol) was added under N_2 atmosphere. The reaction was conducted in an oil bath at 90 ℃ for 6.5 h under stirring. The monomer turned into a brown solid with time.

8.2.4 Purification of the product

The cationic polymerization product was added into excess of diethyl ether and a part of the product was found to be soluble in diethyl ether (Et-soluble). Further, another part of the product was insoluble in diethyl ether (Et-insoluble). The obtained products were isolated and characterized by ^{1}H-NMR spectroscopy.

8.3 Results and Discussion

After conducting the reaction at 90 °C for 6.5 h, the product was isolated by precipitating in excess of diethyl ether. The NMR spectra (**Figure 8.1**) indicate the presence of carboxylic acid (COOH) groups in the Et- soluble part, which are lost in the Et-insoluble part. This suggests the formation of by-products upon polymerization, which are removed upon isolation. The reaction scheme for the cationic polymerization is shown in **Scheme 8.1**. The cationic reaction occurs in the presence of trifluoromethanesulfonic acid catalyst preferably attacks the vinyl group of the monomer leading to the preferential vinyl polymerization. This can be correlated from the ^{1}H-NMR spectra shown in **Figure 8.2** which shows that the ethylidene group is preserved in the reaction system and vinyl group undergoes polymerization.

Along with vinyl polymerization, the ring-open structure may also be formed in the product. The open chain units of the polymer may attack the monomeric units leading to the formation of dimeric units as shown in **Scheme 8.2(a)**. Further, the presence of moisture in the monomer may lead to the formation of hydrolysed monomeric units. This may lead to the possibility of hydrolysed monomer units attacking the lactone units of the polymer as shown in **Scheme 8.2(b)**.

The reaction in the presence of highly reactive acid catalyst may thus lead to the formation of cationic product containing dimeric units along with vinyl chain polymerization. The structural analysis of the product is thus established.

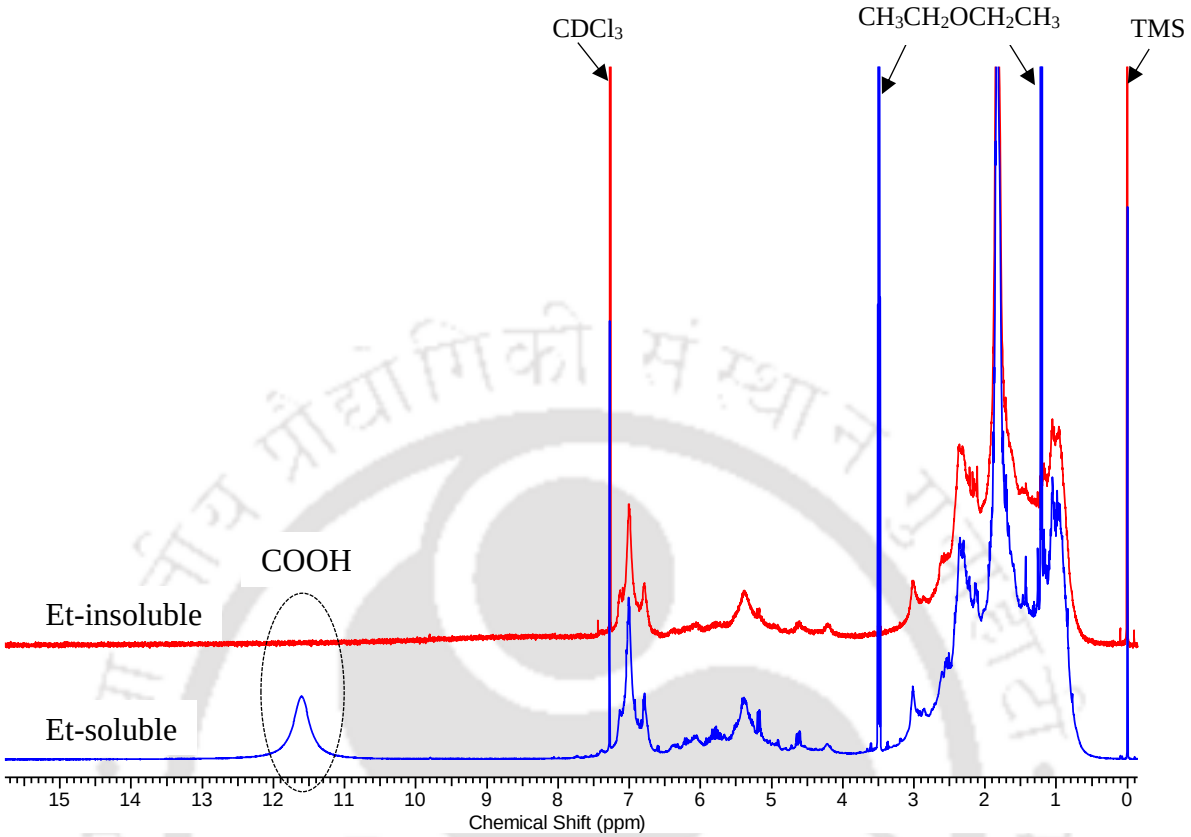

Figure 8.1: ^{1}H-NMR spectra of the product of cationic polymerization (Et-soluble and Et-insoluble).

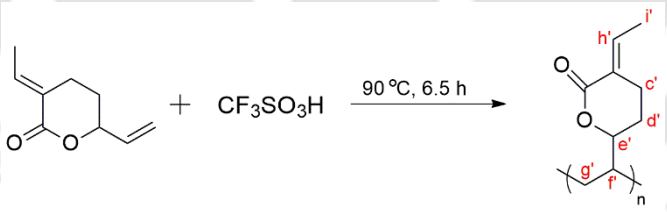

Scheme 8.1: Reaction scheme for the cationic polymerization (Et-insoluble product).

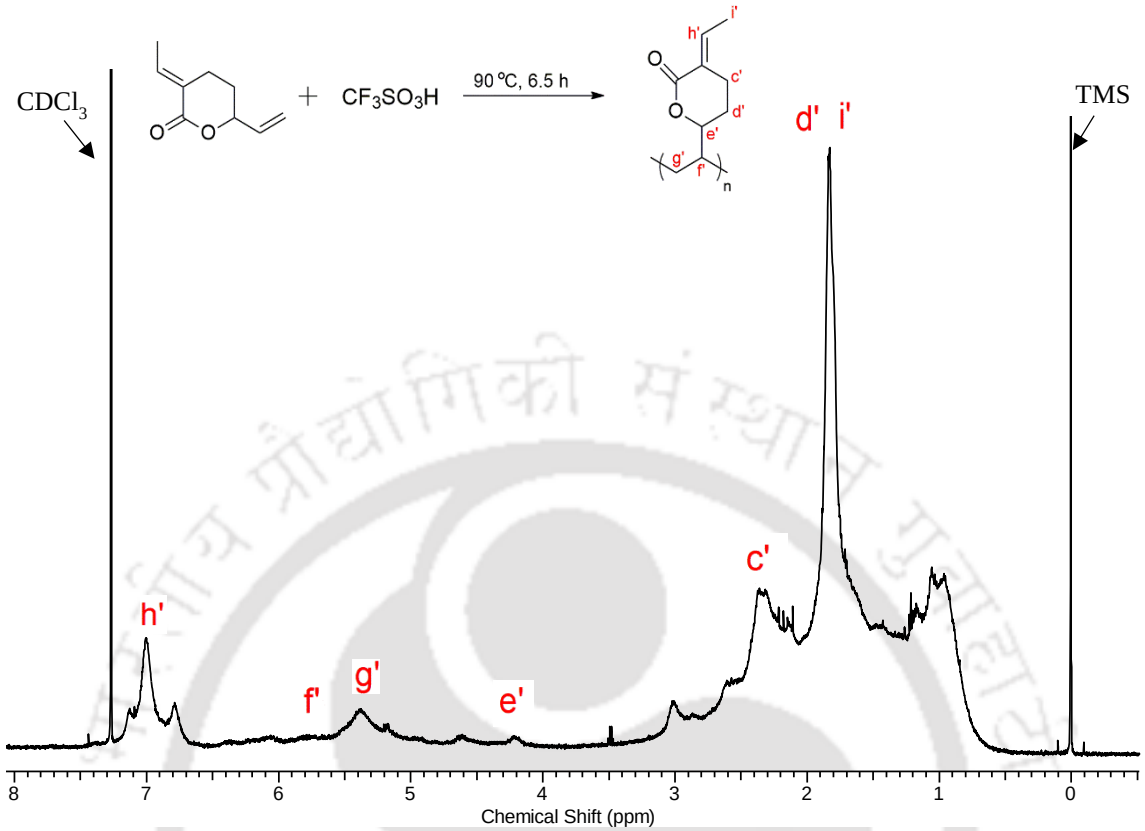

Figure 8.2: ^{1}H-NMR spectra of the product of cationic polymerization (Et-insoluble).

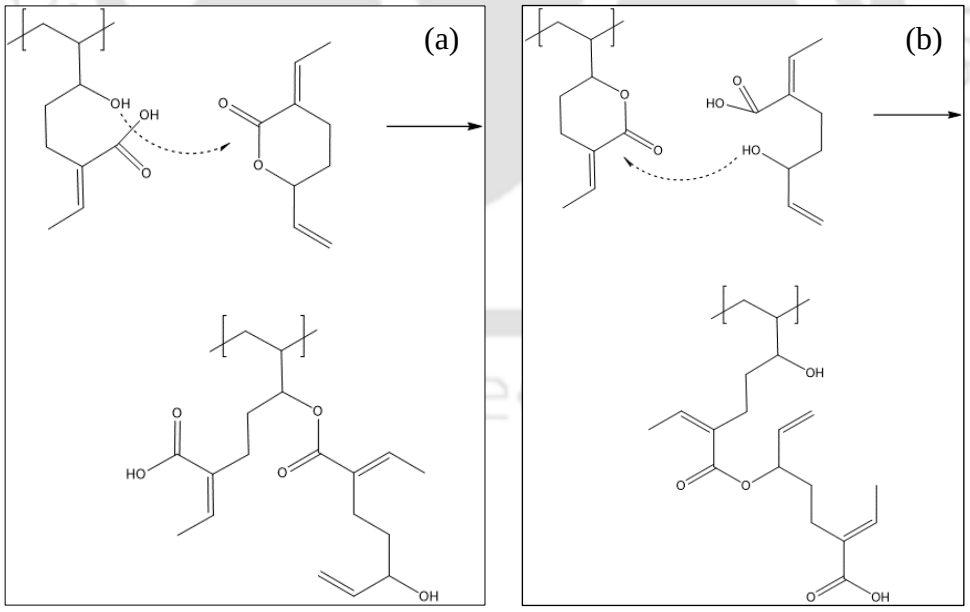

Scheme 8.2: The possible formation of dimeric units (a) due to the open chain units of the polymer attacking the monomer and (b) the hydrolyzed monomers attacking the lactone units of the polymer.

8.4 Conclusion

The cationic polymerization of CO_2 derived EVV was conducted in the presence of highly reactive protic acid catalyst in the bulk system. The preferential vinyl polymerization was induced in the monomer along with the formation of dimeric units due to the open chain structure attacking the monomer. The structure of the product was determined from ^{1}H-NMR spectroscopic analysis. It may be noteworthy to remark the reactivity of the acid catalyst in inducing the reaction of the highly substituted monomer, rendering as a basis for conducting further reactions to optimize the yield and selectivity of the product and utilize for desired applications.

Chapter: 9

Conclusions and Future Scope

9.1 Conclusions

The current doctoral research aimed at developing environmentally benign lactone based polymers and their composites for biomedical applications. The intent of the research was to investigate various strategies of developing environmentally benign materials wherein the monomers lactide and ε-caprolactone were primarily utilized for synthesizing block and random copolymers of PLA and PCL. Furthermore, CO_2 was used as a precursor in synthesizing δ-lactone which was further subjected to polymerization in order to develop a new class of materials. A detailed investigation on the effect of block length of PLA and PCL revealed numerous possibilities of developing customized materials by tailoring their backbone architecture. Various class of materials such as diblock, triblock and stereoblock copolymers resulted in achieving a wide range of mechanical properties which may be utilized for customized applications. The block copolymers were also processed by using the conventional injection and extrusion processes to develop representative implants/scaffolds. The stereoblock terpolymers further resulted in the formation of preferential stereocomplexation with tailored mechanical strength and elongation. The random copolymers of L-lactide and ε-caprolactone with the varying content of caproyl and lactyl segments also resulted in the wide range of mechanical properties (5 – 55 MPa strength) and (5 - 800%) elongation at break. The shape memory and near elastomeric behavior of the copolymers was determined. The bioglass reinforced

(5 – 50%) composites also resulted in near elastomeric behavior. These materials can be suitable for soft tissue applications.

A naïve attempt was further made to polymerize the highly substituted monomer (α-ethylidene, δ-vinylvalerolactone) which was synthesized from the reaction of CO_2 and 1,3-butadiene. The olefin metathesis reaction was conducted by using Hoveyda Grubb's II generation catalyst and the obtained products consisted of a multi-units structure which was elucidated from nuclear magnetic resonance spectroscopy. Furthermore, the cationic polymerization of δ-lactone was performed in presence of a highly reactive protic acid (trifluoromethanesulfonic acid) which resulted in preferential vinyl polymerization.

9.2 Future Scope

- Although the current research reports *in vitro* studies for various block copolymers, it may be vital to perform *in vivo* studies of the synthesized materials.
- Attempts may further be made to reduce the polydispersity index of the block/random copolymers while using the bulk ROP technique in order to exploit their potential for commercial biomedical applications.
- Use of different fillers such as hydroxyapatite, tricalcium phosphase may be utilized to develop the biocomposites for targeted biomedical applications.
- The cost and life cycle assessment along with biodegradation studies may be performed to assess the cradle to grave cycle of the block/random copolymers. This may also be particularly important for the stereocomplex blends and stereoblock terpolymers.

- The enzymatic and hydrolytic degradation studies may be done for the synthesized materials to assess the effect of block length on the degradation behavior.
- The polymerization of CO_2 derived lactone may further be carried out by using controlled techniques to develop naïve materials in a larger scale for a sustainable future.

Patents filed/in process:

1. PLA-r-PCL based Shape Memory, Elastomeric Composites and Method of Preparation Thereof (**Application No: 202131013652**)
2. Stereocomplex Terpolymers and Composites of PLA and PCL, and a Method of Preparation Thereof (**Application No: 202131013736**)
3. Method of Utilizing CO2 based Monomer and Polymerization Thereof (in process).

Peer-reviewed publications from PhD thesis:

1. **Mulchandani, N.,** Masutani, K., Kumar, S., Sakurai, S., Kimura, Y., & Katiyar, V. **(2021)** Toughened PLA-b-PCL-b-PLA Triblock Copolymer based Biomaterials: Effect of Self-Assembled Nanostructure and Stereocomplexation on the Mechanical Properties. Polymer Chemistry, 12, 3806-3824. doi: 10.1039/D1PY00429H
2. **Mulchandani, N.**, Gupta, A., Masutani, K., Kumar, S., Sakurai, S., Kimura, Y., & Katiyar, V. **(2019)**. Effect of Block Length and Stereocomplexation on the Thermally Processable Poly(ε-caprolactone) and Poly(Lactic acid) Block Copolymers for Biomedical Applications. ACS Applied Polymer Materials, 1(12), 3354-3365. doi: 10.1021/acsapm.9b00789
3. **Mulchandani, N.**, Masutani, K., Sakurai, S., Kimura, Y., & Katiyar, V. Valorization of a CO_2 Derived Lactone by Acyclic Diene Metathesis Polymerization (to be submitted).
4. **Mulchandani, N.**, Masutani, K., Sakurai, S., Kimura, Y., & Katiyar, V. Cationic Polymerization of a CO_2 Derived Lactone (to be submitted).
5. **Mulchandani, N.**, Masutani, K., Sakurai, S., Kimura, Y., & Katiyar, V. Effect of Chain Microstructure on the Properties of Poly(L-lactide-co- ε-caprolactone) Random Copolymers: Materials for Customized Applications (to be submitted).
6. **Mulchandani, N.**, Masutani, K., Sakurai, S., Kimura, Y., & Katiyar, V. Stereoblock Terpolymers of PLA and PCL with Preferential Stereocomplexation (to be submitted).

Peer-reviewed publications other than PhD thesis:

1. Ghosh T, Nakano K, **Mulchandani, N.**, & Katiyar, V. Curcumin loaded iron functionalized biopolymeric nanofibre reinforced edible nanocoatings for improved shelf life of cut pineapples. Food Packaging and Shelf Life, 28, 100658. doi: 10.1016/j.fpsl.2021.100658
2. Monika, **Mulchandani, N.**, & Katiyar, V. **(2019)**. Generalized kinetics for thermal degradation and melt rheology for poly (lactic acid)/poly (butylene succinate)/functionalized chitosan based reactive nanobiocomposite. International Journal of Biological Macromolecules, 141, 831-842. doi: 10.1016/j.ijbiomac.2019.09.058
3. Patwa, R., Soundararajan, N., **Mulchandani, N.,** Shah, M., Kumar, S., & Katiyar, V. **(2018)**. Silk Nano Discs: A Natural Material for Cancer Therapy. Biopolymers, 109 (11), e23231.
4. Gupta, A., **Mulchandani, N.,** Shah, M., Kumar, S., & Katiyar, V. **(2018)**. Functionalized chitosan mediated stereocomplexation of poly (lactic acid): Influence on crystallization, oxygen permeability, wettability and biocompatibility behavior. Polymer, 142, 196-208. doi: 10.1002/bip.23231
5. Gupta, A., Prasad, A., **Mulchandani, N.,** Shah, M., Ravi Sankar, M., Kumar, S., & Katiyar, V. **(2017)**. Multifunctional Nanohydroxyapatite-Promoted Toughened High-Molecular-Weight Stereocomplex Poly (lactic acid)-Based Bionanocomposite for Both 3D-Printed Orthopedic Implants and High-Temperature Engineering Applications. ACS Omega, 2(7), 4039-4052. doi: 10.1021/acsomega.7b00915

Book(s) edited:

1. Katiyar, V., Kumar, A., **Mulchandani, N.** (Eds.). (2020, Feb). Advances in Sustainable Polymers: Synthesis, Fabrication and Characterization. In Series, Materials Horizons: From Nature to Nanomaterials. Springer Singapore. ISBN: 978-981-15-1251-3. doi: 10.1007/978-981-15-1251-3

Book Chapters:

1. **Mulchandani, N,**, Kimura Yoshiharu., & Katiyar, V. (2022). Preparation, Structure and Properties of Stereocomplex-Type Poly(Lactic Acid). In Poly(lactic acid): Synthesis, Structures, Properties, Processing, and Applications. Wiley.
2. **Mulchandani, N.**, Ghosh, T., & Katiyar, V. (2020). Nanocellulose for biomedical applications. In Cellulose Nanocrystals (pp. 209-228), De Gruyter. doi: 10.1515/9783110648010-007
3. **Mulchandani, N.,** & Katiyar, V. (2020). Polymers from Carbon Dioxide—A Route Towards a Sustainable Future. In Advances in Sustainable Polymers (pp. 35-49). Springer, Singapore. doi: 10.1007/978-981-15-1251-3_3
4. **Mulchandani, N.**, & Katiyar, V. (2020). Synthesis Strategies for Biomedical Grade Polymers. In Advances in Sustainable Polymers (pp. 1-20). Springer, Singapore. doi: doi.org/10.1007/978-981-15-1251-3_1
5. Das, D., **Mulchandani, N.,** Kumar, A., & Katiyar, V. (2020). Fabrication of Stimuli-Responsive Polymers and their Composites: Candidates for Resorbable Sutures. In Advances in Sustainable Polymers (pp. 121-144). Springer, Singapore. doi: 10.1007/978-981-15-1251-3_6
6. Mondal, K., **Mulchandani, N.**, Mondal, S., & Katiyar, V. (2020). Development of Biomass-Derived Cellulose Nanocrystals and its Composites. In Advances in Sustainable Polymers (pp. 237-269). Springer, Singapore. doi: 10.1007/978-981-15-1251-3_11
7. **Mulchandani, N.**, & Katiyar, V. (2019). Bioactive Glasses: Prospects in Bone Tissue Engineering. In Advances in Sustainable Polymers (pp. 67-83). Springer, Singapore. doi: 10.1007/978-981-32-9804-0_4
8. **Mulchandani, N.**, Prasad, A., & Katiyar, V. (2019). Resorbable polymers in bone repair and regeneration. In Materials for Biomedical Engineering (pp. 87-125). Elsevier. doi: 10.1016/B978-0-12-818415-8.00004-8
9. **Mulchandani, N.,** Gupta, A., & Katiyar, V. (2018). Polylactic Acid Based Hydrogels and Its Renewable Characters: Tissue Engineering Applications. Cellulose-Based Superabsorbent Hydrogels (pp. 1-24). Springer. doi: 10.1007/978-3-319-76573-0_51-1

Conferences/Seminars/Symposia/Workshops/Training:

1. **Mulchandani, N.**, Masutani, K., Kumar, S., Hideki, Y., Sakurai, S., Kimura, Y., & Katiyar, V. (2020, Nov). Toughened PLA-PCL-PLA Triblock Copolymers for Biomedical Applications. 31st Elastomer Debate, Rubber Society of Japan.
2. **Mulchandani, N.**, Masutani, K., Kumar, S., Sakurai, S., Kimura, Y., & Katiyar, V. (2019, Oct). Thermally Processable and Heat Stable Block Copolymers Comprising Poly(ε-caprolactone) and Poly(Lactic acid): Influence of Block Length and Stereocomplexation on the Thermal and Mechanical Properties and Crystallization Behaviors. Advances in Sustainable Polymers (ASP-19), Kyoto Institute of Technology Japan.
3. **Mulchandani, N.**, Masutani, K., Sakurai, S., Kimura, Y., & Katiyar, V. (2019, Oct). Controlling the molecular architecture to tailor the thermal and mechanical properties and water vapor transmission rate of the biodegradable block copolymers: Versatile materials for food packaging. In International Symposium on a New Era in Food Science and Technology 2019, Gifu University, Japan.
4. **Mulchandani, N.**, Masutani, K., Kumar, S., Sakurai, S., Kimura, Y., & Katiyar, V. (2019, August). Synthesis of Poly(ε-caprolactone)-r-Poly(lactic acid): Thermal and Mechanical Properties. International Symposium on Sustainable Polymers & Launch of SPSI-North East Chapter, IIT Guwahati.
5. **Mulchandani, N.**, Masutani, K., Kumar, S., Sakurai, S., Kimura, Y., & Katiyar, V. (2019, March). Bioresorbable and biocompatible block copolymers: *In vitro* studies for targeted biomedical applications. In ABSTRACTS OF PAPERS OF THE AMERICAN CHEMICAL SOCIETY (Vol. 257). 1155 16TH ST, NW, WASHINGTON, DC 20036 USA: AMER CHEMICAL SOC.
6. **Mulchandani, N.**, Masutani, K., Sakurai, S., Kimura, Y., & Katiyar, V. (2019, March). Biodegradable triblock copolymers: Tailoring the block length to control the physical properties. In ABSTRACTS OF PAPERS OF THE AMERICAN CHEMICAL SOCIETY (Vol. 257). 1155 16TH ST, NW, WASHINGTON, DC 20036 USA: AMER CHEMICAL SOC.
7. **Mulchandani, N.**, Masutani, K., Sakurai, S., Kimura, Y., & Katiyar, V. (2019, March). Multicomponent block copolymers consisting of soft and hard segments:

Effect of copolymer architecture on the thermal, mechanical, and crystallization properties. In ABSTRACTS OF PAPERS OF THE AMERICAN CHEMICAL SOCIETY (Vol. 257). 1155 16TH ST, NW, WASHINGTON, DC 20036 USA: AMER CHEMICAL SOC.

8. **Mulchandani, N.**, Masutani, K., Sakurai, S., Kimura, Y., & Katiyar, V. (2019, Jan). Poly(ε-caprolactone)-co-Poly(lactic acid): Influence of Comonomer Backbone Architecture on the Crystallization Behavior, Mechanical and Thermal properties. 10th International Conference on Advances in Polymeric Materials (APM-2019), CIPET, Chennai.
9. **Mulchandani, N.**, Masutani, K., Sakurai, S., Kimura, Y., & Katiyar, V. (2018, Oct). Stereocomplex Blends of Poly(ε-caprolactone)-b-Poly(L-lactic acid) and Poly(ε-caprolactone)-b-Poly(D-lactic acid): Effect of Block Length on the Structural, Thermal and Mechanical Properties. Kathmandu Symposia on Advanced Materials – 2018, Kathmandu, Nepal.

Awards/Achievements/Research Internships:

1. Awarded with **INSPIRE** (**IF160681**) fellowship from the Department of Science and Technology (DST) for the doctoral research.
2. **Short-Term Exchange Student** at Kyoto Institute of Technology (KIT), Japan for conducting a part of doctoral research during September 2017 to March 2018.
3. Best **Poster Award** for the poster entitled "Controlling the molecular architecture to tailor the thermal and mechanical properties and water vapor transmission rate of the biodegradable block copolymers: Versatile materials for food packaging." Presented in: International Symposium on a New Era in Food Science and Technology 2019, Organized by Gifu University, Japan.
4. **Short-Term Exchange Student** at Kyoto Institute of Technology (KIT), Japan for conducting a part of doctoral research during April 2019 to March2 2020.

References:

1. M. Okada, *Progress in Polymer Science*, 2002, **27**, 87-133.
2. H. Danner and R. Braun, *Chemical Society Reviews*, 1999, **28**, 395-405.
3. P. Alagi and S. C. Hong, *Macromolecular Research*, 2015, **23**, 1079-1086.
4. C. Zhang, T. F. Garrison, S. A. Madbouly and M. R. Kessler, *Progress in Polymer Science*, 2017, **71**, 91-143.
5. M. N. Belgacem and A. Gandini, *Monomers, Polymers and Composites from Renewable Resources*, 2009.
6. Brian P. Mooney, *Biochemical Journal*, 2009, **418**, 219-232.
7. J. L. Fortman, S. Chhabra, A. Mukhopadhyay, H. Chou, T. S. Lee, E. Steen and J. D. Keasling, *Trends in Biotechnology*, 2008, **26**, 375-381.
8. *Journal*.
9. M. Super, E. Berluche, C. Costello and E. Beckman, *Macromolecules*, 1997, **30**, 368-372.
10. Z. Gao, H. Zhao, Z. Li, X. Tan and X. Lu, *Energy & Environmental Science*, 2012, **5**, 9857-9865.
11. S. N. Riduan, Y. Zhang and J. Y. Ying, *Angewandte Chemie International Edition*, 2009, **48**, 3322-3325.
12. D. J. Darensbourg and M. W. Holtcamp, *Coordination Chemistry Reviews*, 1996, **153**, 155-174.
13. R.-R. Ang, L. Tin Sin, S.-T. Bee, T.-T. Tee, A. A. H. Kadhum, A. R. Rahmat and B. A. Wasmi, *Journal of Cleaner Production*, 2015, **102**, 1-17.
14. H. Zhang, B. Liu, H. Ding, J. Chen and Z. Duan, *Polymer*, 2017, **129**, 5-11.
15. Y. Sasaki, Y. Inoue and H. Hashimoto, *Journal of the Chemical Society, Chemical Communications*, 1976, DOI: 10.1039/C39760000605, 605-606.
16. J. M. Balbino, J. Dupont and J. C. Bayón, *ChemCatChem*, 2018, **10**, 206-210.
17. P. Braunstein, D. Matt and D. Nobel, *Journal of the American Chemical Society*, 1988, **110**, 3207-3212.
18. A. Behr and M. Heite, *Chemical Engineering & Technology*, 2000, **23**, 952-955.
19. J. Song, X. Feng, Y. Yamamoto, A. I. Almansour, N. Arumugam, R. S. Kumar and M. Bao, *Tetrahedron Letters*, 2016, **57**, 3163-3166.
20. R. Nakano, S. Ito and K. Nozaki, *Nature Chemistry*, 2014, **6**, 325-331.
21. M. Liu, Y. Sun, Y. Liang and B.-L. Lin, *ACS Macro Letters*, 2017, **6**, 1373-1378.
22. K. Masutani and Y. Kimura, in *Poly(lactic acid) Science and Technology: Processing, Properties, Additives and Applications*, The Royal Society of Chemistry, 2015, DOI: 10.1039/9781782624806-00001, pp. 1-36.
23. V. Novy, B. Brunner and B. Nidetzky, *Microbial Cell Factories*, 2018, **17**, 59.
24. M. Singhvi and D. Gokhale, *RSC Advances*, 2013, **3**, 13558-13568.
25. N. Mulchandani and V. Katiyar, in *Advances in Sustainable Polymers: Synthesis, Fabrication and Characterization*, eds. V. Katiyar, A. Kumar and N. Mulchandani, Springer Singapore, Singapore, 2020, DOI: 10.1007/978-981-15-1251-3_3, pp. 35-49.
26. Y. Zhang, W. Jiang, K. Lv, Y. Sun, X. Gao, Q. Zhao, W. Ren, F. Wang and J. Liu, 2020, **36**, e2901.

27. G. Chávez, J.-A. Rasmussen, M. Janssen, G. Mamo, R. Hatti-Kaul and R. A. Sheldon, *Topics in Catalysis*, 2014, **57**, 349-355.
28. S.-H. Pyo, J. H. Park, V. Srebny and R. Hatti-Kaul, *Green Chemistry*, 2020, **22**, 4450-4455.
29. E. J. O. Kompanje, T. C. Jansen, B. van der Hoven and J. Bakker, *Intensive Care Med*, 2007, **33**, 1967-1971.
30. A. Gupta and V. Katiyar, *ACS Sustainable Chemistry & Engineering*, 2017, **5**, 6835-6844.
31. T. S. Srivatsan, *Materials and Manufacturing Processes*, 2014, **29**, 1510-1511.
32. M. A. Ghalia and Y. Dahman, *Journal of Polymer Research*, 2017, **24**, 74.
33. P. Saini, M. Arora and M. N. V. R. Kumar, *Advanced Drug Delivery Reviews*, 2016, **107**, 47-59.
34. K. L. Pickering, M. G. A. Efendy and T. M. Le, *Composites Part A: Applied Science and Manufacturing*, 2016, **83**, 98-112.
35. Y. Dong, A. Ghataura, H. Takagi, H. J. Haroosh, A. N. Nakagaito and K.-T. Lau, *Composites Part A: Applied Science and Manufacturing*, 2014, **63**, 76-84.
36. H. Tsuji, *Macromolecular Bioscience*, 2005, **5**, 569-597.
37. A. Gupta, A. Prasad, N. Mulchandani, M. Shah, M. Ravi Sankar, S. Kumar and V. Katiyar, *ACS Omega*, 2017, **2**, 4039-4052.
38. L. L. Hench, *Biomaterials*, 1998, **19**, 1419-1423.
39. J. A. Hunt, R. Chen, T. van Veen and N. Bryan, *Journal of Materials Chemistry B*, 2014, **2**, 5319-5338.
40. A. B. Kutikov and J. Song, *ACS Biomaterials Science & Engineering*, 2015, **1**, 463-480.
41. B. Yu, Y. Cao, H. Sun and J. Han, *Journal of Polymers and the Environment*, 2017, **25**, 510-517.
42. K. Sriwongsa, K. Hemvichian, W. Kangsumrith, P. Suwanmala and T. Pongprayoon, 2011.
43. T. M. Quynh, H. Mitomo, N. Nagasawa, Y. Wada, F. Yoshii and M. Tamada, *European Polymer Journal*, 2007, **43**, 1779-1785.
44. H. T. Oyama and S. Abe, *ACS Sustainable Chemistry & Engineering*, 2015, **3**, 3245-3252.
45. A. Guinault, C. Sollogoub, S. Domenek, A. Grandmontagne and V. Ducruet, *International Journal of Material Forming*, 2010, **3**, 603-606.
46. C. Nakafuku and H. Yoshimura, *Polymer*, 2004, **45**, 3583-3585.
47. P. B. Maurus and C. C. Kaeding, *Operative Techniques in Sports Medicine*, 2004, **12**, 158-160.
48. J. B. Moser, E. P. Lautenschlager and B. J. Horbal, *Journal of dental research*, 1974, **53**, 804-808.
49. J. J. Park, E. J. Yu, W.-K. Lee and C.-S. Ha, *Polymers for Advanced Technologies*, 2014, **25**, 48-54.
50. S. Eshraghi and S. Das, *Acta Biomaterialia*, 2010, **6**, 2467-2476.
51. M. Brzeziński and T. Biela, in *Encyclopedia of Polymeric Nanomaterials*, eds. S. Kobayashi and K. Müllen, Springer Berlin Heidelberg, Berlin, Heidelberg, 2014, DOI: 10.1007/978-3-642-36199-9_394-1, pp. 1-10.
52. Y. Ikada, K. Jamshidi, H. Tsuji and S. H. Hyon, *Macromolecules*, 1987, **20**, 904-906.

53. *United States Pat.*, 1988.
54. F. Luo, A. Fortenberry, J. Ren and Z. Qiang, *Frontiers in chemistry*, 2020, **8**, 688.
55. D. Karst and Y. Yang, *Polymer*, 2006, **47**, 4845-4850.
56. H. Tsuji, *Biomaterials*, 2003, **24**, 537-547.
57. M. Kakuta, M. Hirata and Y. Kimura, *Polymer Reviews*, 2009, **49**, 107-140.
58. H. Tsuji, F. Horii, S. H. Hyon and Y. Ikada, *Macromolecules*, 1991, **24**, 2719-2724.
59. K. Scheuer, D. Bandelli, C. Helbing, C. Weber, J. Alex, J. B. Max, A. Hocken, O. Stranik, L. Seiler, F. Gladigau, U. Neugebauer, F. H. Schacher, U. S. Schubert and K. D. Jandt, *Macromolecules*, 2020, **53**, 8340-8351.
60. S. Nagarajan, D. Krishnan, V. P. Sivaprasad and E. Bhoje Gowd, in *Crystallization in Multiphase Polymer Systems*, eds. S. Thomas, M. Arif P, E. B. Gowd and N. Kalarikkal, Elsevier, 2018, DOI: https://doi.org/10.1016/B978-0-12-809453-2.00005-0, pp. 93-122.
61. R. Lv, N. Peng, T. Jin, B. Na, J. Wang and H. Liu, *Polymer*, 2017, **116**, 324-330.
62. E. M. Woo and L. Chang, *Polymer*, 2011, **52**, 6080-6089.
63. L. Bouapao and H. Tsuji, *Macromolecular Chemistry and Physics*, 2009, **210**, 993-1002.
64. T. Biela, A. Duda and S. Penczek, *Macromolecules*, 2006, **39**, 3710-3713.
65. H. Tsuji, *Advanced Drug Delivery Reviews*, 2016, **107**, 97-135.
66. M. Saravanan and A. J. Domb, *European Journal of Nanomedicine*, 2013, **5**, 81-96.
67. P. Pan and Y. Inoue, *Progress in Polymer Science*, 2009, **34**, 605-640.
68. L. Han, P. Pan, G. Shan and Y. Bao, *Polymer*, 2015, **63**, 144-153.
69. Y. Furuhashi, Y. Kimura and N. Yoshie, *Polymer Journal*, 2006, **38**, 1061-1067.
70. L. Cartier, T. Okihara, Y. Ikada, H. Tsuji, J. Puiggali and B. Lotz, *Polymer*, 2000, **41**, 8909-8919.
71. T. Okihara, M. Tsuji, A. Kawaguchi, K.-I. Katayama, H. Tsuji, S.-H. Hyon and Y. Ikada, *Journal of Macromolecular Science, Part B*, 1991, **30**, 119-140.
72. L. Cartier, T. Okihara and B. Lotz, *Macromolecules*, 1997, **30**, 6313-6322.
73. D. Brizzolara, H.-J. Cantow, K. Diederichs, E. Keller and A. J. Domb, *Macromolecules*, 1996, **29**, 191-197.
74. D. Sawai, Y. Tsugane, M. Tamada, T. Kanamoto, M. Sungil and S.-H. Hyon, *Journal of Polymer Science Part B: Polymer Physics*, 2007, **45**, 2632-2639.
75. K. Tashiro, N. Kouno, H. Wang and H. Tsuji, *Macromolecules*, 2017, **50**, 8048-8065.
76. K. Tashiro, H. Wang, N. Kouno, J. Koshobu and K. Watanabe, *Macromolecules*, 2017, **50**, 8066-8071.
77. M. Spinu, C. Jackson, M. Y. Keating and K. H. Gardner, *Journal of Macromolecular Science, Part A*, 1996, **33**, 1497-1530.
78. Z. Kan, W. Luo, T. Shi, C. Wei, B. Han, D. Zheng and S. Liu, *Frontiers in chemistry*, 2018, **6**, 547-547.
79. M. Hirata, K. Masutani and Y. Kimura, *Biomacromolecules*, 2013, **14**, 2154-2161.
80. R. H. Platel, L. M. Hodgson and C. K. Williams, *Polymer Reviews*, 2008, **48**, 11-63.
81. M. J. Stanford and A. P. Dove, *Chemical Society Reviews*, 2010, **39**, 486-494.
82. C. M. Thomas, *Chemical Society Reviews*, 2010, **39**, 165-173.
83. H. Tsuji and T. Tajima, *Macromolecular Materials and Engineering*, 2014, **299**, 430-435.
84. M. Hirata, K. Kobayashi and Y. Kimura, *Journal of Polymer Science Part A: Polymer Chemistry*, 2010, **48**, 794-801.

85. K. Masutani, C. W. Lee and Y. Kimura, *Macromolecular Chemistry and Physics*, 2012, **213**, 695-704.
86. N. Mulchandani, A. Gupta, K. Masutani, S. Kumar, S. Sakurai, Y. Kimura and V. Katiyar, *ACS Applied Polymer Materials*, 2019, **1**, 3354-3365.
87. N. Mulchandani, A. Prasad and V. Katiyar, in *Materials for Biomedical Engineering*, eds. V. Grumezescu and A. M. Grumezescu, Elsevier, 2019, DOI: https://doi.org/10.1016/B978-0-12-818415-8.00004-8, pp. 87-125.
88. C. Garofalo, G. Capuano, R. Sottile, R. Tallerico, R. Adami, E. Reverchon, E. Carbone, L. Izzo and D. Pappalardo, *Biomacromolecules*, 2014, **15**, 403-415.
89. W. Zhang, D. Zhang, X. Fan, G. Bai, g. Yuming and Z. Hu, *RSC Advances*, 2016, **6**, 20761-20771.
90. C. Feng, M. Piao and D. Li, *Polymers (Basel)*, 2016, **8**, 165.
91. Y. Yu, J. Zou, L. Yu, W. Ji, Y. Li, W.-C. Law and C. Cheng, *Macromolecules*, 2011, **44**, 4793-4800.
92. N. Mulchandani, A. Gupta and V. Katiyar, in *Cellulose-Based Superabsorbent Hydrogels*, ed. M. I. H. Mondal, Springer International Publishing, Cham, 2019, DOI: 10.1007/978-3-319-77830-3_51, pp. 1537-1559.
93. S. Noack, D. Schanzenbach, J. Koetz and H. Schlaad, *Macromolecular Rapid Communications*, 2019, **40**, 1800639.
94. C. Wang, N. Feng, F. Chang, J. Wang, B. Yuan, Y. Cheng, H. Liu, J. Yu, J. Zou, J. Ding and X. Chen, *Advanced Healthcare Materials*, 2019, **8**, 1900312.
95. Y. Sun and C. He, *ACS Macro Letters*, 2012, **1**, 709-713.
96. A. Gupta, A. K. Pal, E. M. Woo and V. Katiyar, *Scientific Reports*, 2018, **8**, 4351.
97. A. Gupta, N. Mulchandani, M. Shah, S. Kumar and V. Katiyar, *Polymer*, 2018, **142**, 196-208.
98. L. L. Hench and J. M. Polak, *Science (New York, N.Y.)*, 2002, **295**, 1014-1017.
99. L. L. Hench, *Journal of the American Ceramic Society*, 1998, **81**, 1705-1728.
100. L. L. HENCH, *Annals of the New York Academy of Sciences*, 1988, **523**, 54-71.
101. A. Hoppe, N. S. Güldal and A. R. Boccaccini, *Biomaterials*, 2011, **32**, 2757-2774.
102. D. Mondal, S. J. Dixon, K. Mequanint and A. S. Rizkalla, *ACS Applied Bio Materials*, 2018, **1**, 1369-1381.
103. B. A. Allo, A. S. Rizkalla and K. Mequanint, *Langmuir*, 2010, **26**, 18340-18348.
104. C. Wu, L. Xia, P. Han, L. Mao, J. Wang, D. Zhai, B. Fang, J. Chang and Y. Xiao, *ACS Applied Materials & Interfaces*, 2016, **8**, 11342-11354.
105. Y. Mawani and C. Orvig, *Journal of Inorganic Biochemistry*, 2014, **132**, 52-58.
106. C. A. Barta, K. Sachs-Barrable, J. Jia, K. H. Thompson, K. M. Wasan and C. Orvig, *Dalton Transactions*, 2007, DOI: 10.1039/B705123A, 5019-5030.
107. C. R. Patra, S. S. Abdel Moneim, E. Wang, S. Dutta, S. Patra, M. Eshed, P. Mukherjee, A. Gedanken, V. H. Shah and D. Mukhopadhyay, *Toxicology and applied pharmacology*, 2009, **240**, 88-98.
108. K. S. Rana, L. P. d. Souza, M. A. Isaacs, F. N. S. Raja, A. P. Morrell and R. A. Martin, *ACS Biomaterials Science & Engineering*, 2017, **3**, 3425-3432.
109. P. Collery, B. Keppler, C. Madoulet and B. Desoize, *Critical Reviews in Oncology/Hematology*, 2002, **42**, 283-296.

110. R. Ortega, A. Suda and G. Devès, *Nuclear Instruments and Methods in Physics Research Section B: Beam Interactions with Materials and Atoms*, 2003, **210**, 364-367.
111. R. Revelle and H. E. Suess, *Tellus*, 1957, **9**, 18-27.
112. M. Packer, *Energy Policy*, 2009, **37**, 3428-3437.
113. G. A. Olah, A. Goeppert and G. K. S. Prakash, *The Journal of Organic Chemistry*, 2009, **74**, 487-498.
114. Y. Zhang, J. Xia, J. Song, J. Zhang, X. Ni and Z. Jian, *Macromolecules*, 2019, **52**, 2504-2512.
115. M. L. Gray, K. J. Champagne, D. Fauth, J. P. Baltrus and H. Pennline, *International Journal of Greenhouse Gas Control*, 2008, **2**, 3-8.
116. S. N. Riduan and Y. Zhang, *Dalton Transactions*, 2010, **39**, 3347-3357.
117. A. ElMekawy, H. M. Hegab, G. Mohanakrishna, A. F. Elbaz, M. Bulut and D. Pant, *Bioresource Technology*, 2016, **215**, 357-370.
118. M. S. Islam Mozumder, L. Garcia-Gonzalez, H. D. Wever and E. I. P. Volcke, *Biochemical Engineering Journal*, 2015, **98**, 107-116.
119. Y. Qin, X. Sheng, S. Liu, G. Ren, X. Wang and F. Wang, *Journal of CO2 Utilization*, 2015, **11**, 3-9.
120. J. Albo, M. Alvarez-Guerra, P. Castaño and A. Irabien, *Green Chemistry*, 2015, **17**, 2304-2324.
121. X. Sun, Q. Zhu, X. Kang, H. Liu, Q. Qian, Z. Zhang and B. Han, *Angewandte Chemie International Edition*, 2016, **55**, 6771-6775.
122. S. Inoue, H. Koinuma and T. Tsuruta, *Journal of Polymer Science Part B: Polymer Letters*, 1969, **7**, 287-292.
123. L. Vogdanis and W. Heitz, *Die Makromolekulare Chemie, Rapid Communications*, 1986, **7**, 543-547.
124. G. Trott, P. K. Saini and C. K. Williams, *Philosophical transactions. Series A, Mathematical, physical, and engineering sciences*, 2016, **374**, 20150085.
125. S. Inoue, H. Koinuma and T. Tsuruta, *Die Makromolekulare Chemie*, 1969, **130**, 210-220.
126. P. Wang, J. H. Park, M. Sayed, T.-S. Chang, A. Moran, S. Chen and S.-H. Pyo, *Polymer Chemistry*, 2018, **9**, 3798-3807.
127. B.-G. Woo, K. Y. Choi, K. H. Song and S. H. Lee, *Journal of Applied Polymer Science*, 2001, **80**, 1253-1266.
128. C. M. Byrne, S. D. Allen, E. B. Lobkovsky and G. W. Coates, *Journal of the American Chemical Society*, 2004, **126**, 11404-11405.
129. N. Kindermann, À. Cristòfol and A. W. Kleij, *ACS Catalysis*, 2017, **7**, 3860-3863.
130. B. Song, B. He, A. Qin and B. Z. Tang, *Macromolecules*, 2018, **51**, 42-48.
131. R. Nakano, S. Ito and K. Nozaki, *Nature Chemistry*, 2014, **6**, 325.
132. T. J. Kemp, *Science progress*, 2014, **97**, 249-260.
133. H. Sugimoto and S. Inoue, *Journal*, 2006, **78**, 1823.
134. C. Barreto, E. Hansen and S. Fredriksen, *Polymer degradation and stability*, 2012, **2012 v.97 no.6**, pp. 893-904.
135. K. U. D. Calvinho, A. B. Laursen, K. M. K. Yap, T. A. Goetjen, S. Hwang, N. Murali, B. Mejia-Sosa, A. Lubarski, K. M. Teeluck, E. S. Hall, E. Garfunkel, M. Greenblatt and G. C. Dismukes, *Energy & Environmental Science*, 2018, **11**, 2550-2559.

136. M. A. Hillmyer and W. B. Tolman, *Accounts of Chemical Research*, 2014, **47**, 2390-2396.
137. D. K. Schneiderman and M. A. Hillmyer, *Macromolecules*, 2016, **49**, 2419-2428.
138. S. Pisani, R. Dorati, B. Conti, T. Modena, G. Bruni and I. Genta, *Reactive and Functional Polymers*, 2018, **124**, 77-89.
139. M. Fu, Z. Liu, D. Bai, F. Ling, H. Bai, Q. Zhang and Q. Fu, *Macromolecular Materials and Engineering*, 2018, **303**, 1800178.
140. J. Yang, H. Pan, X. Li, S. Sun, H. Zhang and L. Dong, *RSC Advances*, 2017, **7**, 46183-46194.
141. S. R. Rojo, Á. Martín, E. S. Calvo and M. J. Cocero, *Journal of Chemical & Engineering Data*, 2009, **54**, 962-965.
142. C. E. Nyitray, R. Chang, G. Faleo, K. D. Lance, D. A. Bernards, Q. Tang and T. A. Desai, *ACS Nano*, 2015, **9**, 5675-5682.
143. C. Chen, P. Watkins-Curry, M. Smoak, K. Hogan, S. Deese, G. T. McCandless, J. Y. Chan and D. J. Hayes, *ACS Biomaterials Science & Engineering*, 2015, **1**, 94-102.
144. A. K. Matta, R. U. Rao, K. N. S. Suman and V. Rambabu, *Procedia Materials Science*, 2014, **6**, 1266-1270.
145. M.-H. Huang, S. Li, J. Coudane and M. Vert, *Macromolecular Chemistry and Physics*, 2003, **204**, 1994-2001.
146. B. K. Goriparthi, K. N. S. Suman and M. R. Nalluri, *Polymer Composites*, 2012, **33**, 237-244.
147. Q. Lv, D. Wu, H. Xie, S. Peng, Y. Chen and C. Xu, *RSC Advances*, 2016, **6**, 37721-37730.
148. G. Sivalingam, S. P. Vijayalakshmi and G. Madras, *Industrial & Engineering Chemistry Research*, 2004, **43**, 7702-7709.
149. X. Shuai, F. E. Porbeni, M. Wei, I. D. Shin and A. E. Tonelli, *Macromolecules*, 2001, **34**, 7355-7361.
150. Y. Liu, W.-S. Dong, J.-Y. Liu and Y.-S. Li, *Dalton Transactions*, 2014, **43**, 2244-2251.
151. A.-C. Albertsson and I. K. Varma, *Biomacromolecules*, 2003, **4**, 1466-1486.
152. D. Bratton, M. Brown and S. M. Howdle, *Macromolecules*, 2005, **38**, 1190-1195.
153. Z. Wei, L. Liu, F. Yu, P. Wang, C. Qu and M. Qi, *Polymer Bulletin*, 2008, **61**, 407-413.
154. H. Shirahama, A. Ichimaru, C. Tsutsumi, Y. Nakayama and H. Yasuda, *Journal of Polymer Science Part A: Polymer Chemistry*, 2005, **43**, 438-454.
155. O. Jeon, S.-H. Lee, S. H. Kim, Y. M. Lee and Y. H. Kim, *Macromolecules*, 2003, **36**, 5585-5592.
156. *Canada Pat.*, 2016.
157. *China Pat.*, CN106433052A.
158. A. Manea, S. Bran, M. Baciut, G. Armencea, D. Pop, P. Berce, D.-C. Vodnar, M. Hedesiu, C. Dinu, A. Petrutiu, D. Tomina and G. Baciut, *Clujul Med*, 2018, **91**, 452-457.
159. I. Lamego, I. F. Duarte, M. P. M. Marques and A. M. Gil, *Journal of Proteome Research*, 2014, **13**, 6033-6045.
160. T. Rosen, I. Goldberg, W. Navarra, V. Venditto and M. Kol, *Angewandte Chemie International Edition*, 2018, **57**, 7191-7195.
161. O. Persenaire, M. Alexandre, P. Degée and P. Dubois, *Biomacromolecules*, 2001, **2**, 288-294.

162. L. Han, C. Yu, J. Zhou, G. Shan, Y. Bao, X. Yun, T. Dong and P. Pan, *Polymer*, 2016, **103**, 376-386.
163. M. Fujimura, T. Hashimoto and H. Kawai, *Rubber Chemistry and Technology*, 1978, **51**, 215-224.
164. S. Sakurai, J. Sakamoto, M. Shibayama and S. Nomura, *Macromolecules*, 1993, **26**, 3351-3356.
165. X. Wang, H. Zhao, L.-S. Turng and Q. Li, *Industrial & Engineering Chemistry Research*, 2013, **52**, 4939-4949.
166. G. Yin, D. Zhao, X. Wang, Y. Ren, L. Zhang, X. Wu, S. Nie and Q. Li, *RSC Advances*, 2015, **5**, 79070-79080.
167. T. Konishi, K. Nishida, T. Kanaya and K. Kaji, *Macromolecules*, 2005, **38**, 8749-8754.
168. J. Zhang, Y. Duan, A. J. Domb and Y. Ozaki, *Macromolecules*, 2010, **43**, 4240-4246.
169. D. Funt and T. Pavicic, *Clin Cosmet Investig Dermatol*, 2013, **6**, 295-316.
170. Y. Srisuwan and Y. Baimark, *Heliyon*, 2018, **4**, e01082-e01082.
171. D. J. Lohse and N. Hadjichristidis, *Current Opinion in Colloid & Interface Science*, 1997, **2**, 171-176.
172. B. P. Bastakoti and Z. Liu, in *Nanostructures for Cancer Therapy*, eds. A. Ficai and A. M. Grumezescu, Elsevier, 2017, DOI: https://doi.org/10.1016/B978-0-323-46144-3.00010-6, pp. 261-283.
173. A.-V. Ruzette and L. Leibler, *Nature Materials*, 2005, **4**, 19-31.
174. J. F. Kenney, *Polymer Engineering & Science*, 1968, **8**, 216-226.
175. V. Katiyar and H. Nanavati, *Polymer Engineering & Science*, 2011, **51**, 2078-2084.
176. A. John, V. Katiyar, K. Pang, M. M. Shaikh, H. Nanavati and P. Ghosh, *Polyhedron*, 2007, **26**, 4033-4044.
177. V. Katiyar, N. Gerds, C. B. Koch, J. Risbo, H. C. B. Hansen and D. Plackett, *Polymer Degradation and Stability*, 2010, **95**, 2563-2573.
178. N. Mulchandani and V. Katiyar, in *Advances in Sustainable Polymers: Synthesis, Fabrication and Characterization*, eds. V. Katiyar, A. Kumar and N. Mulchandani, Springer Singapore, Singapore, 2020, DOI: 10.1007/978-981-15-1251-3_1, pp. 1-20.
179. Y.-H. Na, Y. He, X. Shuai, Y. Kikkawa, Y. Doi and Y. Inoue, *Biomacromolecules*, 2002, **3**, 1179-1186.
180. I. Fortelny, A. Ujcic, L. Fambri and M. Slouf, *Frontiers in Materials*, 2019, **6**.
181. Y. Huang, R. Chang, L. Han, G. Shan, Y. Bao and P. Pan, *ACS Sustainable Chemistry & Engineering*, 2016, **4**, 121-128.
182. M. Abubekerov, J. Wei, K. R. Swartz, Z. Xie, Q. Pei and P. L. Diaconescu, *Chem Sci*, 2018, **9**, 2168-2178.
183. I. Yildirim, P. Sungur, A. C. Crecelius-Vitz, T. Yildirim, D. Kalden, S. Hoeppener, M. Westerhausen, C. Weber and U. S. Schubert, *Polymer Chemistry*, 2017, **8**, 6086-6098.
184. D. C. Aluthge, C. Xu, N. Othman, N. Noroozi, S. G. Hatzikiriakos and P. Mehrkhodavandi, *Macromolecules*, 2013, **46**, 3965-3974.
185. M. Eleuteri, M. Bernal, M. Milanesio, O. Monticelli and A. Fina, *Frontiers in Chemistry*, 2019, **7**.
186. H. Tsuji and Y. Tezuka, *Biomacromolecules*, 2004, **5**, 1181-1186.
187. P. Pan, J. Bao, L. Han, Q. Xie, G. Shan and Y. Bao, *Polymer*, 2016, **98**, 80-87.

188. M. A. Woodruff and D. W. Hutmacher, *Progress in Polymer Science*, 2010, **35**, 1217-1256.
189. E. M. Elmowafy, M. Tiboni and M. E. Soliman, *Journal of Pharmaceutical Investigation*, 2019, **49**, 347-380.
190. L. Calandrelli, A. Calarco, P. Laurienzo, M. Malinconico, O. Petillo and G. Peluso, *Biomacromolecules*, 2008, **9**, 1527-1534.
191. Y. Ito, Y. Ochii, K. Fukushima, N. Sugioka and K. Takada, *International Journal of Pharmaceutics*, 2010, **384**, 53-59.
192. J. Conn, R. Oyasu, M. Welsh and J. M. Beal, *The American Journal of Surgery*, 1974, **128**, 19-23.
193. A. J. Tsugawa and F. J. M. Verstraete, in *Oral and Maxillofacial Surgery in Dogs and Cats*, eds. F. J. M. Verstraete and M. J. Lommer, W.B. Saunders, Oxford, 2012, DOI: https://doi.org/10.1016/B978-0-7020-4618-6.00007-5, pp. 69-78.
194. M. J. O. E. Bertleff, M. F. Meek and J.-P. A. Nicolai, *The Journal of Hand Surgery*, 2005, **30**, 513-518.
195. H. Samadian, S. Farzamfar, A. Vaez, A. Ehterami, A. Bit, M. Alam, A. Goodarzi, G. Darya and M. Salehi, *Scientific Reports*, 2020, **10**, 13366.
196. I.-K. Park, H. Sun, S.-H. Kim, Y. Kim, G. E. Kim, Y. Lee, T. Kim, H. R. Choi, J. Suhr and J.-D. Nam, *Scientific Reports*, 2019, **9**, 7033.
197. A. Ostafinska, I. Fortelny, M. Nevoralova, J. Hodan, J. Kredatusova and M. Slouf, *RSC Advances*, 2015, **5**, 98971-98982.
198. Y. S. Thio, J. Wu and F. S. Bates, *Macromolecules*, 2006, **39**, 7187-7189.
199. H. Uehara, Y. Karaki, S. Wada and T. Yamanobe, *ACS Applied Materials & Interfaces*, 2010, **2**, 2707-2710.
200. D. G. Abebe and T. Fujiwara, *Biomacromolecules*, 2012, **13**, 1828-1836.
201. L. Chen, Z. Xie, J. Hu, X. Chen and X. Jing, *Journal of Nanoparticle Research*, 2007, **9**, 777-785.
202. H. Cui, J. Shao, Y. Wang, P. Zhang, X. Chen and Y. Wei, *Biomacromolecules*, 2013, **14**, 1904-1912.
203. N. Mulchandani, A. Gupta and V. Katiyar, in *Cellulose-Based Superabsorbent Hydrogels*, ed. M. I. H. Mondal, Springer International Publishing, Cham, 2018, DOI: 10.1007/978-3-319-76573-0_51-1, pp. 1-24.
204. T. L. Chantawansri, T. W. Sirk, R. Mrozek, J. L. Lenhart, M. Kröger and Y. R. Sliozberg, *Chemical Physics Letters*, 2014, **612**, 157-161.
205. O. Sangen, Y. Yamamoto and R. Imamura, *Sen'i Gakkaishi*, 1969, **25**, 455-461.
206. P. J. Flory, *Journal of the American Chemical Society*, 1945, **67**, 2048-2050.
207. R. W. Nunes, J. R. Martin and J. F. Johnson, *Polymer Engineering & Science*, 1982, **22**, 205-228.
208. D. J. Haloi, S. Ata, N. K. Singha, D. Jehnichen and B. Voit, *ACS Applied Materials & Interfaces*, 2012, **4**, 4200-4207.
209. H. Schmalz, A. Böker, R. Lange, G. Krausch and V. Abetz, *Macromolecules*, 2001, **34**, 8720-8729.
210. B. M. Boyle, J. L. Collins, T. E. Mensch, M. D. Ryan, B. S. Newell and G. M. Miyake, *Polymer Chemistry*, 2020, DOI: 10.1039/D0PY01007C.
211. E. B. Zhulina and O. V. Borisov, *ACS Macro Letters*, 2013, **2**, 292-295.

212. Z. Jing, X. Shi, G. Zhang and J. Gu, *Polymer*, 2017, **121**, 124-136.
213. M. Jiao, K. Yang, J. Cao, H. Liu, W. Pan and P. Gao, *Journal of Macromolecular Science, Part B*, 2014, **53**, 191-204.
214. L. M. Pitet and M. A. Hillmyer, *Macromolecules*, 2009, **42**, 3674-3680.
215. M.-H. Huang, S. Li and M. Vert, *Polymer*, 2004, **45**, 8675-8681.
216. T. Yu, J. Ren, S. Gu and M. Yang, *Polymers for Advanced Technologies*, 2010, **21**, 183-188.
217. W. Hoogsteen, A. R. Postema, A. J. Pennings, G. Ten Brinke and P. Zugenmaier, *Macromolecules*, 1990, **23**, 634-642.
218. B. Lotz, G. Li, X. Chen and J. Puiggalí, *Polymer*, 2017, **115**.
219. T. Kawai, N. Rahman, G. Matsuba, K. Nishida, T. Kanaya, M. Nakano, H. Okamoto, J. Kawada, A. Usuki, N. Honma, K. Nakajima and M. Matsuda, *Macromolecules*, 2007, **40**, 9463-9469.
220. P. Pan, W. Kai, B. Zhu, T. Dong and Y. Inoue, *Macromolecules*, 2007, **40**, 6898-6905.
221. J. Zhang, K. Tashiro, H. Tsuji and A. J. Domb, *Macromolecules*, 2008, **41**, 1352-1357.
222. A. K. Pandey, V. Katiyar, S. Sasaki and S. Sakurai, *Polymer Journal*, 2019, **51**, 1173-1180.
223. Y. Chatani, Y. Okita, H. Tadokoro and Y. Yamashita, *Polymer Journal*, 1970, **1**, 555-562.
224. R. Li, Y. Wu, Z. Bai, J. Guo and X. Chen, *RSC Advances*, 2020, **10**, 42120-42127.
225. T. Sakurai, H. Nagakura, S. Gondo and S. Nojima, *Polymer Journal*, 2013, **45**, 436-443.
226. S. Nojima, H. Tanaka, A. Rohadi and S. Sasaki, *Polymer*, 1998, **39**, 1727-1734.
227. D. J. Quiram, R. A. Register, G. R. Marchand and A. J. Ryan, *Macromolecules*, 1997, **30**, 8338-8343.
228. T. Shiomi, H. Tsukada, H. Takeshita, K. Takenaka and Y. Tezuka, *Polymer*, 2001, **42**, 4997-5004.
229. Y. L. Loo, R. A. Register, A. J. Ryan and G. T. Dee, *Macromolecules*, 2001, **34**, 8968-8977.
230. P. Huang, L. Zhu, S. Z. D. Cheng, Q. Ge, R. P. Quirk, E. L. Thomas, B. Lotz, B. S. Hsiao, L. Liu and F. Yeh, *Macromolecules*, 2001, **34**, 6649-6657.
231. S. Nojima, Y. Ohguma, S. Namiki, T. Ishizone and K. Yamaguchi, *Macromolecules*, 2008, **41**, 1915-1918.
232. S. Nakagawa, K.-i. Kadena, T. Ishizone, S. Nojima, T. Shimizu, K. Yamaguchi and S. Nakahama, *Macromolecules*, 2012, **45**, 1892-1900.
233. I. Castilla-Cortázar, A. Vidaurre, B. Marí and A. J. Campillo-Fernández, *Polymers (Basel)*, 2019, **11**, 1099.
234. H. Tsuji and Y. Ikada, *Polymer*, 1995, **36**, 2709-2716.
235. P. Thi Ngoc Diep, M. Mochizuki, M. Doi, H. Takagi, N. Shimizu, N. Igarashi, S. Sasaki and S. Sakurai, *Polymer Journal*, 2019, **51**, 283-294.
236. J. C. Meredith and E. J. Amis, *Macromolecular Chemistry and Physics*, 2000, **201**, 733-739.
237. G. Perego, G. D. Cella and C. Bastioli, *Journal of Applied Polymer Science*, 1996, **59**, 37-43.
238. S. Sakurai, T. Momii, K. Taie, M. Shibayama, S. Nomura and T. Hashimoto, *Macromolecules*, 1993, **26**, 485-491.

239. S. Sakurai, H. Kawada, T. Hashimoto and L. J. Fetters, *Macromolecules*, 1993, **26**, 5796-5802.
240. G. S. Lee, B. R. Moon, H. Jeong, J. Shin and J. G. Kim, *Polymer Chemistry*, 2019, **10**, 539-545.
241. M. Feldmann and J. Fuchs, in *Specialized Injection Molding Techniques*, ed. H.-P. Heim, William Andrew Publishing, 2016, DOI: https://doi.org/10.1016/B978-0-323-34100-4.00005-5, pp. 211-237.
242. M. Oliveira, E. Santos, A. Araújo, G. J. M. Fechine, A. V. Machado and G. Botelho, *Polymer Testing*, 2016, **51**, 109-116.
243. D. K. Lee, A. J. Lança, R. Cheng, T. Nguyen, X. D. Ji, F. Gobeil, Jr., S. Chemtob, S. R. George and B. F. O'Dowd, *The Journal of biological chemistry*, 2004, **279**, 7901-7908.
244. V. A. Byvaltsev, L. A. Bardonova, N. R. Onaka, R. A. Polkin, S. V. Ochkal, V. V. Shepelev, M. A. Aliyev and A. A. Potapov, *Frontiers in Oncology*, 2019, **9**.
245. S. H. Im, S. J. Park, Y. Jung, J. J. Chung and S. H. Kim, *ACS Sustainable Chemistry & Engineering*, 2020, **8**, 8752-8761.
246. T. M. Quynh, H. H. Mai and P. N. Lan, *Radiation Physics and Chemistry*, 2013, **83**, 105-110.
247. V. Srinivas, F. Bertella, C. S. J. van Hooy-Corstjens, B. v. Leeuwen, E. G. M. Craenmehr, D. Cavallo, S. Rastogi and J. A. W. Harings, *Additive Manufacturing*, 2020, **36**, 101665.
248. P. Purnama and S. Hyun Kim, *Polymer International*, 2014, **63**, 741-745.
249. P. Purnama and S. H. Kim, *Macromolecules*, 2010, **43**, 1137-1142.
250. Y. Chang, Z. Chen and Y. Yang, *ACS Omega*, 2018, **3**, 7979-7984.
251. S. Huang and S. Jiang, *RSC Advances*, 2014, **4**, 24566-24583.
252. K. Masutani, C. W. Lee and Y. Kimura, *Polymer Journal*, 2013, **45**, 427-435.
253. Y. Ramot, M. Haim-Zada, A. J. Domb and A. Nyska, *Advanced Drug Delivery Reviews*, 2016, **107**, 153-162.
254. H. Tsuji, K. Iguchi and Y. Arakawa, *Polymer*, 2021, **213**, 123226.
255. L. M. D. Loiola, M. A. de Farias, R. V. Portugal and M. I. Felisberti, *Journal of Polymer Science Part A: Polymer Chemistry*, 2018, **56**, 2203-2213.
256. A. V. Kashina, T. K. Meleshko, N. N. Bogorad, M. A. Bezrukova and A. V. Yakimanskii, *Polymer Science, Series C*, 2019, **61**, 174-185.
257. V. Pertici, C. Pin-Barre, C. Rivera, C. Pellegrino, J. Laurin, D. Gigmes and T. Trimaille, *Biomacromolecules*, 2019, **20**, 149-163.
258. M. Alami-Milani, P. Zakeri-Milani, H. Valizadeh, M. Fathi, S. Salatin, R. Salehi and M. Jelvehgari, *Pharmaceutical Development and Technology*, 2020, **25**, 704-719.
259. J. Bai, N. Wu, Y. Wang, Q. Li, X. Wang and L. Zhang, *RSC Advances*, 2016, **6**, 108045-108050.
260. V. Tamboli, G. P. Mishra and A. K. Mitra, *Colloid and Polymer Science*, 2013, **291**, 1235-1245.
261. S. P. Patel, R. Vaishya, D. Pal and A. K. Mitra, *AAPS PharmSciTech*, 2015, **16**, 327-343.
262. H. S. Abandansari, E. Aghaghafari, M. R. Nabid and H. Niknejad, *Polymer*, 2013, **54**, 1329-1340.
263. J.-O. Lin, W. Chen, Z. Shen and J. Ling, *Macromolecules*, 2013, **46**, 7769-7776.
264. M.-T. Popescu, M. Korogiannaki, K. Marikou and C. Tsitsilianis, *Polymer*, 2014, **55**, 2943-2951.

265. L. Gardella, D. Cavallo, S. Colonna, A. Fina and O. Monticelli, *Journal of Polymer Science Part A: Polymer Chemistry*, 2014, **52**, 3269-3282.
266. H. Mao, G. Shan, Y. Bao, Z. L. Wu and P. Pan, *Soft Matter*, 2016, **12**, 4628-4637.
267. C. W. Lee, C. Na, Y. Kimura and K. Masutani, *Macromolecular Materials and Engineering*, 2016, **301**, 1121-1131.
268. C. Tsutsumi, J. Sakafuji, M. Okada, K. Oro and K. Hata, *Journal of Materials Science*, 2009, **44**, 3533-3541.
269. D. J. Darensbourg and O. Karroonnirun, *Macromolecules*, 2010, **43**, 8880-8886.
270. N. Nomura, A. Akita, R. Ishii and M. Mizuno, *Journal of the American Chemical Society*, 2010, **132**, 1750-1751.
271. G. Li, M. Lamberti, D. Pappalardo and C. Pellecchia, *Macromolecules*, 2012, **45**, 8614-8620.
272. D. Dakshinamoorthy and F. Peruch, *Journal of Polymer Science Part A: Polymer Chemistry*, 2012, **50**, 2161-2171.
273. L. Zhang, N. Li, Y. Wang, J. Guo and J. Li, *Macromolecular Research*, 2014, **22**, 600-605.
274. Y. Maruta and A. Abiko, *Polymer Bulletin*, 2014, **71**, 989-999.
275. C. Kan and H. Ma, *RSC Advances*, 2016, **6**, 47402-47409.
276. T. Shi, W. Luo, S. Liu and Z. Li, *Journal of Polymer Science Part A: Polymer Chemistry*, 2018, **56**, 611-617.
277. P. Chumsaeng, S. Haesuwannakij, A. Virachotikul and K. Phomphrai, *Journal of Polymer Science Part A: Polymer Chemistry*, 2019, **57**, 1635-1644.
278. A. Dalmoro, A. A. Barba, M. Lamberti, M. Mazzeo, V. Venditto and G. Lamberti, *Journal of Materials Science*, 2014, **49**, 5986-5996.
279. M. D. Deokar, S. B. Idage, B. B. Idage and S. Sivaram, *Journal of Applied Polymer Science*, 2016, **133**.
280. M. Rizzuto, A. Mugica, M. Zubitur, D. Caretti and A. J. Müller, *CrystEngComm*, 2016, **18**, 2014-2023.
281. Q. Liu, L. Wu, R. Jackstell and M. Beller, *Nature Communications*, 2015, **6**, 5933.
282. Y.-C. Xu, H. Zhou, X.-Y. Sun, W.-M. Ren and X.-B. Lu, *Macromolecules*, 2016, **49**, 5782-5787.
283. A. Behr and K.-D. Juszak, *Journal of Organometallic Chemistry*, 1983, **255**, 263-268.
284. X. Liu and L.-N. He, *Topics in Current Chemistry*, 2017, **375**, 21.
285. F. Ferretti, M. Sharif, S. Dastgir, F. Ragaini, R. Jackstell and M. Beller, *Green Chemistry*, 2017, **19**, 3542-3548.
286. A. Behr and G. Henze, *Green Chemistry*, 2011, **13**, 25-39.
287. L. Chen, Y. Li, S. Yue, J. Ling, X. Ni and Z. Shen, *Macromolecules*, 2017, **50**, 9598-9606.
288. V. Haack, E. Dinjus and S. Pitter, *Die Angewandte Makromolekulare Chemie*, 1998, **257**, 19-22.
289. K. O. Kim, S. Shin, J. Kim and T.-L. Choi, *Macromolecules*, 2014, **47**, 1351-1359.
290. A. Blencowe and G. G. Qiao, *Journal of the American Chemical Society*, 2013, **135**, 5717-5725.
291. D. J. Darensbourg, *Chemical Reviews*, 2007, **107**, 2388-2410.

292. A. Behr and M. Becker, *Dalton Transactions*, 2006, DOI: 10.1039/B608552K, 4607-4613.
293. J. Song, X. Feng, Y. Yamamoto, A. Almansour, A. Natarajan, S. Raju and M. Bao, *Tetrahedron Letters*, 2016, **57**.